CARDIFF UNIVERSITY
PRIFYSGOL CAERDYDD

PhD Thesis:

Investigation of shallow marine Antarctic environments using the annual increment growth pattern of the bivalve mollusc *Aequiyoldia eightsii* (Jay, 1839).

by

Alejandro Román González

2017

Dedicated to Montserrat and Antonio

THE PRESIDENT'S Research Scholarships
CARDIFF UNIVERSITY PRIFYSGOL CAERDYDD
PRIFYSGOL BANGOR UNIVERSITY
British Antarctic Survey
NATURAL ENVIRONMENT RESEARCH COUNCIL
NATURAL HISTORY MUSEUM

Thesis supervised by:

Ian Hall[1], James Scourse[2], Lloyd Peck[3], Paul Butler[2], Caroline Lear[1] and Martin Ziegler[4]

1 School of Earth and Ocean Sciences, Cardiff University, UK

2 School of Ocean Sciences, Bangor University, UK

3 British Antarctic Survey, UK

4 Earth Science Department, Utrecht University, NL

Acknowledgements

First I would like to thank the President's Research Scholarship from Cardiff University which founded this PhD programme, providing the necessary funds to carry out the research presented here. I also want to express my gratitude to all the partner institutions for all their support and resources provided during this research. Especially I would like to thank all my supervisors (Ian Hall, James Scourse, Lloyd Peck, Paul Butler, Caroline Lear and Martin Ziegler), who provided support and intellectual inspiration throughout the entire length of the PhD programme. I would also like to give especial thanks to Dr. Alexandra Nederbragt from Cardiff University, who processed the minuscule geochemical samples for this study and whose technical expertise was invaluable. Carrying underwater work in Antarctica is challenging to say at least, I want to acknowledge the hard work and dedication of the British Antarctic Survey (BAS) divers who collected the specimens for this research. Furthermore, I would like to mention the support I have received from the ARAMACC Marie Curie Training Network partners for thinking of me during their training workshops, for that I am very thankful. I also want to thank the Natural History Museum, London, and especially the marine Mollusca curator Andreia Salvador, for lending some historical specimens, which have extended the original scope of this research project. In addition, I want to thank Mike Meredith and Hugh Venables (BAS) who provided me access to the Rothera Biological Times Series data, which was invaluable for understanding the local environmental processes in the coastal waters of Rothera Station. I am also grateful to the reviewers of this thesis for taking their time and attention to review it and whose comments help to improve the quality of the work presented here. My eternal gratitude goes to Carmen for the love and support that has granted me during the work in this thesis. Last but not least I want to thank my parents for their lifelong support and love they always have shown which knows no limits. Thank you Mum, thank you Dad.

Note from the author

Reference figures labelling – Figures in this thesis are label as **Fig. 1.1**, **Fig 1.2**, etc. The first number indicates the chapter number of the figure whereas the second number is the number of the figure within each chapter. When a figure is composed of two or more panels they are labelled using small print letters in abecedary order, e.g. **Fig. 1.1a**, **Fig. 1.1b**. Figures in the appendices are labelled using a capital A, e.g. **Fig. A1.1**, when an appendix figure has two of more panels, a small print letter is added, e.g. **Fig. A1.1a**, **Fig. A1.1b**, etc.

General acronyms – Standard deviation (SD), standard error (SE), 95 % confidence intervals ($CI_{0.05}$) and significance levels (SL).

Published chapters – Part of the results presented in Chapter III: *Aequiyoldia eightsii* shell growth were published in *Palaeogreography, Palaeoclimatology, Palaeoecology* 465 (2017), 300-306 as:

Román-González, A., Scourse, J.D., Butler, P.G., Reynolds, D.J., Richardson, C.A., Peck, L.S., Brey, T., Hall, I.R. Analysis of ontogenetic growth trends in two marine Antarctic bivalves *Yoldia eightsi* and *Laternula elliptica* : Implications for sclerochronology.

Part of the results presented in Chapter VI: Sclerochronologies were published in *The Holocene* 27 (2017), 271-281 as:

Román-González, A., Scourse, J.D., Richardson, C.A., Peck, L.S., Bentley, M.J., Butler, P.G. A sclerochronological archive for Antarctic coastal waters based on the marine bivalve *Yoldia eightsi* (Jay, 1839) from the South Orkney Islands.

Pre-publishing versions of both manuscripts have been added at the end of this thesis in an appendix.

Summary

The research presented here constitutes the latest advances in the use of the Antarctic bivalve mollusc *Aequiyoldia eightsii* as a sclerochronological proxy for Antarctic coastal waters. *A. eightsii* has the potential to provide annually-resolved records for the Antarctic shallow waters beyond the beginning of the instrumental record. A comprehensive study of *A. eightsii* shell growth was carried out, which highlighted two ontogenetic trends: i) negative exponential and ii) a quasi-cyclic trend of a period of nine years, which may relate to allocation of energetic resources. Using crossmatching techniques, four chronologies from adjacent locations near Rothera Station (West Antarctic Peninsula, WAP) and an additional chronology from historical samples collected near Signy Station (South Orkney Islands, SOIs) were developed. Additionally further work on a pre-existing chronology from the SOIs is presented. Instrumental records and climatic indices were analysed to determine environmental variability and the factors controlling shell growth. Seawater temperature and fast-ice duration seem to be the main environmental drivers of *A. eightsii* shell growth. Shell growth of South Cove (WAP) specimens seem to better reflect to environmental conditions recorded in the Rothera Biological Time Series. Stable oxygen and carbon isotope ($\delta^{18}O$ and $\delta^{13}C$) records were developed from shell carbonate material; these showed sub- and inter-annual variability and all specimens showed similar trends in $\delta^{18}O_{shell}$ and $\delta^{13}C_{shell}$, with the exception of a deep-collected specimen of the SOIs, which showed much reduced interannual variability and a stronger $\delta^{13}C_{shell}$ negative trend with ontogenetic age. Additionally, stable isotope fractionation depending anatomical part of the shell (anterior, ventral and posterior) was studied, which showed intra-increment variability in $\delta^{18}O_{shell}$ and $\delta^{13}C_{shell}$. The present work constitutes a comprehensive calibration of *A. eightsii* as a sclerochronological proxy for Antarctic shallow coastal waters, which will help to expand our understanding of climate trends in the region.

Chapter I: Introduction

This chapter will cover a general description of the Southern Ocean, giving a general oceanographic description and stating the current knowledge of climate trends acting in the region. In addition, especial attention is paid to the West Antarctic Peninsula, in particular to Marguerite Bay, and the South Orkney Islands since these are the location from where the *Aequiyoldia eightsii* specimens were collected. More detailed oceanographic and climate information from these two regions is provided. Moreover, a review is provided concerning the current knowledge about the biology and ecology of *A. eightsii*. Furthermore a brief introduction to the use of sclerochronological archives is given. The rationale, aims and objectives of this thesis are stated at the end of the present chapter.

1.1 Area of interest

1.1.1 Oceanographic setting

The Southern Ocean is a complex and fragile environment which is of major importance for the ocean circulation and therefore plays a major role in the global climate system. According to the Antarctic Treaty (1959) the Southern Ocean is defined geopolitically as the sea region located south of 60 °S, whilst from an oceanographic perspective it is considered as to be the ocean south of the Subtropical Front (Orsi et al., 1995) and from a biological/ecological perspective it is usually defined as oceanic waters contained within the Polar Front (PF; Barnes et al., 2006; Convey et al., 2014). The Southern Ocean is traditionally divided into three sectors based on their corresponding ocean basins: Weddell Sea, Scotia Sea, Lazarev Sea and Riiser-Larsen Sea (Atlantic Ocean sector), Amundsen-Bellinghausen Sea and Ross Sea (Pacific Ocean sector) and Cosmonauts Sea, Cooperation Sea, Davis Sea, Mawson Sea, D'Urville Sea and Somov Sea (Indian Ocean sector). One unique characteristic of the Southern Ocean is that unlike any other ocean it is not constrained by landmasses besides Antarctica to the south and its circumpolar circulation is continuous and only partly limited by the Drake Passage. The Southern Ocean is also unique in being aligned zonally (east-west) in contrast to other oceans which are aligned meridionally (north-south). These characteristics allow a strong geostrophic flow around Antarctica, forming the Antarctic Circumpolar Current (ACC; Orsi et al., 1995). The ACC is the main feature of the Southern Ocean circulation and flows continuously eastwardly at around 140 Sv (140 x 10^6 m^3 sec^{-1}) connecting the three major oceanic basins (Orsi et al., 1995; Cunningham, 2005; Talley et al., 2011). The flow is largely driven by the action of the Southern Hemisphere westerly winds blowing between the Subantarctic Front (SAF) to the north, and the PF to the south, and the northward Ekman transport (**Fig. 1.1**; Trenberth et al., 1990; Orsi et al., 1995; Cunningham, 2005).

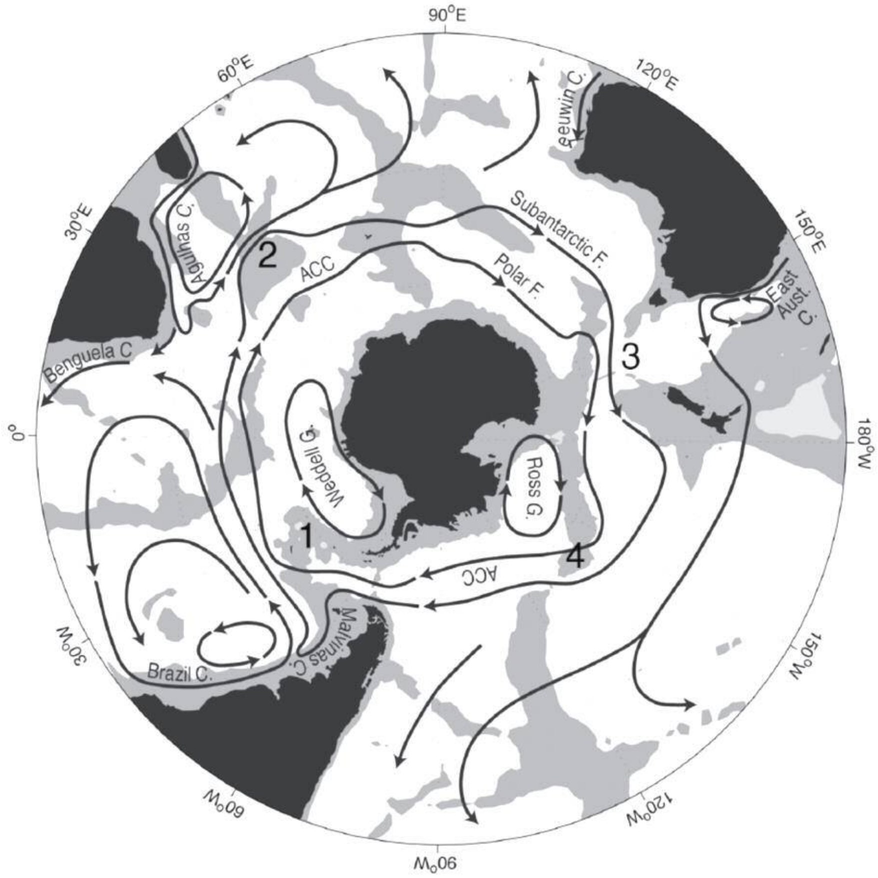

Fig. 1.1 Circulation in the Southern Ocean and climatic zone around Antarctic. The position of the Weddell Sea Gyre, Ross Sea Gyre, Antarctic Circumpolar Current (ACC), Polar Front, Subantarctic Front are also indicated. 1) South Scotia Arch, 2) Kerguelen Plateau, 3) Maxquarie Ridge complex and 4) Pacific Antarctic Ridge (From: Cunningham, 2005).

Closer to the Antarctic continent the easterlies drive oceanic circulation westward along the coastal Antarctic regions. This coastal circulation is interrupted by the Antarctic Peninsula. Katabatic winds blowing from the continent introduce a northward component to coastal circulation (Talley et al., 2011). Two cyclonic (i.e. clockwise) gyres are prominent in Antarctic coastal circulation: the Weddell Sea gyre and the Ross Sea gyre (**Fig. 1.1**). The Weddell Sea gyre, situated south of the ACC, flows westwards along the coastal regions and then turns northwards as it meets the Antarctic Peninsula, its western boundary, then it diverges eastward following the south boundary of the ACC to turn polewards and close the gyre (Orsi et al., 1993). The Ross Sea gyre flows westward along the coast, then turns northward off Victoria Land, until it meets the ACC diverging east towards the Antarctic Peninsula and in the Amundsen Sea, off the coast of Marie Byrd Land, turns polewards again closing the gyre and joining the westward coastal circulation (Jacobs et al., 2002).

The Southern Ocean comprises several stratified water bodies with distinctive physical characteristics. The main water bodies in the Southern Ocean are: Antarctic Surface Water (AASW), Circumpolar Deep Water (CDW), Antarctic Intermediate Water (AAIW), Subantarctic Mode Water (SAMW) and Antarctic Bottom Water (AABW; **Fig. 1.2**). The AASW occupies the upper 200 m of the water column. This water mass is cold and fresh (salinity < 34.5 psu), with high concentrations of oxygen and macronutrients (i.e. nitrate, silicate and phosphate). The physical properties of AASW are strongly modified on a seasonal basis due to sea-ice formation and melt cycle.

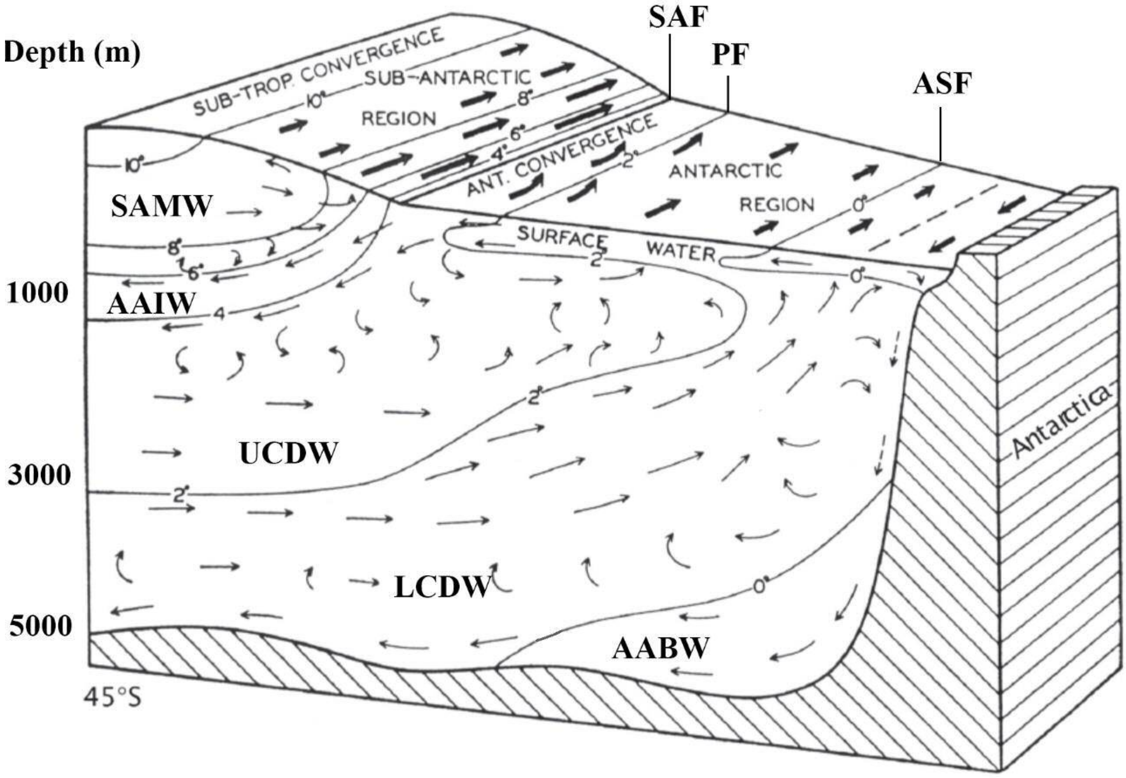

Fig. 1.2 Profile section of the Southern Ocean, showing the position and circulation of the Antarctic Bottom Water (AABW), Lower Circumpolar Deep Water (LCDW), Upper Circumpolar Deep Water (UCDW), Antarctic Intermediate Water (AAIW), Subantarctic Mode Water (SAMW), Sub-Antarctic Front (SAF), Polar Front (PF) and the Antarctic Slope Front (ASF; modified from: Cunningham, 2005).

The CDW is one of the largest water bodies in the Southern Ocean and represents the core of the ACC (**Fig. 1.1** and **Fig. 1.2**; Orsi et al., 1995; Rintoul et al., 2001). It extends from the surface down to approximately 1000 m water depth and it is significantly warmer and more saline (34.7 psu - 34.8 psu) and has a typically lower oxygen concentration than AASW. The CDW is conventionally divided into two different water masses: the Upper (UCDW) and the Lower (LCDW) which have different inherent characteristics. The UCDW is characterised by high levels of oxygen and macronutrients (i.e. nitrate, silicate and phosphate) and the LCDW by high salinity (Orsi et al., 1995; Talley et al., 2011). This combination of high oxygen levels and nutrients in the UCDW is responsible for phytoplankton blooms in the Antarctic Zone (delimited by the Polar Front and the Southern ACC Front) region (Talley et al., 2011). CDW upwells between the Antarctic Slope Front and the SAF (**Fig. 1.2**; Speer et al., 2000; Talley et al., 2011). UCDW flows under AAIW from the SAF region and on the top of LCDW, which flows on the top of AABW. CDW upwells in the Antarctic Zone and in the PF (i.e. across the ACC).

AAIW is generated in the Drake Passage region and it is characterised by its low salinity (33.8 psu), warm temperature (~2.2 °C) and relative high oxygen concentration between 500 and 1500 m water depth (Rintoul et al., 2001; Talley et al., 2011). There are two theories of how AAIW is formed: i) the conventional view is that it is formed from sinking of the AASW in the SAF around Antarctica and carried northwards by Ekman transport (**Fig. 1.2**), ii) on the other hand, Talley (1999) explains the formation of AAIW as a more localized process in the Pacific Ocean sector (i.e. derived from the advected Pacific AAIW) and Drake Passage region (i.e. local modification of the Pacific AAIW).

AABW is formed south of the ACC as a result of brine rejection during ice formation in coastal latent heat polynyas (i.e. ice-free oceanic regions) mainly in the Weddell Sea, Ross Sea and Adélie Coast (**Fig. 1.2**; Foster and Carmack, 1976; Orsi et al., 1999; Rintoul et al., 2001; Talley et al., 2011). The AABW is characterised by its depth (reaching > 3000 m water depth), cold temperature (from -0.8 to 0 °C) and high salinity (from 34.6 psu to 34.7 psu). As sea-ice starts forming the saltier cold surface water sinks following the bottom topography down the continental slope mixing with adjacent water masses such as the LCDW (Orsi et al., 1999). However, the increased meltwater runoff from continental ice due to current climate trends is believed to have a significant effect in the rapid freshening of the AABW (Jacobs, 2006; Rintoul, 2007). AABW characteristics differ depending on the region where it was formed as lateral mixing varies largely between regions; AABW from the Weddell Sea is the freshest and coldest whereas AABW from Ross Sea is the warmest and saltiest, while AABW formed off Adélie Coast has intermediate properties (Orsi et al., 1999; Talley et al., 2011). AABW is constrained due to the complex Southern Ocean bathymetry, and in the Weddell Sea is only able to leave the Southern Ocean through a gap in the South Scotia Ridge (which separated the Weddell Sea from the Scotia Sea to the north) in the south Atlantic (**Fig. 1.1**; Orsi et al., 1999; Talley et al., 2011). As AABW travels northward in the Atlantic Basin it begins to mix with the North Atlantic Deep Water, resulting in an increase in temperature, salinity and oxygen. The vast flow, estimated around 21 Sv (21 x 10^6 m^3 sec^{-1}; Orsi et al., 2002), of the saline and cold AABW has a special importance since it allows the existence of the global thermohaline circulation (Orsi et al., 1999; Rintoul et al., 2001; Orsi et al., 2002), a global circulation process controlled ultimately controlled by temperature and salinity gradients at low and high latitudes.

The Amundsen-Bellinghausen Sea occupies the southeast Pacific Ocean sector of the Southern Ocean (**Fig. 1.1**). It is bounded to the east by the WAP and opens to the west to the Amundsen Sea and in the north to the South Pacific Ocean. The Bellingshausen Sea also connects with the Weddell Sea through the Drake Passage, between the Antarctic Peninsula and South America. In this sector of the Southern Ocean, the ACC flows eastward along the shelf slope (Hofmann and Klinck, 1998). At depth the CDW overflows episodically onto the continental shelf across deep glacial troughs (Hofmann and Klinck, 1998; Moffat et al., 2009; Martinson and McKee, 2012), which in some regions was found to add a significant amount of nutrients to shallower waters (Gordon et al., 2000); however, similar studies in Marguerite Bay have found no difference in nutrient (nitrates and silicates) concentration between the CDW and shallower water masses (Serebrennikova and Fanning, 2004) or even nutrient (silicates) dilution in shallow water masses (Prézelin et al., 2004). The Amundsen-Bellingshausen Sea also presents the most negative trend in sea-ice extent between 1979 and 2012 in the entire Southern Ocean with an annual anomaly of -4.3 % (Vaughan et al., 2013). In addition a later ice advance (+61 ± 15 days), an earlier retreat (-39 ± 13 days) and shorter duration (-3.1 ± 1.0 days year^{-1}) were found for the period 1979-2011 (Stammerjohn et al., 2012). Within the region the upper 100 m of the water column have also experienced a significant warming of 0.5 °C decade^{-1} and summer salinization during the second half of the twentieth century (Meredith and King, 2005).

An analysis of the relationship between El Niño-Southern Oscillation (ENSO), sea-ice cover and climate anomalies in the Southern Ocean between 1982 and 1998 found that the strongest were located in the Amundsen-Bellingshausen and Ross Sea (Kwok and Comiso, 2002a). During ENSO warm (cold) events there was a weakening (strengthening) in the Amundsen-Bellingshausen low pressure centre, which caused a reduction (increase) in the northerly component of surface winds along WAP (Meredith et al., 2004a). In this scenario (ENSO warm events) the Amundsen-Bellingshausen Sea low deepens and the northerly component of surface winds along the WAP strengthens (Harangozo, 2000).

The Weddell Sea is a region of major importance in the Southern Ocean as one of the principal locations for AABW formation (e.g. Orsi et al., 1993; Robertson et al., 2002). It is bounded by the Antarctic Peninsula to the west, the submarine South Scotia Ridge to the north, Antarctica to the south and opens to the Indian Ocean along its easterly side.

The water depth structure of the Weddell Sea is formed by several water masses: Surface mixed layer, Winter Water, shelf waters, Warm Deep Water, Weddell Sea Deep Water and Weddell Sea Bottom Water (**Table 1.1**; Robertson et al., 2002).

Table 1.1 Potential temperature and salinity of the water masses of the Weddell Sea. Data from Robertson et al. (2002).

Water type	Water mass	Potential temperature range (°C)	Salinity range (psu)
Surface waters	Surface mixed layer	-1.88 to 1.0	33.0-34.5
	Winter Water	-1.88 to 1-1.7	34.30-34.44
Shelf waters	Low-salinity shelf water	-1.88 to 1-1.7	34.3-34.4
	high-salinity shelf water	-1.88 to 1-1.7	34.56-34.84
	Ice Shelf Water	< -1.9	34.2-34.7
Transitional water	Modified Warm Deep Water	-0.7 to -1.7	34.4-34.6
Deep waters	Warm Deep Water	0.0 to 1.0	34.6-34.75
	Weddell Sea Deep Water	-0.8 to 0.0	34.62-34.68
	Weddell Sea Bottom Water	-1.3 to -0.7	34.62-34.68

Temperature trends in the Weddell Sea are not linear however the warm and saline Warm Deep Water has warmed approximately 0.012 ± 0.007 °C year^{-1} from the 1970s to 1990s (Robertson et al., 2002), and the dense Weddell Sea Bottom Water has also shown trends of warming at a rate of 0.01 °C year^{-1} between 1989 and 1995 (Fahrbach et al., 2004) although it is constrained within the Weddell Sea basin due to its high density (Turner and Marshall, 2011). In addition, Weddell Sea Deep Water has also shown signs of warming and is able to spill into the Atlantic Ocean basin; this warming signal has been measured as far north as the Equator (Zenk and Morozov, 2007). There are important implications from these oceanographic changes in the formation of the AABW, for deep ocean ventilation, thermohaline circulation and ocean-atmosphere heat transport (Robertson et al., 2002). In spite of these, the annual sea-ice extent anomaly for the Weddell Sea is slightly positive +1.3 % and significantly different from the west side of the Antarctic Peninsula, where in the Amundsen-Bellingshausen Sea it is at -4.3 % (Vaughan et al., 2013).

The Weddell Gyre is a cyclonic (clockwise) oceanic circulation in the Weddell Sea basin. It flows westwards along the Antarctic coast and turns north when it encounters the shallower bathymetry along the east coast of the Antarctic Peninsula. The main component of the gyre then turns east along the South Scotia Ridge driven by the ACC, and subsequently the Coriolis force and Ekman transport drives the circulation south towards Antarctica before it flows westwards again completing the gyre. Several ice shelves are in contact with the Weddell Gyre: Ronne-Filchner (south section), Larsen (west section), Riiser-Larson and Fimbul (east section).

The Weddell Polynya, which developed between 1974 and 1976 and has not reoccurred since (Gordon et al., 2007), was estimated to be approximately 350,000 km^2 (Motoi et al., 1987). This large ice-free region played a significant role in ocean ventilation that led to densification of surface waters and a significant formation of AABW due to convective processes (Turner and Marshall, 2011), increased winter (June-August) surface air temperatures above the polynya (approximately +20 °C) and 50 % increase in cloud formation (Moore et al., 2002). There are several mechanisms hypothesized for the formation of the 1974/76 Weddell Polynya. One possible explanation is that it was formed by the injection of warm deep water into the surface layer due to deep convective processes that inverted the water column stratification leaving a warm deep water layer on the surface and a sub-superficial “cold spot” body of water. This “cold spot" was reported to flow at 1.3 cm sec^{-1} westwards towards South Orkney Islands (Gordon, 1982a). Alternatively, Motoi et al. (1987) suggested the presence of a high-salinity mixed layer during the summer led to deep convection processes that prevented sea-ice formation. In addition, Gordon et al. (2007) suggested a teleconnection forcing by negative Southern Annular Mode (SAM) conditions whereby the Weddell Sea presented an increased surface salinity and reduced pycnocline stability, which in turn favours upwelling and deep convection at Maud Rise; these conditions coupled with La Niña events, that enhances sea-ice formation and therefore increased surface salinity, was argued to be a possible driver of the Weddell Polynya formation.

1.1.2 Climate change in the Southern Ocean

Vaughan et al. (2013) highlighted, in the 5th Intergovernmental Panel on Climate Change (IPCC) report, the major role that the cryosphere plays in the global climate affecting the surface energy budget, primary production, water cycle and sea level. Furthermore, changes in the ice systems have strong repercussions on the biota that depends on ice shelves, ice sheets and ice dynamics (e.g. Moline et al., 2008; Massom and Stammerjohn, 2010).

In the Antarctic most of the sea-ice is first year ice, which melts during the summer season. On average it extends from 3 x 10^6 km^2 in February to 18 x 10^6 km^2 in September (Vaughan et al., 2013). While, current trends in the Arctic show a decrease in both multiyear sea-ice and perennial sea-ice extent (-13.5 ± 2.5 % decade^{-1} and -11.5 ± 2.1 % decade^{-1} respectively) between 1979 and 2012 (Comiso, 2012; Vaughan et al., 2013), the Antarctic shows a slight positive trend of 1.5 ± 0.2 % decade^{-1}. There are, however, strong spatial differences, with sea-ice retreating in the Amundsen-Bellinghausen Sea region and advancing in the Ross Sea linked with climate variability in the tropical eastern Pacific (Vaughan et al., 2013; Meehl et al., 2016). In the process of sea-ice formation salt is released into the water altering the ocean stratification and modifying the ocean circulation. Sea-ice is also important because it insulates the ocean from heat loss, acts as a barrier to gas exchange between the atmosphere and the ocean and reflects energy coming from the sun due to its high surface albedo (Vaughan et al., 2013). Therefore if current trends in sea-ice extent continue, ocean productivity, regional and global heat fluxes and ocean circulation are expected to be altered (Vaughan et al., 2013). The sea-ice cycle affects significantly the water column stability (e.g. Dierssen et al., 2002; Montes-Hugo et al., 2009) which in turn is critical for the development of phytoplankton blooms (Mitchell and Holm-Hansen, 1991). The northern coastal regions of the WAP have experienced a reduction in phytoplankton biomass due to increased cloudiness and wind-driven enhanced vertical mixing whereas southern coastal of the WAP have experienced an increase in phytoplankton biomass due to enhance water column stabilization driven by meltwater runoff, reduced sea-ice and cloudiness (Montes-Hugo et al., 2009).

Ice sheets play a major role to sea level rise as they are grounded on land so that any melting process is not hydrostatically compensated. Ice sheet dynamics are controlled by the following processes: a) basal lubrication, b) cryo-hydrologic warming, c) ice shelf buttressing effect, d) ice-ocean interaction and e) ice calving (Vaughan et al., 2013). Ongoing changes in ice sheet dynamics have been attributed to a combination of atmospheric-ocean-ice processes (i.e. climate forcing), snowfall precipitation (influenced by atmospheric humidity) and ocean thermal forcing (Vaughan et al., 2013). The East Antarctic Ice Sheet seems to have remained stable for the past 14 million years (Young et al., 2011); on the other hand West Antarctic Ice Sheet has been losing mass at an increasing rate during the last century (Vaughan et al., 2013).

Glaciers occur where the topography and climatic conditions are favourable for snow to accumulate, compress and refreeze into firn and later on into snow ice. Glaciers are also a good proxy for climate trends as they adjust and alter in response to changes in environmental parameters such as precipitation or temperature (Vaughan et al., 2013). According to Vaughan et al. (2013), glaciers are major contributors to sea level rise due to the fact that they are grounded on land and therefore any addition of melt water to the sea is not hydrostatically compensated. Glacier mass balance trends in the Antarctic and Sub-Antarctic are not clear, so that complex regional patterns with gains (e.g. Ellsworth Land) and losses (e.g. West Antarctic Peninsula; WAP) in different parts of the continent indicate an overall status that is close to balance (Gardner et al., 2013). Cook et al. (2016) identified the importance of ocean warming leading glacier retreat rate along the coast of the Antarctic Peninsula highlighting the complex interaction between the atmosphere, the ocean and the cryosphere.

The WAP is the region that has experienced the strongest trends in sea-ice loss of the Southern Ocean and strongest warming trends in temperature over the last half of the 20th century (e.g. Vaughan et al., 2003; Meredith and King, 2005; Vaughan et al., 2013). Turner et al. (2016) recently analysed stacked temperature records from the Antarctic Peninsula and reported a change from a warming trend (0.32 ± 0.2 °C decade^{-1} for the period 1979/97) to a cooling trend (-0.47 ± 0.25 °C decade^{-1} for the period 1999/2014) coinciding with the so-called global warming hiatus (i.e. a reduction in the rate of increase of global surface air temperature; Trenberth, 2015). The authors also established that major changes occurred at tropical-high latitudes in the Pacific Ocean, reflected in the switch of the El Niño Interdecadal Pacific Oscillation (IPO) from an El Niño dominated (IPO positive) state during the warming period (1979/97) to a La Niña dominated (IPO negative) state during the cooling period (1999/2014). The negative trend in temperature was driven by the increasing frequency of cold east-to-south easterly winds which in turn favoured cyclonic conditions in the northern Weddell Sea and a strengthening of the Polar Front Jet (Turner et al., 2016a).

Knowledge of Antarctic benthic ecosystem response to climate change has been limited to date due in part to the lack of comparative baselines. In the pelagic realm, a shift polewards in phytoplankton activity was found over the past 30 years with decreasing phytoplankton biomass in the north regions of the WAP, associated with an increased upper mixed layer depth induced by wind stress (Mitchell and Holm-Hansen, 1991), and increasing phytoplankton biomass in the south regions of the WAP, associated with reduced sea-ice duration and reduced upper mixed layer depth (Montes-Hugo et al., 2009). In the benthic realm, major ecosystems shifts have been reported linked to catastrophic events such the collapse of the Larsen ice shelf (e.g. Gutt et al., 2011, 2013), although disastrous at a local scale these type of events are not representative of gradual long-term changes associated with climate change. Iceberg scouring is predicted to increase with current climate trends (Smale et al., 2008; Barnes and Souster, 2011a); this can have significant effects on benthic communities (e.g. Peck et al., 1999; Clarke et al., 2007; Barnes and Souster, 2011; Sahade et al., 2015). Some examples are: shifts from filter feeders-ascidian domination to a mixed assemblage mediated by increasing sediment runoff was reported for Potter Cove, King George Island (Sahade et al., 2015), increased physical disturbance and increased mortality of mega- and macro-fauna (Harper et al., 2012; Barnes et al., 2014a) and increased patchiness in the shallow benthic ecosystem with alterations between dominant and pioneering species (Clarke et al., 2007).

1.1.3 Rothera Research Station, West Antarctic Peninsula setting

Rothera Research Station is a British Antarctic Survey (BAS) base on the Antarctic Peninsula, located at Rothera Point on the south-east Coast of Adelaide Island (67°35’8”S, 68°7 ’59”W) in the Bellingshausen Sea (**Fig. 1.3**). Rothera Point delimits to the north the opening of Ryder Bay, the closest coastal embayment to Rothera Research Station. Ryder Bay opens into the wider Marguerite Bay in the Bellingshausen Sea. Marguerite Bay is bounded by Alexander Island to the south, Adelaide Island to the north and the Antarctic Peninsula to the East (**Fig. 1.4**). The continental shelf in Marguerite Bay is typically about 450 m deep and it presents a deep trough running from north-west to south-east called Marguerite Trough. The deepest point in Marguerite Trough is found near Alexander Island around 1600 m water depth (Meredith et al., 2008a).

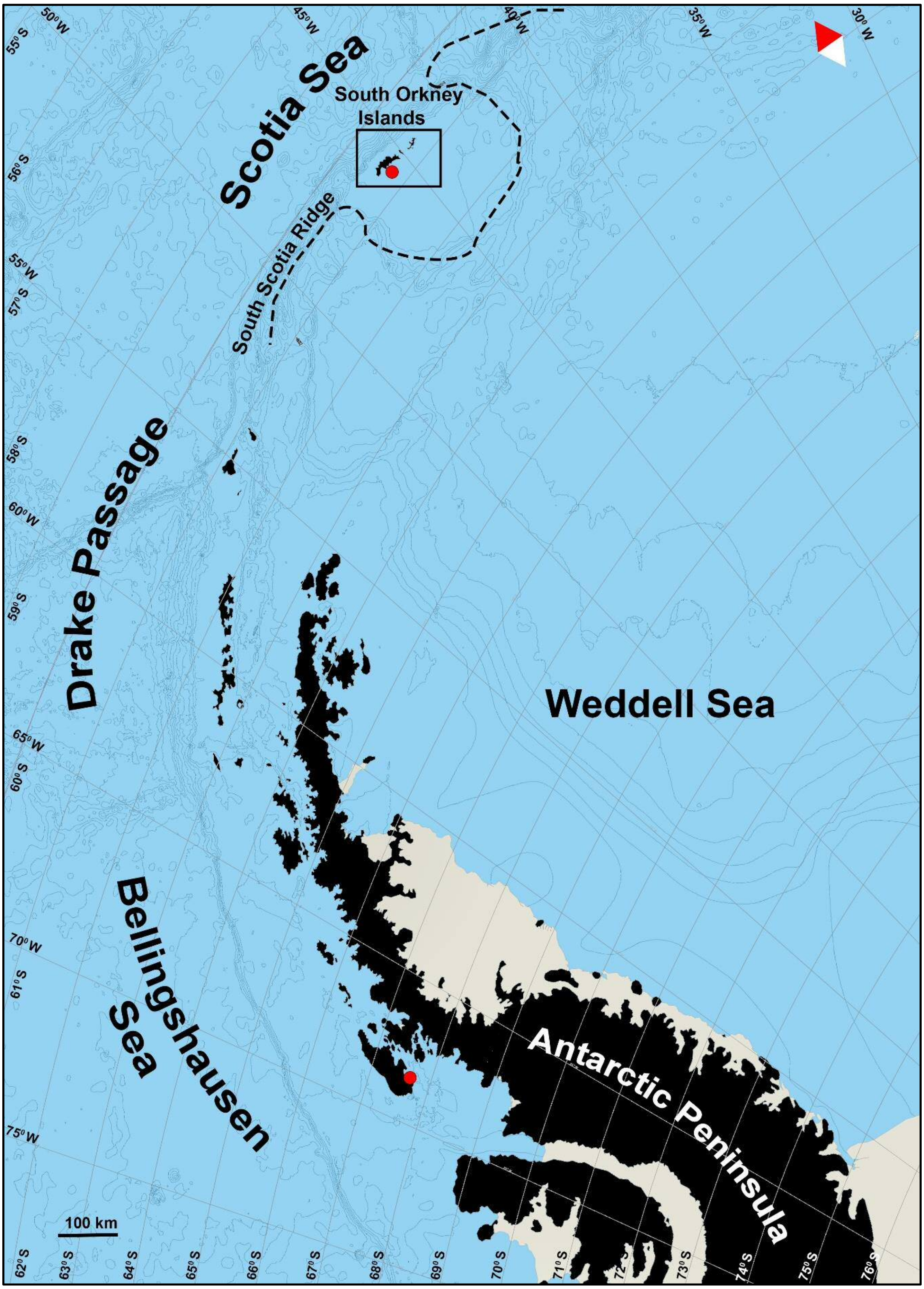
50° W
45° W
40° W
35° W
30° W
55° S
56° S
55° W
57° S
58° S
60° W
59° S
65° W
60° S
70° W
61° S
75° W
Scotia Sea
South Orkney Islands
South Scotia Ridge
Drake Passage
Weddell Sea
Bellingshausen Sea
Antarctic Peninsula
100 km
62° S
63° S
64° S
65° S
66° S
67° S
68° S
69° S
70° S
71° S
72° S
73° S
74° S
75° S
76° S

Fig. 1.3 Map of the Antarctic Peninsula showing the position of Signy Research Station (red dot in the South Orkney Islands) and the position of Rothera Research Station (red dot in the WAP). The dash line represents the location of the South Scotia Ridge. A scale and a compass indicating north (red) are also included.

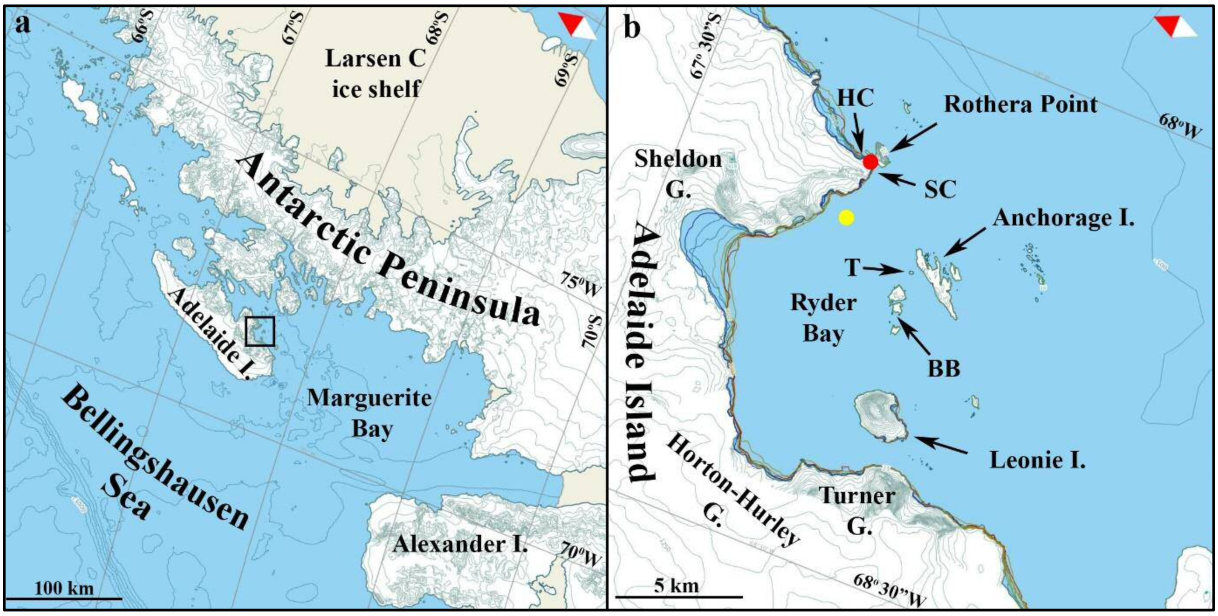

Fig. 1.4 a) Regional map of the West Antarctic Peninsula in the Adelaide Island region **b)** Local map of Ryder Bay with the position of the Rothera Biological Time Series (RaTS) sampling location (yellow dot), Rothera Research Station (red dot), Hangar Bay (HC, South Cove (SC), Trolval (T) and Back Bay (BB, Lagoon Island). The compass indicates north (red).

Oceanographically Marguerite Bay differs from other Antarctic regions as slope front at the shelf break is interrupted by deep troughs. These deep troughs, such as Marguerite Trough, are thought to be key in the incursions of the CDW to shallower regions, the CDW to flow onto the shelf with little modification becoming fresher and colder (Meredith et al., 2004), bringing heat and nutrients that can be used by the phytoplankton assemblages (Klinck et al., 2004). The CDW is traditionally divided into the LCDW, characterised by a potential temperature (θ) of 27.80 °C, and the UCDW, characterised by θ = 27.72 °C (Klinck et al., 2004). The warm and saline UCDW is also characterised by a dissolved oxygen minimum and high concentrations of dissolved nutrients (Meredith et al., 2004a). The UCDW is separated from the AASW by a pycnocline, which is characterised by temperatures higher than 0 °C and a salinity around 33.5 psu in the Marguerite Bay region (**Fig. 1.5**). During the austral summer ice melt, continental runoff freshens the top-most part of the AASW, which also receives an increased input of heat due to insolation. The remnants of the previous winter cold and saline Winter Water (WW), which shows as a marked subsurface temperature minimum, is displaced deeper by the fresher AASW (**Fig. 1.5**). During the austral winter there is a deep vertical mixing down to approximately 200 m water depth as a consequence of sea-ice formation, low temperature and increased salinification, which leads to the formation of the WW (**Fig. 1.5**; Moffat et al., 2008; Annett et al., 2015).

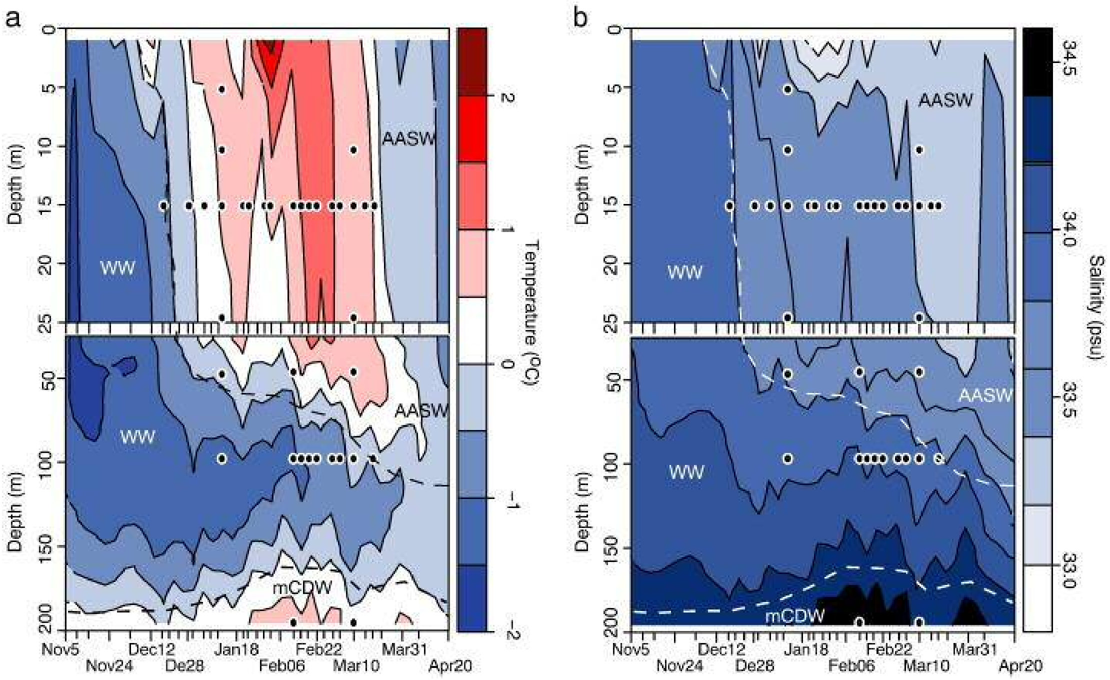

Fig. 1.5 a) Seasonal variation in temperature (°C) and **b)** salinity in the upper 200 m at the RaTS station in Ryder Bay during 2009/10. Water masses are indicated: Antarctic surface water

(AASW), winter water (WW) and modified CDW (mCDW). Note the increased stratification due to increased temperatures and lower salinities during the austral summer and the break-up of stratification and vertical mixing during the austral winter with the formation of the WW (from: Annett et al., 2015).

Ryder Bay has a maximum water depth of approximately 500 m water depth and is located south-east of Adelaide Island (**Fig. 1.4**). Several islands (Léonie Island, Anchorage Island, Lagoon Island, Trolval Island) and glaciers (e.g. Sheldon, Horton, Turner) are located within Ryder Bay (**Fig. 1.4**). Ryder Bay is thought to be largely representative of the environmental conditions of the wider Marguerite Bay (e.g. Clarke et al., 2008, Venables and Meredith, 2014, Annet et al., 2015). Smale et al. (2007) studied the influence of ice scour intensity (high, low and intermediate respectively) on benthic communities at three sites (i.e. Hangar Cove, South Cove and Lagoon Island; **Fig. 1.4**). The authors found a reduction of 75.9 % in species richness in high intensity scoured communities and concluded that ice scour is the major structuring force on benthic communities at Ryder Bay. Survival of small taxa was determined by ice scour intensity and survival was highly conditioned by local physical conditions, disturbance size and frequency (Smale et al., 2007). Increased scouring is predicted to occur with future rising temperatures and the loss of sea-ice, since sea-ice buffers seabed against iceberg activity; this would potentially result in further loss of species richness and ecosystem stability (Barnes and Souster, 2011a; Barnes et al., 2014a). The use of concrete markers at either sides of Rothera Point (i.e. Hangar Cove and South Cove) showed reduced rates of iceberg scouring in the inner side of Rothera Point (i.e. South Cove) compared to the outer side of Rothera point (i.e. Hangar Cove; Brown et al., 2004).

Sediment in Ryder Bay varies depending on specific local conditions. Smale et al. (2007) reported that the substratum at Hangar Cove was primarily formed of soft sediment (68.0 ± 4.3 % fines), whilst at South Cove it was formed of semi-stable substrata (39.0 ± 5.9 % cobbles and 30.5 ± 2.8 % pebbles), with Lagoon Bay, Lagoon Island, as an intermediate case (58.5 ± 6.3 fines and 34.0 ± 5.4 pebbles) between the other two sites (see **Fig. 1.4** for specific site locations). Also further differences were found in the smaller particle size fractions; whereas Hangar Cove and Lagoon Bay were formed of very fine silt and sand, South Cove was formed of fine/medium sand (Smale et al., 2007).

Year-round environmental measurements have been taken by BAS since 1997 in the Rothera Oceanographic and Biological Time Series programme (RaTS; https://www.bas.ac.uk/project/rats/). The RaTS programme has allowed the generation of a comprehensive long-term environmental time series of: seawater temperature, salinity, chlorophyll, density, sea-ice (duration, concentration and type), macronutrients, dissolved organic carbon and photosynthetic active radiation; this programme is crucial for the assessment of long term changes in the WAP (Venables and Meredith, 2014a). The main RaTS sampling site is situated at the deepest point (approximately 520 m water depth) of Ryder Bay (67.570°S, 68.225°W); however, when the main site is not accessible a secondary site is used (67.581°S, 68.156°W), although this is situated in shallower water (approximately 300 m water depth). The RaTS programme aims to collect measurements twice weekly during the austral summer and as often as weather allows during the austral winter (Venables and Meredith, 2014). A detailed description of RaTS sampling methodology is given by Venables and Meredith (2014).

The hydrographic structure of Ryder Bay broadly coincides with that described above for Marguerite Bay. Annual temperature and salinity depth profiles are provided in **Fig. 1.5** (Clarke et al., 2008, Venables and Meredith, 2014, Annet et al., 2015). Locally, the main sea surface temperature (SST) peak (between 0.3 °C and 1.7 °C) occurs around January-February and sea-ice tends to start forming around April-July (Clarke et al., 2008a). Clarke et al. (2008) reported substantial interannual variability in the sea-ice cover in Ryder Bay, ranging from more than 200 days to just a few weeks. Furthermore, Venables and Meredith (2014) reported a positive feedback mechanism by which reduced sea-ice cover during the austral winter reduces stratification in the water column, which extends to the following summer season. This in turn allows increased warming which further reduces sea-ice formation in the following winter (Venables and Meredith, 2014). Generally, sea-ice is blown away from Ryder Bay rather than melting *in situ* by the action of northerly winds (Clarke et al., 2008). The structure of the water column, although ultimately controlled by salinity, temperature and sea-ice, is also linked to wider climatological forcings such as ENSO, with El Niño events causing deepening of the austral winter mixed layer depth (Meredith et al., 2004; Wallace, 2008 in Clarke et al., 2008). The phytoplankton activity in Ryder Bay exhibits the well-defined cycle for southern high latitudes, regularly reaching a maximum in chlorophyll concentration of 20-25 mg m^{-3} in December-January, often with a secondary peak around March (Clarke et al., 2008).

1.1.4 Signy Research Station, South Orkney Islands setting

The South Orkney Islands are situated between the Weddell Sea and the Scotia Sea on the South Scotia Ridge (**Fig. 1.3**) in the maritime Antarctic zone. The South Scotia Ridge area has a complex oceanographic regime as it is situated in the Weddell-Scotia Confluence between the Weddell Gyre and the ACC. The Weddell-Scotia Confluence is characterised by high chlorophyll concentration (Korb et al., 2004), thought to be due to advective supply of micronutrients from the Antarctic Peninsula and vertically mixed at the seamounts present in the region (Korb et al., 2005).

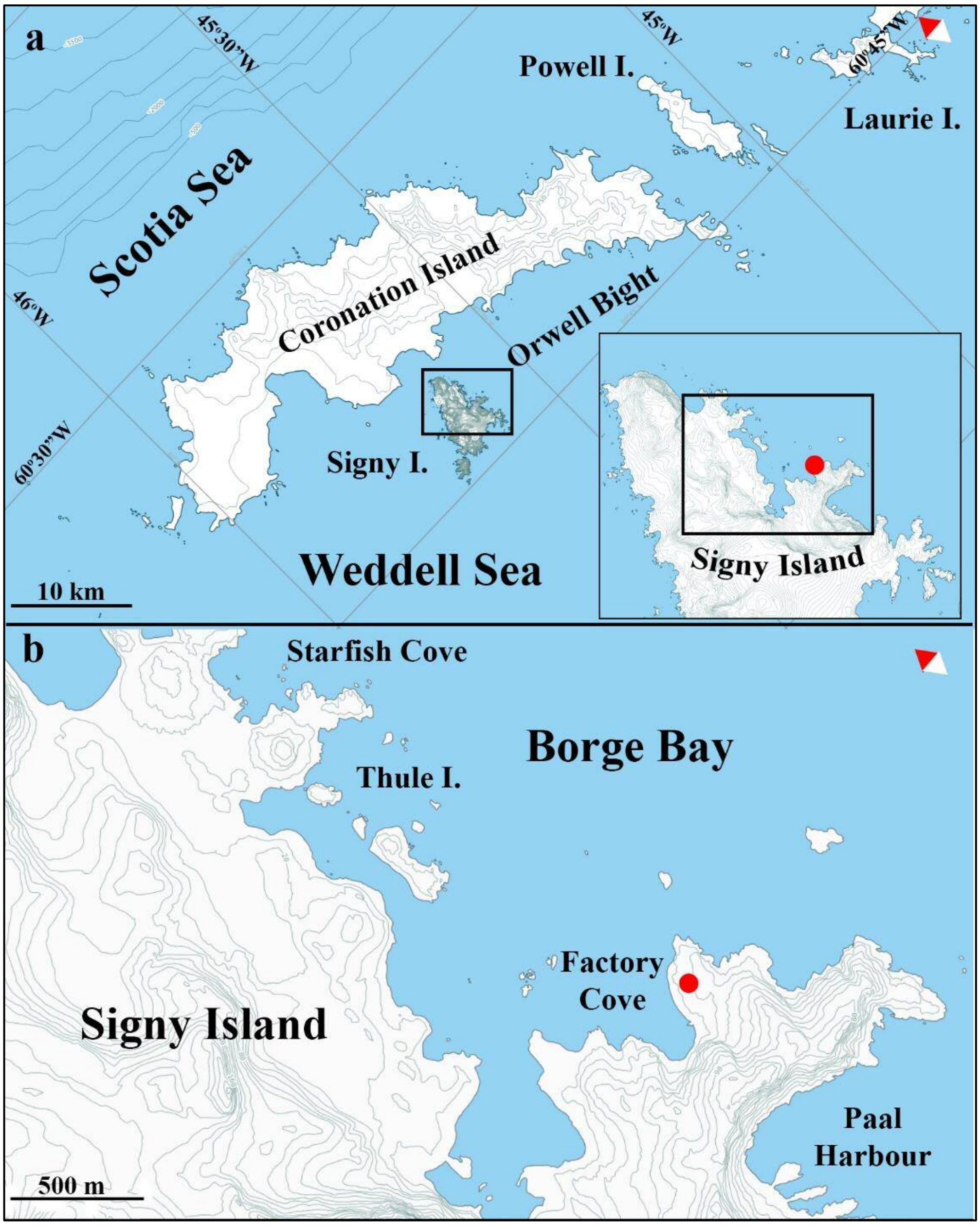

Fig. 1.6 a) Map of the South Orkney Islands and the position of Signy Research Station (red dot) and **b)** local map of Borge Bay in the east coast of Signy Island showing the position of Signy Research Station (red dot). Scale bars and a compass indicating north (red) are also included.

The archipelago of the South Orkney Islands is composed of: Coronation Island, Signy Island, Powell Island and Laurie Island (**Fig. 1.6**). Signy Research Station is situated in Factory Cove (60°43'S, 45°36'W), a small embayment of Borge Bay on the east coast of Signy Island. Borge Bay bathymetry ranges from 10 m to 30 m water depth and it opens directly to the Orwell Bight situated to the east from Signy Island (**Fig. 1.6**). Historically Signy Research Station has been operating as a meteorological station since 1947, being converted in 1963 into a year-round biological research facility until the mid-1990s when it switched to austral summer-only operations.

The paucity of *in situ* environmental records from the South Orkney Islands has limited the climatological and environmental understanding of this region. Year-round (e.g. Meredith et al., 2011) or long-term multi-year (e.g. Clarke, 1988; Clarke et al., 1988; Clarke and Leakey, 1996) studies are available although data are still limited, especially as Signy Research Station has been operational only during the summer season since 1995/96. An exception is the long-term instrumental record carried out at the Orcadas Base (60°44'25"S, 44°44'33"W), an Argentine research station, on Laurie Island (**Fig. 1.6**) situated approximately 46 km east from Signy Research Station. The Orcadas Base time series is the longest Antarctic observational *in situ* record (Zitto et al., 2015), with daily meteorological observations since April 1903. The Orcadas record comprises hourly values of atmospheric pressure and temperature, daily sea-surface temperature, relative humidity, wind speed and direction, sunshine duration and snowy days (Datos climatologicos y geomagneticos Islas Orcadas del Sur. Periodo 1903 - 1950, 1951).

The annual sea temperature pattern in Factory Cove is that the minimum temperature occurs in August and then starts to rise in September/October reaching its maximum in February (Clarke et al., 1988a). Average temperature ranges between -1.78 °C (August) and 0.14 °C (February) at Factory Cove and between -1.76 °C (August) and 0.31 °C (February) at Orwell Bight were reported for the period 1969/82 (**Fig. 1.6**; Clarke et al., 1988). Warming climate trends in the region have been determined to be around 1 °C from the mid-1950s to the early 2000s in air temperatures (Zazulie et al., 2010), which is the range of climate trends reported for the WAP (3.7 ± 1.6 °C century^{-1}; Vaughan et al., 2003).

Sea-ice formation and breakout dates from the South Orkney Islands are representative of the regional sea-ice concentrations in the northern Weddell Sea (Murphy et al., 2014). In addition, sea-ice formation and breakout in the South Orkney Islands are associated with larger climate variability (ENSO and SAM respectively) showing a preconditioning in sea-ice formation lagging 18 months (Murphy et al., 2014). Locally, there is little difference in the sea-ice annual pattern between Factory Cove and the wider Borge Bay (**Fig. 1.6**; Clarke et al., 1988). Normally fast-ice tends to form around the 1st of June (± 24 days SD) and remains in the bay until the 18th of October (± 37 days SD) with an average sea-ice duration between 141 days (± 57 days SD, 1969-83; Clarke et al., 1988) and 149 days (for the period 1957/72; White, 1977). Furthermore, the interannual variability in sea-ice duration is large, ranging between 59 sea-ice days in 1977 and 230 sea-ice days in 1973 (Clarke et al., 1988a). Murphy et al. (1995) reported a long-term non-linear decline in sea-ice duration of about 0.75 days year^{-1} between 1903 and 1995 using a combined record from Signy and Laurie Islands. The authors also reported a sub-decadal cycle of about seven to nine years in the fast-ice duration at Signy Island between the mid-1960s and 1990s which subsequently disappeared (Murphy et al., 1995a). This cyclicity was attributed to the precessional mode of the Antarctic Circumpolar Wave, a coupled ocean/atmosphere wave that circles the Southern Ocean in approximately eight years (White and Peterson, 1996), although its causes are not yet fully-understood (c.f. Connolley, 2002).

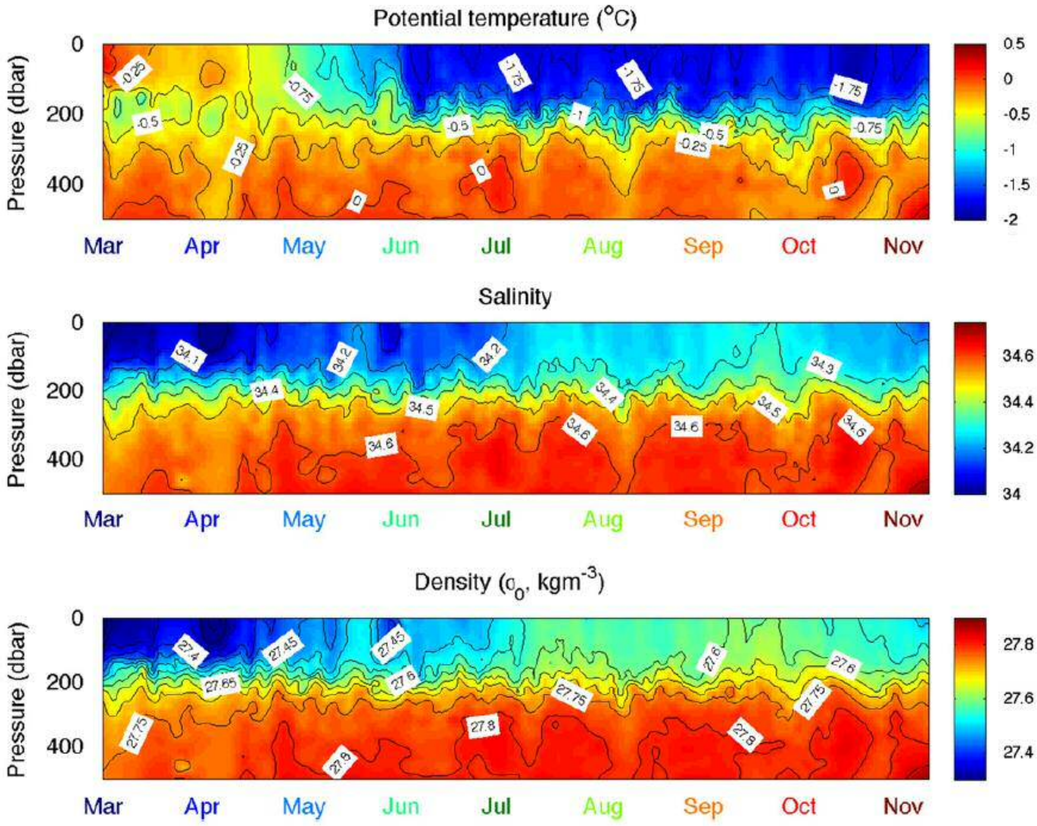

Fig. 1.7 Potential temperature, salinity and density profiles from the upper ocean near the South Orkney Islands recorded by a CTD Satellite-Relay Data Logger attached to a southern elephant seal in 2007 (from: Meredith et al., 2011).

The vertical structure of the water column near the South Orkney Islands is similar to the coastal regions in Antarctica. Meredith et al. (2011) reported summer (March) sea-surface temperature close to 0 °C (surface mixed layer) and the presence of a cold layer (-0.75 °C) approximately at 200 m water depth (Winter Water). Below the Winter Water lies a warm and saline water body (Warm Deep Water) which is derived from the CDW and modified through advection and mixing with shelf waters (Meredith et al., 2011). Gradually from mid-April until June, this structure breaks into a two-layer system formed by a cold surface layer, down to 200 m water depth, above the Warm

Deep Water. The seasonal change can also be observed in the salinity profiles with a less saline surface layer during the summer caused by sea-ice melting, which becomes more saline during the winter due to brine rejection during sea-ice formation (**Fig. 1.7**; Meredith et al., 2011)

The phytoplankton activity in Borge Bay reflects the intense seasonality in the region (Clarke et al., 1988a; Gilbert, 1991). The austral winter suspended chlorophyll levels remain very low, 0.23 mg Chl m^{-3} (July) on average and as low as < 0.001 mg Chl m^{-3} (August), until November when the bloom starts to develop (Clarke et al., 1988a). Microphytobenthic communities have been reported to be able to survive under the ice during winter and to account for most of the increase in sediment chlorophyll concentration, which indicates a low suspended chlorophyll sedimentation (Gilbert, 1991). Then phytoplankton activity rises rapidly during December and peaks in January, at 19.3 mg Chl m^{-3} on average (1972/79), with values as high as 50.9 mg Chl m^{-3} (January; Clarke et al., 1988). Subsequently the chlorophyll level declines rapidly until April when it falls below 1 mg Chl m^{-3} (Clarke et al., 1988). Inter-annual variability in the bloom duration is significant, ranging from 41 days (1981/82) to 170 days (1976/77; Clarke et al., 1988). Chlorophyll levels in Orwell Bight are consistently lower than those reported for Factory Cove although the seasonal pattern remains similar (Clarke et al., 1988). Macronutrients (phosphate, nitrate, nitrite, ammonia and silicate) in Factory Cove and Orwell Bight reflect the seasonal phytoplankton activity. Dissolved phosphate levels vary from 2.05 µmol kg^{-1} during winter (September-October) down to 1.2 µmol kg^{-1} during summer (January), whereas nitrate level varies from 28.7-30.7 µmol kg^{-1}during the winter (September-October) to 13.3-16.4 µmol kg^{-1} during the summer (January, Clarke et al., 1988). Nitrite is present at much lower concentrations and varies less throughout the year, ranging from 0.2-0.4 µmol kg^{-1} (Clarke et al., 1988).

The variability recorded at Orwell Bight and Factory Cove are likely due to differences in the sample water depth and distance to the coast between the stations with Orwell Bight at 10 m water depth and approximately 4 km offshore and Factory Cove collected at 6 m water depth (Clarke et al., 1988). In addition, coastal runoff from melting ice is likely to have a greater influence at Factory Cove than Orwell Bight. Seasonal changes in all environmental parameters take place earlier (i.e. early temperature rise, sea-ice formation, macronutrients recovery after bloom) in Factory Cove than at Orwell Bight (Clarke et al., 1988). This is likely due to the shallower bathymetry at Factory Cove when compared to Orwell Bight.

Comparisons between the instrumental records from Rothera Research Station and Signy Research Station must be undertaken with caution. The location of the South Orkney Islands between the Atlantic basin and the western edge of the Weddell Gyre presents a different oceanographic setting to that of Rothera Station and although there is a relatively short distance from the South Orkney Islands to the Antarctic Peninsula, a clear latitudinal gradient affects many of the environmental parameters along the Antarctic Peninsula (e.g. Martinson et al., 2008; Stammerjohn et al., 2008a). In addition, the shallower nature of the Signy Research Station sampling site (15 m of approximately 30 m total water depth) poses a difference when comparing the 15 m of approximately 520 m at Rothera Station (Clarke et al., 2008). Clarke et al. (2008) offer a further comparison between sites reporting a shorter summer season, based on SST data, and extended phytoplankton bloom for Rothera although phytoplankton blooms are stronger at Signy.

1.1.5 Climatic modes

SAM is an atmospheric annular mode in the Southern Hemisphere between 40°S (high pressure) and 70°S (low pressure) which involves synchronous atmospheric pressure anomalies of opposite sign. It is the main atmospheric mode of variability in the Southern Hemisphere (Talley et al., 2011; Turner and Marshall, 2011) and represents the variability (intensity and position) in the westerlies belt. Positive SAM anomalies are represented by positive atmospheric pressure anomalies at mid-latitudes and negative anomalies at high latitudes, resulting in the strengthening westerly winds around Antarctic, and *vice versa* for negative SAM anomalies (Thompson and Wallace, 2000; Marshall, 2007; Stammerjohn et al., 2008a). During the last half century SAM has shown a trend towards more positive values especially during austral summer months (Thompson and Wallace, 2000a). This trend towards a more positive SAM has been related to significant cooling over Antarctica, especially west of the Ross Sea (East Antarctica), and to significant warming over the Antarctic Peninsula and Amundsen-Bellingshausen Sea (Thompson and Wallace, 2000a; Thompson and Solomon, 2002a; Marshall and Connolley, 2006; Gillett et al., 2008; Massom and Stammerjohn, 2010a). The origin of this trend in the SAM has been traced to anthropogenic impacts on the atmosphere such as greenhouse gas emissions and depletion of tropospheric ozone (Sharon E. Stammerjohn et al., 2008). If the current trends in the SAM and greenhouse gas emissions continue, further declines in sea-ice, ice shelves and glaciers in the Amundsen-Bellingshausen sector are expected (Massom and Stammerjohn, 2010a; Vaughan et al., 2013). Alterations in sea-ice formation cycles and sea-ice seasonality are likely to have major impacts on the physical environment and on the biotope. Water column stratification, UV penetration, stability of pack-ice, atmosphere-ocean heat flux, gas exchange processes and iceberg scouring frequency are some of the characteristics that are likely to be impacted by alterations of sea-ice formation and seasonality (Smale and Barnes, 2008; Massom and Stammerjohn, 2010a; Barnes and Souster, 2011a; Venables et al., 2013; Constable et al., 2014).

ENSO is a subdecadal climatic cycle in the Pacific Basin (Turner and Marshall, 2011). ENSO is regulated by differences in atmospheric pressure between the west and east Pacific and is characterized by a cyclicity from three to seven years (Murphy et al., 2007; Talley et al., 2011). The ENSO-normal state is defined by strong easterly trade winds at the equator, high atmospheric pressure on the east and low atmospheric pressure on the west (associated with low [east] and high [west] precipitation), which results in a sea-level slope, rising on the west Pacific (Talley et al., 2011). Ocean balance processes due to this slope include: a) thermocline deepening in the west Pacific and shoaling in the east Pacific, b) cold upwelling processes along the equator and in the east Pacific generated by Ekman transport. The La Niña state represents an amplified form of ENSO-normal conditions where trade winds produce a further shift of warm water masses to the west, further deepening the thermocline (Talley et al., 2011). During an El Niño state a relaxation in trade winds decreases meridional transport to the west, and an ebb-flow current forms along the equator bringing warm water to the east (Talley et al., 2011). This shallow warm water blocks upwelling in the east Pacific with significant consequences for the regional ecosystems.

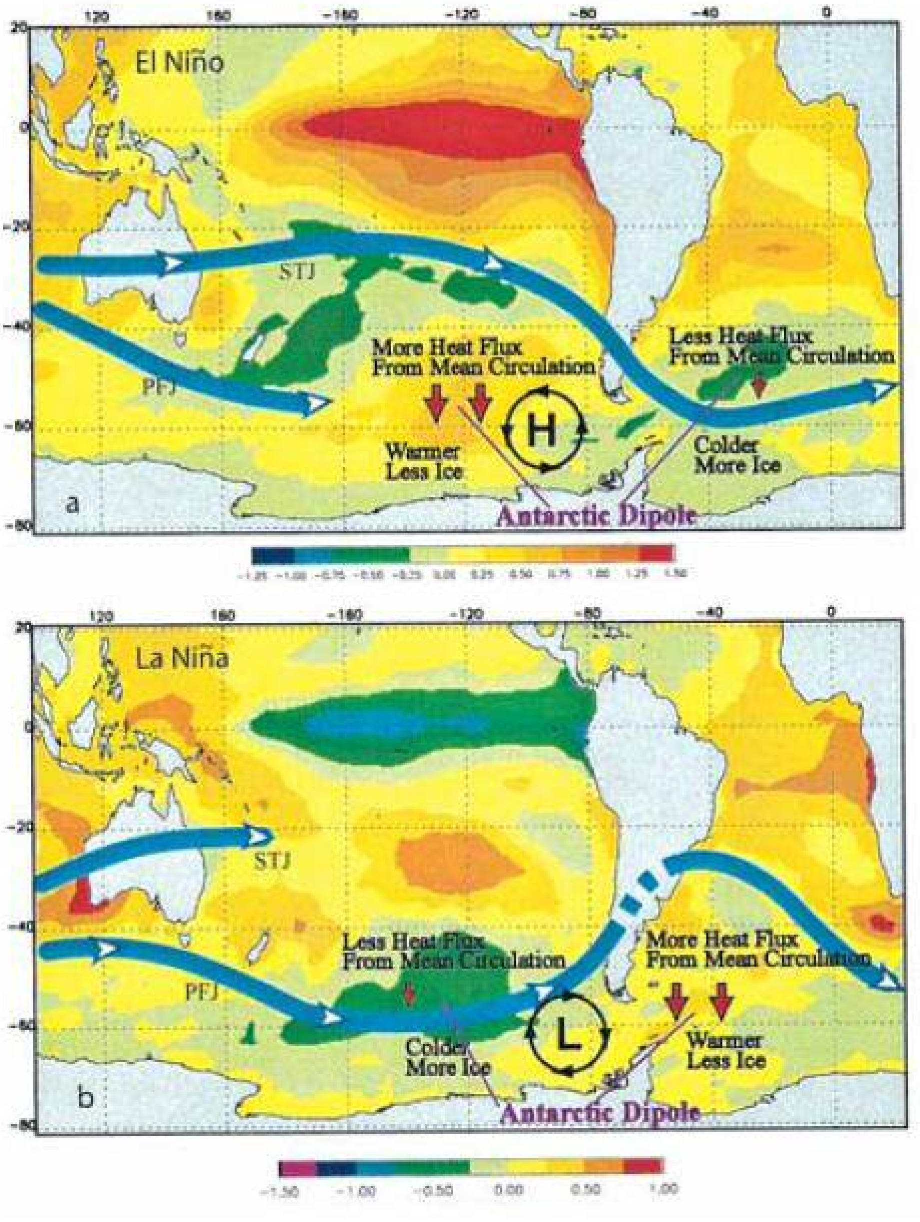

Fig. 1.8 Changes in the ADP modes in the SST anomaly composites (°C) **a)** during an El Niño event and **b)** during a La Niña event STJ: Subtropical jet, PFJ: Polar Front Jet, H: High pressure system and L: Low pressure system (from: Yuan, 2004).

ENSO propagates through from the subtropical western Pacific to the south Pacific and south Atlantic in a wave-like progression in the SST anomaly field (Murphy et al., 2007; Turner and Marshall, 2011). This ENSO teleconnection propagates to the Southern Ocean through a strong coupling with the Antarctic Dipole (ADP), and in that sense, the ADP represents the largest ENSO temperature anomaly outside of the tropical Pacific (**Fig. 1.8**; Yuan and Martinson, 2001; Yuan, 2004; Turner and Marshall, 2011). The ADP is a high latitude climate mode of variability in the air-sea-ice system characterised by its quasi-stationary nature and an out-of-phase relationship in sea-ice and surface temperature anomalies between the Pacific pole and the south Atlantic pole (Yuan, 2004; Yuan and Martinson, 2001). The ADP propagates strongly through the surface air temperature and sea-ice edge fields and moderately through the sea level pressure field (Yuan and Martinson, 2001). Yuan (2004) suggested that heat flux due to meridional circulation of the regional Ferrel Cell and regional anomalous circulation associated with stationary atmospheric heat eddies as mechanisms originating the ADP. These two mechanisms over the seasonal ice zone are in phase and possess a similar magnitude although the heat flux during a La Niña event is not characterised by a linear reversal from El Niño conditions (Yuan, 2004). In addition, the ADP is highly modulated by ENSO; during warm (cold) ENSO events, El Niño (La Niña), generates positive (negative) temperature anomalies and negative (positive) anomalies in the sea-ice field in the Pacific pole (Bellingshausen Sea) and the opposite response in the Atlantic pole (Weddell Sea; Yuan, 2004). These regional changes associated with the ADP and forced by ENSO activity can persist for three to four seasons after the original ENSO forcing has disappeared (Yuan, 2004). Such is the importance of these ENSO-originated atmospheric cycles at southern high latitudes that they modulate the strength of the Weddell Gyre (Martinson and Iannuzzi, 2003).

As explained above, ENSO is a complex natural phenomenon, therefore depending on the research focus and the specific geographical area of interest one or another ENSO climatic index, from several available, can be used to measure the ENSO state. The most used ENSO-related index is the Oceanic Niño Index (ONI; https://www.ncdc.noaa.gov/teleconnections/enso/indicators/sst.php) produced by NOAA. The ONI is the three month running mean of the Extended Reconstructed Sea Surface Temperature version 4 (ERSST.v4; https://www.ncdc.noaa.gov/data-access/marineocean-data/extended-reconstructed-sea-surface-temperature-ersst-v4) in the Niño 3.4 region (5°N-5°S, 120°-170°W) that surpasses a minimum of ± 0.5 °C for five successive months. Another ENSO-related index is the Multivariate ENSO index (MEI; https://www.esrl.noaa.gov/psd/enso/mei/) which is based on measurements, collected by NOAA since December 1949, of sea-level pressure, zonal and meridional components of the surface wind, SST, surface air temperature and total cloudiness fraction of the sky (Wolter and Timlin, 1993, 1998). The measurements are computed in sliding bimonthly seasons (e.g. December/January, January/February) and the resulting index assigns positive values to the El Niño phase and negative values to La Niña phase. For further detail, a full description of the computation of MEI is provided by NOAA at https://www.esrl.noaa.gov/psd/enso/mei/.

1.2 The Antarctic Aequiyoldia (*Aequiyoldia eightsii*, Jay 1839)

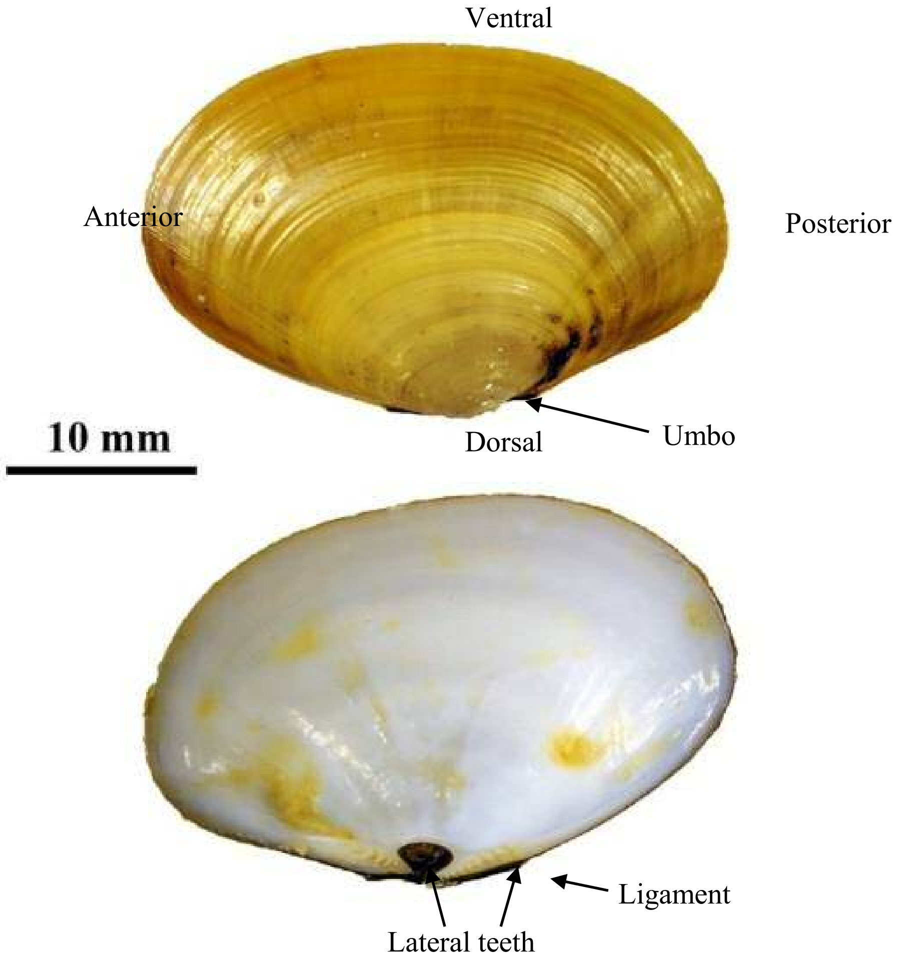

Fig. 1.9 Specimen of *A. eightsii* showing the dorsal and the exterior and the interior sides of a right valve. Periostracum is still attached on the exterior side of the valve and no deterioration is obvious at the umbo region (characteristic of young specimens). Lateral teeth and ligament can be observed on the interior side.

The Antarctic Aequiyoldia **(Fig. 1.9)**, *Aequiyoldia eightsii* (Jay 1839), previously known as *Yoldia eightsi* reviewed by André F. Sartori on 23/01/2016 and consulted at World Register of Marine Species http://www.marinespecies.org/aphia.php?p=taxdetails&id=868255, is one of the most abundant benthic species in Antarctic waters. Its distribution ranges from Tierra del Fuego (southern Argentina), Falkland Islands, and southern Chile to circumpolar waters (Nolan and Clarke, 1993). Although it has a pan-Antarctic distribution, local population distribution seems to be patchy (Dell, 1990) and very dense in some cases, with reported values up to 1,540 individuals m^{-2} in Factory Cove, Signy Island (Peck and Bullough, 1993). *Aequiyoldia eightsii* habitat ranges from 4 m to 824 m water depth, though it is most commonly found in the uppermost 100 m depth (Dell, 1990) and it usually inhabits the top 2-3 cm of the soft-sediment, being rarely found at greater depths even though adult individuals are known to possess the ability to dig deeper into the sediment (Davenport, 1988). Burrowing activity by *A. eightsii* happens in three phases: i) foot extension and penetration of the sediment, ii) rocking movements in the upright position and iii) shell anchorage (**Fig. 1.10**; Peck et al., 2004). *Aequiyoldia eightsii* is one of the most active burrowing bivalves in the Southern Ocean with a Burrowing Rate Index (BRI) of 8.8 - 49.8, although this is relatively low compared with temperate bivalves, BRI ranging between 3 and 2000 (Peck et al., 2004). The frequent burrowing activity by *A. eightsii* exert great damage to the shell around the umbo region; adult specimens show significant deterioration of the periostracum (i.e. organic layer covering the outer surface of the shell) and carbonate part of the shell near the umbo (**Fig. 1.9**).

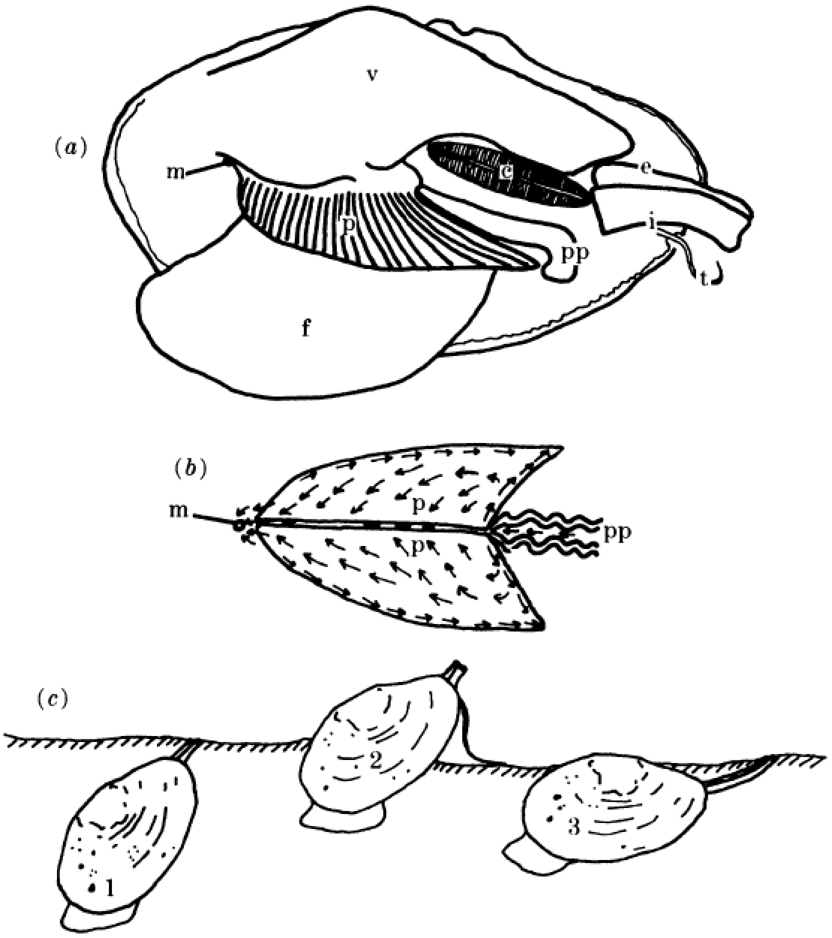

Fig. 1.10 (a) General anatomy of *A. eightsii*. c: ctenidium, e: exhalant siphon, f: foot, i: inhalant siphon, m: mouth, p: palp, pp: palp proboscis, t: sensory tentacle and v: visceral mass (b) View of parted apposed palp surfaces (p) and palp proboscis (pp) from ventral view. m: mouth. Arrows indicate the ciliary tracts (c) Burrowing behaviour of *A. eightsii*. 1: subsurface feeding (most common), 2: surface feeding (deposit feeding) and 3: subsurface feeding on a horizontal plane (common in large individuals; from: Davenport 1988).

As with other nuculanids, *A. eightsii* is a deposit/suspension feeder, being able to change its feeding behaviour according to the concentration of organic particulate matter in the surrounding waters (Davenport, 1988; Abele et al., 2001). This feeding behaviour allows the species to take advantage of the more nutritious seasonal blooms when filtering microplankton. For further information about the feeding anatomy and physiology of *A. eightsii* see (Davenport, 1988). Filter feeding is believed to happen all year round, though it is probably only profitable energetically during the austral summer when diatom blooms occur (Davenport, 1988). These environmental conditions consequently have a great impact on *A. eightsii* growth rates with high growth rates coinciding with the austral summer phytoplankton bloom. Nevertheless, *A. eightsii* growth is still slow compared to other similar species from lower latitudes (Rabarts, 1970; Davenport, 1989; Nolan and Clarke, 1993a; Peck et al., 2000a). Analysis undertaken by Nolan and Clarke (1993) identified clear increment series in the shells of *A. eightsii*. Although the increments were assumed to be deposited annually there was no independent assessment of this assumption. Peck and Bullough (1993) estimated the length of the growing season at Factory Cove, Signy Island as about five months, from mid-November to early April.

Estimates of the longevity of *A. eightsii* differ considerably depending on the analysis technique applied. Rabarts (1970) estimated its longevity as 19 years using external winter check marks on the shells. By contrast, Davenport (1989), Nolan and Clarke (1993) and Peck and Bullough (1993) estimated a much longer life span above 60 years, using mark-recapture (Davenport, 1989; Peck and Bullough, 1993a) and ^{45}Ca incorporation into the shell techniques to measure growth (Nolan and Clarke, 1993a). A more recent study estimated the longevity of *A. eightsii* at Factory Cove as more than 30 years using sclerochronology techniques (Roman-Gonzalez, 2011).

Peck and Bullough (1993) found that populations of *A. eightsii* are subject to density-dependent stresses which significantly affect recruitment. They described how high adult densities affect recruitment rates due to ingestion of the larvae and/or young individuals while adult individuals feed on the sediment. Smale et al. (2007) also reported that *A. eightsii* was notably abundant in the scoured communities at South Cove, Ryder Bay, which suggests the resilience of the population to ice scouring.

1.3 Sclerochronology

The term sclerochronology was defined by Jones (1983) as the counterpart of dendrochronology (i.e. the study of tree-rings), where it has its methodological origin (Jones, 1983; Cook et al., 1995; Mann and Lees, 1996; Cook and Peters, 1997; Esper et al., 2003), for the marine realm. Sclerochronological analysis involves the study of growth patterns in skeletal carbonate structures which can have different periodicities: tidal, daily, fortnightly and annual (e.g. Clark, 1968; Jones, 1983; Richardson, 2001; Schöne and Gillikin, 2013) and has been applied in a wide range of organisms: fish otoliths (e.g. Sturrock et al., 2015), corals (e.g. Hendy et al., 2003; Allison et al., 2010; Halfar et al., 2011; DeLong et al., 2013)), gastropods (e.g. Hollyman et al., 2014) and bivalves (e.g. Brey et al., 2011; Wanamaker et al., 2012; Brocas et al., 2013; Reynolds et al., 2013). Recent studies have shown how sclerochronological records can be applied to determine the role of ocean dynamics *vs.* atmospheric forcing in climate dynamics (Reynolds et al., 2016), as environmental recorders of the local physical hydrographic parameters (e.g. Bušelić et al., 2015; Mette et al., 2016; Peharda et al., 2016; Roman-Gonzalez et al., 2016) and as a proxy for large scale climatic processes (Wanamaker et al., 2012a; Reynolds et al., 2017a).

The use of growth patterns in sclerochronology requires that: the periodicity of the growth pattern can be determined, growth occurs synchronously within a population (reflecting environmental parameters driving growth), the growth pattern is formed continuously throughout the life of the organisms, the species has a significant longevity (in order to develop long records to analyse long-term environmental change) and the species has a wide distribution (in order to analyse spatial variability in the environment; Thompson and Jones, 1977). Some of the bivalve mollusc species that have been found to fulfil these criteria are: *Arctica islandica* (e.g. Wanamaker et al., 2012; Mette et al., 2016; Reynolds et al., 2016), *Cerastoderma edule* (Richardson et al., 1980; Milano et al., 2017), *Glycymeris bimaculata* (Bušelić et al., 2015a), *Glycymeris glycymeris* (e.g. Brocas et al., 2013; Reynolds et al., 2013), *Glycymeris pilosa* (Peharda et al., 2016), *Laternula elliptica* (Brey et al., 2011a) and *A. eightsii* (Roman-Gonzalez et al., 2016, 2017).

1.4 Rationale, aim and objectives

The lack of long-term instrumental records from Antarctica and the Southern Ocean has limited our understanding of long-term key feedbacks between the atmosphere, the ocean and the ice systems. The use of sclerochronology can provide long-term and absolutely-dated records for the marine environment that can be extended beyond the instrumental record; using the instrumental records from the most modern period for calibration purposes. Therefore it is crucial to understand the variability of local environmental parameters and the drivers of such variability (local or forced via teleconnections) as some of these parameters will be the main drivers of shell growth and will influence shell geochemical composition. Currently sclerochronological studies from the Southern Ocean are limited (Brey et al., 2008; Lartaud et al. 2010; Ivany et al., 2011; Roman-Gonzalez, 2011), especially those analysing the geochemical composition of the shells of modern collected bivalves (Brey and Mackensen, 1997, Trevisiol et al., 2013). The Southern Ocean has presented very stable temperatures for several million years (Zachos, 2001), which has resulted in very stenothermal evolutionary adaptations making many Antarctic species very sensitive to global warming (Peck, 2005; Peck et al., 2006; Clarke et al., 2007). The Southern Ocean ecosystems are likely to be severely affected if current climatic trends continue, especially benthic communities which are highly dependent on sea-ice dynamics (Barnes and Peck, 2008; Smale and Barnes, 2008; Constable et al., 2014). Understanding the effects of present and past climatic variability in benthic ecosystems will be key to assess the vulnerability of such ecosystems in the future.

The aim of this project is extend the work and knowledge of the use of *A. eightsii* as a sclerochronological proxy, based on a pilot study (Roman-Gonzalez, 2011), for Antarctic shallow coastal waters and constrain the onset of intense regional warming occurring in the WAP by the use of sclerochronology.

The project presents several objectives: determine the main environmental drivers of shell growth, determine ontogenetic shell growth pattern in *A. eightsii*, produce robust chronology(ies) from newly collected specimens from Rothera Research Station and explore historical museum collections, extend the existing chronology from the South Orkney Islands, develop stable oxygen and carbon isotope (i.e. $\delta^{18}O_{shell}$ $\delta^{13}C_{shell}$) records and study the relationship with them and environmental parameters (i.e. seawater temperature, salinity, chlorophyll concentration), investigate the relationship between seawater $\delta^{18}O$ ($\delta^{18}O_{water}$) and $\delta^{18}O_{shell}$ so the later can be used as a temperature/salinity proxy, study lateral fractionation in the stable isotope depending on the position of sampling (i.e. anterior, ventral, posterior) and investigate possible teleconnections between shell growth and climatic modes such as ENSO and SAM.

Chapter II: Materials and Methods

This chapter will cover the methodology used for sample collection, processing and analysis. Geolocation, time and depth of the sample collection are indicated as well as number of samples collected per location and for each fieldwork season. A description of the techniques used for the making of acetate peel replicas and the posterior imaging of the samples are given. A detailed account is provided of how growth increments in *A. eightsii* are measured and how these growth histories are compared between specimens in order to construct master chronologies. Special attention is given to the analysis of *A. eightsii* growth patterns and several statistical techniques applied to detrend those patterns associated with pure biological causes to those patterns environmentally driven. Data handling of the different instrumental records used is also described. Lastly the techniques used for the collection of shell powder samples for stable isotope analysis (i.e. oxygen and carbon) for three different experiments are also provided.

2.1 Site selection and description

As reviewed in detail in the introduction the West Antarctic Peninsula (WAP) has become an increasingly important location for climate research due to the recent and rapid warming trends in the region. Site selection was conditioned by logistical support (e.g. British Antarctic Survey, BAS, divers have to work within 45 min from a decompression chamber), availability of long term instrumental series (e.g. Rothera Biological Time Series) and knowledge of living *A. eightsii* populations. Taking advantage of the infrastructure of the BAS samples were collected from different shallow marine localities surrounding Rothera Research Station (67°34′S 68°08′W). Rothera Research Station is situated at Rothera Point on the South-East coast of Adelaide Island on the Loubet Coast (**Fig. 1.4** and **Fig. 2.1**). Ryder Bay (RB) is located west of Rothera Research Station and is approximately 11 km wide and presents several islands in its mouth: Leonie Isl., Limpet Isl., Lagoon Isl., Donnelly Isl. and Anchorage Isl. (**Fig. 1.4**). In addition, four glaciers flowing into RB: Sheldon (67°30′S, 68°23′W), Horton (67°33′S, 68°30′W), Hurley (67°34′S, 68°32′W) and Turner (67°37′S, 68°29′W; **Fig. 1.4**).

Health and safety regulations from BAS estipulate that for the scuba divers can only work from a range within 45 min reach of a decompression chamber (available at Rothera Research Station), therefore sampling locations had to be chosen accordingly. The sampling locations near Rothera Research Station are the following: Hangar Cove (HC, 67°33′S, 68°7′W), South Cove (SC, 67°34′S, 68°8′W), Trolval (T, 67°35′S, 68°12′W) and Back Bay (BB, 67°35′S, 68°15′W; **Fig. 2.1b**). The selection of these sites allows the especial comparison within Ryder Bay (T, SC and BB) and a comparison with the outer Ryder Bay location (i.e. HC). In addition, the micro-local conditions present at each site allow independent interpretation of the environmental data available.

The second study location is situated in the South Orkney Islands, at Signy Island (**Fig. 1.6** and **Fig. 2.1**). Signy Station, situated on the east coast of Signy Island, served as the main BAS research station from 1947 to 1996. Borge Bay is the main coastal embayment in the Signy Station region although many of the previous environmental and ecological studies carried out at Signy Station were located at Factory Cove, a shallow embayment adjacent to Signy Station (**Fig. 1.6** and **Fig. 2.1c**).

The comparison of these two regions also allows a latitudinal comparison (e.g. climatological trends) of the results as well as a comparison in the context of the regional oceanographic context.

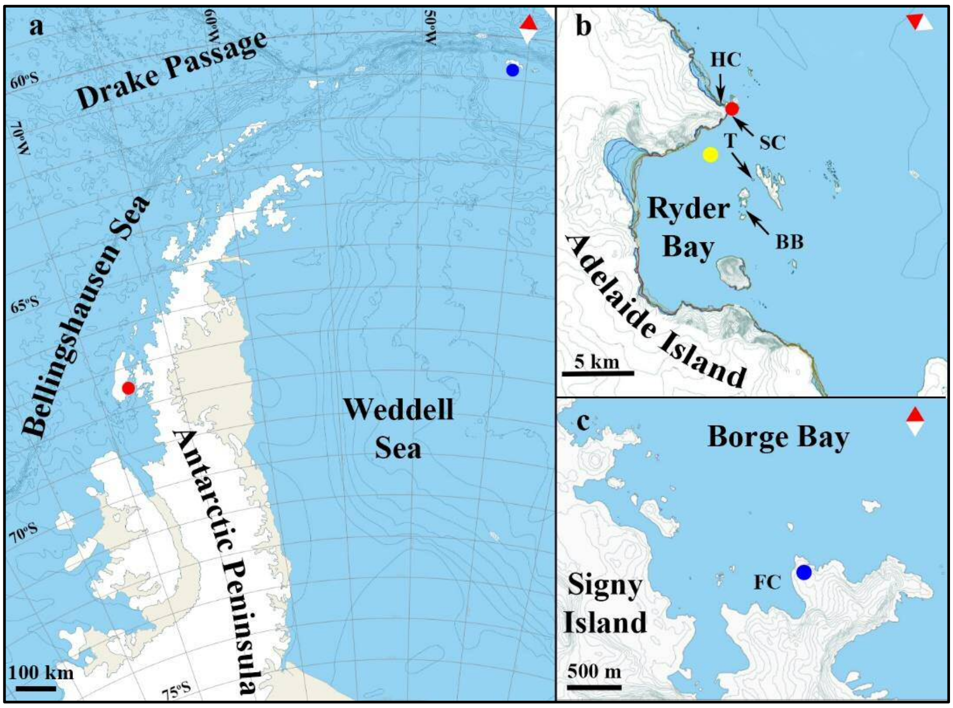

Fig. 2.1 a) Map showing the Antarctic Peninsula. The position of Rothera Research Station (red dot) and Signy Station (South Orkney Islands; blue dot) **b)** Map of Ryder Bay showing the sampling locations: Hangar Cove (HC), South Cove (SC), Trolval (T) and Back Bay (BB). Red dot indicates the position of Rothera Research Station, yellow dot indicates the position of the RaTS sampling station **c)** Map of Borge Bay and Factory Cove (FC) showing the location of Signy Station (blue dot). Scale bars and compass indicating north (red) are also included.

2.2 Sample collection and curation

Sample collection from Rothera Research Station was carried out during two austral summer seasons: 2013/14 and 2014/15. During the 2013/14 season a total of 50 specimens were live-collected at Trolval from around 25-30 m water depth, and 122 live-collected specimens from Hangar Cove (50 specimens from a shallow depth approximately of 15 m water depth and 72 specimens from a deeper site around 25-30 m water depth; **Fig. 2.1b**). The 2014/15 season provided a total of 57 live-collected and seven dead-collected specimens from South Cove from approximately of 15 m water depth, 19 live-collected and 18 dead-collected specimens from Hangar Cove from approximately of 15 m water depth and 58 live-collected specimens from Back Bay from approximately of 11 m water depth (**Fig. 2.1b**).

Samples were either hand-collected by BAS scuba divers and by the use of manually-operated suctions pumps. Large specimens were specifically targeted in order to maximise the chance of obtaining long-lived specimens.

Aequiyoldia eightsii samples from the South Orkney Islands live-collected in 1988 from Factory Cove (**Fig. 2.1c**) from around 8 m water depth by the BAS were already available and curated at Bangor University. This collection was composed of a total of 174 live-collected specimens (21 specimens collected in March, 112 specimens collected in April, 10 specimens collected in August and 31 specimens collected in November). Additional *A. eightsii* specimens from the South Orkney Islands were obtained from the Natural History Museum in London, hereafter NHM collection. NHM collection consists of a total of 29 specimens that were live-collected in 1915 from 9 to 11 m water depth (A. Bennett collection, hereafter referred as AB1915) and three valves from live-collected specimens in 1927 by the *Discovery* expedition from 320 m water depth. Two deep-collected specimens were preserved in ethanol with the soft tissues still attached to the shell whereas the other specimen was dry-preserved with no soft tissues present. The flesh was carefully removed from the two specimens in order to preserve the soft tissues in the preservative and one valve of each specimen was extracted.

2.3 Laboratory processing

2.3.1 Shell material

Live collected specimens were sacrificed by placing them in a freezer at -20 °C; this procedure was carried out at Rothera Research Station by Prof. Lloyd Peck (BAS). Subsequently the samples were shipped to the UK for further analysis, being kept frozen until arrival at the School of Ocean Sciences at Bangor University. After arrival, the samples were defrosted and weighed (shell and soft tissues) to the nearest 0.1 g using an Adventurer OHAUS® analytical balance. The specimens were subsequently defleshed using a scalpel by carefully inserting the tip of the blade into the posterior part and sectioning the adductor muscles joining the valves; having especial care to remove the small portions of the adductor muscle and other soft tissues that remained attached to the shell. The soft tissues and shell material were catalogued with a cross-referenced ID code. An example of the ID codes for the WAP specimen is 21502001, the first three digits (215) indicate the year of collection (2015), the next two digits (02) indicate the sampling location and the last three digits (001) indicate a specific specimen. An example ID codes for the South Orkney Islands specimen is 8804087, 88 refers to the year of collection (1988), 04 refer to the month of collection (April) and 087 is the specimen number. In the case of the NHM collection, since the specimen codes are as follow: 191501001, 1915 refers to the year of collection, 01 (02) refers to shallow-collected (deep-collected) at Signy and 001 is indicates a specific specimen. Immediately after the soft tissues were weighed (hereafter soft wet weight) to the nearest 0.1 g and frozen at -80 °C. The remaining flesh was cleaned from the shell material, which was then washed and air-dried.

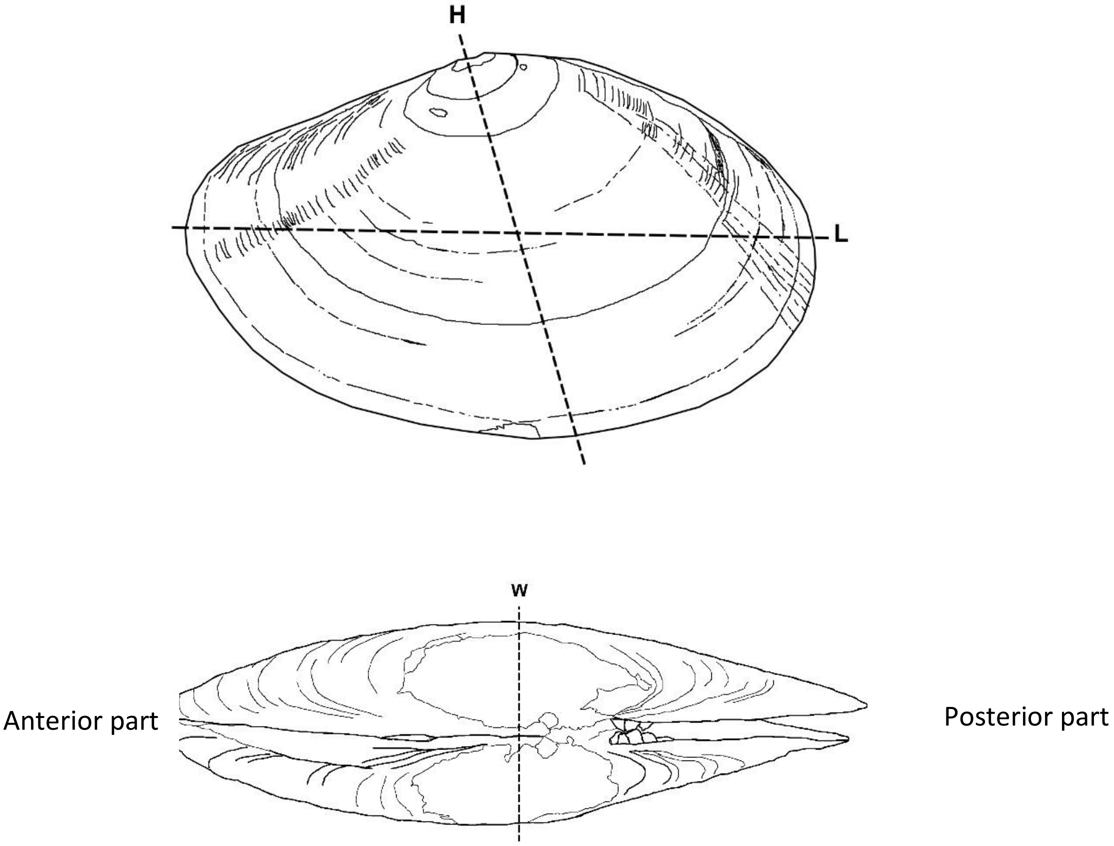

Fig. 2.2 Diagrams of an *A.eightsii* shell showing the three biometrical measurements: height (H), length (L) and width (W).

Once dried, the length, width, height (**Fig. 2.2**) and mass of the shell material were measured using a digital calliper to the nearest 0.1 mm and recorded in a logbook. In addition, other parameters such as periostracum condition (i.e. % preservation) and shell condition (i.e. ligament condition, % of bioerosion, shell margin preservation) were recorded. A numerical index ranging from one to four was used to mark these parameters. Information in the logbook was subsequently digitized and compiled into a master Excel spread sheet.

Subsequently a total of 20 left valves were selected, from each sampling location, for further processing based on length values (longest valves) and shell condition (minimum bioerosion, high periostracum preservation, no chipping present at the shell margin). The valves were selected according to shell length (larger valves were prioritized) and shell condition (if a large shell was significantly damaged, erosion present on more than 20 % of its surface or presented major breaks, it was not selected). The selected left valves were embedded in MetPrep Kleer polyester resin. MetPrep Kleer polyester resin is a bicomponent resin with a setting process that is thermoactive around 60-80 °C and takes about 8-12 h to set completely. First, valves were filled with resin to avoid the formation of bubbles on the interior side. The resin-filled valves were left overnight to set and embedded completely the next day in two stages with a printed ID code inside the resin block; again these were left overnight to allow the resin to set.

2.3.2 Sectioning and Polishing

Resin blocks with the embedded valves were initially trimmed in order to remove the resin excess using a wafering blade saw. Then a line was drawn with a permanent marker pen along the maximum growth axis drawn with a marker pen on the resin block in order to help guide the precision cutting.

Precision cutting was carried out using a Buehler IsoMet 5000 saw. The reference cutting lines were aligned parallel to the saw and the blade was positioned next to the reference line so the umbo region would not be lost during the cutting. Valves were cut at 3200 rpm and a feeding rate of 16 mm sec^{-1}. Once a block was cut, the two halves were removed from the saw and another block was fitted for cutting. The water tank of the precision saw had to be changed every ten cuts due to the increasing amount of resin residue building up in the water.

After sectioning, one half block of each specimen was selected by visual analysis of the block and the shell; parameters such as position of the cutting transect and shell condition were the most important considerations. Half blocks with the cutting transect coinciding with the maximum growth axis were selected versus half blocks with an offset cutting transect (this was due to the removed part of the shell during cutting). Also the shell condition was assessed by looking for significant amounts of bioerosion in the shell and for shell fractures due to cutting. If any air bubbles were present in the resin near the specimen (usually this occurring in the inner side of the shell) they were filled with a drop of resin and left to harden before continuing with the sample processing. This step is important as the ethyl acetate, used in the following steps, can accumulate in the air pockets, affecting the quality of the acetate peel replica. The corners of the resin block were sanded down using a P120 carborundum grinding pad to prevent damage of the more delicate grinding pads. The exposed surface of the shell was then ground down using progressively finer carborundum grinding pads (P400, P1200, P2500, P4000) attached to an automated rotatory table with tap water as lubricant. Between P2500 and P4000 grinding pads the exposed surface was gently dried with a paper cloth and the specimen was visually checked for the presence of significant scratches. This is important as sometimes tiny resin shards/grains can stick to a grinding pad and significantly scratch a well-polished resin surface. If any significant scratch was present the surface was polished again using the P1200 grinding pad. Following grinding, the exposed shell surfaces were polished using Presi Mecaprex GH diamond paste (grain size of approximately 3 μm in diameter) diluted in Presi Mecaprex GH lubricant on a Presi Mecapol P230 polishing table at 250 rpm for two minutes. Finally, polished blocks were washed with lukewarm tap water and soap to remove the oily lubricant.

2.3.3 Etching and peel replica preparation

The polished exposed surfaces were then photographed using a Lumenera Infinity3 colour camera attached to a Meiji MT8100 microscope under x5 magnification using Image Pro software package. Due to the thickness of the resin block, transmitted light was not a feasible option and reflective light was applied using an Olympus Highlight 3001 light source. Lighting of the samples was set in order to create maximum contrast between the sample and the resin.

After photographing the polished shell surface, the specimens were brought back to the laboratory for etching and to produce the acetate peel replicas. Etching in other bivalve species (e.g. *Glycymeris glycymeris, Arctica islandica*) is standardized to two minutes in 0.1 M HCl (c.f. Scourse et al., 2006). In the case of *A. eightsii*, due to its fragile nature, etching was carried out for between 20-30 min in 0.01 M HCl depending on the specimen. Immediately after etching the blocks were submerged in tap water in order to prevent the acid dissolving the specimen any further. Blocks were then left to air dry; once dry a thin layer of ethyl acetate was pipetted on the exposed etched shell surface and a 35 µm thick acetate sheet (G255 replication material Agar Scientific) was rolled over the block with the ethyl acetate. This favours the attachment of the acetate sheet to the specimen as well as causing the excess of ethyl acetate to overflow. Specimens were subsequently left to air dry between one and two hours. Once dry, the acetate peel replicas were carefully removed, trimmed and mounted on a microscope slide. Two glass slides instead of one glass slide plus cover slide proved to be more useful due to the curly nature of the acetate peel replica. Acetate peel replicas were labelled (ID code, species name and date were annotated) and stored in microscope sample boxes. All specimens (i.e. resin blocks and acetate peel replicas) are stored to date (11/01/2018) at Penryn Campus, University of Exeter.

2.3.4 Imaging

Images of the acetate peel replicas were taken using a Meiji MT8100 microscope under x5 magnification lens with a Lumenera Infinity3 colour camera. Transmitted light was used for acetate peel replicas and reflected light for polished resin blocks.

Images were adjusted for brightness and contrast and stitched together using Image Pro Premier 9.1 in order to produce a composite picture of the polished shell and of the acetate peel replica. Composite pictures of both the acetate peel replica and the polished block were then exported to Adobe Photoshop CS6 and were overlapped in order to provide a quick comparison for increment assessment between the polished shell and the peel replica. Primary and secondary increment lines were highlighted in Adobe Photoshop for both composite images. Increment identification in *A. eightsii* proved to be challenging in either within a specimen life history and between specimens. A general definition of an *A. eightsii* increment width is the distance between two consecutive annual increment lines. Shell growth increments in *A. eightsii* generally consist of a lower part and a darker part near the increment line (**Fig. 2.3**). In addition, secondary lines are frequently present adjacent to the annually-formed lines. Primary annually-formed growth lines can be identified from disturbance lines in that: i) annual growth lines are always located at a dark-coloured part of the shell, ii) annual growth lines are clear and do not become faint when followed to the interphase between the outer and the inner shell layers and iii) annual growth lines often present a small indentation in the inner side of the periostracum. On the other hand, disturbance lines tend to present a fainter colouration and definition (they disappear when followed towards the boundary between the outer and the inner shell layers) and they tend to be associated with shell damage (e.g. shell deformation, intrusions, breaks).

Some exploratory scanning electron microscope (SEM) images were taken using a Thermo Scientific™ Quanta™ FEG 250 SEM located in University of Exeter, Penryn campus, in order to explore differences in the crystallography of *A. eightsii* shell (i.e. intra increment and inter shell layer differences). Two samples were randomly selected, specimen 21403048 had been already embedded in resin, polished and etched for an acetate peel production and specimen 21504053 was just a snapped shell with no additional treatment. Both samples were carbon coated prior to being imaged. A range of voltage between 3 KV and 15 KV was used for taking the images. The SEM images were compared with the images of the polished shell in order to accurately identify the position of the growth lines.

2.3.5 Measuring

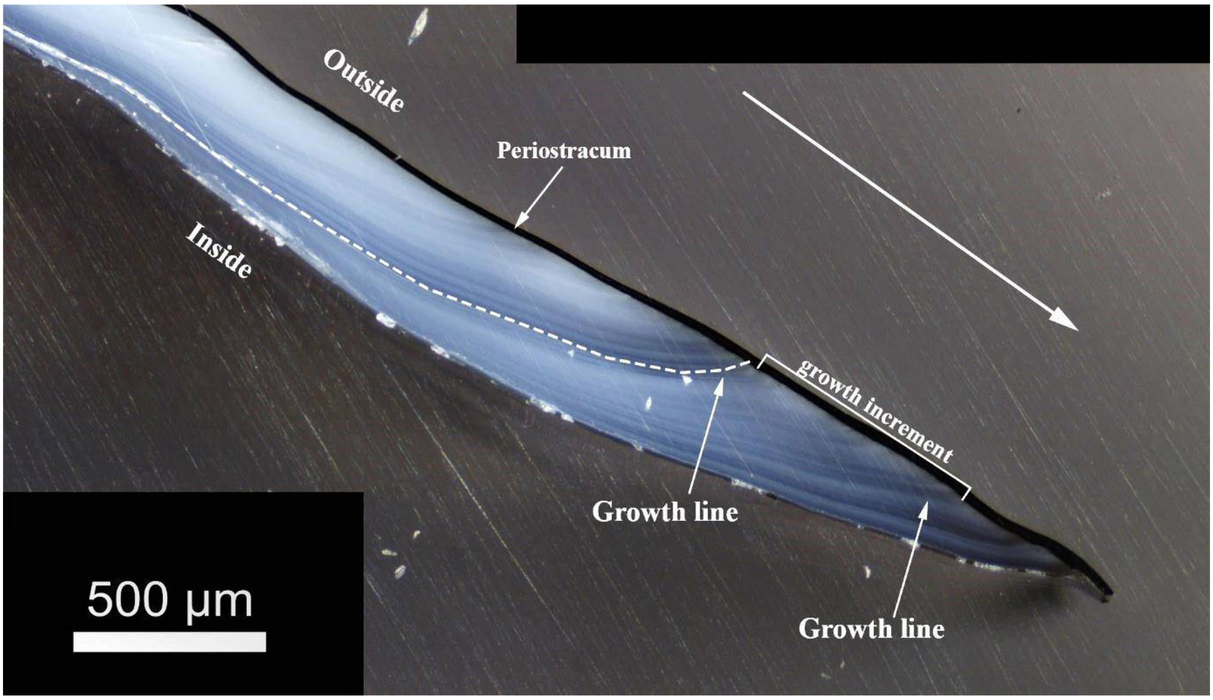
[redacted]

Fig. 2.3 Microphotograph of a polished section of an *A. eightsii* shell, embedded in a resin block, showing growth increments, growth lines and the different colouration within the shell, meaning light blue after the growth line is formed and dark blue adjacent to the growth line. The arrow indicates the direction of growth.

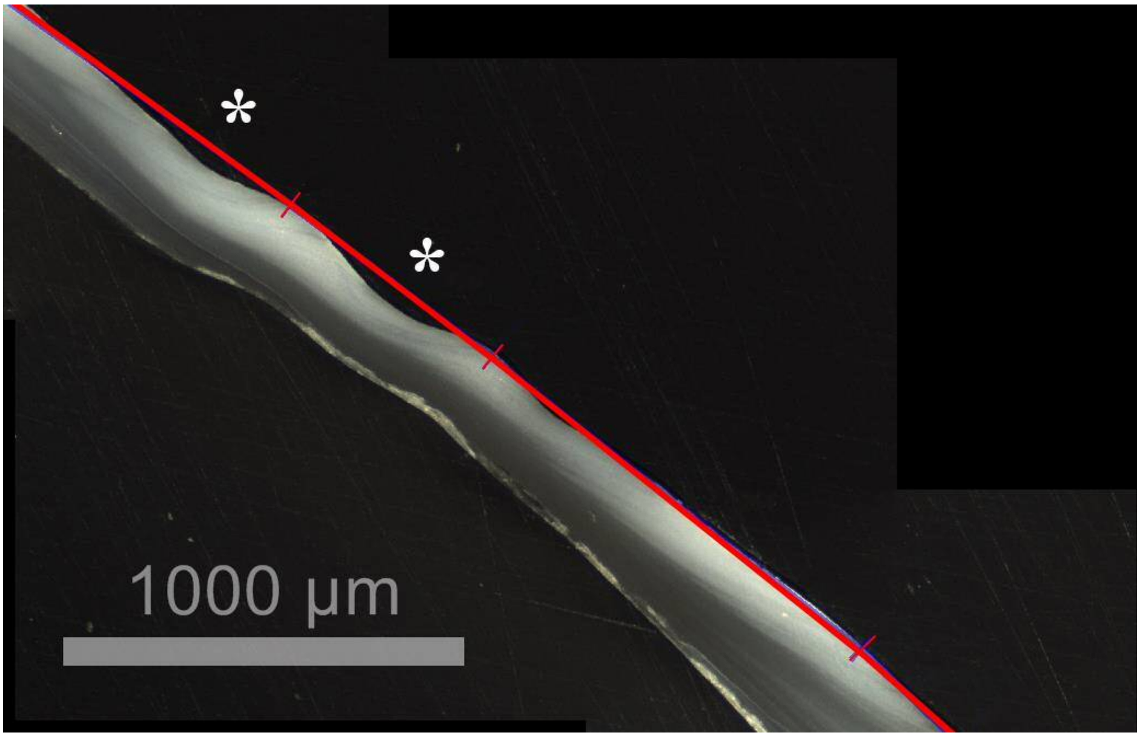

Fig. 2.4 Microphotograph of a polished section of *A. eightsii* showing deformations of the shell (i.e. troughs and ridges) and how the increments were measured avoiding introducing bias due to the deformations (*). The red lines indicate the measured increments.

Prior to measuring, the common growth pattern of each sampling location was determined by visual analysis of the composite pictures. The traditional approach to find the common growth pattern is to analyse particular good or bad years of growth in the life of the specimen and use them as "marker" years, then identify similar temporal sequences in growth increment series in other specimens. If the specimens are live-collected the last increment is dated as the year of collection and the rest of the increments are back dated (i.e. crossdating). On the other hand, when a specimen is dead-collected crossmatching techniques (discussed in detail in the following section) play a major role in constraining the timing of the growth series. Increment width was measured in Image Pro Premier 9.1; the composite comparison carried out in Adobe Photoshop between the resin block and the acetate peel replica was used to aid in the identification of the growth increments. It was decided to standardize increment measurement to the length between the first primary lines of two consecutive dark increment sections (**Fig. 2.3**). Increments were measure alongside the interface between the periostracum and the calcareous part of the shell. Where a shell abnormality was present, this was ignored and the general shape of the valve was followed in order to avoid introducing bias in the increment measurements (**Fig. 2.4**). Measurement records were then exported into a master Excel logbook for further statistical analysis.

2.4 Investigation of shell growth

The relationships between shell length, width, height and mass were analysed and linear regressions were applied to the data. In addition growth curves (i.e. accumulative growth) were calculated by carrying out a cumulative sum of the increment width series. Averages for the different sampling locations of the individual growth curves were calculated to check for differences in growth rates between the different populations.

One crucial aspect of the chronology development is the understanding of shell growth and the possible ontogenetic trends in the growth increment time series. The removal of the variability in the time series associated with biological growth whilst retaining the low-frequency variability associated with climatic trends is the key goal of detrending. This is important as ontogenetic trends have a significant effect on the growth pattern of living creatures and have the potential to bias the correlation between specimens and mask any underlying environmental signal (Cook et al., 1980; Cook and Peters, 1981; Cook, 1985; Briffa et al., 1996; Butler et al., 2010). In bivalve molluscs a high rate of growth (i.e. wide increments) is present during the early years of life which then reaches an asymptote as the individuals grow older (Seed, 1980). Several methods can be used to remove this characteristic ontogenetic trend of mollusc bivalves. One commonly used detrending method is the use of the modified negative exponential (NE) curve suggested by Cook et al. (1990) which models a rapid growth during the first years of life and becomes progressively reduced with increasing age. A slight variation of NE detrending is the use of a negative exponential -30 function (NE-30) in which the first 30 years are removed (Butler et al., 2010), which equates some long-lived bivalves (e.g. *A. islandica*, *G. glycymeris*) for the main portion of the strong ontogenetic trend during rapid early years of growth (Butler et al., 2010; Brocas et al., 2013).

An alternative to NE detrending is the use of smoothing spline functions with different flexibility. Smoothing spline functions make *a priori* no assumption about the shape of the fitted curve and apply a centrally weighted moving average (Cook and Peters, 1981). The cut-off point, which normally describes 50 % of the variance, are set *a priori* and acts then as a high-pass filter in removing frequencies below the cut-off point from the curve to be standardized (Cook and Peters, 1981). The use of smoothing splines should be considered when NE detrending curves provide a poor fit to the curve to be standardized (Cook and Peters, 1981). Butler et al., 2010 used cubic smoothing splines with a flexible 30 year cut-off point (Sp30) and a stiffer (set to 67 % of the mean length of the studied time series) 88 year cut-off point (Sp88) in analysing the effect of detrending techniques upon chronology construction based on the marine bivalve *A. islandica*. The flexible Sp30 was found to be more suitable than the stiffer Sp88 for removing the ontogenetic variability during the early years of rapid growth of *A. islandica* although it was unable to retain low-frequency variability in the mature part of the curve (Butler et al., 2010). The use of any specific cut-off point has to be considered on a case-by-case basis (Wanamaker et al., 2012; Brocas et al., 2013; Schöne, 2013).

A comparison between two established detrending methods: regional curve standardization (RCS) and NE was carried out using 47 *A. eightsii* specimens collected in 1988 from Factory Cove, Signy Island.

The RCS method is an alternative for the preservation of low-frequency variability (Mitchell, 1967; Briffa et al., 1992, 1996; Esper et al., 2003, 2009). The RCS methods relies on greater sample depth (i.e. number of growth increment series added to a chronology) and correct identification of the first annual increment formed (Esper et al., 2003). The growth increment series for each specimen of each species are aligned ontogenetically and averaged for each ontogenetic year. This averaged ontogenetic growth curve is conventionally termed the regional curve (Briffa et al., 1992; Cook et al., 1995; Esper et al., 2003, 2009). The principle is that the regional curve (RC) describes the ontogenetic trend for a specific species in a specific location and assumes that this is relatively constant throughout time (Esper et al., 2003). Departures from the RC curve are therefore interpreted as non-biological, i.e. climatic or otherwise, and can be calculated as ratios or residuals to produce a RCS-chronology (Briffa et al., 1996; Cook and Peters, 1997). A potential source of error in the RCS technique is the misalignment of the series during the first years of growth due to missing increments, termed pith offset (Briffa et al., 1992; Cook et al., 1995; Esper et al., 2009). This means that either the number of missing increments needs to be estimated based on the size of the shell, the portion of the umbo eroded and the shape growth increment pattern or alternatively it must be assumed that there is no pith offset and that the first measured growth increment is also the first ontogenetic increment. This second option is reasonable where the analysed specimens present similar biometric characteristics and a similar degree of preservation (see subsection 2.3.1); as this was the case in all selected samples no correction for pith offset was carried out. If pith offsets of the individual growth increment series are evenly distributed the overall effect on the RC is small when compared to the RCS-chronology calculation methods (Esper et al., 2003). This may result in the RCS indices to be somewhat biased although potential effects on chronologies will be limited once the series are aligned by calendar date instead of ontogenetic age (Cook et al. 1995; Esper et al. 2009) during the chronology construction. Nonetheless, in order to provide a possible estimation of the error due to the lack of pith offset correction, the standard deviation and standard error of the original uncorrected series and a set of growth series with randomly introduced offsets were compared. To produce these offset series a random offset between -5 and +5 years was introduced to the individual specimen-specific growth increment series, then growth by ontogenetic year class was averaged (i.e. regional curve construction); this process was repeated 30 times. Finally standard deviation and standard error of the 30 offset series were calculated per year class.

The NE ontogenetic growth trend was removed by first carrying out a regression on the regional curve fitted to a NE model, which produced an empirically-calculated NE detrending curve. The NE model applied is defined by:

(Equation 2.1)

Where $f(x)$ is shell growth (µm), y_0 is the animal size at $f(\infty)$, x represents age (yr), a is the intercept or size at first year of life and b is the slope or rate of change in shell growth. Y_0, a and b are empirical constants which must be calculated for each species. The NE detrending curve calculated was then subtracted from the original regional curve to generate residuals. As a result of this detrending process, the data were normalized to the population mean shell growth. Positive deviations from the mean represent enhanced population shell growth whereas negative deviations represent a decrease in population shell growth, with values close to zero representing a homeostatic balance in shell growth. It is important to note that as the time series are ontogenetically aligned rather than calendar-date aligned the environmental drivers of shell growth are not affecting the RCS curve as they are reduced to a noise signal within the ontogenetic growth.

An analysis of the standard error was carried out in order to estimate the effect upon variability of decreasing sample depth associated with increasing biological age in the RCS, created by a lack of ontogenetically old specimens. A cut-off point of sample depth was adopted as a compromise between series length and stable data variability. This was set at 50 % reduction of the maximum standard error, for which the equivalent sample depth was 21 *A. eightsii* specimens. Below this cut-off point data should be interpreted cautiously as the low sample depth and increased variability may lead to erroneous interpretations.

Multitaper spectral analysis (MTM) was used to analyse the growth cycles present in the residual ontogenetic growth pattern (ROGT, Mann and Lees, 1996). The program K-Spectra (v3.4.3, SpectraWorks Inc.) was set for a comparison against red noise, i.e. temporally integrated white noise, for narrowband and harmonic signals (Ghil et al., 2002). K-Spectra was configured with a resolution = 2 and number of tapers = 1. Frequencies were tested against their amplitude relative to the estimated background noise (i.e. narrowbands), using an F-test for periodic signals (i.e. harmonics; Ghil et al. 2002). Robust noise background estimation and a log fit of the misfit between the robust estimated background noise and the spectral densities were also tested.

2.5 Crossdating

The process of crossmatching, which has its roots in dendrochronological analysis, involves the year-by-year alignment of specimen-specific growth increment series (Wigley et al., 1984; Briffa and Jones, 1990; Cook et al., 1990). Crossmatching was carried out using the program SHELLCORR written for Matlab (c.f. Scourse et al., 2006). SHELLCORR compares pairs of growth increment series with specific correlation windows at different set lagged positions. SHELLCORR is characterised by its graphical output, showing colour coded Pearson's product-moment correlation (r) at different configurable temporal lags (**Fig. 2.5**). In this way, the program helps to “anchor” dead-collected specimens in time by comparing its increment width series with one live-collected specimen, and therefore absolutely dated, specimen. The temporal lag shown by the strongest correlation indicates the date of death of the undated specimen (**Fig. 2.5a**). In addition, possible offsets due to the misidentification or omission of an increment during the measurement of the growth increments can be detected and corrected (**Fig. 2.5b**). Prior to comparison the increment width data are normalized, logged and residuals are taken (e.g. Scourse et al., 2006; Butler et al., 2010; Bušelić et al., 2015). In this instance, a spline of 11 years was applied to the growth increment series and SHELLCORR was programmed to display correlation at lags of ± 21 years in a 21 year window. The length of the smoothing spline was chosen based on the length of the shortest time series. The number of the lagged correlations was selected to check not only for possible offsets introduced during measuring in the life growth histories but also for autocorrelation in the data.

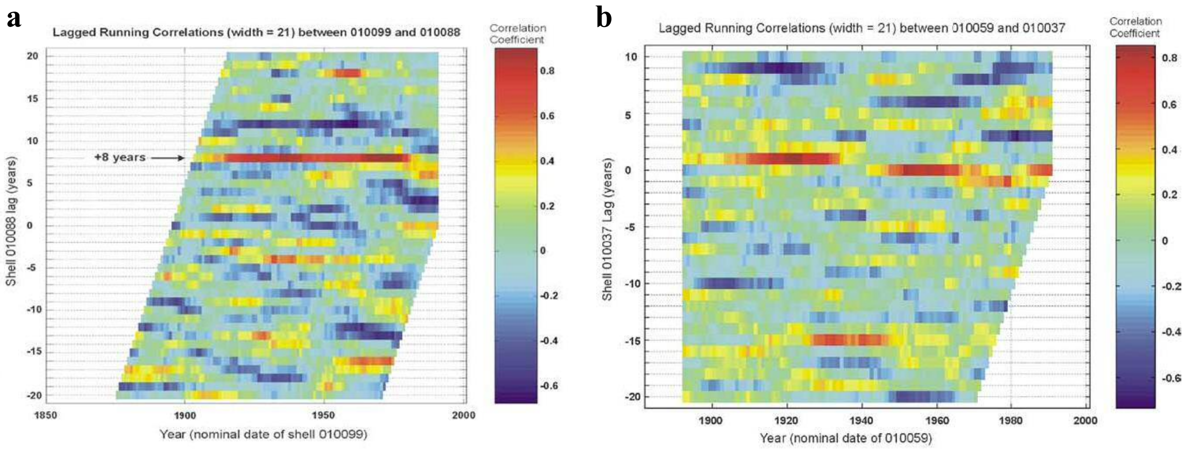

Fig. 2.5 a) Graphical output of SHELLCORR showing a strong positive correlation (solid red line) between two shell specimens at +8 year lag and **b)** Graphical output of SHELLCORR showing three possible offsets in the increment width series of two shell specimens (*A. islandica*) around year 1940 and around mid-1970s. The scale bar shows the Pearson’s product-moment of

correlation (r) in a graphical scale assigning red to positive correlations and blue for negative correlations (from: Scourse et al., 2006).

Specimens from the different sampling locations were compared independently. Where there was a disagreement (i.e. offset) between a growth increment series with the shell growth signature of a specific location, a visual re-assessment under the microscope and of the composite images of the acetate peel replica and the polished exposed shell surface was carried out.

Once specimens from the different sampling locations had been independently crossmatched, an inter-site comparison was carried out using the previously described SHELLCORR settings.

2.6 Detrending and chronology construction

After crossmatching the growth increment series were compiled into a compact file (.cmp) using the MS-DOS program Farm Management Technology (FMT, http://web.utk.edu/~grissino/software.htm). This required the creation of tab-delimited text files for each specimen with two columns: calendar year and increment width. Calendar year must be in decreasing order. Subsequently the compact file was imported into the dendrochronology program Autoregressive Standardization (ARSTAN, which can be obtained from http://web.utk.edu/~grissino/software.htm, Cook and Krusic, 2007). The compact file was loaded into ARSTAN and the data type was indicated to the program (option 1 in ARSTAN and 4 for compact files). The variance in the time series was stabilized by the use of an adaptive power transformation (option 3 in ARSTAN and 4 for the adaptive power transformation). The life growth histories were then detrended using the RCS method (option 4 in ARSTAN and -2 for RCS detrending). After detrending the chronology was built using a robust biweight mean (option 12 in ARSTAN and 2 for the robust biweight mean). In order to assess how robust a chronology is, the expressed population signal (EPS) was calculated. EPS is a function of the sample depth (i.e. number of specimens in the chronology) and the intercorrelation between the growth increment series (Wigley et al., 1984; Briffa, 1995). The EPS is defined as:

(Equat

ion 2.2)

Where *n* stands for the number of standardized growth increment series (SGIs; i.e. sample depth), or Rbar stands for the effective chronology signal and *t* stands for time unit (i.e. annual in this case). The EPS ranges between zero and one, with EPS = 1 indicating a perfect agreement between the standardized growth increment series. A threshold of EPS = 0.85 has been suggested as a minimum (Wigley et al., 1984) in order to consider the signal in the chronology sufficiently representative of the signal in the underlying population so that it can be reliably used for comparison with environmental and climatological records. The EPS index can be increased either by the addition of new time series to the master chronology, or by improved agreement between the growth increment series already added. Environments with high fluctuations in physical variables (e.g. strong seasonal variability, as in Antarctica) were found to increase the common variability between the growth increment series, and therefore a smaller number of samples were needed to acquire strength in the EPS (Mäkinen and Vanninen, 1999). For the calculation of the EPS in ARSTAN the Rbar window length and the Rbar window overlap were set to seven and six years respectively, which corresponds approximately to a third of the average length of the SGIs. Finally, the core series were saved in tab-delimited text files (option 18 in ARSTAN and 6 for tab-delimited text files) and summary plots were displayed (option 19 in ARSTAN and 3 for all summary plots).

ARSTAN produces a set of output files containing the different chronologies constructed (i.e. standard, residual and arstan), EPS and Rbar values. ARSTAN produces three versions of the chronology: a) standard chronology, b) residual chronology and c) ARSTAN chronology. The standard chronology uses the standardized series combined with a biweight robust mean estimation, the residual chronology is based on the residuals from autoregressive modelling of the individual time series and a biweight robust mean estimation and the ARSTAN chronology adds to the residual chronology the autocorrelation common to the entire population (Holmes et al., 1986; Butler et al., 2010) The ARSTAN chronology was used in further statistical analysis as it retains only that autocorrelation which is common to multiple time series and therefore it is preferable for assessing long-term climatic trends (c.f. Butler et al., 2010). EPS and Rbar values were extracted from the res_rbar file in order to assess the robustness of the chronology.

2.7 Instrumental Records

2.7.1 West Antarctic Peninsula records

The BAS has been carrying out year-round environmental measurements in Ryder Bay at Rothera Research Station since 1997 under the Rothera Time Series (RaTS) project. The main RaTS sampling site is located in the deepest section of Ryder Bay (67°31'12.0"S, 68°13'30.0"W) at 520 m water depth (**Fig. 2.1b**). A secondary site exists (67°34'51.6"S, 68°09'28.8"W), in case the main site cannot be accessed, closer to Rothera Research Station and at 300 m water depth. Sampling methodology for the RaTS programme is described in detail by Venables and Meredith (2014). As a summary of the methodology followed, measurements are taken twice a week during the summer season and as often as weather and ice allow during the winter season. RaTS sampling is carried out by the use of a SeaBird 19+ conductivity-temperature-depth instrument (CTD), a WetLabs in-line fluorometer and a LiCor photosynthetically available radiation (PAR) sensor through the entire water column (Venables and Meredith, 2014). RaTS temperature and salinity accuracy are estimated to be 0.002 °C and 0.005 respectively, achieved through the comparison of joint casts between the RaTS and the Palmer Long Term Ecological Research grid survey and by the use of a BAS glider equipped with CTD instruments (Venables and Meredith, 2014). Sea ice observations (i.e coverage and type of ice) are made daily from Rothera Research Station and although there is some subjectivity depending on the observer, interannual and seasonal changes are greater than the observer bias (Venables and Meredith, 2014).

The RaTS record between 2002 and 2016 was provided by Dr. Hugh Venables (BAS) and the RaTS record between 1997 and 2001 was obtained from the British Oceanographic Data Centre (BODC, http://www.bodc.ac.uk/about/news_and_events/rats_data.html). Data time series from the climatic indices were downloaded from the web: Multivariate El-Niño-Southern-Oscillation (ENSO) Index (MEI; http://www.esrl.noaa.gov/psd/enso/mei/) and the Southern Annular Mode index (SAM; http://www.nerc-bas.ac.uk/icd/gjma/sam.html). Subsequently the data were compiled into an Excel master database along with data of fast-ice duration (also provided by Dr. Hugh Venables).

The RaTS dataset is comprised of measurements of seawater temperature (ºC), chlorophyll (mg m^{-3}), salinity, density (kg m^{-3}) and photosynthetically active radiation data (PAR, µmol photon m^{-2} sec^{-1}; not considered in the present study). Due to the shallow sampling locations only measurements of the upper 100 m of the water column from the RaTS dataset were considered for subsequent analysis.

Monthly, annual (August-July) averages, summer (December-April), winter (May-November) and core winter (July-September) maximum, minimum and quartiles (Q1 to Q3) were calculated for each parameter for the upper 5 m, upper 10 m, upper 15 m, upper 20 m, upper 25 m, upper 50 m, upper 75 m and upper 100 m of the water column (i.e. sequentially averaging deeper layers of the water column). This sequential averaging allows the investigation of stratification in the water column. Additionally annual (August-July) averages were calculated for every meter of the water column, which provides information about the variability meter-to-meter in depth. In order to provide a continuous record, if a value was missing for any particular calendar month it was interpolated by averaging the values of the previous and the following months if available. If data for more than one consecutive month were missing, no interpolation was carried out leaving a discontinuity in the record. Annual start and end date of the fast-ice formation were calculated as the count of days from the 1st of January to the date of the formation of fast-ice (index = 6 in the sea ice Rothera time series; start date) and the count of days from the 1st of January to the date of final break-up of the fast-ice (end date).

Two indices assessing the winter length were calculated based on the seawater temperature record. First winter length (days) is defined as the time during which the seawater temperature remained below the second temperature quartile (Q2); this coincides approximately with May-November period, which was taken as a standard for the time series. The second index, core winter length (days) is defined as the time during which the temperature remained below the first temperature quartile (Q1), which coinciding approximately with the July-September period, which was also taken as a standardization for the time series. Similarly, summer was defined as the time when the seawater temperature was higher than the third quartile (Q3), which corresponds with December-April period.

Long-term trends (i.e. covering the entire length of the record) in the time series were studied and a comparison between the upper 5 m, upper 25 m, upper 50 m and upper 100 m profiles was carried out. This allows the investigation of the temporal changes between near surface waters with deeper sections of the water column.

A record of seawater oxygen isotopes ($\delta^{18}O_{water}$) was collected from August 2001 to March 2015 from 15 m water depth at RaTS site in Ryder Bay (Rothera Research Station) provided by Prof. Michael Meredith (BAS). The record consisted of tab delimited data containing: event number, salinity value, potential temperature (°C), $\delta^{18}O_{water}$ value (‰ SMOW), year and day of collection. The relationship between $\delta^{18}O_{water}$ and salinity was calculated by applying a linear regression to the data. In addition monthly averages of $\delta^{18}O_{water}$ were calculated and were compared with monthly salinity averages in order to analyse possible temporal changes.

2.7.2 South Orkney Islands records

Due to the historical nature of the specimens available from the South Orkney Islands a systematic search of historical instrumental records was carried out. This search included several academic search engines: Google Scholar, Science Direct, Web of Knowledge and a selection of search keywords (e.g. South Orkney Islands, Signy Island, Orwell Bight, Factory Cove, long-term record, sea-ice, temperature, phytoplankton, annual cycle and seasonal cycle). A range of publications was found, using different instrumental records, which varied in length, for the region. When the data were not available online, the authors or in case of old publications the institution was contacted in order to access the data.

The updated (until 2008) year-long sea-ice duration record from Murphy et al. (1995) was obtained for the South Orkney Island. The South Orkney Islands sea-ice record is composed of three independent records: i) From 1903 to 1975 fast-ice duration was measured in Scotia Bay, Laurie Island (**Fig. 1.6**), ii) from 1947 to 1994 fast-ice duration was measured in Factory Cove and iii) from 1995 to 2008 fast-ice duration was measured in Factory Cove by using a sea-ice camera. The Scotia Bay and the 1947-1994 Factory Cove record were combined into the South Orkney Island sea-ice record using a regression during the overlap period; however the 1995-2008 Factory Cove record remains uncalibrated. Centred moving averages of three, nine and fifteen years were calculated using Excel, and fifteen and thirty years low-pass filter were calculated in AnClim. According to Murphy et al. (1995) the start day of fast-ice was defined as "the date on which the ice will first support the weight of a "typical" scientist and the end date was defined as the date of the seasonal departure of the fast-ice, which in Factory Cove occurs either simultaneously with or sooner after the departure of the consolidated pack-ice. In addition fast-ice duration was defined as the period between the fast-ice start date and fast-ice end date; short ice-free periods may occur between the start date and the end date but these were ignored in the analysis (Murphy et al., 1995).

Clarke et al. (1988) developed multi-annual (from 1969 to 1982) seawater temperature, salinity chlorophyll and major nutrients (i.e. PO_4, NO_3, NO_2 and SiO_4; although not considered in the present study) records from Factory Cove and from the Orwell Bight (i.e. offshore of Borge Bay at Signy Island). Prof. Lloyd Peck (BAS) provided these instrumental time series, although only the part of the record between 1972 and 1982 was available, and subsequently digitized and incorporated into a database in Excel; monthly averages for the entire length of the record available were calculated. The Clarke et al. (1988) record contains several gaps, presumably due to adverse weather conditions preventing instrumental readings. In order to provide a continuous record as much as possible, missing monthly measurements were interpolated only in the cases when adjacent monthly measurements were available. If, for example, there was a gap of two or more consecutive months the values for that gap were left blank and were not interpolated. In addition, two outliers (June 1972 with a salinity of 35.72 and June 1975 with a salinity of 38.34) in the salinity record were omitted for analysis. Mean annual (August-July), mean summer (December-April) and mean core winter (July-September) temperature, mean annual (August-July) chlorophyll concentration and salinity time series were calculated.

Sea-surface temperature (SST) data were extracted from the HadISST1 dataset from the MET Office gridded for the area 58-62° S, 43-47° W centred on the South Orkney Islands and for the period 1948/88. The HadISST1 dataset consists of global monthly median SST and sea-ice concentration values from one degree latitude, longitude spatial resolution (c.f. Rayner et al., 2003). The SST time series was downloaded from the MET Office Data Bank (http://www.metoffice.gov.uk/hadobs/hadisst/) and later compiled in Excel. Monthly correlation coefficients with the robust (EPS > 0.85) part of the relevant chronology (i.e. developed from the specimens collected in 1988 at Factory Cove, Signy Island) were calculated in order to identify the most relevant months for shell growth. Subsequently the monthly SST time series was weighted by multiplying the temperature value with the monthly correlation coefficient. Then mean annual (August-July), mean summer (December-April) and mean core winter (July-September) temperature time series were produced. In addition, a comparison between the instrumental dataset produced by Clarke et al. (1988) and the weighted HadISST1 dataset was carried out for the mean annual, mean summer and mean core winter temperature time series for the overlapping period (i.e. 1972/82).

2.8 Geochemistry

The laboratory procedures for the preparation of samples for microdrilling in order to obtain carbonate powder from the shell material for geochemical analysis are described in this section. In addition, a new method for sampling 3D delicate carbonate structures (e.g. bivalve shells) using the New Wave Micromill was developed and is presented here. Three different experiments were carried out: one developing high-resolution geochemical records (i.e. subannual), one developing low-resolution geochemical records (i.e. annual) and one analysing potential lateral stable isotope fractionation ($\delta^{18}O_{shell}$ and $\delta^{13}C_{shell}$) depending on the drilling position along an annual growth increment.

The first step in the preparation of specimens was the removal of periostracum (i.e. organic outer layer covering the shell). The periostracum of the selected valves was removed by inserting a razor blade between the carbonate material and the organic layer, being careful not to damage or scrape the carbonate part of the shell. Once the periostracum was fully removed the internal part of the valve was filled with polyester resin (Metprep Kleer set) in order to give the sample structural integrity avoiding breakage when drilling. Subsequently the resin-filled valves were mounted on thin (0.5 cm thick approximately) polyester resin slides. The samples were secured to the micromill stage by using Blue-Tack around the resin slides. The micromill was equipped with a 300 µm Ø carbide drill bit (Brasserler USA HP round H52.11.003 HP) and was configured to one pass spot drilling at 15 % drill speed (i.e. 5250 rpm), 3 sec dwell time, 40 µm sec^{-1} plunge rate and zero µm drill depth. In all experiments the outer surface of the shell was analysed by using the micromill camera and the lines present in the shell were highlighted using the line tool of the micromill software. This technique helps to improve accuracy when drilling as it prevents the introduction of sequential offsets that after a time can be quite significant. More of these guiding lines were drawn during the high-resolution experiment as the effect of offset could have a much greater impact than in the low-resolution or in the lateral fractionation experiment (only annually-formed growth lines were highlighted).

Traditionally shell material is drilled on the exposed shell profile after being sectioned along its maximum growth axis (e.g. Reynolds et al., 2016). After several trials using different established techniques it was decided that this approach was not feasible in *A. eightsii* due to the small, thin and fragile nature of its shell. Also manual drilling using a hand drill was tested but it was not considered reliable for accurate sampling. Instead, drilling on the outer surface of the shell appeared to be the best approach for drilling *A. eightsii* shells. This approach is not free of technical difficulties, since during the trial phase using this technique it became apparent that the New Wave Micromill cannot cope well with significant differences in the Z-axis due to the curved nature of the shell. The software surface profile tool could not be used due to the fast plunge rate (this cannot be adjusted in the software) of the drill bit, which caused the shell to break in a test specimen in several occasions. Consequently no automatization of the drilling process could be used and a more “manual” approach was adopted. After setting the drill spots to be drilled and a calibration of X-Y axis of the micromill stage, the drill bit was positioned approximately 200 µm above the first drilling spot, and then the “run” button was activated. When the drill bit touched the surface of the shell the micromill was manually stopped, using the “abort” button, and then the drill bit was moved to the position of the next drilling spot. The determination of the touch-down of the drill bit on the shell was carried out visually, by the use drilling micromill camera, but it was mainly based on an audible cue, which was a distinct change of pitch in the sound produced by the micromill. The lack of automatization in this method can introduce several errors during sampling. For example the abort button is hit later than it should have been and the drill bit is allowed to go deeper into the shell. If it was thought that drill bit had penetrated too deep into the shell, or in any other case where there was a cast of doubt on the accuracy of the sampling, the powder generated around the drill spot was carefully collected with the tip of a scalpel and subsequently discarded. Subsequent visual analysis of the drilled shells under a high power magnification microscope confirmed the accuracy and reproducibility of this method. Sampling spots ranged from approximately 100 µm to 160 µm in diameter.

The first experiment carried out was the development of high-resolution (i.e. subannual) geochemical records. One specimen from each sampling location and temporal frame (**Fig. 2.1**), with the exception of Trolval, were drilled (total of six specimens: 191501025, 192702003, 8804045, 21402010, 21403025 and 2150403). In this experiment a sample is defined as the powder collected from a row of sampling spots, where the row is parallel to the increment growth pattern (**Fig. 2.6a**). The number of sampling spots, within a sampling row, is variable depending on the position on the shell (near the umbo vs near the margin), ranging normally between 33 (closer to the umbo) and 120 spots (closer to the margin). In order to limit the possible effects of lateral fractionation, if any, during drilling the centre of the sampling rows was centred approximately with the maximum growth axis of the shell. Note that the-resolution during this experiment changes as the increments become narrower towards the margin, becoming annual or even multiannual depending on the increment width. Following the drilling sampling, the drilled specimens were photographed under 4x magnification in a Meiji MT8100 high power microscope using an INFINITY 3 Lumen*era* colour camera. Images were processed using Image Pro Premier 9.1 and post-processed in Adobe Photoshop CC for adding ID labels. This enables every geochemical sample to be assigned to a specific growth increment and ultimately to a specific calendar year. The images taken of the outer drilled surface of the shells were then compared to the images taken of the profile sections of the paired valves (i.e. polished shell and acetate peel replicas). This was not possible in the case of the specimens 8804025 and 192702003 as there were no paired valves available for sectioning. The markings present on the external surface of the shell and the annually-formed growth checks present in the profile sections were matched in order to provide a robust assignation of geochemical samples to annually-formed increments.

The second experiment addressed the development of the low-resolution (i.e. annual) geochemical records. In this experiment a sample is defined as the powder collected from several rows of sampling spots but all contained within an annually-formed growth increment (**Fig. 2.6b**). In contrast to the high-resolution sampling, the temporal resolution per sample in this experiment is always annual and does not change with narrowing growth increments. The same specimens were used as in the high-resolution experiment, drilling either the same valve as for the high-resolution sampling or the paired valve if it was not possible to drill the same valve. The comparison between the photographs of the drilled shells and the high-resolution geochemical profiles allowed the accurate identification of annually-formed growth lines. If the already-drilled valve was selected, the low-resolution drilling ran parallel to the high-resolution drill transect (**Fig. 2.6b**); annually-formed growth lines were identified and highlighted using the micromill software line tool. If the other valve was selected, a cross-identification of annually-formed growth lines was carried out between valves by images taken with a Novex RZ Range low power microscope and an OptixCam OCS-HDMI-NH1080 camera.

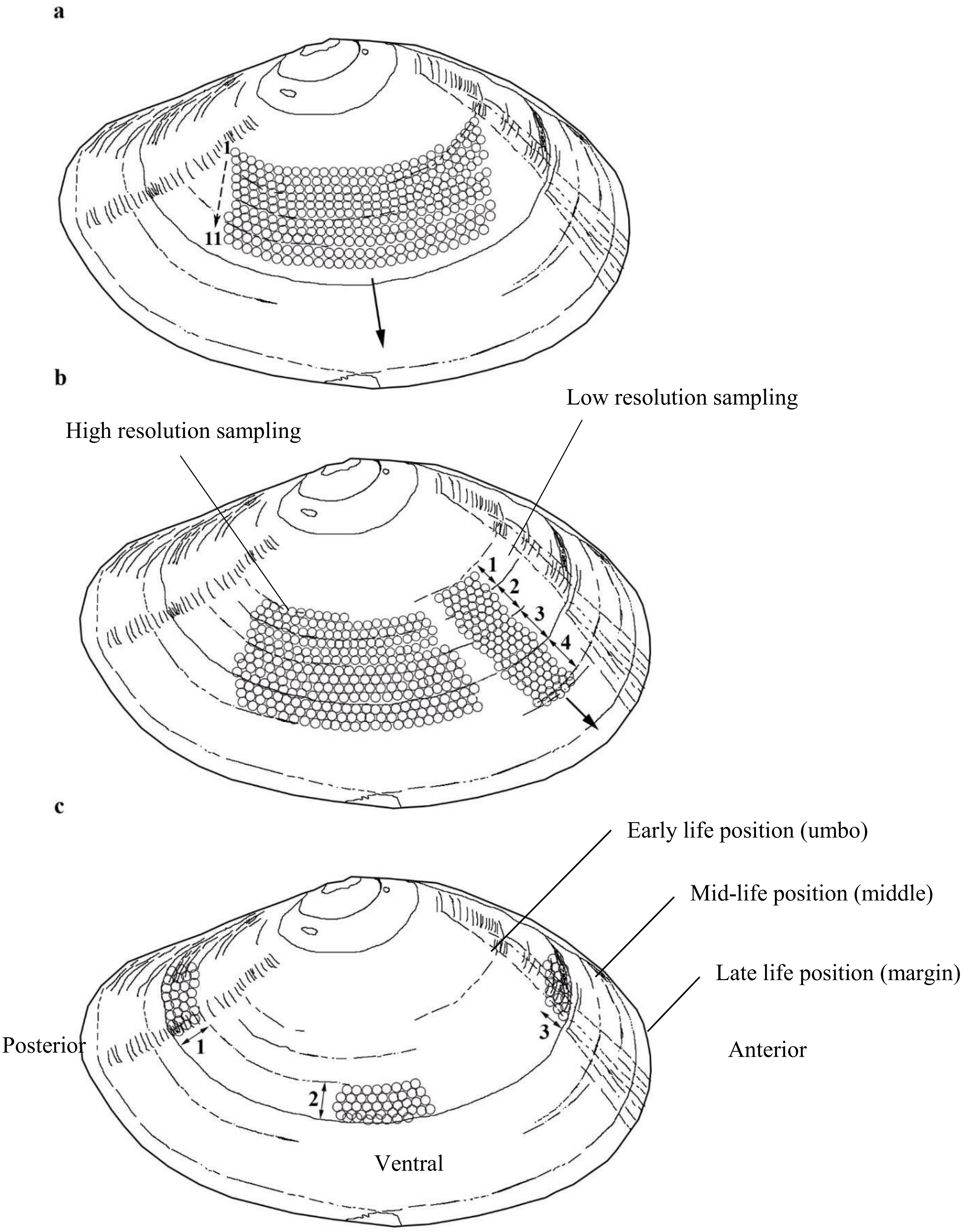
a
1
11
b
Low resolution sampling
High resolution sampling
1
2
3
4
c
Early life position (umbo)
Mid-life position (middle)
Late life position (margin)
Posterior
1
3
Anterior
2
Ventral

Fig. 2.6 Drawing showing the sampling strategy for **a)** high-resolution sampling, the arrow indicated the direction of drilling **b)** low-resolution sampling, the arrow indicates the direction of drilling and the dots present in the middle section of the shell are from the high-resolution sampling previously carried out in the valve and **c)** lateral fractionation sampling, showing three sampling location within the same increment located in the anterior, ventral and posterior parts of the shell Numbers indicate what is referred to as a sample in each experiment. Note the number of dots and samples in the drawing do not represent the total amount of dots/samples drilled.

The final experiment addressed lateral fractionation in the stable isotope ratios in the shell carbonate material depending on the position of the sampling transect (i.e. anterior, ventral and posterior parts of the shell; **Fig. 2.6c**). A set of three *A. eightsii* valves was selected (one specimens collected from Rothera in 2015, ID 21504010; one specimen collected from Signy in 1988, ID 8804034, and one specimen collected from Signy in 1915, ID 191501036). Specimens were selected for which paired valves were available and medium size shells (> 25 mm in shell length) were selected in order to facilitate increment identification under the New Wave Micromill camera. Also medium size shells (approximately 25 mm in length) were selected to facilitate the drilling work (e.g. shell manipulation, increment identification). Additionally the 21504010 specimen was drilled in three independent increments (one at the first years of growth, one at mid-life and one during the last years of growth) in order to provide some insight into the relationship between isotope fractionation and ontogeny; in the other two specimens only the part corresponding to mid-life increment was drilled.

The shell carbonate powder from the different samples was collected using the tip of a scalpel and placed in a weighing paper envelope. The weighing paper envelopes with the samples were stored in pre-labelled eppendorfs and recorded in a log book (sampling ID, specimen ID and drill date). Samples drilled at the School of Ocean Sciences, Bangor University, were sent for analysis to the School of Earth and Ocean Sciences, Cardiff University.

The $\delta^{13}C$ is defined as the ratio between the two stable carbon isotopes (^{12}C and ^{13}C; McKenzie, 1985), being ^{12}C more abundant in nature than ^{13}C, in the sample and in a standard (Vienna Peedee Belemnite, VPDB, was used as a standard) and is calculated as:

(Equation 2.3)

Similarly, $\delta^{18}O$ is defined as the ratio between the stable oxygen isotopes ^{16}O and ^{18}O in the sample and in the standard and is calculated as:

(Equation 2.4)

The shell powder samples were analysed in a Thermo Finnigan MAT 253 dual inlet mass spectrometer coupled to a Kiel IV carbonate preparation device at Cardiff University. Instrumental precision depends on sample size; for samples > 15 µg the long-term precision of the in-house Carrara marble is < 0.05 ‰ in the case of $\delta^{18}O$ and < 0.03 ‰ in the case of the $\delta^{13}C$; for samples between 5 µg and 15 µg a correction is applied to adjust for the variation in the ratio between the amount of sample and the reference gas (Brand, 2004). The resultant instrumental precision of the in-house standard in the case of the *A. eightsii* samples was on average 0.05 ‰ ± 0.02 SD, 0.20 ‰ in range in the case of $\delta^{18}O_{shell}$ and on average 0.03 ‰ ± 0.01 SD, 0.1 ‰ in range in the case of the $\delta^{13}C_{shell}$.

Once the geochemical data were available, they were compiled into a master database in Excel. In cases where it was possible to carry out a replicate analysis of a geochemical sample, the average between the two or more samples was carried out in order to provide a single geochemical value per sample (i.e. in all geochemical experiments). Subsequently with the comparison pictures between the external surface and section profile of the shells calendar years were assigned to the geochemical samples for the high and low-resolution records. In addition, high-resolution series were averaged to produce series of annual resolution; this was achieved with the help of sectioned shell profiles and with the images from the outer surface of the shell. Subsequently, those annual averages from the high-resolution sampling were compared to their equivalent samples from the low-resolution for both $\delta^{18}O_{shell}$ and $\delta^{13}C_{shell}$. Due to the variable width of the growth increments, each sample represents a variable length of time, thus temporal variation had to be standardized for each geochemical sample prior to a comparison between the trends in the isotope series was carried out. The temporal standardization based on a linear model of growth of five months which then was divided between the number of samples drilled out of a single annually-formed growth increment. After standardization, a comparison between the trends within both sampling locations (i.e. South Orkney Islands and WAP) and between sampling locations (latitudinal) was carried out.

In the case of the WAP samples the availability of the contemporary long-term environmental records of $\delta^{18}O_{water}$, seawater temperature, salinity and chlorophyll concentration allowed a comparison with the $\delta^{18}O_{shell}$ and $\delta^{13}C_{shell}$ series. For the South Orkney Islands samples, the limited environmental data available (seawater temperature, salinity and chlorophyll concentration) only allowed a comparison with the 8804034 specimen.

In the case of the geochemical lateral fractionation experiment, the samples were labelled: anterior, ventral or posterior (anatomical parts of the shell) for each specimen and in the case of the specimen 21504010 for each drilled section (i.e. early, mid and late life position; **Fig. 2.6**). The samples within each drilling section and trends between each shell anatomical part were then compared and the variability contained within each dataset was analysed.

Chapter III: *Aequiyoldia eightsii* shell growth

This chapter covers the results related to shell growth and ontogenetic growth trends in *Aequiyoldia eightsii*. Characterising shell growth is crucial for the development of sclerochronological records as multiple can mask the common environmental forcing on shell growth. In addition a description of the shell specimens is provided describing their morphometrics and physical appearance and a comparison between the different *A. eightsii* populations. The results are discussed considering the biology of the species as well its natural habitat. The hypothesis tested in this chapter are: i) all *A. eightsii* populations exhibit similar biological growth patterns and similar morpho-characteristics and ii) Growth trends associated in pure biological causes can be removed preserving the high frequency variability in the growth pattern.

3.1 Morphometrics and specimen description

Clear phenotypical differences were found between the *A. eightsii* specimens from the different sampling locations. These included: i) colour differences, samples collected from Factory Cove, South Orkney Islands (SOI), showed predominantly a pale-yellow periostracum (lower specimen in **Fig. 3.1**) whereas samples from the West Antarctic Peninsula (WAP) showed predominantly a dark brown periostracum colouration, ii) shell size, the deep-collected specimens from the *Discovery* investigations showed abnormally large shells (upper specimen in **Fig. 3.1**) and were particularly elongated compared to the rest of the specimens (**Fig. 3.2**). A summary of the averaged shell sizes for the different sampling locations is provided in **Table 3.1**.

Table 3.1 Average biometrics (i.e. shell length, L, shell height, H and shell width, W; see **Fig. 2.2** for reference; all measurements in mm) ± standard deviation of the specimens from different locations: Factory Cove (FC), South Cove (SC), Hangar Cove (HC), Back Bay (BB) and Trolval (T).

	FC	SC	HC	BB	T

L	24.78 ± 4.16	23.31 ± 3.46	22.54 ± 2.43	22.15 ± 1.97	25.54 ± 2.84
H	7.17 ± 1.47	7.56 ± 1.25	7.13 ± 0.92	6.99 ± 0.87	7.79 ± 1.06
W	15.78 ± 2.53	16.93 ± 14.36	14.29 ± 1.30	14.48 ± 1.12	16.25 ± 1.56

Fig. 3.1 Photograph showing two specimens of *A. eightsii* shells collected from the SOI. The upper specimen was collected in 1927 at 320 m water depth, the lower specimen was collected in 1915 at 10 m water depth. The lower specimen represents the "typical" *A. eightsii* adult shell size.

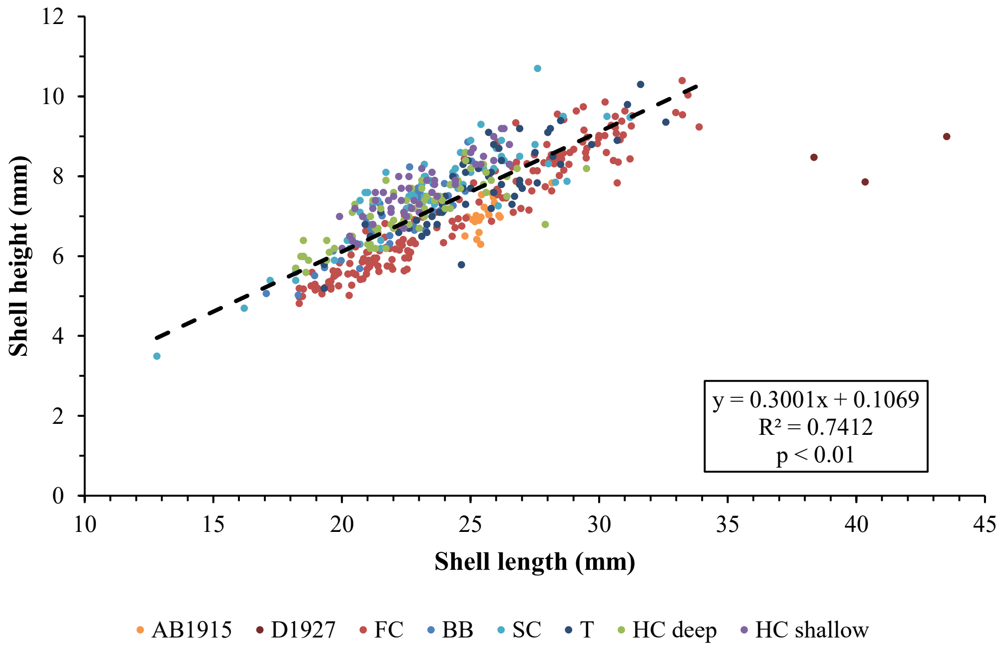

Fig. 3.2 Relationship between shell length (mm) and shell height (mm) of the *A. eightsii* specimens arranged by sampling location: 1915 A. Bennett collection (AB1915, SOI), 1927 *Discovery* investigations (D1927, SOI), Factory Cove (FC, SOI), Back Bay (BB, WAP), South Cove (SC, WAP), Trolval (T, WAP), Hangar Cove deep (HC deep, WAP) and Hangar Cove shallow (HC shallow, WAP). A linear trend (dashed black line) including all except the 1927 *Discovery* deep specimens was fitted to the data, the equation and R^2 of the trend line are provided in the inset.

After the periostracum was removed clear differences were apparent between modern collected shells and shells from historical collections. All specimens showed a pockmarked pattern in the carbonate part of the shell, and only the modern collected specimens showed an orange pigmentation, of an unknown origin, associated with this pattern (**Fig. 3.3**). This pockmarked pattern was usually restricted to the region between the umbo and the mid part of the shells and was rarely found closer to the shell margin. The orange dots were also obvious in the sectioned valves and the orange pigmentation extended to the boundary between the external and the internal carbonate layers but rarely crossed this boundary (**Fig. 3.4**). In addition, the presence of these orange dots was commonly associated with either shell damage or with abnormal shell mineralization (only assessed visually, **Fig. 3.4**). During the process of taking reference pictures it was noted that the *A. eightsii* shell appear to polarise light when images taken under reflected and transmitted light are compared (**Fig. 3.5**). The light polarisation shows as dark bands in the reflected light images (e.g. **Fig. 3.5a**) appear as light bands when using transmitted light (e.g. **Fig. 3.5b**).

Fig. 3.3 Photograph of two *A. eightsii* specimens, collected in shallow water from the SOI, without the periostracum. The upper specimen was collected in 1915, shows some degree of umbo erosion and a pockmarked pattern of white dots that occur especially during the first years of life. The lower specimen was collected in 1988 and does not show any significant erosion at the umbo. The pockmarked pattern shows a distinct orange colouration and is more widespread, although it is mostly located between near the umbo and in the mid-section of the shell.

The state of preservation (see subsection 2.3.1) of the dead-collected material was varied. No dead-collected specimen were found during the 2013/14 season and while the 2014/15 season did provide some dead-collected shells, most of them were not useful for analysis as they were severely damaged and/or eroded, and only three single valves were suitable for analysis. The 2015/16 season was the most productive in providing dead-collected samples, including a total of six paired-valve specimens from South Cove, 22 single valves and one paired-valve from Hangar Cove, four single valves and one paired-valve specimen from Trolval. Dead-collected samples from Hangar Cove tended to be significantly smaller (shell length 20.38 mm ± 2.35 SD; **Table 3.2**) than those from Trolval (shell length 26.43 mm ± 4.30 SD) or from South Cove (shell length 27.75 mm ± 2.39 SD). The dead-collected material showed a significant amount of erosion both external and internal, and the periostracum was often damaged and even missing in the more eroded shells.

Table 3.2 Results from Fisher's LSD test carried out after a significant differences were found in one-way ANOVA test between in shell length from the dead-collected shells from Hangar Cove, South Cove and Trolval (one-way ANOVA, $F_{2,29} = 19.273$, $p < 0.01$).

(I) Location	(J) Location	Mean Difference (I-J)	Std. Error	Sig.	95% Confidence Interval	
					Lower Bound	Upper Bound
South Cove	Hangar Cove	6.97^*	1.35	.00	4.21	9.74
	Trolval	0.69	1.56	.66	-2.50	3.88
Hangar Cove	South Cove	-6.97^*	1.35	.00	-9.74	-4.21
	Trolval	-6.28^*	1.29	.00	-8.92	-3.64
Trolval	South Cove	-0.69	1.56	.66	-3.88	2.50
	Hangar Cove	6.28^*	1.29	.00	3.64	8.92

*. The mean difference is significant at the 0.05 level.

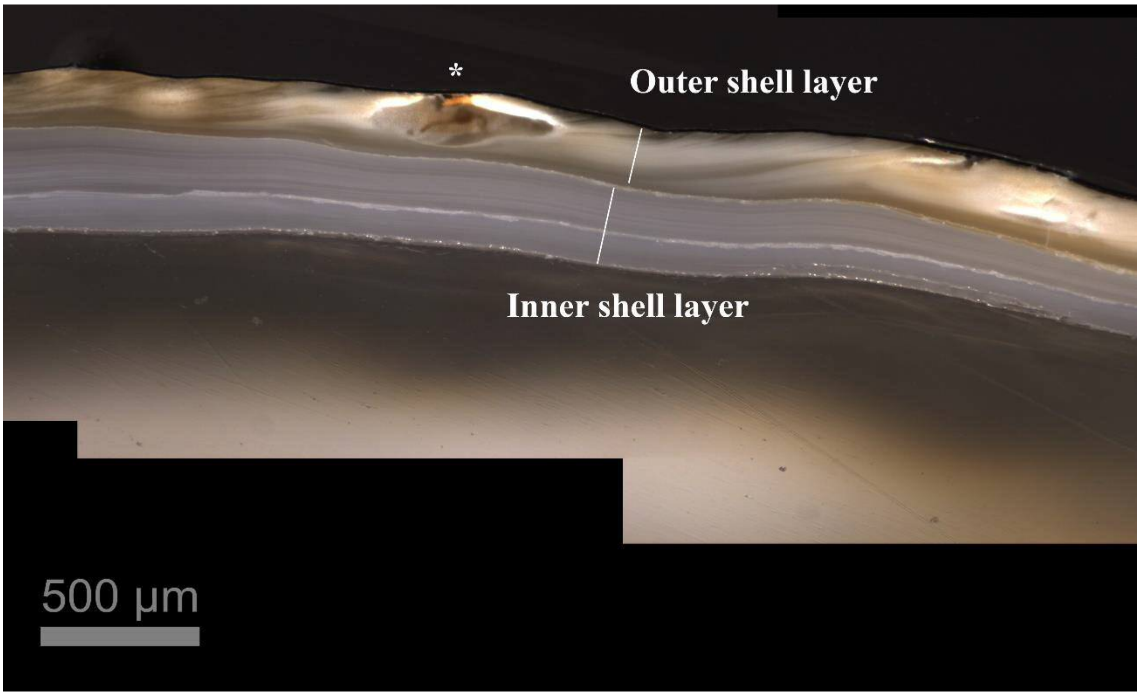

Fig. 3.4 Microphotograph of the profile of a sectioned *A. eightsii* valve collected from Trolval (specimen 21401022) showing shell damage associated with the orange dots (*). Note that the anomalous orange pigmentation and the shell damage does not seem to cross the boundary between the outer and the inner shell layers.

The scanning electron microscope (SEM) images revealed differences between the two specimens analysed. Whereas the snapped shell did not show any significant internal shell structure (**Fig. 3.6**), the lightly etched (0.01 M HCl for about 30 to 45 min) specimen showed the internal structures (e.g. growth increments, shell layers) of the shell (**Fig. 3.7**).

The etched shell presented clear lines both in the shell margin and in the hinge plate (**Fig. 3.7**). The comparison between the SEM images and the polished shell images allowed an accurate identification of the position of the growth lines. This comparison showed that in the case of the ventral margin, some annual growth increments are not very clear in the SEM images (**Fig. 3.7a**, second arrow from the left). On the other hand, the SEM images from the hinge plate highlighted a myriad of "secondary" lines, possibly disturbance lines, in the shell growth record that were not clearly visible in the polished shell image (**Fig. 3.7b**).

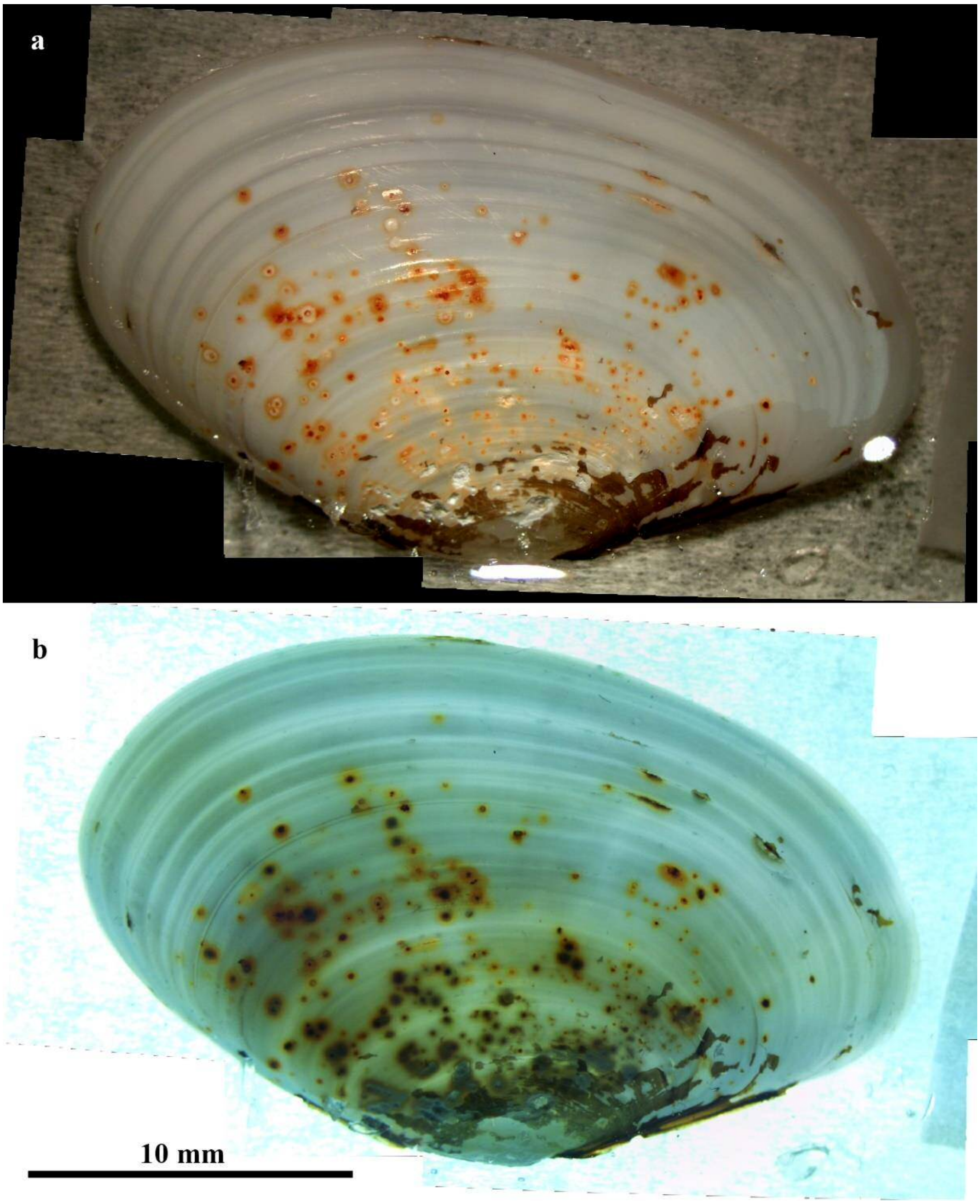

Fig. 3.5 Photographs taken using a dissecting microscope of an *A. eightsii* valve (specimen 21504034) under **a)** reflected light and **b)** transmitted light. Note the light polarisation as dark bands in the reflected light picture appear as light bands in the transmitted light picture. A scale bar is also included.

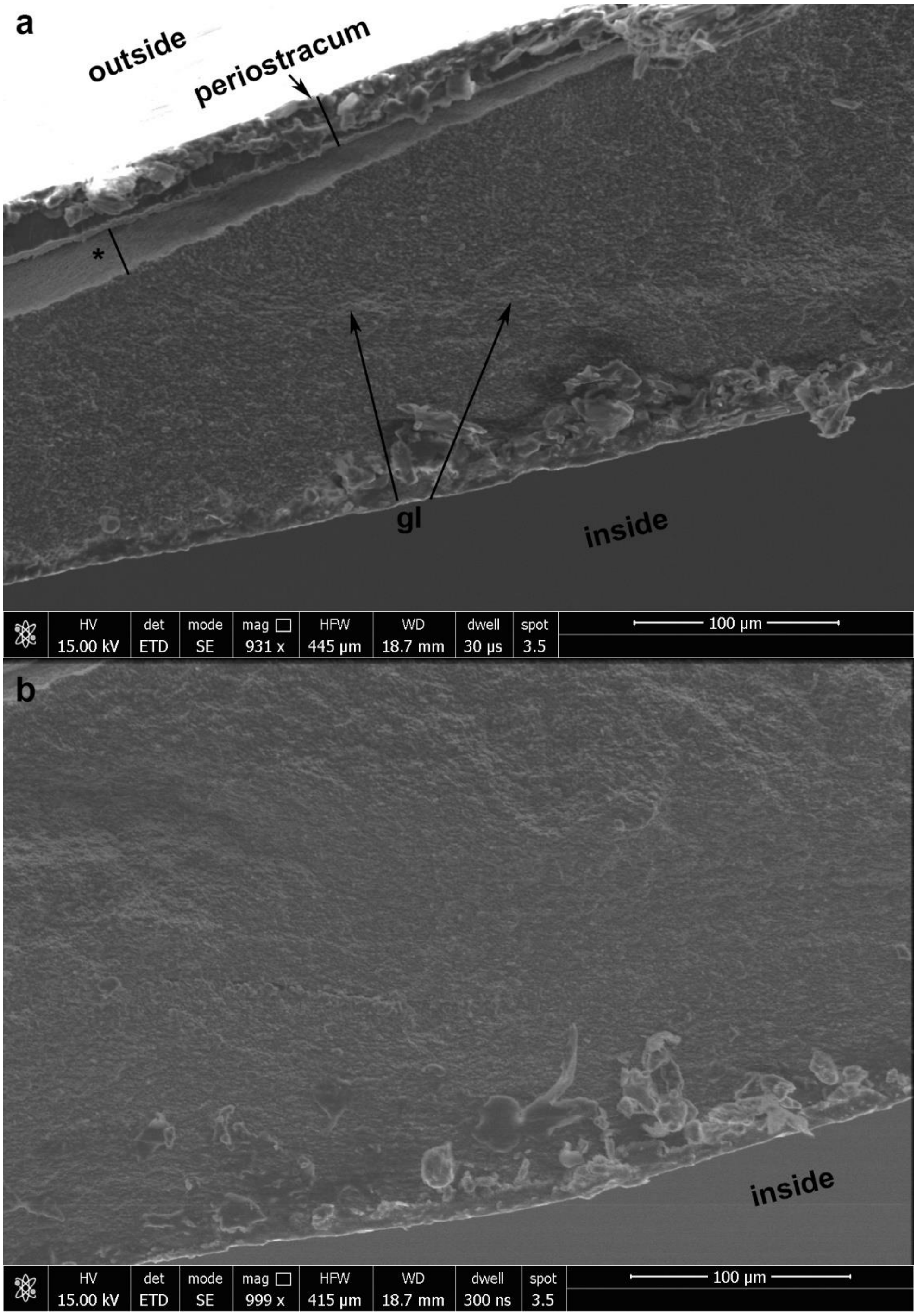
a
outside
periostracum
*
gl
inside
HV 15.00 kV
det ETD
mode SE
mag ☐ 931 x
HFW 445 µm
WD 18.7 mm
dwell 30 µs
spot 3.5
100 µm
b
inside
HV 15.00 kV
det ETD
mode SE
mag ☐ 999 x
HFW 415 µm
WD 18.7 mm
dwell 300 ns
spot 3.5
100 µm

Fig. 3.6 SEM photographs of a snapped *A. eightsii* shell showing: **a)** a region closer to shell margin tip, the periostracum layer is indicated and the asterisk shows the region where the periostracum has detached from the aragonitic part of the shell, gl: shows the possible position of a growth increment **b)** a different region of the shell closer to the mid-section of the shell. Details of the image capture and scale bars are also provided.

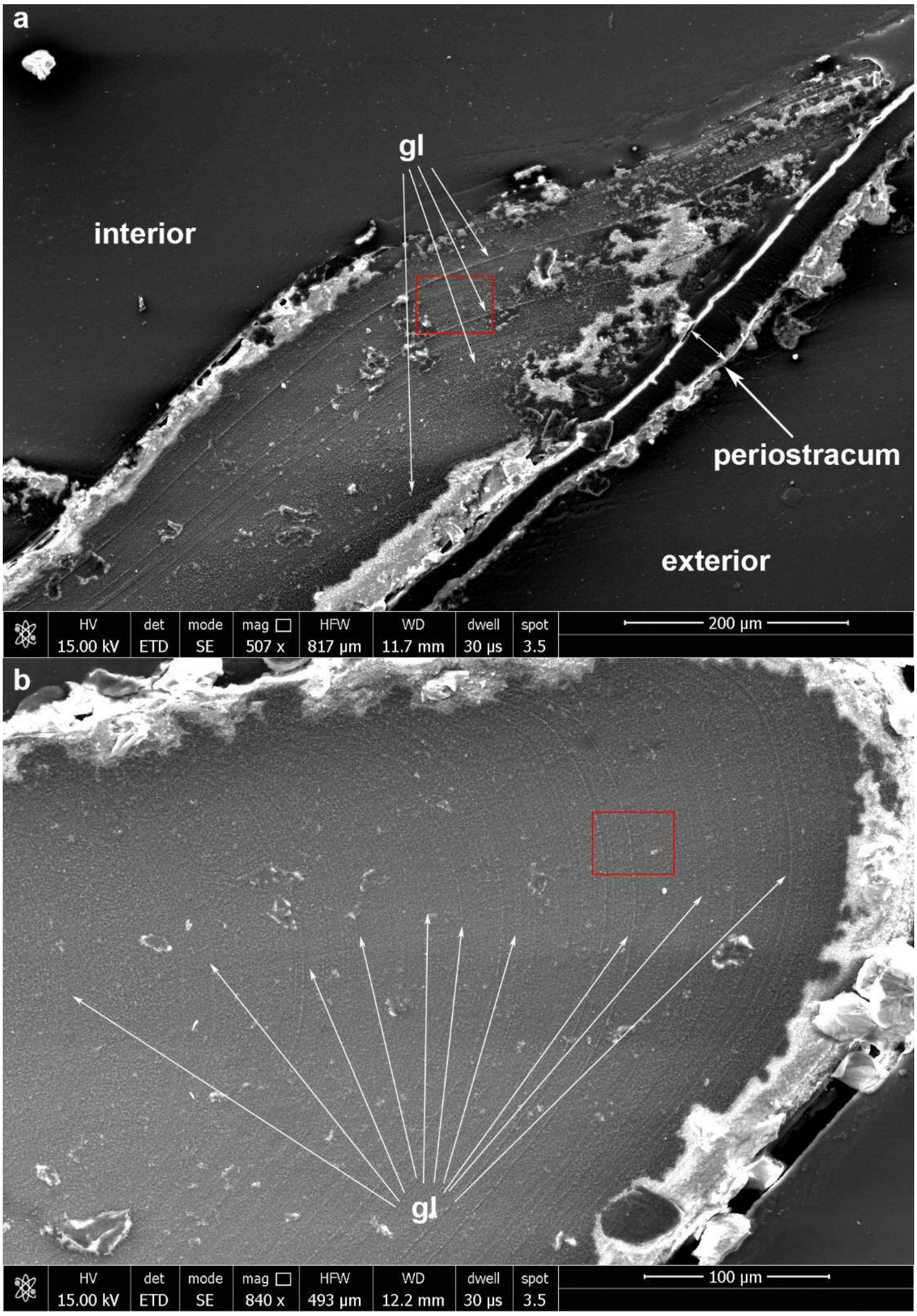
a
gl
interior
periostracum
exterior
HV 15.00 kV
det ETD
mode SE
mag 507 x
HFW 817 µm
WD 11.7 mm
dwell 30 µs
spot 3.5
200 µm
b
gl
HV 15.00 kV
det ETD
mode SE
mag 840 x
HFW 493 µm
WD 12.2 mm
dwell 30 µs
spot 3.5
100 µm

Fig 3.7 SEM photographs of an etched *A. eightsii* shell showing **a)** the tip of the shell margin and **b)** the hinge plate. The position of the growth lines (gl) is indicated with arrows. The red squares indicate the regions of the detailed images shown **Fig. 3.8** and **Fig. 3.9** (highlighted in panel a and b respectively). Details of the image capture and scale bars are also provided.

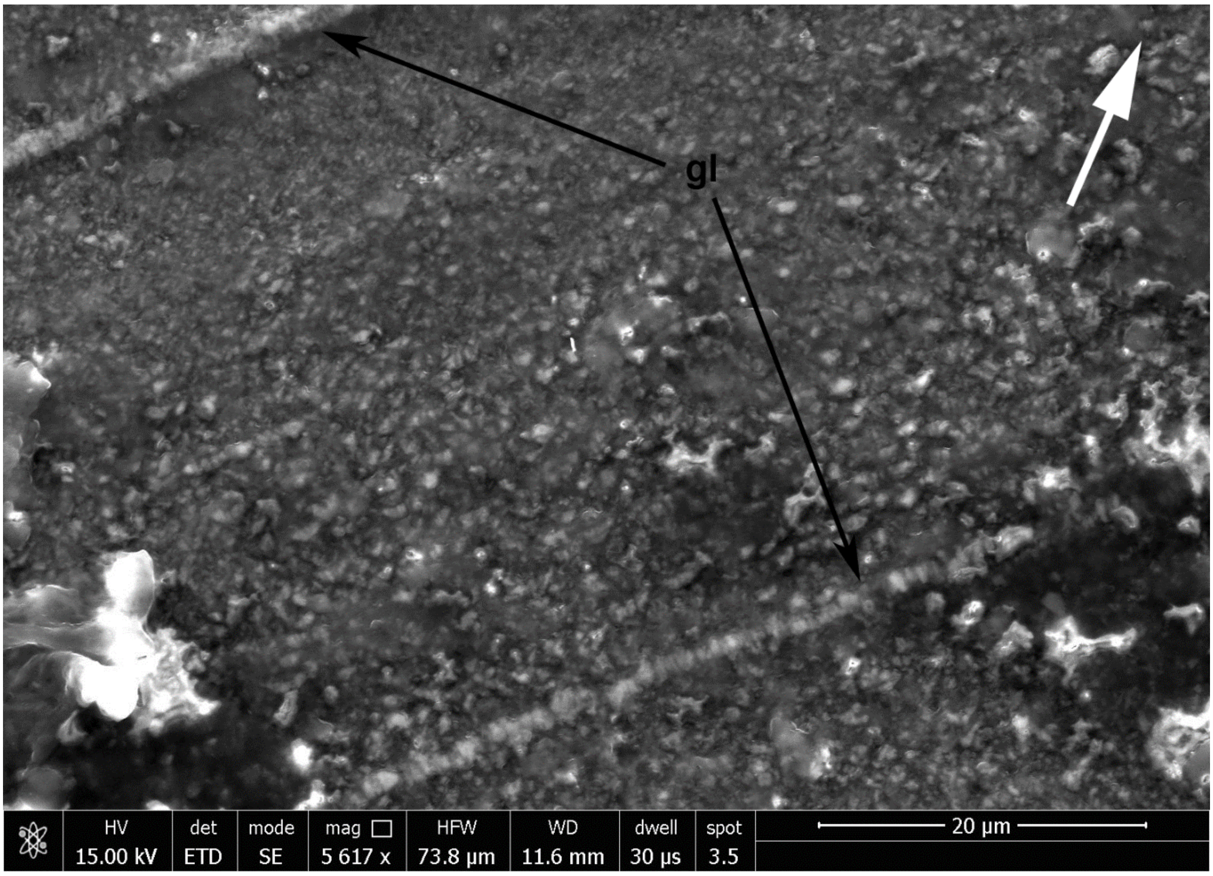

Fig. 3.8 SEM photographs of an etched *A. eightsii* shell of the tip of the margin region. Two growth lines (gl) are highlighted with black arrows. The white arrow indicates the direction of growth. Details of the image capture and scale bars are also provided.

In the ventral margin the orientation of the crystal of the growth line were tangent to the direction of growth (**Fig. 3.8**) whereas the growth increment showed crystal of globular shape of varying size (**Fig. 3.8**).

In the hinge plate region, the crystal orientation of the growth line differs from that one of the rest increment. In addition, the crystal orientation within the annually formed increments showed a zig-zag pattern (**Fig. 3.9**). The zig-zag was more visible using 15 KV although the image taken using 5 KV was sharper, mainly due to the reduced backscatter from the reduced voltage. The crystal orientation of the growth line was perpendicular to those crystals from the growth increment (**Fig. 3.9**).

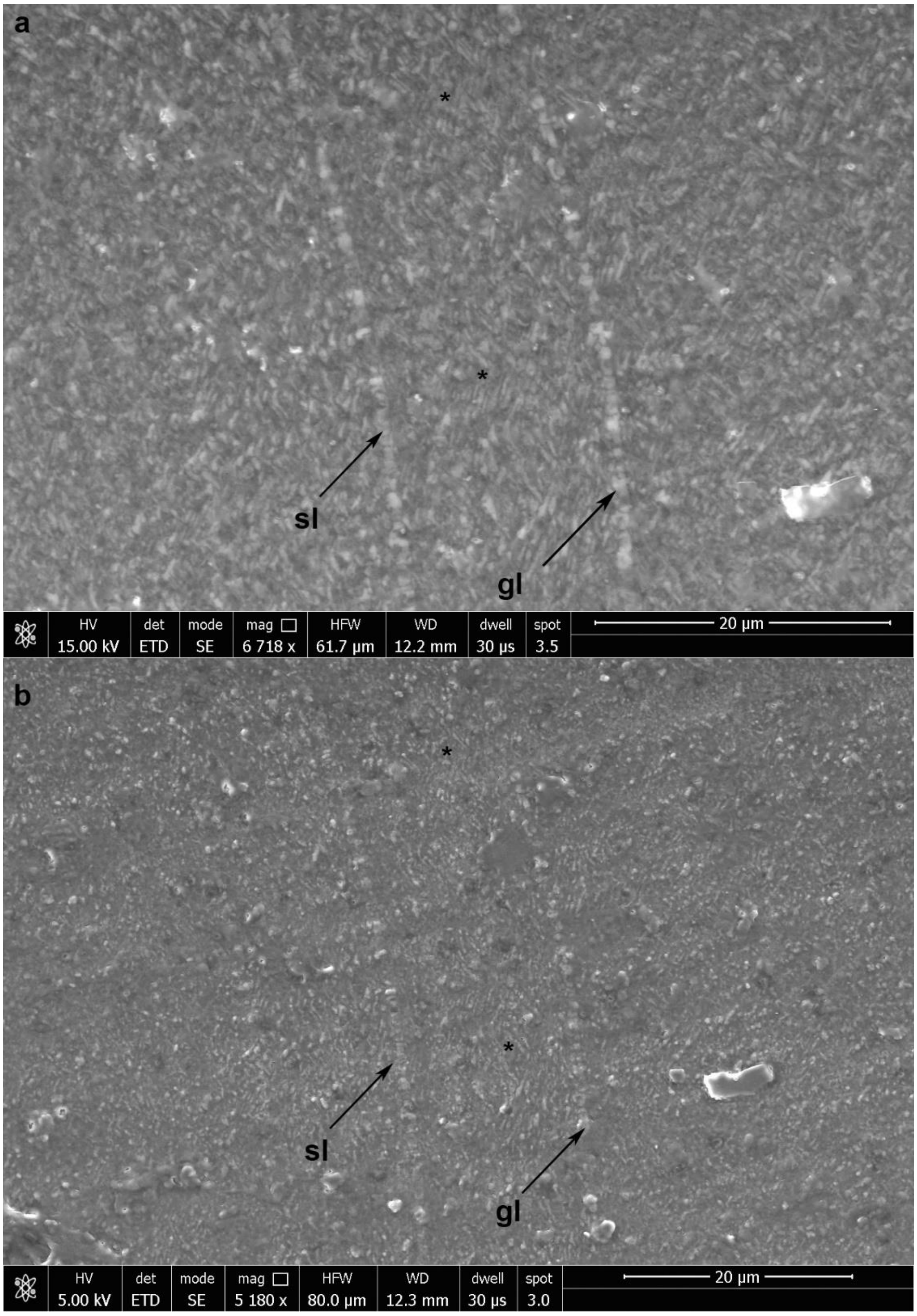
a
*
*
sl
gl
HV 15.00 kV
det ETD
mode SE
mag 6 718 x
HFW 61.7 µm
WD 12.2 mm
dwell 30 µs
spot 3.5
20 µm
b
*
*
sl
gl
HV 5.00 kV
det ETD
mode SE
mag 5 180 x
HFW 80.0 µm
WD 12.3 mm
dwell 30 µs
spot 3.0
20 µm

Fig. 3.9 SEM photographs of an etched *A. eightsii* shell in the hinge plate using different voltage **a)** 15.00 KV and **b)** 5.00 KV. A growth line (gl) and a secondary line (sl) are shown. Regions with the zig-zag pattern in the crystal structure are indicated with asterisks. Details of the image capture and scale bars are also provided.

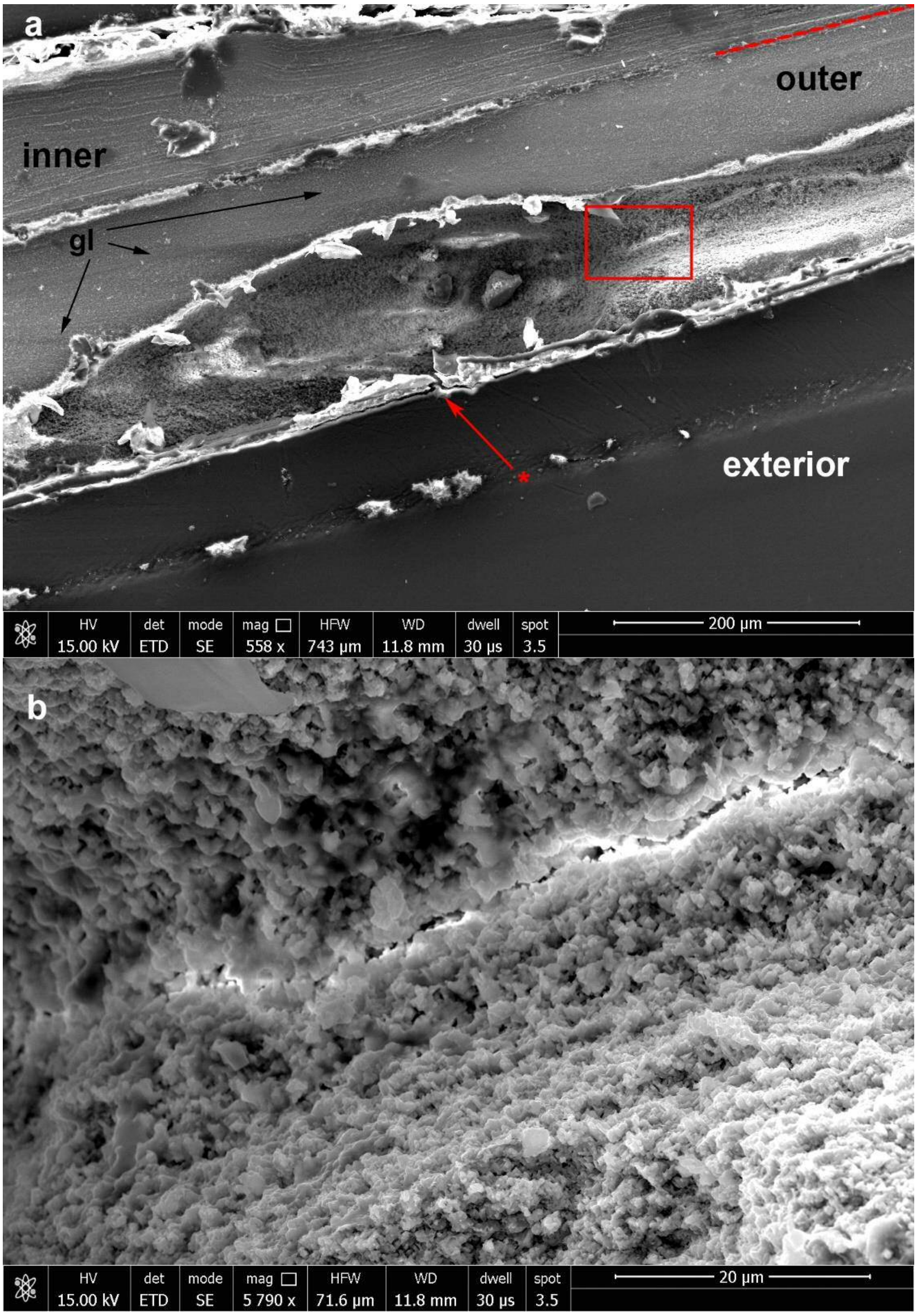
a
outer
inner
gl
exterior
*
HV
15.00 kV
det
ETD
mode
SE
mag
558 x
HFW
743 µm
WD
11.8 mm
dwell
30 µs
spot
3.5
200 µm
b
HV
15.00 kV
det
ETD
mode
SE
mag
5 790 x
HFW
71.6 µm
WD
11.8 mm
dwell
30 µs
spot
3.5
20 µm

Fig. 3.10 SEM photographs of an etched *A. eightsii* shell showing: **a)** the damage in the shell in form of a pit. The inner and outer shell layers are indicated and the separation between layers is indicated with a dashed red line. Gl indicates the position of annually-formed growth lines and the asterisk indicates the position where the periostracum is pierced. The red rectangle shows the position of the detail picture in **b)** where aragonite crystals can be observed. Details of the image capture and scale bars are also provided.

The analysis of the acetate peel replica and the polished of the specimen 21403048 showed a couple of regions with extensive shell damage (i.e. a pit within the shell) associated with periostracum damage/erosion. One of these regions was analysed using the SEM and is shown in **Fig. 3.10**. The pit in the shell, which has a longitudinal oval shape, only affects the outer shell layer and an incision in the periostracum can be observed (**Fig. 3.10a**). In **Fig. 3.10a** it can also be observed the boundary layer between the inner and the outer shell layer, a few annually-formed increments in the outer shell layer and growth lines running parallel in the inner shell layer. Closer observation of the pit showed aragonite crystals and fissures within the pit (**Fig. 3.10b**).

3.2 Ontogenetic growth trends

The longest-lived specimen was from Factory Cove and reached an ontogenetic age of 41 years, whereas the longest-live specimen from the WAP reached 21 years and was collected from South Cove (**Table 3.3**). Within the WAP location, specimens from South Cove and Back Bay were longer-lived than those from Hangar Cove (shallow or deep) although no statistical difference is present between WAP locations. No information regarding Trolval specimens is provided as it was not possible to construct a chronology and therefore age estimation is not considered reliable enough.

Table 3.3 Average longevity (in years, yr) ± standard deviation, maximum longevity (max, years) and sample size (n) for *A. eightsii* populations from the South Orkney Islands (SOI) and the west Antarctic Peninsula (WAP). AB1915: 1915 A. Bennett collection, FC: Factory Cove, SC: South Cove, HC: Hangar Cove, HC d: Hangar Cove deep, HC s: Hangar Cove shallow and BB: Back Bay.

	SOI		**WAP**				
	AB1915	**FC**	**SC**	**HC**	**HC d**	**HC s**	**BB**
Age (yr)	15 ± 5	30 ± 6	17 ± 3	14 ± 3	14 ± 3	14 ± 3	16 ±3
Max	34	41	21	20	20	18	20

n	17	20	11	16	9	7	11

The relationship between ontogenetic age and shell length for specimens collected from the SOI (1915 A. Bennett collection and 1988 Factory Cove) and from the WAP (South Cove, Hangar Cove and Back Bay) is shown in **Fig. 3.11**. Specimens from the SOI were longer-lived (one-way ANOVA, $F_{1,73} = 23.379$, $p < 0.001$, **Fig. 3.11** and **Table 3.3**) and also were slightly larger in size (Mann-Whitney U test, $U = 22813$, $p < 0.001$ and **Fig. 3.2**) than those specimens from the WAP. The WAP (South Cove, Back Bay and Hangar Cove) and the Factory Cove specimens show a positive trend between shell length and age, being slightly higher in the case of the Factory Cove specimens, whereas the AB1915 specimens show a negative trend (**Fig. 3.11**).

Further differences between the studied *A. eightsii* populations are observed when the cumulative growth curves of each population are compared (**Fig. 3.12**). All the WAP specimens and the AB1915 showed very similar ontogenetic average increment-width trends, whereas the Factory Cove specimens showed extended growth during the mid-life of the animals and a delay in the reduction of increment width with ontogenetic age (**Fig. 3.12**). No pith offset adjustment (i.e. correction for missing increments at the beginning of the series) was applied to any of the individual series, consequently the beginning of the series does not represent the true first year of life but the first measurable year of life. This means that any of the individual series (specimen specific) could be displaced along the x-axis for a number of years (± five years pers. obs.).

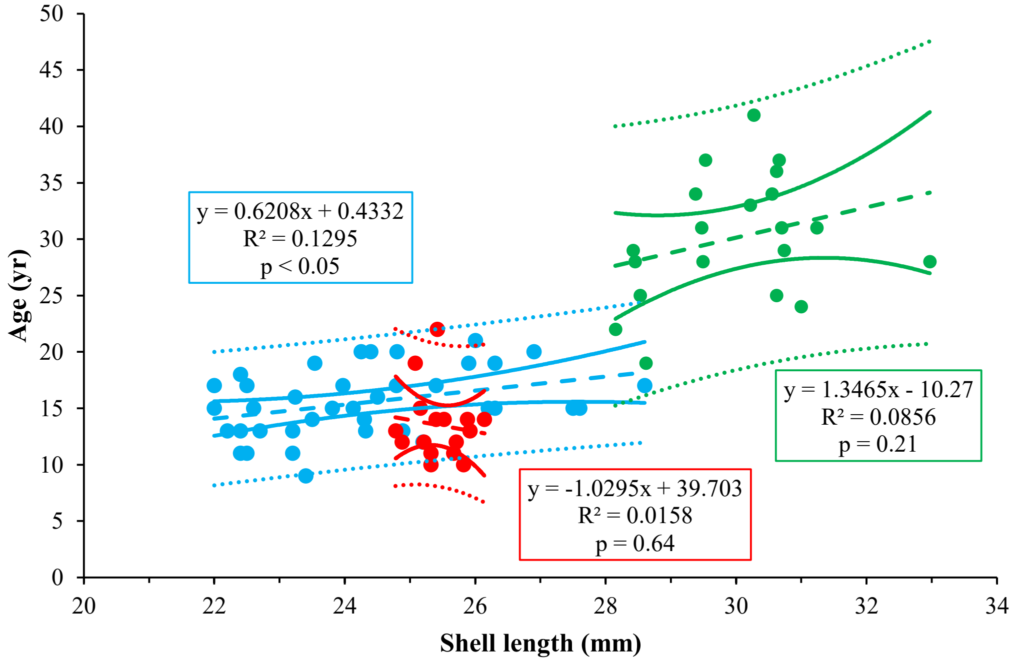

Fig. 3.11 Relationship between shell length (mm) and ontogenetic age (years) of 75 *A. eightsii* specimens from the 1915 A. Bennett collection (red), Factory Cove (green) and all sampling locations at the West Antarctic Peninsula (i.e. South Cove, Back Bay, and Hangar Cove; blue). All specimens used here were crossdated and therefore age determination considered accurate. Linear trends (dashed lines) were fitted to the data with 95 % confidence intervals (solid lines) and 95 % prediction intervals (dotted lines), equations and R^2 values are provided in the insets (colour coded).

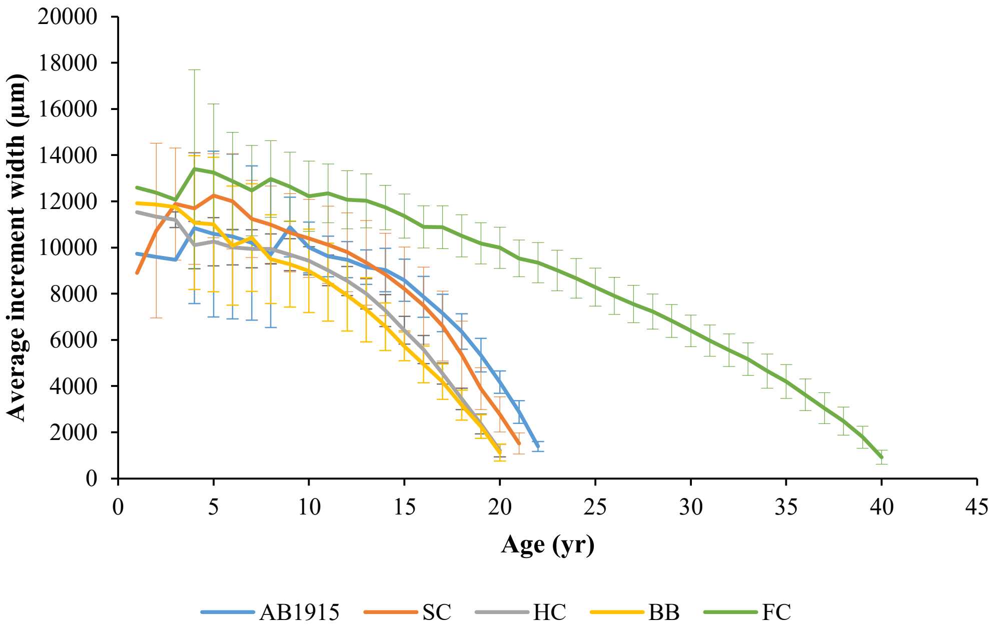

Fig. 3.12 Averaged cumulative increment width specimens from the A. Bennett 1915 collection (AB1915), South Cove (SC), Hangar Cove (HC), Back Bay (BB) and Factory Cove (FC). Error bars represent the 95 % confidence intervals of each series (colour coded).

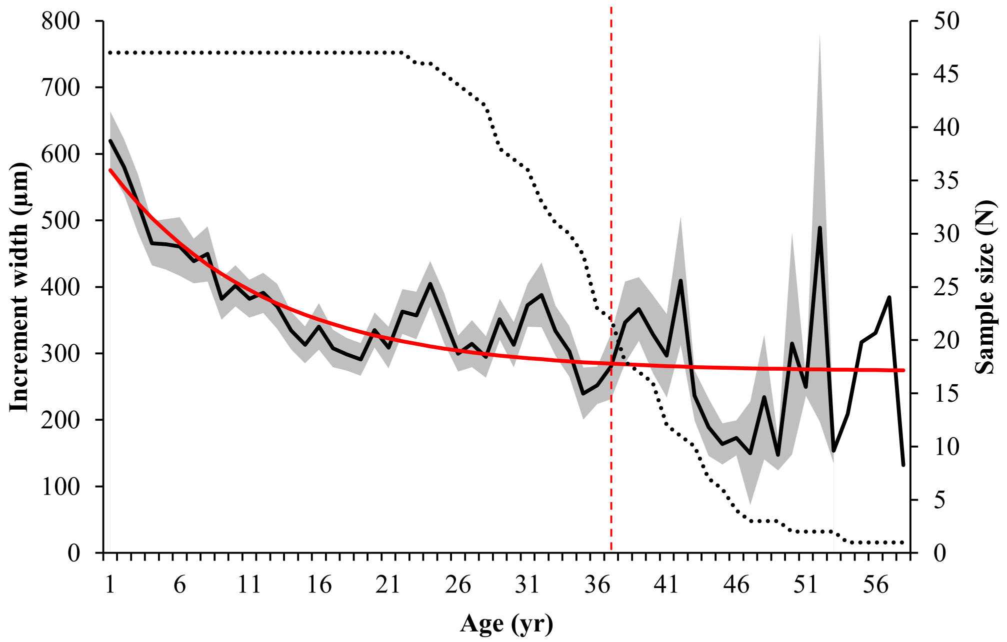

Fig. 3.13 Ontogenetic growth trend (also termed regional curve) calculated from 47 ontogenetically-aligned *A. eightsii* specimens from Factory Cove (solid black line), standard error (grey-shaded area) and the empirically calculated negative exponential function (solid red line). Sample size (dotted line, number of specimens) used to calculate the ontogenetic growth trend is also provided. The dashed red line represents the cut-off point of n = 21 (Roman-Gonzalez et al., 2016).

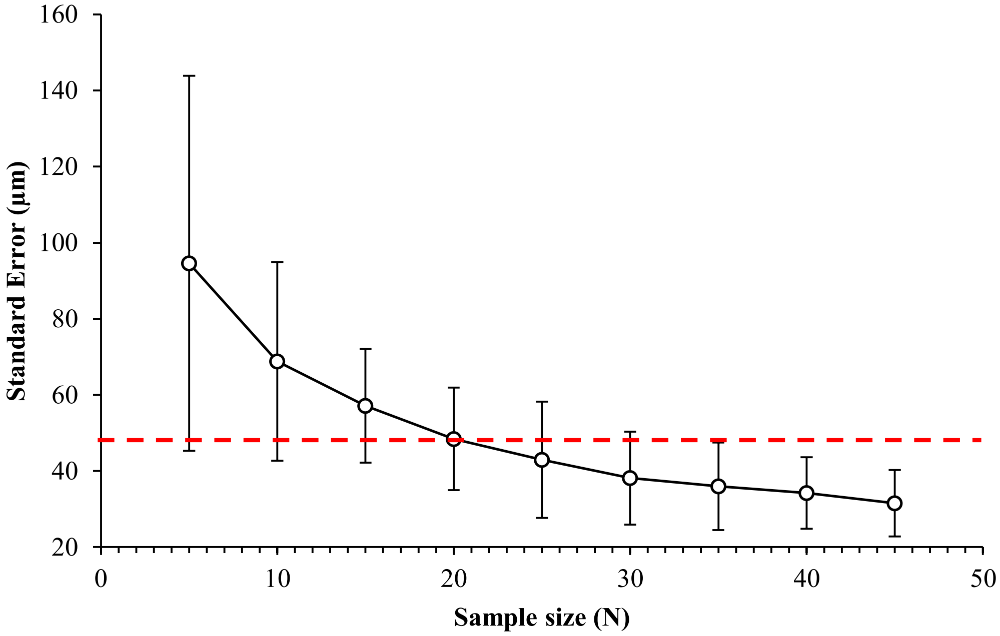

Fig. 3.14 Standard error analysis for the mean ontogenetic growth of the *A. eightsii* population in Factory Cove showing decreasing standard error (solid black line) with increasing sample size (N). The red dashed line represents 50 % of the maximum standard error. The intercept of the red dashed line with the standard error line indicates the minimum sample size (n = 21) required for further analysis. The error bars represent ± the standard deviation (Roman-Gonzalez et al., 2016).

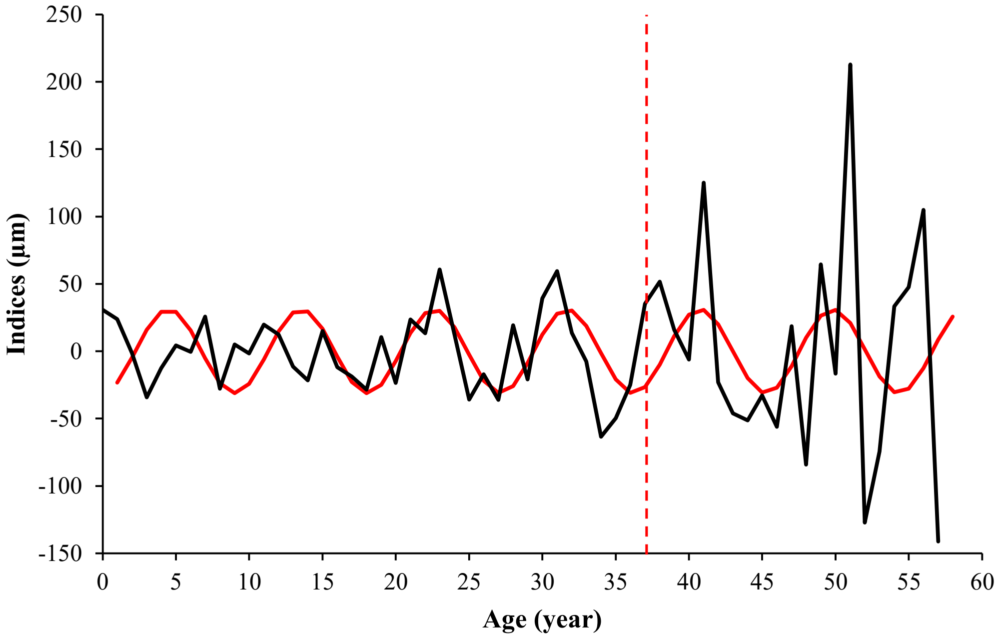

Fig. 3.15 Residuals (solid black line) after the empirically-calculated negative exponential growth curve has been removed. The red line shows the likely cyclicity based on the centre weighted and band pass filtered MTM spectral analysis. The sample depth cut-off point for stable data variability is shown with a vertical red dashed line (Roman-Gonzalez et al., 2016).

The alignment of 47 Factory Cove specimens by biological age shows that the shell growth pattern of *A. eightsii* at this site contains two ontogenetic growth patterns (**Fig. 3.13**). The following data were published in Roman-Gonzalez et al. (2016). Sample size declined rapidly after 20 years of age (**Fig. 3.13**) and only six specimens showed an age above 45 years (these specimens have not been crossdated and therefore are not included in **Table 3.3** and **Fig. 3.13**). The first trend presents a negative exponential shape typical from bivalve molluscs, in which the animal grows rapidly during the first years of age after which growth becomes progressively reduced with increasing age. The empirical negative exponential detrending curve applied to the ontogenetic growth trend is defined by the equation ($R^2 = 0.572$; **Fig. 3.13**):

(Equation 3.1)

Where *y* is increment width (µm) and *x* is age (yr). The standard error analysis shows a negative trend with increasing sample size (N, **Fig. 3.13**). The minimum number of specimens required to achieve a 50 % reduction in the standard error was 21 (**Fig. 3.14**), which corresponds to 37 ontogenetic years in **Fig. 3.13**. This sample size (n = 21) was used as a cut-off point beyond which interpretations of the growth trend should be made with caution as individual shell growth records can exert significant bias. The residual ontogenetic growth pattern (hereafter ROGP) after the negative exponential trend was removed using the empirical-calculated function is provided in **Fig. 3.15**. A secondary cyclical growth trend can be observed in the ROGP starting around 16 years of age, which presents a period of approximately 9 to 11 years (**Fig. 3.13** and **Fig. 3.15**). Three distinct cycles can be observed (centred at 24, 32 and 41-42 years of age). A possible fourth cycle may also be present (centred at 52 years of age) although this cannot be verified because of the increased variability in the growth signal resulting from reduced sample size (**Fig. 3.15**).

The multitaper spectral analysis method (MTM) shows the alignment with the cyclicity in the residuals centred at 24, 32 and 41-42 years of age (**Fig. 3.16a**). The MTM of the ROGP identified two significant frequencies $f_1 = 0.0869$ (90 % SL; $T_1 = 11.5$ years) and $f_2 = 0.4990$ (90 % SL; $T_2 = 2$ years; **Fig. 3.16b**). Although f_1 corresponds to a period within the range of the secondary ontogenetic pattern, its period does not match with that observed in the raw shell growth data, which is of around seven to nine years (**Fig. 3.13**). Therefore a more conservative approach was chosen for setting the MTM, a 15 year high pass filter (which removes any variability with a period above 15 years) was applied to the detrended shell growth series (**Fig. 3.15**) and the MTM analysis was carried out after applying more conservative settings in K Spectra (resolution = 2, number of taper = 1). The selection of a 15 year high pass filter was intended to remove low frequency variability not relevant to this study. The revised MTM analysis highlighted a single significant frequency of $f_3 = 0.1103$ years (99 % SL) corresponding to a period of $T_3 = 9.06$ years (**Fig. 3.17**).

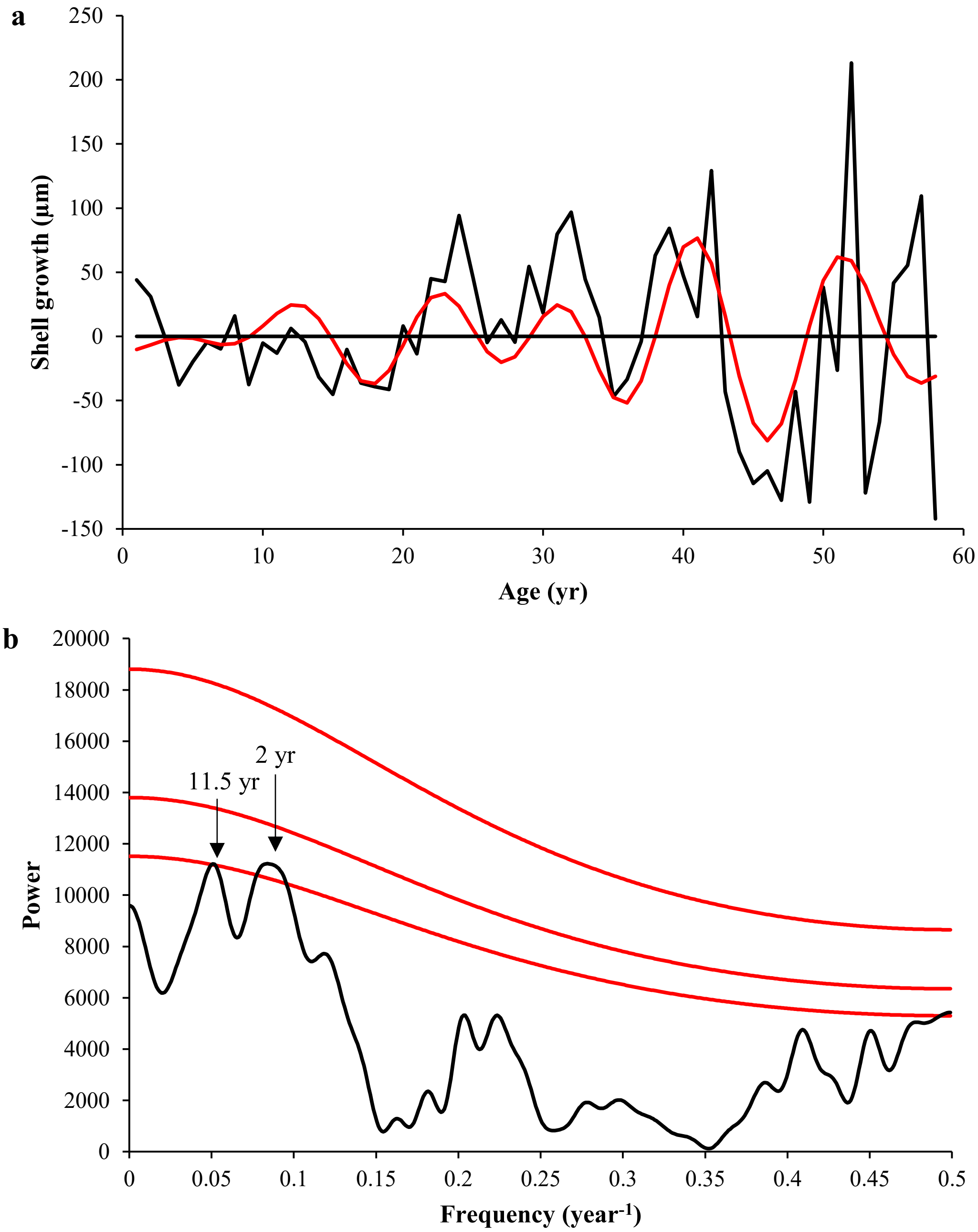

Fig. 3.16 Results of the flexible MTM analysis (K spectra resolution = 2, number of tapers = 3) without carrying a 15 year high pass filter on the negative exponential detrended growth series. All *A. eightsii* specimens collected in 1988 from Factory Cove. **a)** Negative exponential detrended growth series (black line) and most significant frequency spectrum (i.e. 11.5 yr, red line) **b)**

spectral analysis (black lines) and the confidence levels for 90 %, 95 % and 99 % (red lines, ascending order; Roman-Gonzalez et al., 2016).

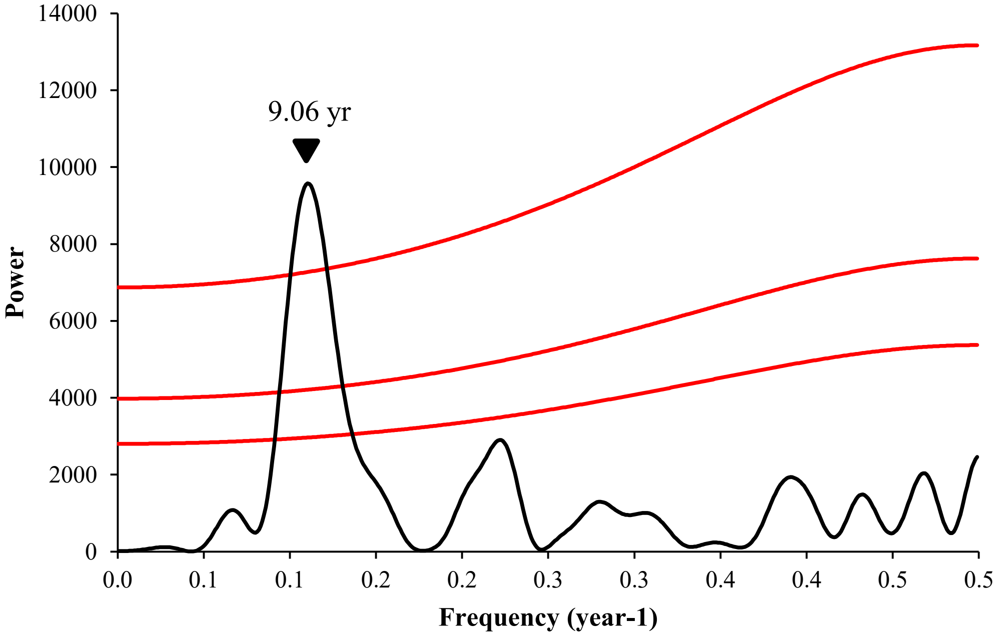

Fig. 3.17 Spectral analysis of *A. eightsii* (collected in 1988 from Factory Cove) ontogenetic growth trend using the MTM method. Spectral frequencies (solid black line), and 90 %, 95 % and 99 % significance levels (solid red lines in ascending order) are shown. The period of significant frequencies is also indicated (Roman-Gonzalez et al., 2016).

3.3 Discussion

The biometrics analyses from the different shell collections (**Fig. 3.2**) reflect the sampling strategy selected for this study, in which large adult specimens were specifically targeted explaining the lack of small, young individuals in the collection. The differences in the phenotype type between the different populations may also suggests a difference in the seabed type as it was reported that *A. eightsii* shells of the pale-yellow phenotype were more commonly found in sandy bottoms whereas the dark brown phenotype was more commonly found in muddy bottoms; however a change of colour from the pale-yellow phenotype to dark brown might be a consequence of aging

(Rabarts, 1970). The 1927 *Discovery* sample did not have an eroded umbo, it is usual that adult *A. eightsii* specimens present an eroded umbo region associated with the reburial activity, the lack of erosion (less than 5 % of the outer shell surface) in the deep-collected specimen may indicate that specimens from deep environments are less subjected to be unearthed (e.g. due to either physical disturbance or predatory attacks) than shallow inhabiting specimens. In addition to the mechanical break of the shell due to reburial activity, a component of chemical dissolution must be considered. *A. eightsii* has been reported to be one of the most sensitive Antarctic macrobenthic mollusc species to ocean acidification (McClintock et al. 2009). Current average Southern Ocean pH levels (pH = 8.48) and calcium carbonate mineral saturation state at Ryder Bay indicates a supersaturation of aragonite (Ωara. ~ 3.1), calcium carbonate polymorph of which *A. eightsii* shell is made, during austral summer months is coastal water (Jones et al. 2017). However, regions affected by intrusions of the Upper Circumpolar Deep Water (CDW) upon the shelf showed more acidic and undersaturated conditions (Jones et al. 2017). These vertical mixing episodes can pose a risk to shallow calcifying Antarctic organisms, which show an especial sensitivity to ocean acidification (McClintock et al. 2009 and references therein). The presence of protective organic layers (such as the periostracum in mollusc bivalves) against dissolution is crucial for the survival of sessile marine calcifying organisms (Tunnicliffe et al. 2009). If the shallow *A. eightsii* specimens have to rebury more often than deep-inhabiting populations, this can have deleterious consequences for the periostracum health (mechanical break) and therefore making them more susceptible to chemical shell dissolution (even though the deep inhabiting specimens live in the more undersaturated and acidic waters of the CDW).

The biometric data from the three deep-collected specimens from the *Discovery* investigations (**Fig. 3.2**) suggest a significant difference between these specimens and the rest of specimens from all sampling locations. Although the cause of this shell elongation (**Fig. 3.2**) is still unknown, several possible explanations can be hypothesised: i) there is a difference in shell formation with depth ii) the different shell shape from the deep-collected specimens from the *Discovery* investigations is an adaptation to a deep environment and iii) the deep-collected specimens from the *Discovery* investigations are from a different and undescribed deep Antarctic *Aequiyoldia* species. Eurybathy is a particular characteristic of many Antarctic benthic species (Brey et al., 1996), although some believed eurybathic species may be actually species complexes rather than a single species (Held and Waegele, 2005). Since this is the only study carried on using the *Discovery* specimens, it is difficult to determine which of the suggested hypotheses might be true. In order to assess the influence of depth (pressure) on shell formation (i.e. hypothesis i) several specimens could be caged and placed at increasing water depth; another option would be the study in a laboratory with pressure aquarium-chambers where environmental conditions could be controlled. Alternatively, specimens could also be collected across different water depths at the same location. Assessing whether the deep-collected *Discovery* specimens belong to a different undescribed *Aequiyoldia* species (i.e. hypothesis iii) or they belong to *A. eightsii* although displaying a different phenotype, further genetic analysis could be carried out in the soft tissues preserved in the Natural History Museum in London and compared to the genome of modern-collected *A. eightsii* (available at Bangor University).

Comparison between the data shown in **Fig. 3.11** and **Fig. 3.12** further highlights differences in shell growth between the different *A. eightsii* populations. Whereas **Fig. 3.11** shows that Factory Cove specimens are larger and ontogenetically older than AB1915 and the WAP specimens, **Fig. 3.12** shows that Factory Cove specimens have an extended growth during mid-life. In addition, the AB1915 specimens showed very similar average ontogenetic increment-width curve to WAP specimens (**Fig. 3.12**) and also due to the narrow shell length distribution AB1915 specimens with age (**Fig. 3.11**); it is likely that the negative trend between shell length and age of the AB1915 (**Fig. 3.11**) is an statistical artefact caused by the lack of a wider range in shell length from the AB1915 specimens. The difference in maximum lifespan between populations is likely due to sampling bias, as selected large specimens were specifically targeted for collection at Factory Cove whereas little is known about the collection of the AB1915 (**Fig. 3.2** and **Fig. 3.11**). However, it is also important to consider stress responses to environmental processes and how these can affect longevity (Abele and Philipp, 2013).

The origin of orange spots under the periostracum (**Fig. 3.3**) of *A. eightsii* shells is still unclear and requires further investigation. The nature of the spots (circular with a deeper central section) could be interpreted as unsuccessful predatory attacks to the individuals, especially during the first years of growth (where most of the spots concentrate) when the individual may be more vulnerable due to the fragility of the shell. It is common that mollusc bivalve species (e.g. *Arctica islandica*, *Glycymeris glycymeris*, *Laternula elliptica, A. eightsii*) show signs of predatory attacks during the early stages of life when they are more vulnerable (e.g. Ramsay et al., 2000; Harper and Peck, 2003; Peck et al., 2004; Ridgway and Richardson, 2010). Another possible explanation is that the orange spots are due to the action of endolithic algae (personally observed in the Antarctic limpet *Nacella concinna*; Roman-Gonzalez, 2011) or chemical dissolution which dissolves and/or make more vulnerable the calcareous part of the shell (e.g. Cerrano et al., 2001). Based on visual observation of the polished sectioned valves, the carbonate around the spots has an amorphous appearance (**Fig. 3.4**), which might suggest some degree of remineralization. The SEM picture of a pit where the periostracum was pierced shows signs of chemical dissolution of the aragonite crystals in the out shell layer (**Fi. 3.10**). This example could be a more developed stage of the orange spots (**Fig. 3.4 and Fig. 3.5**) and would point physical chemical dissolution of the shell as an explanation for these features. As indicated previously, marine calcifying organisms are affected by increasing ocean acidification (McClintock et al., 2009; Gazeau et al., 2013), most of Antarctic coastal regions are expected to reach aragonite undersaturation in the near future (McNeil and Matear, 2008; Gutt et al., 2015) with some areas already showing some degree of seasonal aragonite undersaturation (Jones et al., 2017). The integrity of the external organic layer covering the carbonate parts of the shell, i.e. periostracum, is a shield against chemical dissolution. Lack of large wandering predators, such as crabs, in the Antarctic coastal ecosystems has most likely help in the conservation of a healthy, unpierced periostracum in mollusc bivalves; especially in thin-shelled shallow burrowers such as *A. eightsii*. Associated with warming trends, there is a trend in retreating glacier and ice-sheets systems which in turn are expected to export more icebergs into the Antarctic coastal areas (e.g. Barnes and Souster, 2011; Gutt et al., 2015 Cook et al., 2016). The increasing iceberg scouring of soft bottom could result not only in the crushing of the sea bottom dwellers but also in an increased occurrence of damage periostracum in marine molluscs, which then would be more vulnerable ocean acidification. The dominant position of the orange dots in the mid part of the shell also agrees with this theory. The frequent burrowing activity of *A. eightsii* rapidly degrades the periostracum at the umbo region, this facilitates the shell dissolution and mechanical breakdown of the carbonates creating extensive shell damage, as seen the majority of adult specimens. Whereas random damage of the periostracum at the mid portion of the shell over the years causes the orange dots. The lack of orange dots closer to the shell margin can be explain as there has been not enough time to for these random periostracum-damaging events to occur.

The results concerning the ontogenetic growth rhythm of *A. eightsii* presented in this chapter have been published by Roman-Gonzalez et al. (2017) and compared with another common Antarctic marine mollusc bivalve (i.e. *L. elliptica*). Endogenous shell growth rhythms are innate variations of growth within an individual independent of external environmental factors. These endogenous rhythms can be caused by cyclical innate variations in resource allocation to growth and probably reflect trade-offs between growth and other energetic life history requirements (e.g. Bayne and Newell, 1983; Richardson, 1988; Shumway and Parsons, 2006; Abele and Philipp, 2013). One possible explanation for the innate growth rhythm in *A. eightsii* may be related to spawning events during its life history. Shell growth can be limited as a result of the preferential allocation of energy resources to developing gonads and the production of gametes (Bayne and Newell, 1983; Shumway and Parsons, 2006). Spawning in *A. eightsii* may be constrained by the available resources needed for gametogenesis and finally spawning to occur. In many marine benthic species spawning occurs annually providing that energy resources have been accrued. In *A. eightsii* the accumulation of sufficient resources for spawning to occur may take several years and this might be manifested in innate rhythmic changes in shell growth. Extended gametogenic phases in Antarctic species have been reported for several phyla, which can take from two to five times longer than in temperate species (reviewed in Peck et al., 2006). The initiation of this cyclicity coincides the onset of maturity (i.e. between 12 and 17 years of age) in *A. eightsii*, reported for the same sampling location (i.e. Factory Cove; Nolan and Clarke, 1993; Peck et al., 2000). Nolan and Clarke (1993) reported the *A. eightsii* population at Signy Island to have a wide range in age although recruitment may be sporadic in areas of high adult density. Peck et al. (2000) reports a personal observation by J.G. Colman in which animals showed gonad development at around 13 mm of shell length and they were considered fully mature at around 20 mm of shell length. Since the specimens used in our study were all over 28 mm in shell length and can be therefore considered fully mature and therefore the ROGP should be observable in all of them. For future studies, it would be interesting to select specimens of 13 mm and 20 mm in shell length and investigate the number of cycles of the ROGP present in the shell record. However, the process of resource reallocation during gametogenesis seems to be species-specific in that some species (i.e. *Ruditapes decussatus*) show significant shell growth during periods of active gametogenesis (e.g. Urrutia et al., 1999) whereas others (including: *Argopecten irradians*, *Notovola meridionalis* and *Patinopecten yessoensis*) show none (Shumway and Parson 2006). A recent study comparing growth rhythms in *A. eightsii* and *L. elliptica*, also a common Antarctic bivalve species, showed that a conservative MTM analysis (as reported here for *A. eightsii,* **Fig. 3.15** and **Fig. 3.17**) on *L. elliptica* regional curve, constructed using 250 specimens, presented two significant periodicities at 5 and 6.6 years (Roman-Gonzalez et al., 2017); however the cause of these periodicities is still unknown. Resource limitation has been suggested to be a major factor dictating marine animal adaptations and life history characteristics in Antarctica (Clarke, 1988; Clarke and Peck, 1991). This has been used to explain the seasonal decoupling of shell growth and body mass increase in the Antarctic brachiopod *Liothyrella uva* (Peck et al., 1997). As a result of the seasonally scarce and intermittent food supply and the strong inter-annual variability of phytoplankton blooms, it may take several years for *A. eightsii* to accumulate sufficient resources to undergo a successful gamete production. This also relates to the hypothesis suggested by Peck et al. (2000) regarding the decoupling between shell growth and tissue mass growth in juvenile *A. eightsii* specimens: i) shell and tissue growth were decoupled with shell growth remaining constant throughout the year and tissue growth being limited to the austral summer when energetic resources are available and ii) shell and tissue growth are not decoupled and are constant throughout the year in which there is a production of storage compounds used for tissue growth during the austral winter. If it is confirmed that the ROGP relates to gamete production, then shell and tissue growth coupling would be much more closely related than expected surpassing seasonality in the environmental parameters. The developmental strategy in which several years are needed in order to undergo gamete production successfully is not unheard of, with species such as the Arctic Woolly Bear Caterpillar (*Gynaephora groenlandica*; Wocker, 1874) requiring between 7 and 14 years of resource stocking in order to undergo metamorphosis, with long periods of diapause during the Arctic winter (Kukal et al., 1988; Morewood and Ring, 1998). As the basal energetic budget of *A. eightsii* remains unknown and little information is available about *A. eightsii* reproductive cycle is, it is still not possible to test this hypothesis.

Due to the short length of the *A. eightsii* increment growth time series the results of the MTM have to be interpreted cautiously (**Fig. 3.15** and **Fig. 3.17**). Ghil et al. (2002) suggested that the significance levels (SL) have to be about 1-(1/N), which in the case of the *A. eightsii* time series SL is 0.98, so the significant frequencies of the MTM are not due to statistical chance. Although there is some degree of uncertainty in the spectral data mainly due to the short length of the series, the internal growth rhythm is still obvious in the raw growth increment series (**Fig. 3.13**). The analysis carried out to determine the error associated with no pith offset correction suggests that internal growth rhythm is still significant even when no pith offset correction was applied (**Fig. 3.18**) for at least a ± five year offset, which is what is expected in *A. eightsii* due to umbo erosion. The conservative MTM analysis (**Fig. 3.17**) did find a significant frequency f_{Y3} (T_{Y3} = 9.06 years, 99 % confidence interval), which complies with this criterion of being at a significance level of at least 98 %. On the other hand, the more flexible MTM (**Fig. 3.16b**) did highlight two periodicities (T_{Y1} = 11.5 years and T_{Y2} = 2 years) at lower significance level (90 % confidence interval). Therefore the 15 year high pass filter and the more conservative settings in the MTM analysis seem to have removed some of the variability highlighted by the flexible MTM. The periodicity highlighted by the conservative MTM (T_{Y3} = 9.06 years) coincides with the period of the rhythm observed in the growth increment series (24, 32 and 41 and 52 ontogenetic years; **Fig. 3.15** and **Fig. 3.17**); this indicates that the results provided in the conservative MTM are more robust than those from the flexible MTM. Regarding the shorter periodicity T_{Y2} = 2 years (flexible MTM, **Fig. 3.16**), this periodicity is probably due to high frequency variability in the data and was not even highlighted by the conservative MTM. Cook et al. (1995) discussed the relationship between series length and signal detection as “the segment-length curse”, the authors stated that the maximum possible fluctuation detectable is limited in theory by the maximum length of series and in a more pragmatic way by a third of the length of the series. The *A. eightsii* growth series analysed here is 57 years long and therefore the maximum detectable fluctuation is approximately 19 years and even if the series is limited to the cut-off point of 37 years the maximum detectable fluctuation is approximately 12 years; this indicates that the period T_{y3} = 9.06 years detected by the conservative MTM analysis is within sound statistical limits.

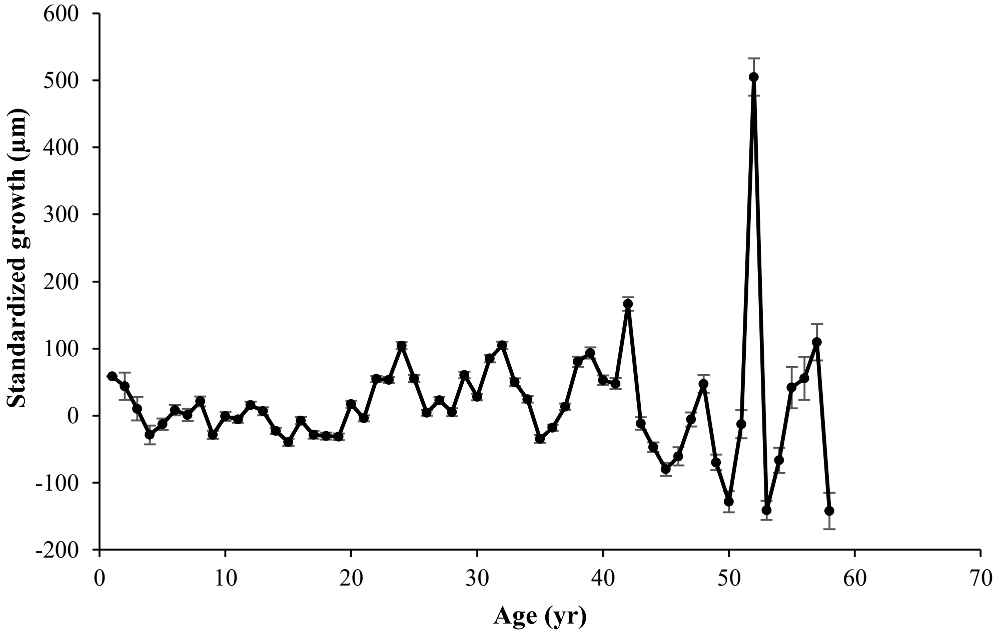

Fig. 3.18 Standardized shell growth of *A. eightsii* (black line) after negative exponential detrending was applied. Error bars represent the standard error. The standard error plotted for *Y. eightsi* was calculated from the 30 offset growth series. Note that for the case of *A. eightsii* the internal rhythm is still present even when the error is considered.

In terms of population dynamics these innate growth rhythms should not, in theory, represent a handicap (i.e. a period of slow growth in the regional ontogenetic growth pattern, ROGP, in a year of abundant resources) if the population receives sufficient recruitments each year. This seems to be the case with the *A. eightsii* population at Factory Cove (Peck and Bullough, 1993a), although Nolan and Clarke (1993) demonstrated sporadic *A. eightsii* recruitment at Signy Island. In addition Peck and Bullough (1993) suggested the possibility of density-dependent control on recruitment based on the low abundance of young individuals in the presence of adults. A normally distributed population, in terms of age class, would be able to take advantage of plentiful years, with some of the individuals (those at the low growth part of the cycle) allocating resources towards gametogenesis and others (those at the rapid growth part of the cycle) allocating resources towards somatic growth.

These ontogenetic cycles are important not only for their biological relevance but also for other research fields such as the development of sclerochronological archives based on annually-resolved growth increments measured in the shells of marine bivalves (e.g. Butler et al., 2009). Sclerochronological analysis uses growth patterns in carbonate structures of molluscs as a proxy for environmental/climatological parameters (with shell growth shown to be dependent on parameters such as food availability or water temperature (e.g. Reynolds et al., 2013; Schöne, 2013; Bušelić et al., 2015), and as a chronological template for geochemical analysis. Detrending methods are a crucial part of dendrochronological and sclerochronological studies, since they remove low frequency trends (i.e. biological and climatological) and aim to preserve the underlying high frequency external environmental component present in the growth of these organisms. The ontogenetic deviations from the mean observed in *A. eightsii* (**Fig. 3.13**) were not expected and are not removed by the standard use of negative exponential detrending. Although the selection of the cut-off point for stable data variability (**Fig. 3.14**) was made as a subjective compromise between series length and data variability, this is not necessarily optimal. The reduced number of long-lived specimens of *A. eightsii* remains a limiting factor in developing robust shell growth series; the addition of few (ten specimens should be sufficient) long-lived (between 40 and 50 years of age) *A. eightsii* specimens to the current analysis should, in theory, reduce significantly the error associated to the regional curve in the latter part of the curve (i.e. above the cut-off point; **Fig. 3.13**) and should also provide a confirmation of the possible cycles centred at 41-42 and 52 years of age.

Chapter IV: Instrumental records

This chapter presents the analyses from the instrumental datasets acquired from the Rothera time series (RaTS) programme (i.e. seawater temperature, chlorophyll, salinity and fast-ice duration). A comparison between seawater salinity and $\delta^{18}O_{water}$, historical instrumental time series from the South Orkney Islands (i.e. seawater temperature, chlorophyll, salinity and fast-ice duration) and long-term climatic indices (i.e. Southern Annular Mode, SAM and El Niño Southern Oscillation, ENSO) are also presented.

While the instrumental data series presented in this chapter were not collected specifically for the PhD programme (c.f. Clarke et al., 1988; Clarke et al., 2008; Meredith et al., 2004, 2010; Murphy et al., 1995; Rayner et al., 2003; Venables et al., 2013, 2014) the analysis of the data presented in this thesis is novel, unless where clearly stated. Understanding the background information of the environmental conditions that the records provide for the period covered by the shell growth records (i.e. calibration period) is key to determine the drivers of shell growth formation and shell geochemistry.

Specific hypotheses tested in this chapter are: i) Long term climatic trend (e.g. warming) can be detected in the instrumental data, ii) the instrumental data series possess interannual variability, iii) there is a variability in the instrumental series with depth, iv) the different parameters from the data series covary together (e.g. water salinity *vs* sea ice production) and v) major climate processes, such as SAM and ENSO, have an impact in the variability of physical characteristics (e.g. seawater temperature, sea ice production) of the studied regions.

4.1 Rothera time series instrumental record

4.1.1 Seawater temperature

Monthly seawater temperature values between 1998 and 2016 across different averaged water depths are presented in **Fig. 4.1**. The interannual variability present during the summer (December-April) is much greater (1.23 °C range) than during winter (July-September, 0.26 °C range). Note that measurements from August to November 2000 and September to October 2001 are missing, due to adverse weather conditions which prevented data collection and due to an instrumental fire respectively (Venables and Meredith, 2014, **Fig. 4.1**). As expected, during the austral summer season (December-April) more heat is stored in surface waters (e.g. -0.09 °C ± 0.35 SD average for the upper 15 m) relative to when deeper waters are considered (e.g. -0.48 °C ± 0.24 SD for the upper 100 m); this increased thermal stratification seen within the depth averaged temperature time series which shows lower temperature values with increasing water depth (**Fig. 4.1**). This pattern reverses during the austral winter season when more heat is stored in the deeper waters (e.g. -1.29 °C ± 0.19 SD for the upper 100 m) than in surface waters (e.g. -1.59 °C ± 0.07 SD for the upper 15 m, **Fig. 4.1**).

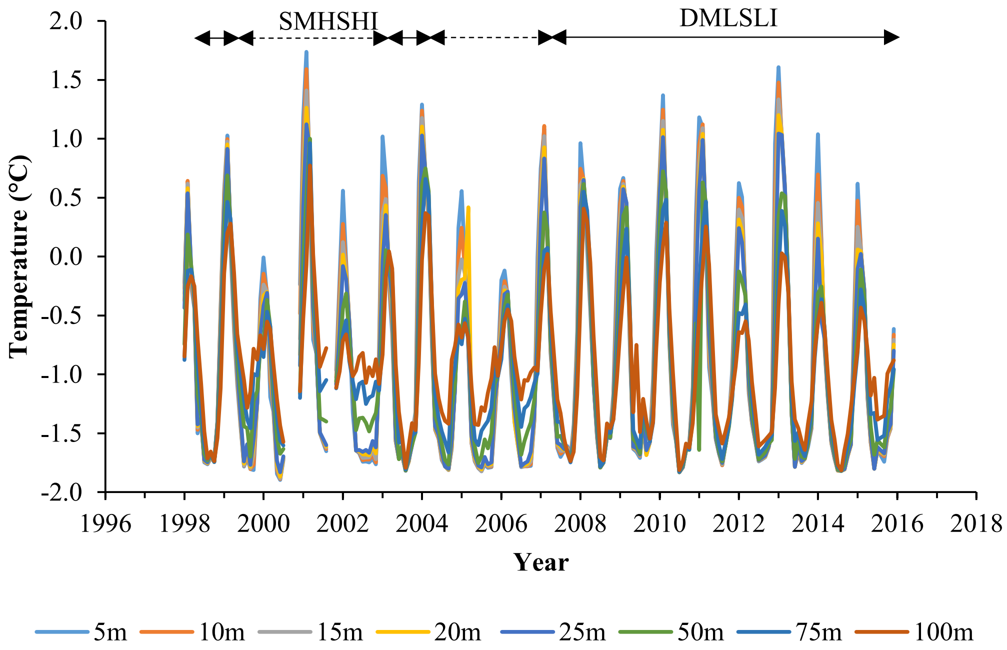

Fig. 4.1 Monthly seawater temperature (°C) averaged over sequential water depths (upper 5 m, upper 10 m, upper 15 m, upper 20 m, upper 25 m, upper 50 m, upper 75 m and upper 100 m) from the RaTS programme between 1998 and 2016. Note the missing values for the winter season 2000 and 2001. The periods of deep mixing (as indicated in Venables and Meredith, 2014), low stratification and low sea-ice concentration (DMLSLI) are indicated with solid double pointed arrows, and periods of shallow mixing, high stratification and high sea-ice concentration (SMHSHI) are indicated with dashed double pointed arrows.

Annual (August-July) averaged seawater temperature profiles averaged over sequential water depths between 1998 and 2014 are shown in **Fig. 4.2**. The profiles up to the upper 25 m profile show a high degree of similarity although there is a slight trend towards lower temperature with depth, in some years there is a more marked differentiation (e.g. 0.05 °C range during 2010 *versus* 0.16 °C range during 2014) in this negative (cooler) temperature trend with depth (**Fig. 4.2**). A clear change in trends is observed in 2007 in the deep averaged profiles (i.e. upper 75 m and upper 100 m, **Fig. 4.2**). Prior to 2007 (with the exception of 2004) the deep average profiles show higher temperature than shallower profiles (i.e. up to the upper 50 m profile, **Fig. 4.2** and **Fig. 4.4**). After 2007, the deep average profiles show lower temperature values than the shallower profiles (**Fig. 4.2** and **Fig. 4.4**). In addition, prior to 2007 the upper 50 m profile seems to be more similar to shallower profiles whereas after 2007 the upper 50 m profile shows an increasing difference with shallower profiles and more similarity with deeper profiles. During 2015 the upper 100 m temperature profile shows higher temperature relative to the other shallower temperature profiles (**Fig. 4.2**). Another notable feature of the annually averaged temperature record is a marked cooling event during 2004/05, which shows a maximum difference in the upper 25 m profile of -0.41 °C becoming subsequently less strong with water depth (-0.15 °C in the upper 100 m profile, **Fig.4.2**). A similar cooling event is observed during 2013/14 with a maximum cooling of -0.42 °C in the upper 25 m profile and the temperature range also decreasing with depth (-0.17 °C in the upper 100 m profile, **Fig. 4.2**). Seawater temperature trends over the entire length of the record vary depending on the temperature profile considered (**Fig. 4.3a**), whereas surface profiles (i.e. up to the upper 25 m profile) show a warming trend over the 1999/2015 period; profiles considering deeper waters (i.e. from the upper 50 m profile) show a cooling trend, which becomes more intense with depth, over the same the same period. However, only the top 100 m trends for the annual and for the core winter average seawater temperature are statistically significant (**Fig. 4.3**), which suggest a winter control of the average annual seawater temperature for the top 100 m of the water column.

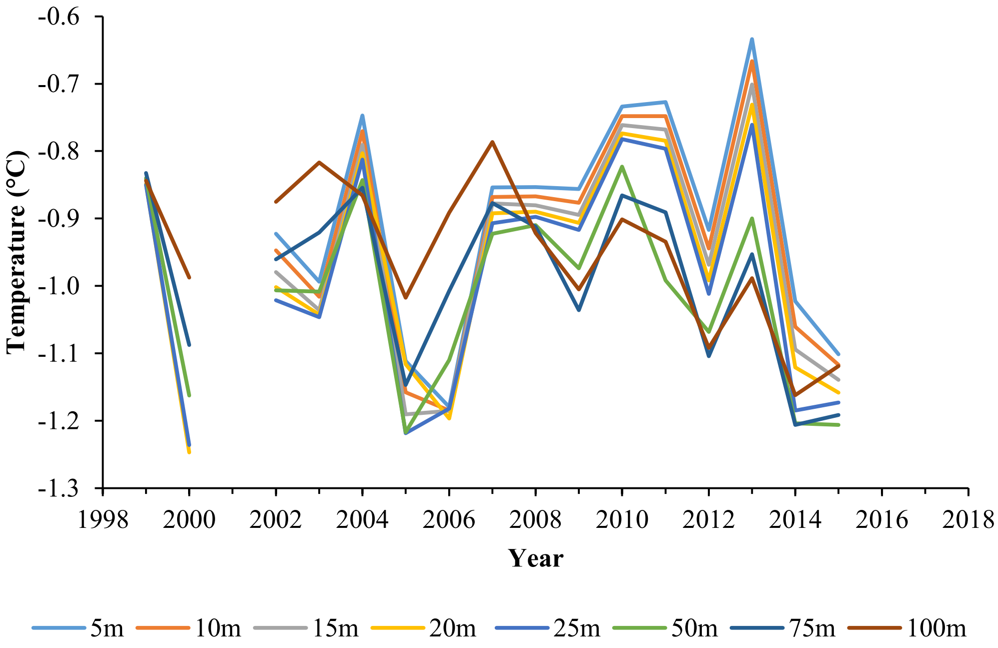

Fig. 4.2 Annual (August-July) averaged seawater temperature (°C) averaged over sequential water depths (upper 5 m, upper 10 m, upper 15 m, upper 20 m, upper 25 m, upper 50 m, upper 75 m and upper 100 m) from the RaTS programme between 1999 and 2015. Values for the 1999/2001 period are not given due to missing winter measurements in the dataset that could bias the record towards warmer temperature.

Annual depth temperature profiles between 1999 and 2015 are provided in **Fig. 4.4**. Two different types of profiles are observed: 1) linear decrease of temperature with depth (e.g. 2008, 2010 in **Fig. 4.4**) and 2) a decrease of temperature with depth that stabilising to subsequently rise again with increasing depth. The depth at which the temperature trend changes, shows some degree of interannual variability (51 m ± 24 m water depth, **Fig. 4.4**). Temperature variability at surface (1 m water depth) was -0.47 °C ± 1.15 SD decreasing subsequently with depth: -0.85 °C ± 0.66 SD at 50 m water depth and -0.75 °C ± 0.49 SD at 100 m water depth. Note that the 2002 profile (**Fig. 4.4**) is biased, as there are no instrumental data available from the September to October 2001.

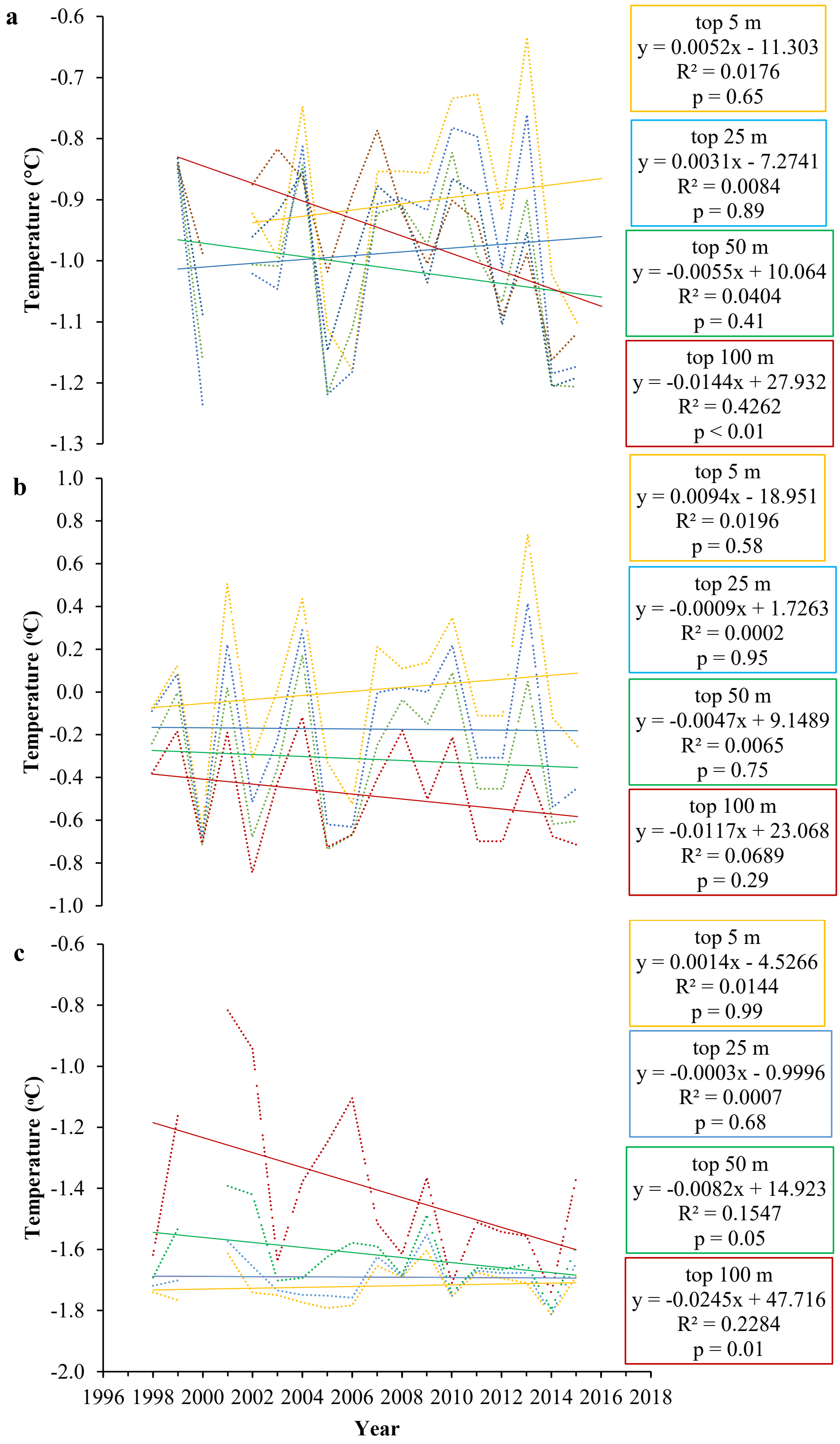
a
-0.6
-0.7
-0.8
-0.9
-1.0
-1.1
-1.2
-1.3
Temperature (°C)
top 5 m
y = 0.0052x - 11.303
R² = 0.0176
p = 0.65
top 25 m
y = 0.0031x - 7.2741
R² = 0.0084
p = 0.89
top 50 m
y = -0.0055x + 10.064
R² = 0.0404
p = 0.41
top 100 m
y = -0.0144x + 27.932
R² = 0.4262
p < 0.01
b
1.0
0.8
0.6
0.4
0.2
0.0
-0.2
-0.4
-0.6
-0.8
-1.0
Temperature (ºC)
top 5 m
y = 0.0094x - 18.951
R² = 0.0196
p = 0.58
top 25 m
y = -0.0009x + 1.7263
R² = 0.0002
p = 0.95
top 50 m
y = -0.0047x + 9.1489
R² = 0.0065
p = 0.75
top 100 m
y = -0.0117x + 23.068
R² = 0.0689
p = 0.29
c
-0.6
-0.8
-1.0
-1.2
-1.4
-1.6
-1.8
-2.0
Temperature (ºC)
top 5 m
y = 0.0014x - 4.5266
R² = 0.0144
p = 0.99
top 25 m
y = -0.0003x - 0.9996
R² = 0.0007
p = 0.68
top 50 m
y = -0.0082x + 14.923
R² = 0.1547
p = 0.05
top 100 m
y = -0.0245x + 47.716
R² = 0.2284
p = 0.01
1996 1998 2000 2002 2004 2006 2008 2010 2012 2014 2016 2018
Year

Fig. 4.3 a) Annually (August-July) averaged seawater temperature profiles (dotted lines) **b)** annually averaged summer (December-April) seawater temperature profiles (dotted lines) and **c)** annually averaged core winter (July-September) seawater temperature profiles (dotted lines) over sequential water depths (upper 5 m yellow, upper 25 m blue, upper 50 m green and upper 100 m red) from the RaTS sampling point, Linear trends are also shown, the regression equation and the R^2 values are shown in the insets, which are also colour coded.

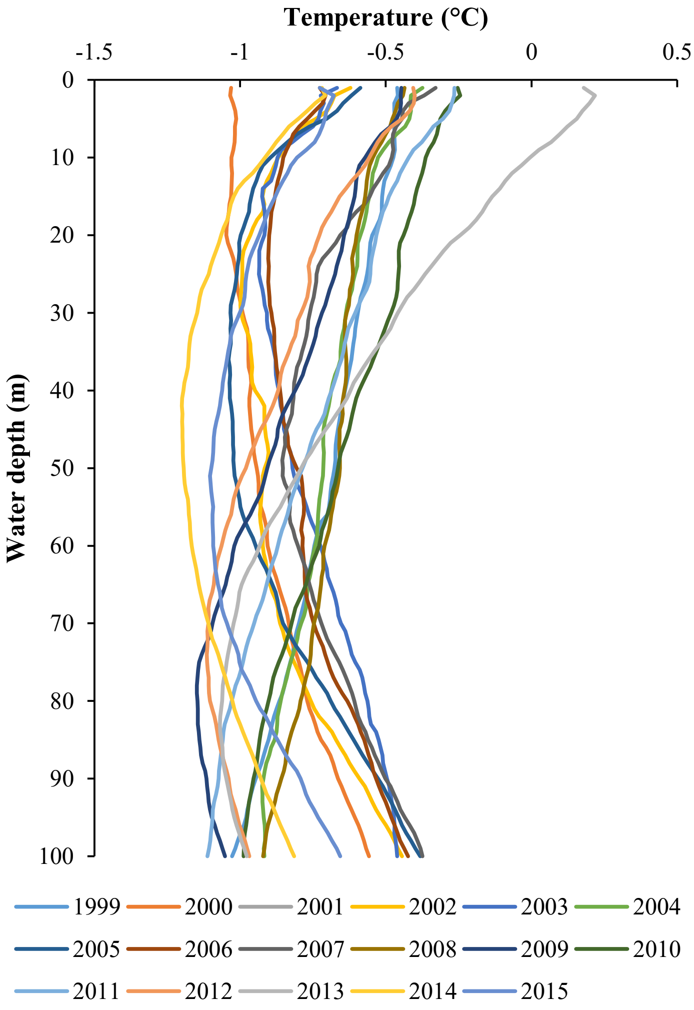

Fig. 4.4 Annual (August-July) averaged temperature (°C) profiles from 1 m to 100 m water depth between 1998 and 2015 at the RaTS site, Ryder Bay. Note that some years (e.g. 1999, 2001 and 2013) temperature starts to steadily increase below around 40-50 m. Note that 2001 is excluded as there were missing winter measurements between August and November 2000 that biased the profile towards warmer temperature.

The annually averaged summer (December-April) seawater temperature records are shown in **Fig. 4.5**. The general trend in the record is warm surface waters that cool with water depth with a few exceptions (e.g. 2000, 2005 and 2014) when mid depth profiles (i.e. upper 50 m and upper 75 m) showed lower temperatures than the upper 100 m profile (**Fig. 4.5**). A high degree of interannual variability is observed between warm summer (e.g. 2001, 2004, 2013) and cold summer temperatures (e.g. 2000, 2002, 2005, 2006, 2014). Years with warm summers show higher thermal stratification (cooling trend, e.g. 0.7 °C range in 2001) with water depth in comparison to years with cold summers (e.g. 0.09 °C range in 2000) when the top 100 m of the water column was much more homogeneous. Again a change of pattern is observed in 2007; prior to 2007 the summer water column shows a high degree of homogeneity, although the cooling trend with depth is present (0.9 °C range on average between 1998 and 2007), whereas after 2007 the cooling trend with depth becomes much more obvious (1.46 °C range between 2008 and 2015; **Fig. 4.5**). No significant trend was found in the average summer (December-April) seawater temperature record for any of the sequentially averaged water depths (**Fig. 4.3b**). On the contrary, this trend reverses with depth with deeper averaged temperature profiles showing a cooling trend which becomes stronger with depth (**Fig. 4.3b**).

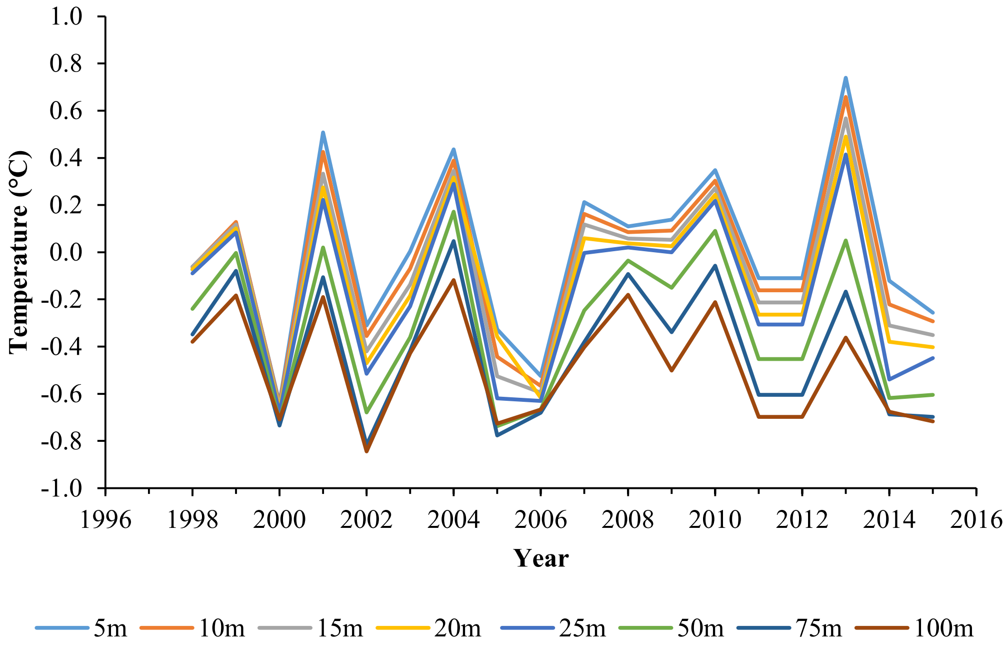

Fig. 4.5 Summer (December-April) seawater temperature (°C) averaged over sequential water depths (upper 5 m, upper 10 m, upper 15 m, upper 20 m, upper 25 m, upper 50 m, upper 75 m and upper 100 m) from the RaTS programme between 1998 and 2016.

The core winter (July-September) temperatures record is shown in **Fig. 4.6**. Core winter temperatures show a marked difference between shallow profiles (i.e. up to the upper 25 m profile) and deep averaged profiles (i.e. from the upper 50 m profile). A warming trend with water depth is present in the entire length of the record although this is highly variable. Frequent alternating episodes of warming/cooling throughout the entire upper 100 m are observed (**Fig. 4.6**); these episodes are mostly multiannual, taking between three and six years from minimum to minimum temperature. Similar to what was reported for the average annual record and the annually averaged summer record, prior to 2007 the water column exhibits a much higher degree of variability (0.98 ^{o}C range between 1998 and 2006) with water depth whereas after 2007 depth profiles show a higher degree of homogeneity (0.45 ^{o}C range between 2007/15) through the upper 100 m of the water column (**Fig. 4.6**). The averaged core winter temperature for 2000 and 2001 are not provided as there is no temperature data available for the periods August-November of 2000 and October-November of 2001 and their inclusion could bias the average towards higher temperature. Long trends in the data show that during the core winter (July-September) surface waters were not affected by any significant warming (**Fig. 4.3c**). However, a negative temperature trend is present in deeper averaged temperature profiles principally modulated by the decreasing intensity of the deep warming episodes.

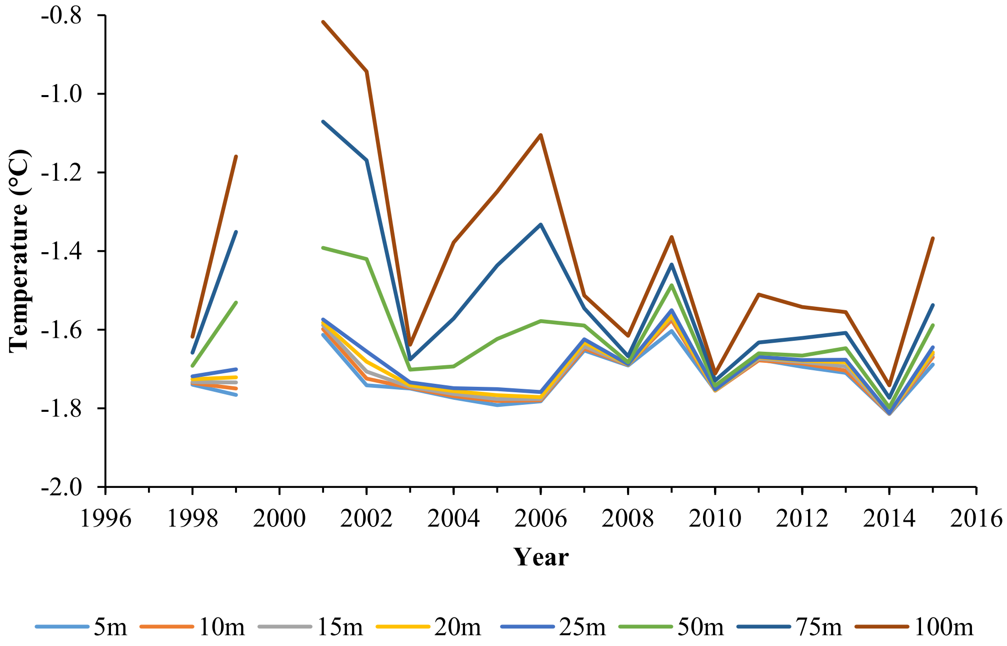

Fig. 4.6 Core winter (July-September) temperature (°C) averaged over sequential water depths (upper 5 m, upper 10 m, upper 15 m, upper 20 m, upper 25 m, upper 50 m, upper 75 m and upper 100 m) from the RaTS programme between 1998 and 2015. Values for 2000 and 2001 were not calculated as major gaps in the instrumental record could have introduced biases in the calculation of the averages. Note the significant departure of temperatures in the upper 50 m, upper 75 m and upper 100 m profiles when compared to the upper 25 m of water prior to 2007. After 2007 the upper 100 m is much more homogeneous, indicating enhanced deep mixing.

Comparing average summer (December-April) seawater temperature (**Fig. 4.5**) and average core winter (July-September) seawater temperature (**Fig. 4.6**), an increase in the seawater heat content during warm summers does not translate into an increase of the seawater heat content during the winter ($r = 0.06$, $R^2 = 0.004$, $p = 0.81$, $n = 17$). In addition, some years characterised by cold summers (e.g. 2002, 2005, 2015; **Fig. 4.5**) showed a high degree of temperature stratification during the following (core) winter (**Fig. 4.6**); this apparent contradiction indicates an alternative source of heat preferentially affects the deeper portions of the water column. This becomes more obvious in 2006, in summer the water column shows a high degree of homogenization in the top 100 m with low temperature values (**Fig. 4.5**); however, in the following winter a high degree of stratification is apparent with shallower layers of the water column presenting the lowest temperature values (**Fig. 4.6**).

Comparing average summer (December-April) seawater temperature (**Fig. 4.5**) and average core winter (July-September) seawater temperature (**Fig. 4.6**) with average annual (August-July) seawater temperature (**Fig. 4.2**), the summer temperature shows a positive correlation with annual temperature ($r = 0.87$, $R^2 = 0.75$, $p \geq 0.01$, $n = 16$) whereas the core winter temperature did not ($r = 0.02$, $R^2 \leq 0.001$, $p = 0.94$, $n = 15$).

Comparing annually averaged summer and core winter temperatures after 2007 an inverse relationship is observed in the behaviour of the depth profiles; whereas during summer, temperature started to change much more rapidly with depth (**Fig. 4.5**), during winter, temperature depth profiles became much more homogeneous (**Fig. 4.6**). The opposite behaviour occurred prior to 2007. In addition when the upper 100 m water depth annual, summer and core winter profiles are considered together, it is seen that the cooling trend observed in the annual profile is due to winter cooling and not to summer cooling.

A comparison between the seawater temperature measurements at 15 m and at 25 m water depth with the upper 15 m and upper 25 m averaged series is provided in **Fig. 4.7**. It is noted that the annual (August-July) averages do not differ significantly (one-way ANOVA, $F_{1,31} = 0.18$, $p = 0.89$ for the 15 m *vs.* upper 15 m records and $F_{1,31} = 0.01$, $p = 0.92$ for the 25 m *vs.* upper 25 m records) as well as for summer (one-way ANOVA, $F_{1,34} = 0.69$, $p = 0.41$ for the 15 m *vs.* upper 15 m records and $F_{1,34} = 1.20$, $p = 0.28$ for the 25 m *vs.* upper 25 m records), winter (one-way ANOVA, $F_{1,32} = 1.13$, $p = 0.30$ for the 15 m *vs.* upper 15 m records and $F_{1,32} = 3.78$ $p = 0.06$ for the 25 m *vs.* upper 25 m records), and core winter (one-way ANOVA, $F_{1,32} = 0.46$, $p = 0.50$ for the 15 m *vs.* upper 15 m records) and only more significant differences are found for the comparison of the core winter temperatures for the 25 m *vs.* upper 25 m records (one-way ANOVA, $F_{1,32} = 3.08$ $p = 0.09$).

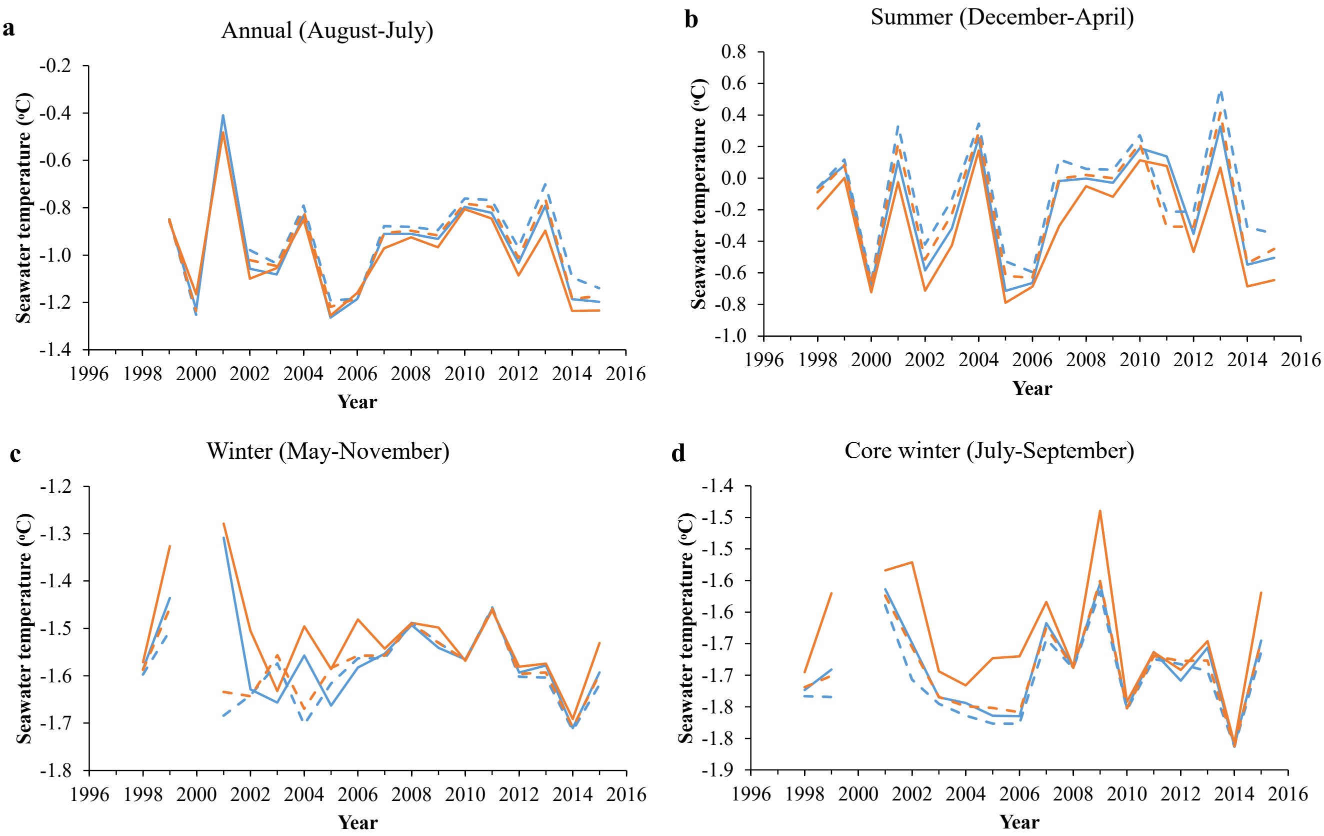

Fig. 4.7 Comparison seawater temperature variability between measurements at 15 m water depth (solid blue line) and at 25 m water depth (solid orange line) with the seawater temperature variability for the upper 15 m of the water column (dashed blue line) and for the upper 25 m of the water column (dashed orange) averaged for **a)** August-July (annual average), **b)** December-April (summer average), **c)** May-November (winter average) and **d)** July-September (core winter average) between 1998 and 2015 for the RaTS sampling site.

4.1.2 Salinity

Monthly salinity values between 1998 and 2016 are presented in **Fig. 4.8**. Note the missing winter measurements for 2000/01 and 2001/02. Annually (August-July) averaged salinity record between 1999 and 2015 is shown in **Fig. 4.9**. The general trend in the salinity record is increasing salinity values with water depth. The most obvious feature of the salinity record is the freshening between 2004 and 2006 down to 100 m water depth (**Fig. 4.9**); this freshening trend was followed by a period of increasing salinity between 2006 and 2008. From 2008 a period of mixing of the upper 100 m of the water column is observed (salinity range 0.32 psu for 1999/2007 and 0.15 psu for the period 2008/10); further stratification in the salinity profiles with depth is observed after 2010 (salinity range 0.24 psu for the period 2011/15; **Fig. 4.9**). The phase of increased mixing that occurred between 2008 and 2010 was due to an increased salinity across the upper 100 m of the water column significantly affecting surface waters (< 50 m water depth). The average salinity for the upper 5 m of the water column was 33.36 between 1999 and 2007 and 33.58 psu between 2008 and 2010 (difference of 0.22), whereas when considering the upper 100 m the difference was smaller (33.65 psu between 1999 and 2007 and 33.73 psu between 2008 and 2010, 0.08 psu in difference). These changes in salinity do not appear to be associated with changes in any particular season but rather due to process that acted throughout the year (**Fig. 4.10**).

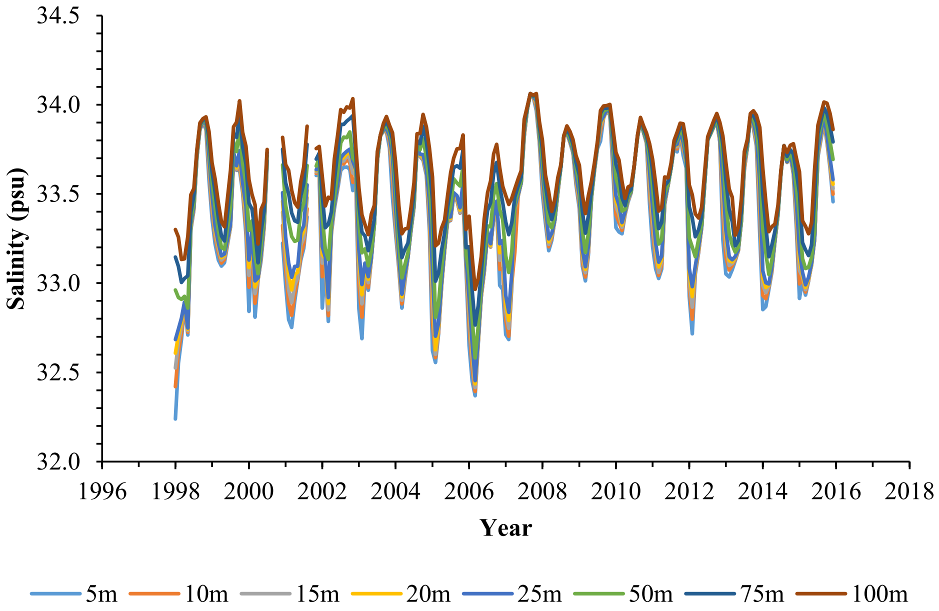

Fig. 4.8 Monthly salinity averaged over sequential water depths (upper 5 m, upper 10 m, upper 15 m, upper 20 m, upper 25 m, upper 50 m, upper 75 m and upper 100 m) from the RaTS programme between 1998 and 2016. Note the missing values for the winter season 2000 and 2001.

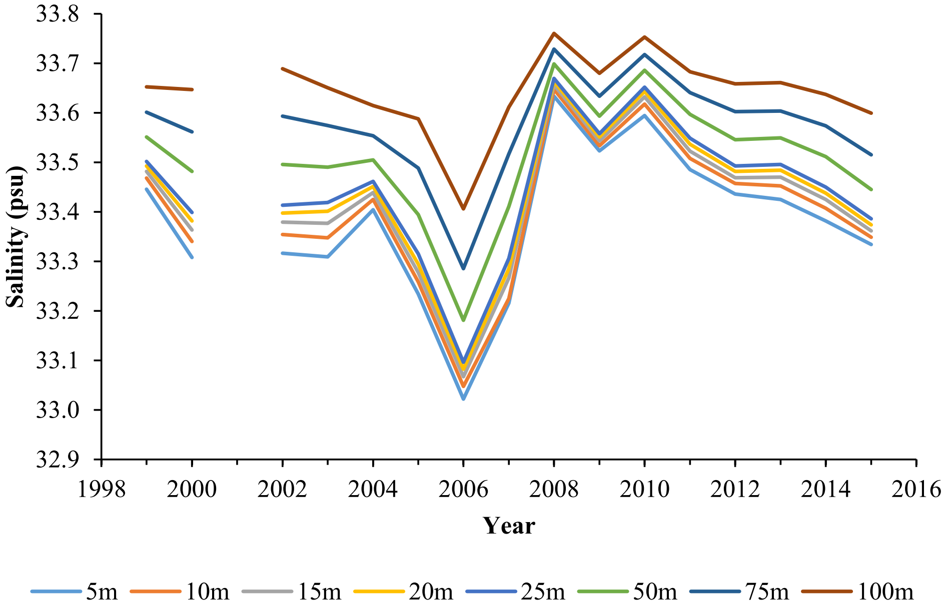

Fig. 4.9 Annually (August-July) averaged salinity averaged over sequential water depths (upper 5 m, upper 10 m, upper 15 m, upper 20 m, upper 25 m, upper 50 m, upper 75 m and upper 100 m) from the RaTS programme between 1999 and 2015. Note that the 2001 value is not shown as no data are available between August and November 2000 and averages calculated provide a biased low salinity value. In addition 2002 values are somewhat biased towards a lower salinity as the values from September and October 2001 are missing.

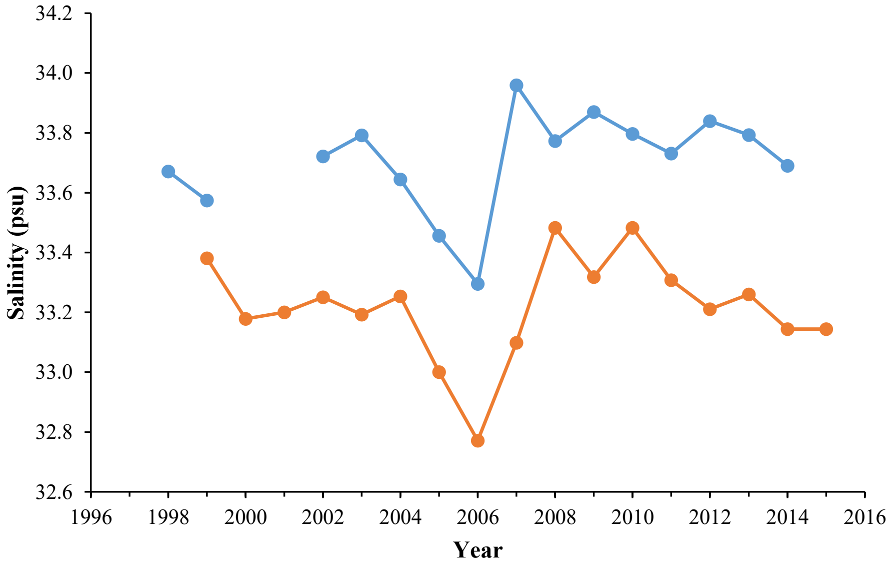

Fig. 4.10 Salinity profiles for the upper 25 m of the water column at the RaTS site, Rothera for summer (December-April, orange line) and for core winter (July-September, blue line) between 1998 and 2015.

Depth salinity profiles between 1999 and 2015 down to 100 m water depth are shown in **Fig. 4.11**. Surface waters present a much higher interannual variability (0.90 psu for the upper 10 m) than deeper waters (0.28 psu between 90 m and 100 m). An anomalous year, as already shown in **Fig. 4.9**, is 2006 that shows a much fresher profile almost down to 100 m water depth (**Fig. 4.11**). Note that the 2001 and 2002 depth salinity profiles are somewhat biased towards lower salinity since the measurements from August to November 2000 and September to October 2000 are missing. The 2001 profile shows a departure towards fresher salinity values, especially in the first 10-20 m of the water column, which are likely to be due to the missing measurements (**Fig. 4.11**).

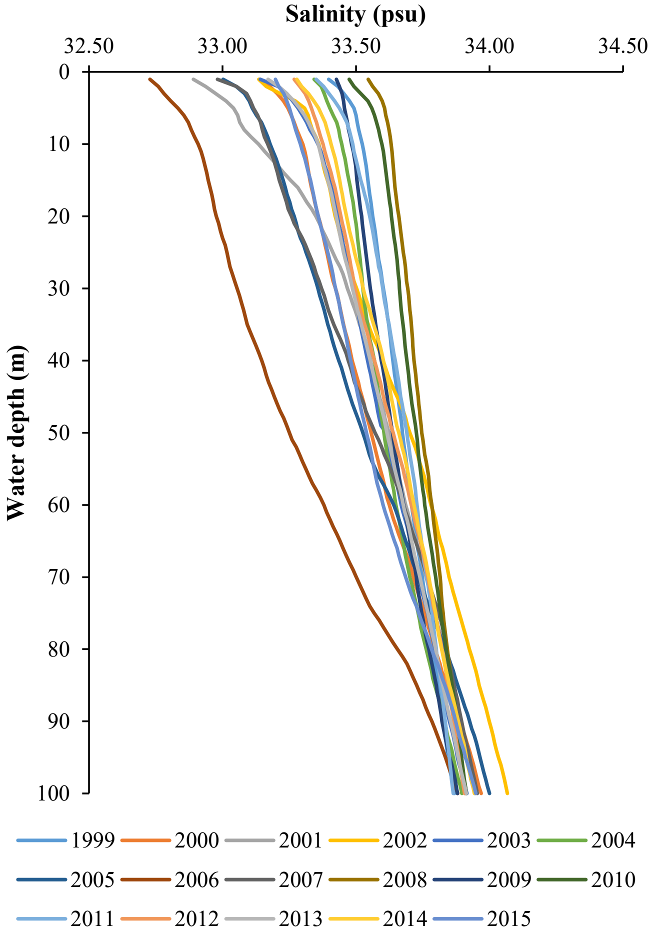

Fig. 4.11 Annual (August-July) averaged salinity profiles from 1 m to 100 m water depth between 1999 and 2015 at the RaTS site, Ryder Bay.

When comparing the salinity data with the temperature data, it can be observed that the onset of the freshening period between 2004 and 2006 (**Fig. 4.9**) coincided with rising temperatures across the upper 100 m of the water column in 2004 (**Fig. 4.2**). Subsequently between 2005 and 2006 seawater temperature dropped, especially in surface waters (< 75 m water depth; **Fig. 4.2**), although this did not translate into increased salinity as freshening continued with salinity reaching the lowest level on record in 2006 (**Fig. 4.9**).

4.1.3 Chlorophyll

Monthly chlorophyll concentrations between 1998 and 2016 across different averaged water depths are presented in **Fig. 4.12**. There are no data available for the periods: August-November 2000 and for September-October 2001; these months encompass the end of the winter season and the beginning of the seasonal productivity peak associated with the spring phytoplankton bloom; therefore, annual averages for these years are likely to be biased towards stronger bloom conditions. A decrease in chlorophyll concentration with water depth is observed for the entire record (**Fig. 4.12**).

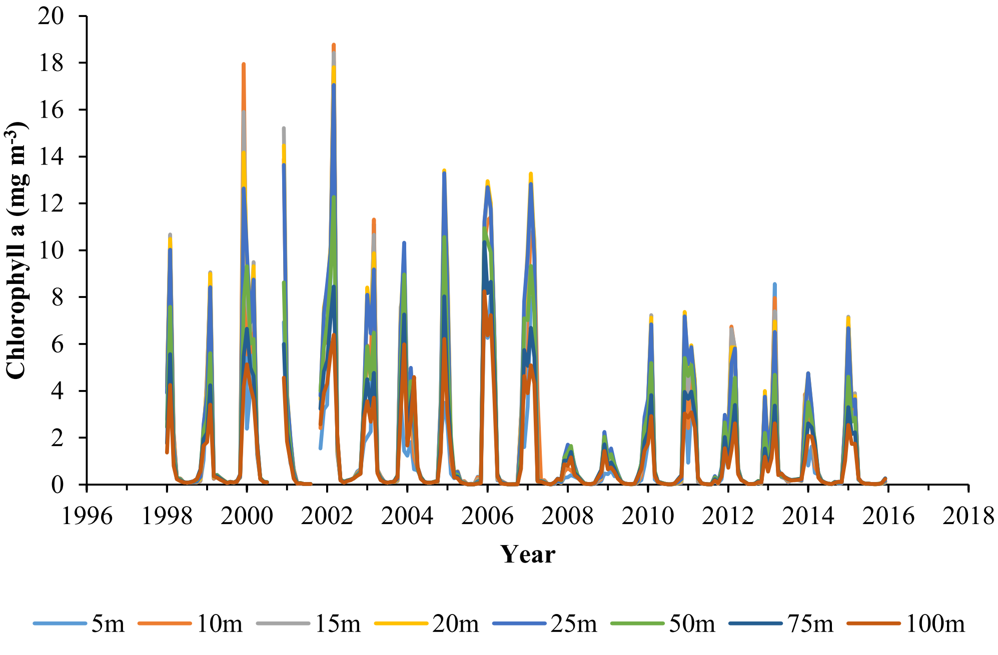

Fig. 4.12 Monthly chlorophyll (mg m^{-3}) averaged over sequential water depths (upper 5 m, upper 10 m, upper 15 m, upper 20 m, upper 25 m, upper 50 m, upper 75 m and upper 100 m) from the RaTS programme between 1998 and 2016. Note the missing values for the winter season 2000 and 2001.

One of the most remarkable features of the chlorophyll record is the marked seasonality of the phytoplankton bloom, compared to extended blooms from lower latitudes. During the summer (December-April) high chlorophyll concentration (4.66 mg m^{-3} ± 5.57 SD averaged over the upper 25 m of the water column) was present, whereas very low chlorophyll concentration levels (0.08 mg m^{-3} ± 0.08 SD averaged over the upper 25 m of the water column) were present during the winter (July-September). The record shows that the peak of chlorophyll concentration typically occurs during February (1998, 1999, 2003 and 2005/08), although earlier chlorophyll peaks (2000/01, 2004, 2010, 2013 in December and 2014 in January) and later chlorophyll peaks (2002, 2011/12 in March) are also recorded. The chlorophyll concentration also shows large interannual variability (**Fig. 4.12**); during 2007/08 an almost total collapse of the standing crop was recorded and this low chlorophyll level continued into the 2008/09 season.

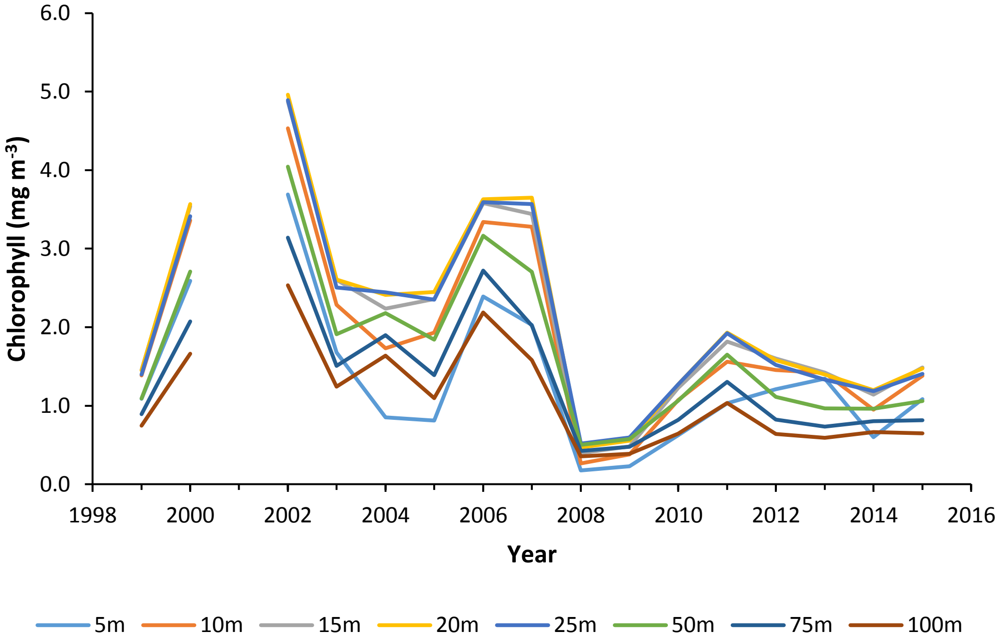

Fig. 4.13 Annual (August-July) averaged chlorophyll concentration (mg m^{-3}) averaged over sequential water depths (upper 5 m, upper 10 m, upper 15 m, upper 20 m, upper 25 m, upper 50 m, upper 75 m and upper 100 m) from the RaTS programme between 1999 and 2015. Note that the 2001 value is not shown as it could be biased towards higher chlorophyll concentration as no data are available between August and November 2000. In addition 2002 values are somewhat biased towards a higher chlorophyll concentration as the values from September and October 2001 are missing.

Annually (August-July) averaged chlorophyll concentration records between 1999 and 2015 are shown in **Fig. 4.13**. Most of the phytoplankton concentrates in the upper 25 m of the water column decreasing into shallower and deeper water. Another important feature in the chlorophyll concentration records is the collapse of the standing crops in 2007/08 (**Fig. 4.12** and **Fig. 4.13**). This collapse marks a transition from high chlorophyll levels prior to 2007, on average 2.25 mg m^{-3} between 1998 and 2006, to low chlorophyll levels after 2007, on average 0.99 mg m^{-3} between 2007 and 2014 (**Fig. 4.13**). Prior to 2007 the water column also showed a marked depth gradient (0.84 mg m^{-3} SD), with a chlorophyll peak around 20 m to 25 m, whereas after 2007 the water column experienced more homogenization (0.45 mg m^{-3} SD, **Fig. 4.13**). Other notable features happened during 2004 and 2014. In 2004, the 50 m, 75 m and 100 m profiles show increased chlorophyll levels although this did not translate into increased surface chlorophyll levels, some surface profiles (i.e. 5 m, 10 m and 15 m) even show reduced chlorophyll concentration. A similar situation happened in 2014 where surface profiles show a marked reduction in chlorophyll concentration but deeper profiles (i.e. 50 m, 75 m and 100 m) do not show any reduction (**Fig. 4.13**).

Depth chlorophyll profiles between 1999 and 2015 to 100 m are shown in **Fig. 4.14**. Chlorophyll distribution in the water column shows that the chlorophyll peak occurs between 10 m and 15 m water depth.

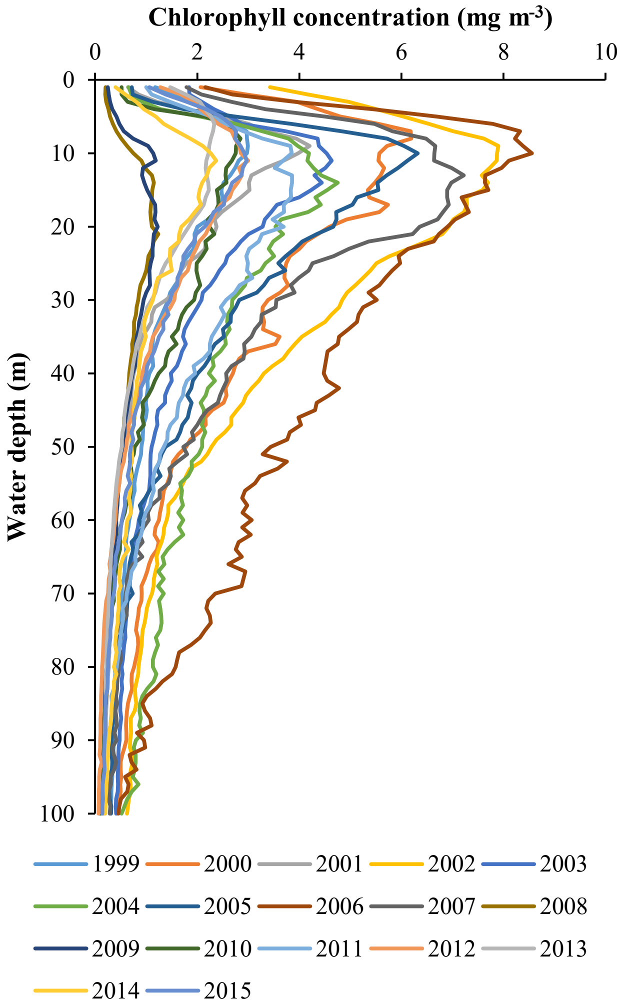

Fig. 4.14 Annual (August-July) averaged chlorophyll (mg m^{-3}) profiles from 1 m to 100 m water depth between 1999 and 2015 at the RaTS site, Ryder Bay. Note the interannual variability in the chlorophyll concentration during high productivity years (e.g. 2002, 2006 and 2007) and very low productivity years (e.g. 2008 and 2009).

A high degree of interannual variability, also seen in **Fig. 4.12** and **Fig. 4.13**, is observed with high productivity years (e.g. 2002 and 2006) and low productivity years (e.g. 2008 and 2009). Chlorophyll concentration declines to half (2.00 mg m^{-3}) at around 35 m water depth and reaching less than 1 mg m^{-3} at around 57 m water depth. Anomalously high chlorophyll levels deeper than 40 m occurred during 2006 (**Fig. 4.14**); the average chlorophyll concentration deeper than 40 m for 2006 is 2.31 mg m^{-3}, whilst for the remainder of the record it is 0.67 mg m^{-3}. It can also be observed that in 2004, chlorophyll concentration was reduced in surface waters (< 25 m water depth), although it presented relative increased values at depth below 50 m water depth (**Fig. 4.14**), similar to reported in the annual averages (**Fig. 4.13**).

4.1.4 Fast-ice

The standardized annually averaged fast-ice duration record is presented in **Fig. 4.15** and monthly fast-ice duration observations are provided in **Fig. 4.16**. The fast-ice duration record shows that prior to 2007 there was an alternation between years when the fast-ice lasted long (e.g. 1997, 2002, and 2005) and years with short fast-ice duration (e.g. 1998, 2001). After a significant decline in the fast-ice duration in 2007, which started in 2005/06, a prolonged period of short fast-ice duration lasted until 2011, when fast-ice began to last longer at the RaTS site (**Fig. 4.15**). The fast-ice duration appears to be strongly modulated by the beginning, rather than the end, of the fast-ice season, as years when the fast-ice started to form earlier are associated with longer annual fast-ice duration than years when the fast-ice started to form later (**Fig. 4.17**). In addition, a comparison between annual (August-July) seawater temperature from the upper 25 m of the water column and the fast-ice duration is provided in **Fig. 4.15**; a significant negative correlation between both parameters for the period 1999/2015 was found ($r = -0.69$, $R^2 = 0.47$, $p < 0.01$, $n = 17$).

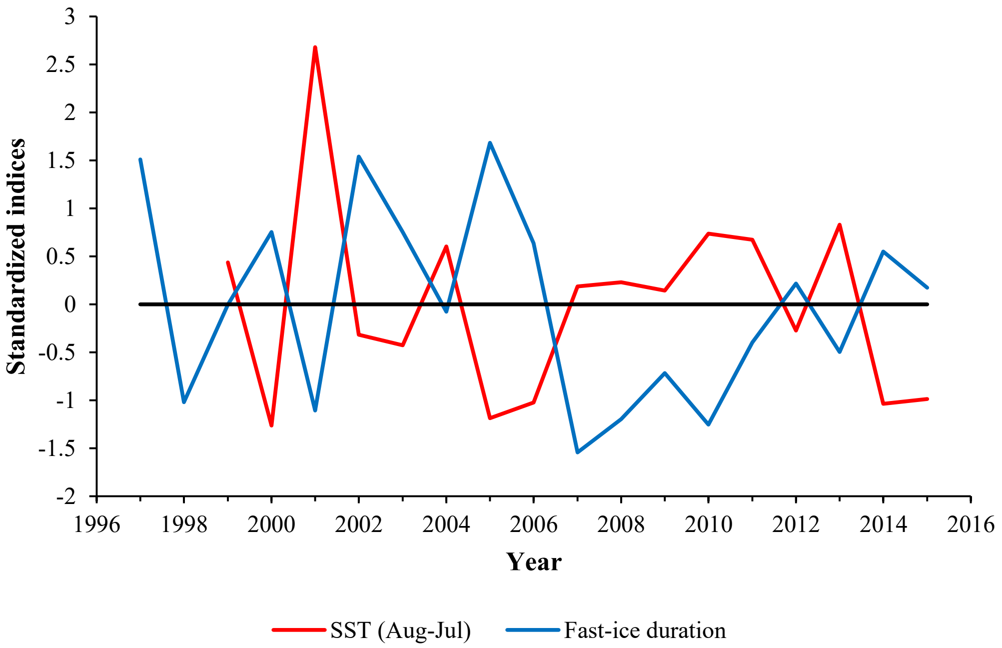

Fig. 4.15 Standardized annual average (August-July) sea surface temperature (SST) for the upper 25 m of water at the RaTS site (red line) and fast-ice duration (blue line).

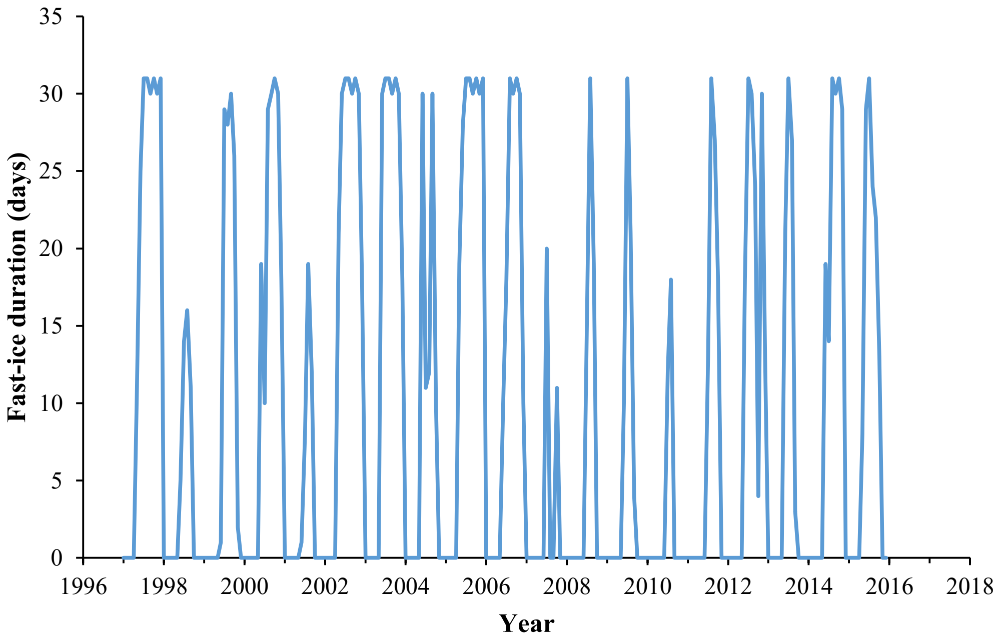

Fig. 4.16 Monthly average of fast-ice duration (days) from the RaTS time series at Rothera station from 1997 to 2016.

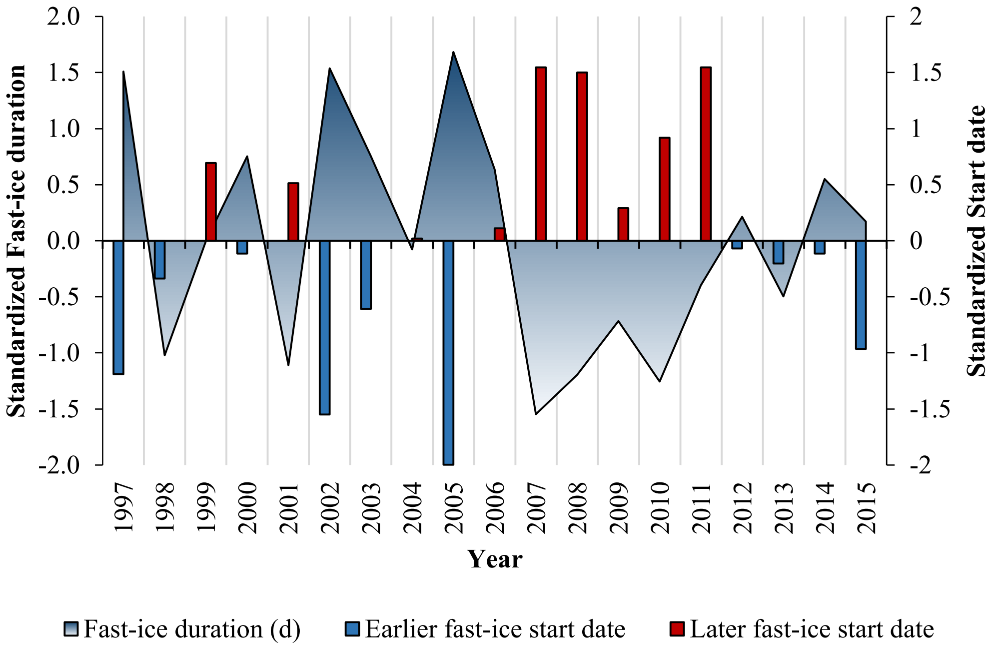

Fig. 4.17 Standardized fast-ice duration (blue shaded area) and fast-ice start date index (early start in blue columns and later start in red columns). Note the inverse relationship between fast-ice duration and start date index (i.e. years when the fast-ice lasted for a longer period showed an earlier fast-ice start).

4.1.5 Geochemistry

The $\delta^{18}O_{water}$ record, developed from samples collected at 15 m water depth at the RaTS sampling site at Ryder Bay, is presented in **Fig. 4.18**. Sub-annual variability is apparent in the $\delta^{18}O_{water}$ record with lower values occurring typically between January and April (austral summer season) and higher values occurring typically between August and December (austral winter season, **Fig. 4.18**). The $\delta^{18}O_{water}$ record also shows a change in annual average $\delta^{18}O_{water}$ value from 2007 onwards (-0.72 ‰ ± 0.1 SD for the period 2002/07 and -0.57 ‰ ± 0.1 SD for the period 2008/15). The range $\delta^{18}O_{water}$ is 0.71 ‰ for the entire length of the record (August 2001 to March 2015). Seasonal variability (from the summer season to the following winter season) in the $\delta^{18}O_{water}$ record is also large, varying from -0.10 ‰ (2010/11) to -0.50‰ (2007/08) and on average -0.28 ‰ ± 0.1 SD (**Fig. 4.18**). In addition, high correlation between the monthly $\delta^{18}O_{water}$ and the salinity records is observed (r = 0.94, **Fig. 4.18**).

The calibration between the $\delta^{18}O_{water}$ values measured from the water samples and the salinity measurements is provided in **Fig. 4.19**. A positive trend in $\delta^{18}O_{water}$ is observed with increasing salinity.

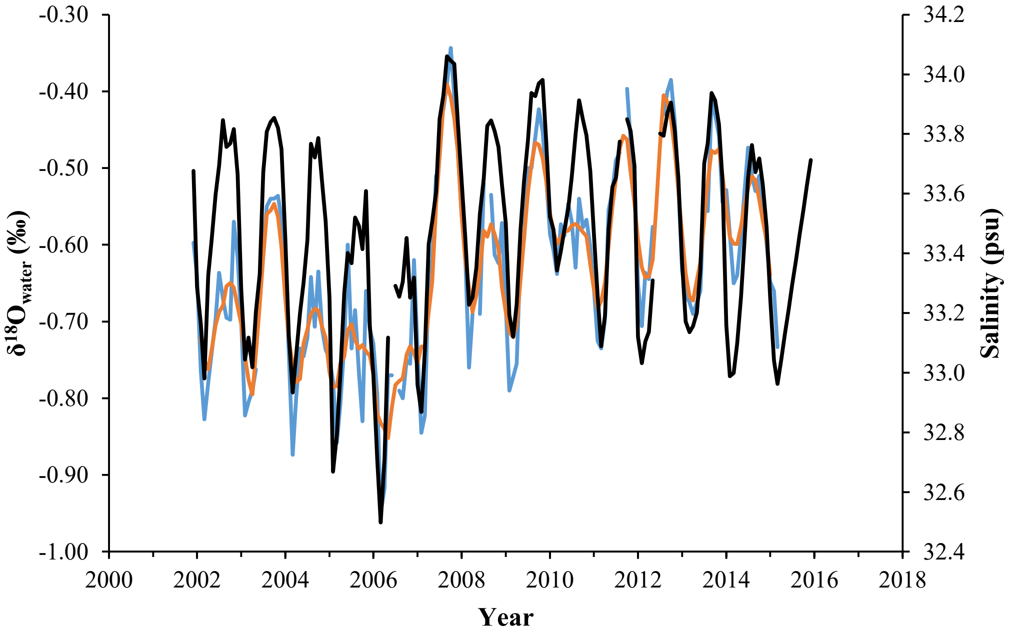

Fig. 4.18 Monthly $\delta^{18}O_{water}$ (‰ SMOW, blue line), five-month running average of the monthly $\delta^{18}O_{water}$ (‰ SMOW, orange line) and salinity record (black line) collected at 15 m water depth at the RaTS site between 2002 and 2016.

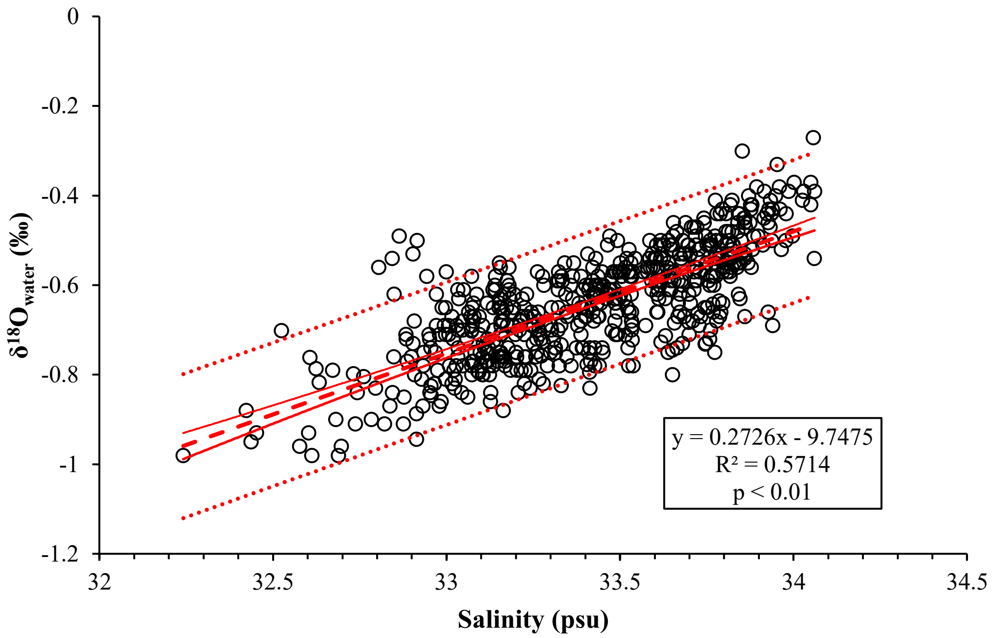

Fig. 4.19 Relationship between seawater salinity and $\delta^{18}O_{water}$ (‰ SMOW) of the water samples collected between 2001 and 2015 at Ryder Bay as a part of the RaTS programme. A linear trend was fitted (dashed red line) to the data, 95 % confidence intervals (solid red lines), 95 % prediction intervals (dotted red lines), the trend line equation and R^2 (inset) are also provided.

4.1.6 Summary

The records from the West Antarctic Peninsula at Rothera Research Station show a marked change of the pattern of variability 2007 onwards. Annually (August-July) temperature averages showed that deeper waters became relatively colder than surface waters (**Fig. 4.2** and **Fig. 4.3a**), fast-ice duration showed a marked negative trend and a delay in the date of formation (**Fig. 4.15** and **Fig. 4.17**), salinity profiles showed a significant decrease in salinity across all depths (**Fig. 4.9**), and finally the collapse of the standing chlorophyll crops in 2007 and 2008 was obvious (**Fig. 4.12** and **Fig. 4.13**) and a shift between high productivity years prior to 2007 to low productivity years after 2007 was also found (**Fig. 4.12** and **Fig. 4.13**).

4.2 South Orkney Islands records

This section presents the results from the observational records collected at the South Orkney Islands (SOI) at Signy Research Base. The British Antarctic Survey routinely collected instrumental records at the SOI between 1947 and 1996, at which point the Signy Research Base started to operate as a summer-only station. Therefore, data series become sparse after 1996, although this is not *a priori* a major disadvantage for this study since the chronologies for this region have been based on historical collections from specimens live-collected in 1915, 1927 and 1988.

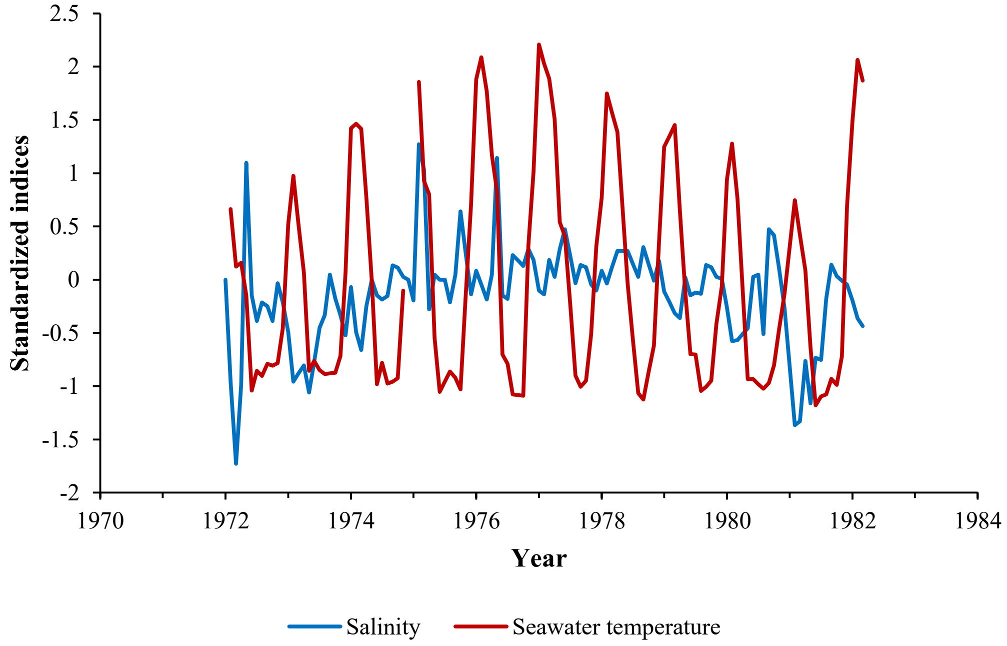

Fig. 4.20 Standardized salinity (blue line) and seawater temperature (°C; red line) between February 1972 and March 1982 collected in Borge Bay, Signy Island at 10 m water depth.

Standardized instrumental salinity and seawater temperature records collected at 10 m water depth between 1972 and 1982 from Factory Cove are shown in **Fig. 4.20**; these datasets were originally collected by Clarke et al. (1988). Summer seawater temperature shows a positive (warming) trend during the early 1970s, which switches to a negative (cooling) trend during the late 1970s (**Fig. 4.20**). In 1982 a significant increase in temperature is also observed, although data from the 1982/83 winter is missing. Due to the difficulty of manually collecting instrumental data there are missing values for the winter season in 1974/75, 1976/77 and 1979/80. Between 1972 and 1982 the maximum seawater temperature was 0.87 °C, the minimum seawater temperature was -1.94 °C and on average seawater temperature was -0.87 °C ± 0.84 SD. In addition, the maximum salinity was 38.34 psu, the minimum salinity was 33.08 psu and on average salinity was 34.00 ± 0.58 psu SD. A significant negative relationship ($r = -0.26$, $n = 100$, $p \leq 0.05$) was found between seawater temperature and salinity when lagged by six months.

Mean annual (August-July), summer (December-April) and core winter (July-September) sea-surface temperature values from the HadISST1 record (c.f. Chapter II subsection 2.7.2) from the UK Meteorological Office from 1949 to 1988 are presented in **Fig. 4.21**. Even though this record extends to 1949, the lack of environmental data (instrumental or telemetric) prior to 1970s presents a caveat for the use of this record for that period. Nonetheless the extension of the temperature record to 1988, the date of collection of the most modern *A. eightsii* specimens from the South Orkney Islands, improves the knowledge of the environmental conditions in the region.

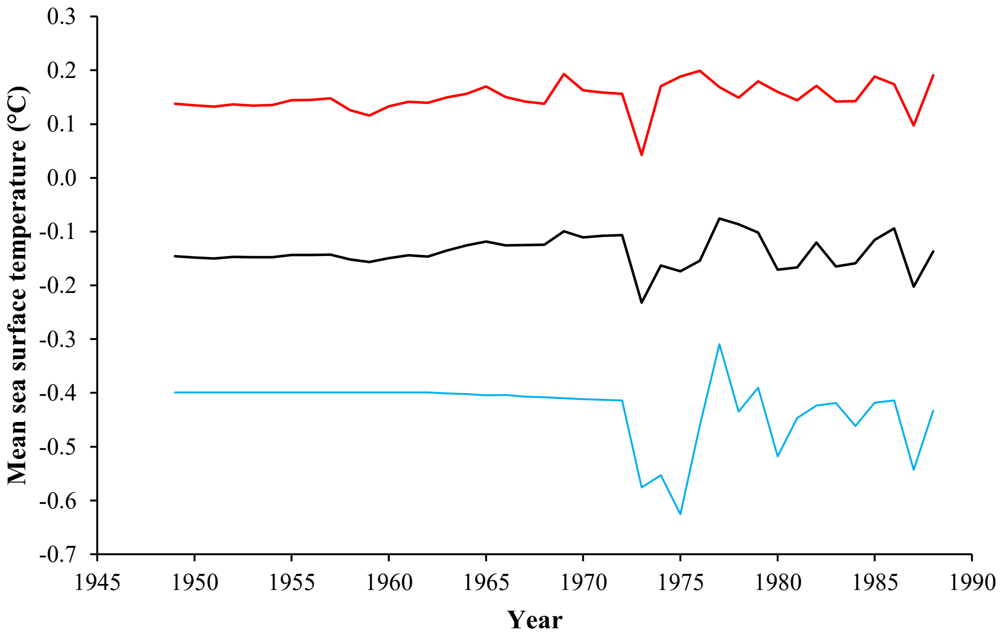

Fig. 4.21 Mean summer (December-April) sea-surface temperature (SST, red line), mean core winter (July-September) SST (blue line) and mean annual (August-July, black line) from the HadISST1 record from 1949 to 1988.

The low variability in the mean winter sea-surface temperature record prior to 1973 is due to the lack of instrumental measurements; this means that the mean annual values are biased towards the variability from the summer sea-surface temperature record (**Fig. 4.21**). The comparison between both the instrumental dataset from Clarke et al. (1988) and the HadISST1 dataset is provided in **Fig. 4.22**. It has to be noted that the instrumental record constructed by Clarke et al. (1988) contains several gaps, presumably due to adverse weather conditions and therefore some of the averaged values presented in **Fig. 4.22a** may be biased or interpolated. Missing measurements from the Clarke et al. (1988) sea surface temperature (SST) record and the approach taken (interpolated and not interpolated) to construct the mean annual, summer and core winter records (**Fig. 4.22a**) are presented in **Table 4.1**. The comparison between the Clarke et al. (1988) instrumental record and the HadISST1 records shows that the

HadISST1 record presents warmer average temperature than the instrumental record (**Fig. 4.22** and **Table 4.2**) although the temperature ranges are higher in the instrumental record (**Table 4.2**). In addition, considering that the majority of the gaps present in the Clarke et al. (1988) record are during the austral winter (**Table 4.1**), the differences in average temperature between the instrumental and the telemetric record are likely to be larger than the estimates given here.

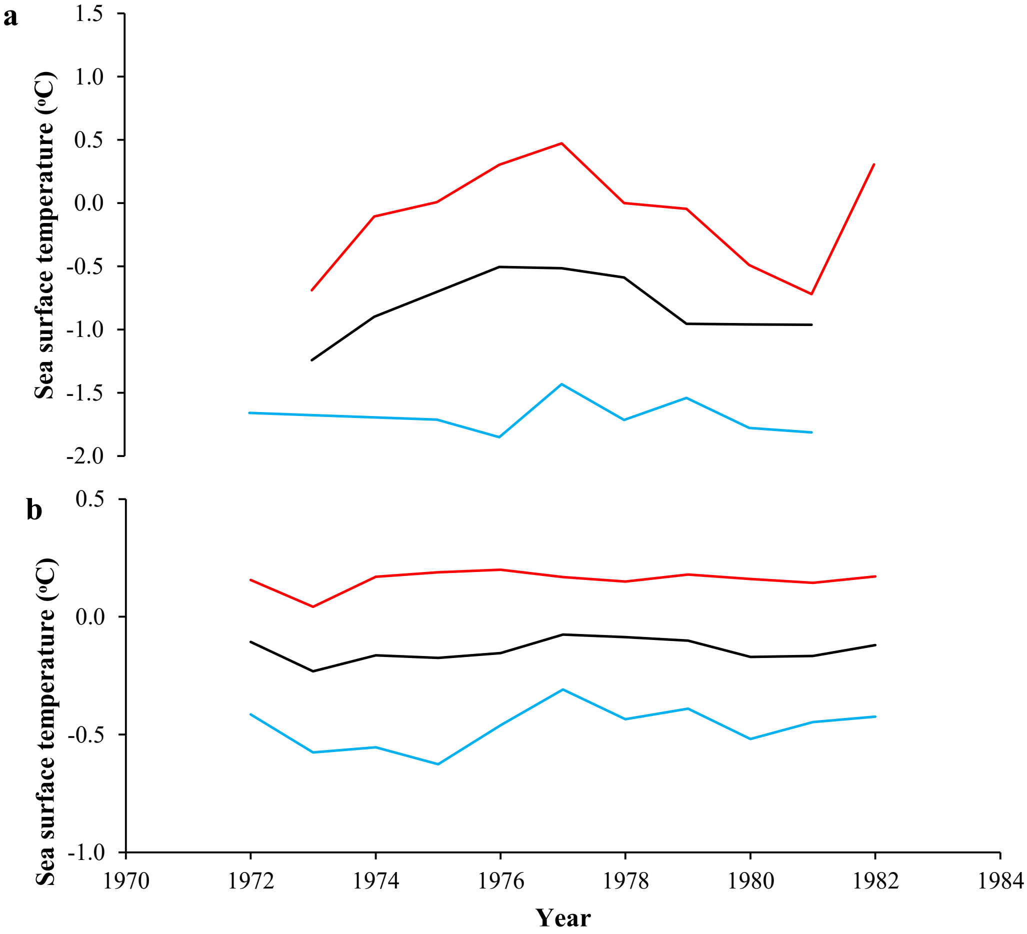

Fig. 4.22 Mean annual summer (December-April, red line), annual (August-July, black line) and mean annual core winter (July-September, blue line) sea surface temperatures of **a)** the

instrumental data collected by Clarke et al. (1988) and **b)** from the HadISST1 data set for the overlapping period 1972/82. Note the difference in range in the Y-axes.

Table 4.1 List of missing measurements present in the Clarke et al. (1988) sea surface temperature record and the approach taken to produce mean annual, mean summer and mean winter core temperature records presented in **Fig. 4.22a**.

	Annual (Aug-Jul)	**Summer (Dec-Apr)**	**Winter Core (Jul-Sep)**
Values interpolated	Mar 1973, Jul 1975, Sep 1976, Jul 1977, Mar, May, Jul 1978, Oct 1978, Feb 1979, Apr 1980, Jan 1981	Mar 1973, Mar 1978, Feb 1979, Apr 1980, Jan 1981, Apr 1982	Jul 1975
Values not interpolated	Jul 1974, Aug-Oct, Dec 1974, Jan 1975, Jun, Jul 1976, Sep, Oct 1977, Apr-Jun 1979, Aug-Nov 1979	Dec 1974, Jan 1975, Apr 1979	Jul 1976, Sep 1977, Sep 1979

Table 4.2 Average, standard deviation (SD), maximum (max) and minimum (min) values and range comparison between the summer (Dec-Apr), Annual (Aug-Jul) and core winter (Jul-Sep) calculated from Clarke et al. (1988) record and the HadISST1 record. Period considered are for the summer (1973/82), annual (1973/81) and core winter (1972/81).

	Clarke et al. (1988)			**HadISST1**		
	Summer (Dec-Apr)	**Annual (Aug-Jul)**	**Core winter (Jul-Sep)**	**Summer (Dec-Apr)**	**Annual (Aug-Jul)**	**Core winter (Jul-Sep)**
average	-0.10	-0.81	-1.69	0.94	-0.13	-1.32
SD	0.42	0.25	0.12	0.26	0.15	0.26
max	0.47	-0.50	-1.43	1.23	0.05	-0.88
min	-0.72	-1.24	-1.85	0.37	-0.43	-1.74
range	1.19	0.74	0.42	0.86	0.48	0.85

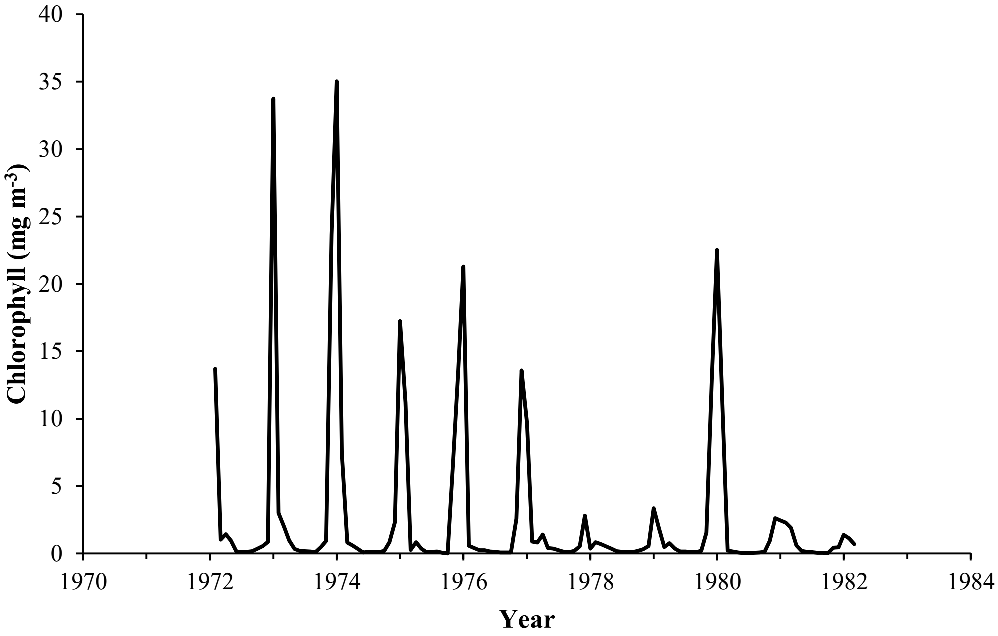

Fig. 4.23 Chlorophyll concentration (mg m^{-3}) collected between February 1972 and March 1982 from the Orwell Bight, Signy Island at 10 m water depth. Note the great interannual variability with high-yield phytoplankton bloom years (e.g. 1972/73, 1973/74) and very low yield years (i.e. 1977/78, 1978/79, 1980/81 and 1981/82).

The chlorophyll concentration shows a unimodal distribution with the highest chlorophyll concentrations around December (austral summer), with some years (1972/73, 1975/76, 1977/78) also characterised by a much weaker autumn bloom (**Fig. 4.23**). Between 1972 and 1982 the maximum chlorophyll level was 35.025 mg m^{-3}; and minimum chlorophyll level was 0.01 mg m^{-3}, on average chlorophyll level remained low at 3.024 mg m^{-3} which highlights the marked seasonality of the shallow Antarctic coastal environment. Chlorophyll concentrations show very high levels in the 1972/73 and 1973/74 seasons and an almost total collapse of the standing crop during the 1977/78, 1978/79, 1980/81 and 1981/82 seasons (**Fig. 4.23**). In general, there is a positive trend in chlorophyll peak between 1972 and 1974 and a negative trend after 1974 with the exception of 1980/81. A relationship between the previous winter fast-ice duration and chlorophyll concentration can be observed (**Fig. 4.24**), although this is not significant ($r = 0.41$, $p = 0.27$, $n = 9$). A comparison of the standardized salinity, seawater temperature and chlorophyll indices are provided in **Fig. 4.25** for the annual (August-July) values and the summer (December-April) season.

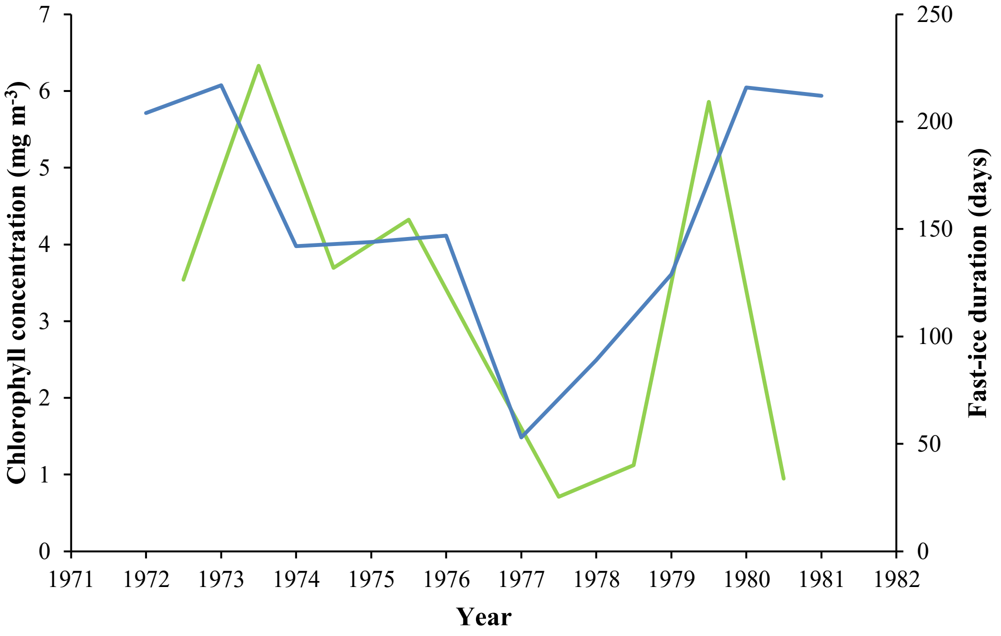

Fig. 4.24 Annual (August-July) chlorophyll *a* concentration (mg m^{-3}, green line) and fast-ice duration (days, blue line) between 1972 and 1981. Note the offset between the series, this offset was introduced to account for the difference between seasons during which the instrumental parameters were measured.

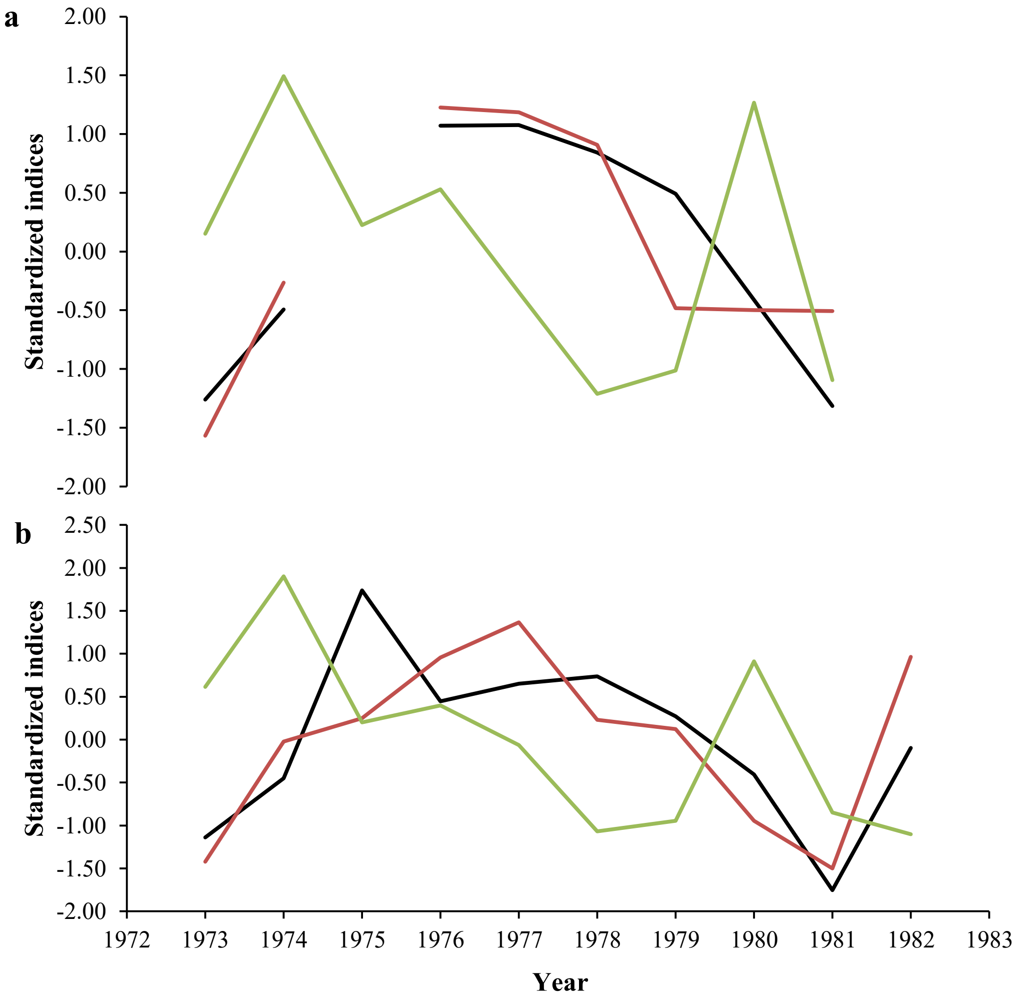

Fig. 4.25 a) Annually (August-July) averaged salinity (black line), seawater temperature (red line) and chlorophyll concentration (green line) time series at Factory Cove, Signy Island from 1973 to 1981 and **b)** Summer (December-April) annual averages for salinity (black line), seawater temperature (red line) and chlorophyll concentration (green line) time series at Factory Cove, Signy Island from 1973 to 1982.

The sea-ice record for the SOI, including moving averages and low-pass filtered data are presented in **Fig. 4.26**. A discontinuity in the fast-ice duration after 1947, already highlighted by Murphy et al. (1995), is observed clearly in the smoothed data as reduction of about 41-46 days (**Fig. 4.26**). In addition, Murphy et al. (1995) highlighted a 7-9 year cyclicity in the fast-ice data since the mid-1960s that lasted until 1991 (**Fig. 4.26**). However, interdecadal variability remained relatively constant (average range 166 days ± 28 SD for the period 1910/99). As a comparison of smoothing techniques, the 15-year moving average (MA15) and the 30-year low-pass filter (LP30) produced similar functions although interannual variability is higher in the moving average function. Similarly, the nine-year moving average (MA9) and the 15-year low-pass filter (LP15) show comparable trends, although they become out of phase in the mid-1960s.

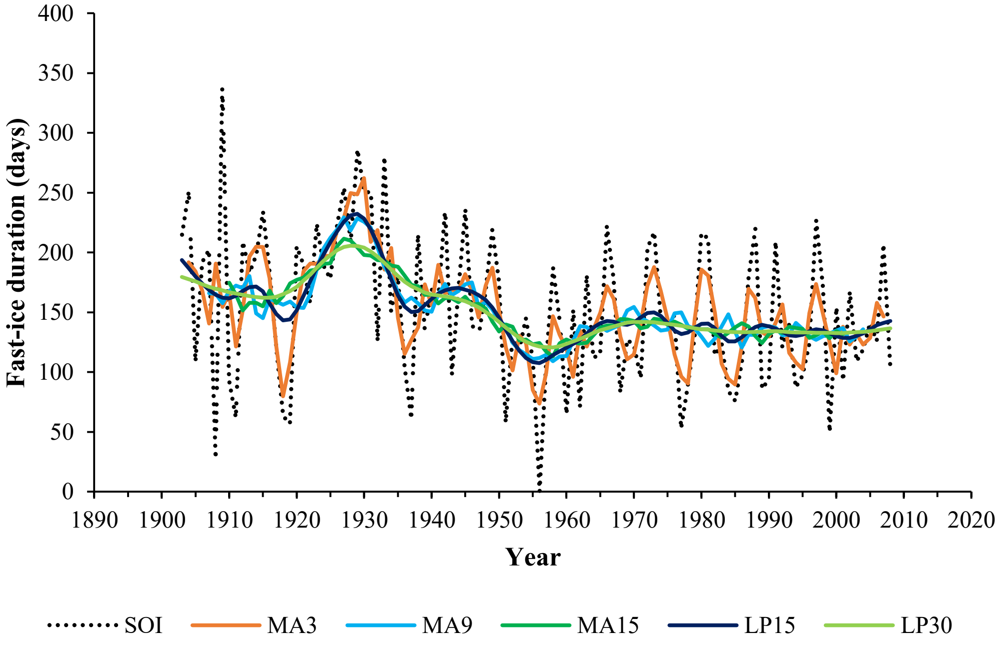

Fig. 4.26 Fast-ice duration (days) for the South Orkney Islands (SOI) between 1903 and 2008. The SOI ice index comprises three independent datasets: 1) from 1903 to 1947 fast-ice duration in Scotia Bay, 2) from 1947 to 1994 observed fast-ice duration in Factory Cove and 3) from 1995 to 2008 sea-ice camera record from Factory Cove. Three year, nine year and 15-year moving averages (MA3, MA9 and MA15 respectively) and a 15-year and 30-year low-pass filters (LP15 and LP30 respectively) are also shown.

4.3 Climatic indices

4.3.1 Southern Annular Mode (SAM)

The monthly SAM index between 1957 and March 2016 is presented in **Fig. 4.27**. When annual summer (January-March) averages are taken a positive trend in the SAM index can be observed (**Fig. 4.28**).

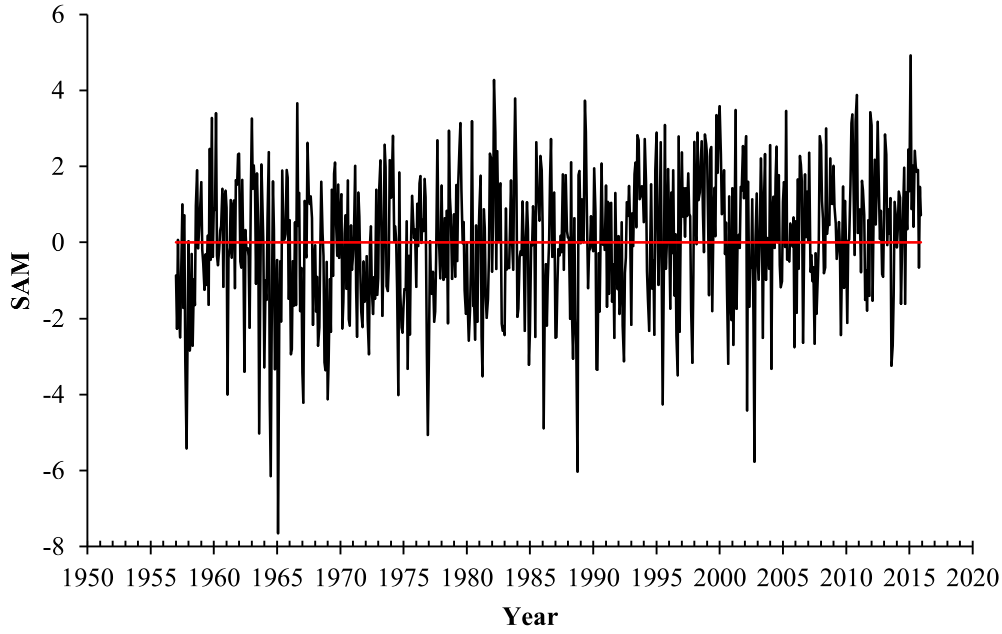

Fig. 4.27 Monthly SAM index (black line) from 1957 to March 2016.

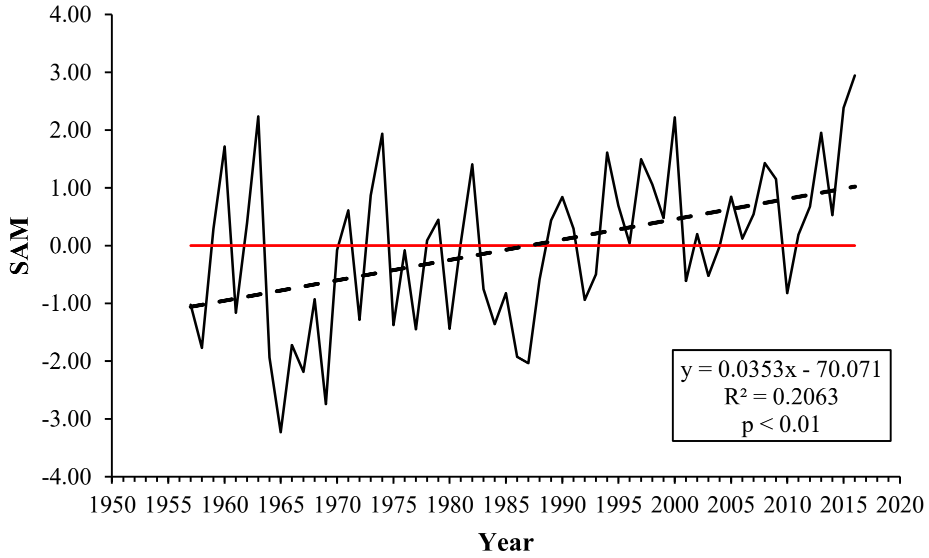

Fig. 4.28 Annually averaged core summer (January-March) SAM index (solid black line) between 1957 and 2016. A linear trend (dashed line) is shown to highlight the trend towards positive SAM values, the line equation is also given in the inset box.

4.3.2 El Niño Southern Oscillation (ENSO)

Monthly average values of the Multivariate ENSO index (MEI) are presented in the **Fig. 4.29**. It is a prevalence towards stronger El Niño events than towards La Niña events.

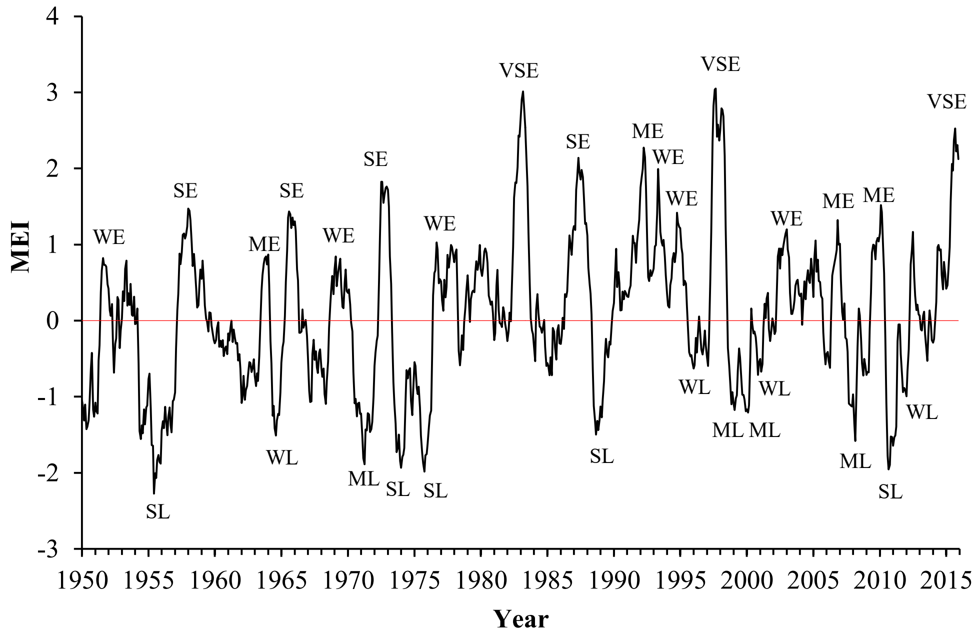

Fig. 4.29 Monthly Multivariate ENSO Index (MEI) between 1950 and 2015. WE: weak El Niño, ME: moderate El Niño, SE: strong El Niño, VSE: very strong El Niño, WL: weak La Niña, ML: moderate La Niña and SL: strong La Niña.

4.4 Discussion

4.4.1 West Antarctic Peninsula

The RaTS programme provides an excellent opportunity to analyse in detail the local environmental conditions present at Ryder Bay during part of the lifespan of the *A. eightsii* specimens collected for this study. Even though the *A. eightsii* specimens were collected from shallow marine environments (i.e. up to 30 m water depth) it is also important to appreciate the wider environmental processes potentially affecting the location of study and for this reason it was considered necessary to extend the examination of the water column down to 100 m.

The study of the different environmental parameters from the RaTS record revealed a complex system which shows strong depth gradients, with a high interannual variability (e.g. Meredith et al., 2004; Clarke et al., 2008; Meredith et al., 2010; Venables et al., 2013). Some of the environmental changes recorded in the RaTS time series occur simultaneously, for example after 2007 Ryder Bay experienced: higher temperature gradients with depth during summer (**Fig. 4.2)**, lower temperature gradients with depth during winter and reduced intensity of deep winter warming events (**Fig. 4.4**), low chlorophyll concentrations (**Fig. 4.13**) intense salinification and homogenization of the upper 100 m of the water column (**Fig. 4.9**) and low fast-ice duration (**Fig 4.15**). Part of the results presented here, covering the period 1998/2006, have been discussed in detail by Clarke et al. (2008). The simultaneous timing of these changes may indicate a common environmental driver affecting the local oceanography. Meredith et al., (2010) discussed in detail changes in freshwater composition of the ocean surface at Marguerite Bay using the RaTS time series, specifically a combination of $\delta^{18}O_{water}$ and salinity instrumental measurements. They reported that during 2003, 2007 and 2008, and also during 1998 in a previous study (Meredith et al., 2004), a deep winter mixed layer caused by polynya-like conditions (i.e. low sea-ice cover, increased sea-ice formation which in turn increased salinity, strong air-sea heat fluxes) acting at Ryder Bay. Similar conditions, although of a lesser strength, to those occurring in 1998 for by El Niño have been reported for 2003 (Wallace, 2008). The lack of sea-ice cover was ultimately caused by the action of anomalously persistent northerly winds, with teleconnections to SAM (positive; **Fig. 4.28**) and ENSO (La Niña; **Fig. 4.29**), which push sea-ice from the coast, similarly to the action of katabatic winds, generating a coastal polynya (Meredith et al., 2004, 2010). In the present analysis of the RaTS time series, it is observed that during 1998, 2003, 2007/08 and also to some extent 2010 and 2014, the winter core (July-September) seawater temperature shows cooling events and a homogenization of the upper 100 m of the water column (**Fig. 4.6**). In addition, Meredith et al. (2004) noted that restratification of the water column after a deep winter mixing event is delayed and reduced and causes a persistence in the reduced extrema in the freshwater content in surface waters. Winter seasons following deep mixed winter layers and low sea-ice cover show an increasing temperature stratification with depth (**Fig. 4.6**), however the amplitude of these cycles shows a negative trend which may be an indication of either a larger driver acting on a multi-decadal scale, or alternatively the action of a multiannual positive feedback acting locally at Marguerite Bay. Differences in temperature between two consecutive cooling/warming/cooling cycles (**Fig. 4.6**) could be interpreted as ventilation of the upper circumpolar deep water and an exchange of heat with surface Antarctic water as suggested by Venables and Meredith (2014). The 1998, 2003 and 2010 deep-mixing cooling episodes (**Fig. 4.6**) are associated with El Niño conditions (very strong El Niño in 1998 and moderate El Niño in 2003 and 2010; **Fig. 4.29**); whereas during 2007/08 moderate La Niña conditions were present and neither positive nor negative ENSO conditions developed during 2014. It is notable that the 1998/2003 and 2003/08 cycles (**Fig. 4.6**) show that following a peak in high temperature stratification with depth (i.e. 2001 and 2006) the subsequent winter shows a trend towards deep mixed winter layer suggesting some pre-conditioning (one year in advance) for the subsequent deep winter mixing events. Meredith et al. (2010) described how the summer season following a winter with deep mixed layers is characterised by a reduced peak in sea-ice melt, which would have in turn affect the stability (i.e. reduced) of near surface water and pre-condition the near surface water for the following winter if the driving atmospheric conditions persist. Furthermore, preconditioning conditions in sea-ice formation lagging 18 months and associated with ENSO variability have been described for the South Orkney Islands (Murphy et al., 2014).

Ultimately the identified climatic drivers controlling the prevalence of abnormally strong northerly winds on the Western Antarctic Peninsula (WAP) are the ENSO and the SAM. During the last half of the 20th century SAM has shown trends towards more positive values especially during the austral summer (Thompson and Wallace, 2000b).

Anthropogenic impacts on the climate system have been considered partly responsible for the positive trend in SAM (**Fig. 4.28**; Thompson and Solomon, 2002; Gillett and Thompson, 2003; Marshall, 2003). South Atlantic SST anomalies were found to present significant lags with SAM of 1-2 months and also at longer periods of around 2-3 years (Meredith et al., 2008b). On the other hand ENSO has shown trends towards a predominance of El Niño events *versus* La Niña events (Thompson et al., 2000; Marshall, 2003; Turner, 2004). The local manifestations of (warm) ENSO events at the WAP include reduced sea-ice concentrations, increased air temperatures, increased winter sea-ice production, which in turns increases salinity and increases the mixed layer depth (Meredith et al., 2004). On the other hand, ENSO local manifestations at the South Orkney Islands have shown to lag approximately 2.5 years (Meredith et al., 2008b), between the development of positive SST anomalies in the southwest Pacific and the arrival of the positive anomalies to the south Atlantic and the Scotia Sea.

These oceanographic trends on the WAP also influence the ecosystems present in the region. The stability of the near-surface water column plays a crucial role for the development of seasonal phytoplankton blooms (Mitchell and Holm-Hansen, 1991; Dierssen et al., 2002; Clarke et al., 2008). The chlorophyll time series sequentially averaged over increasing water depth (**Fig. 4.13**) shows reduced chlorophyll levels following a winter of deep mixed layer (**Fig. 4.6**, note that there is a one year offset between both plots due to the average window), especially in 1999, 2008 and 2009. Interestingly the 2003 deep winter mixed layer (**Fig. 4.6**) did not cause such an abrupt collapse of the phytoplankton stock as in 1999 and 2008 (**Fig. 4.13**); there is, however, a reduction in the chlorophyll concentration in shallower profiles (i.e. up to 20 m **Fig. 4.13**) and an increase in chlorophyll concentration in deeper profiles which suggests a shift from shallow to deeper phytoplankton activity. Similarly, the same situation occurs during 2014 with a reduction of chlorophyll concentration in shallower profiles and abnormal high chlorophyll concentration in deeper profiles (**Fig. 4.13**). In addition a change from high chlorophyll concentration prior to 2008 to low chlorophyll concentration have been discussed in terms of water column stratification by Venables et al. (2013). Increased vertical mixing (i.e. reduced water column stratification) increases the variability in the light conditions experienced by the phytoplankton and is also likely to reduce iron availability, which on the whole reduces the primary production (Venables et al., 2013). This water-column stability control over the phytoplankton is therefore likely to have further effects across the ecosystem through bottom-up cascading effects. During 2003/04 it was reported a steady deepening of the bloom from late January to late March (Clarke et al., 2008); this may be an explanation of the unusual high chlorophyll concentration in the deep profiles of 2004 (**Fig. 4.13**).

The most noticeable event in the salinity time series is the abnormally low average salinity values recorded in 2006 (**Fig. 4.9**). This was caused by a strong and persistent sea-ice cover from June to December 2005 which was followed by strong melting conditions between January until early June 2006 (**Fig. 4.16**; Meredith et al., 2010). Although there were similar conditions between 2002 and 2003, despite reduced sea-ice melting during 2003, no significant freshening of the upper 100 m of the water column was present. This difference between the salinity conditions in 2003 and 2006 is related to the stability of the water column; whereas during 2003 a deep winter mixed layer was present, in 2006 a shallow winter mixed layer was present (**Fig. 4.6**). Enhanced vertical mixing and ventilation of the Upper Circumpolar Deep Water would have increased salinity in near surface waters in 2003 whereas higher stratification and low vertical mixing in 2006 could not prevent freshening of near surface water due to increased sea-ice cover during the previous winter and enhanced sea-ice melting during the summer.

4.4.2 South Orkney Islands

Since the *A. eightsii* specimens from the South Orkney Islands used in this study all belong to historical collections there was no need, nor the means to collect, new instrumental data from the South Orkney Islands and therefore all the instrumental data relate to historical studies carried out in the region. Long-term time series from the South Orkney Islands are more limited compared with Rothera. Clarke et al. (1988) provided a comprehensive analysis of the temperature, chlorophyll and major nutrients cycles at Borge Bay from 1969 to 1982, with instrumental measurements taken from Factory Cove (the same location where the 1988 *A. eightsii* specimens were collected, **Fig. 2.1**). Although the authors possessed monthly measurements of a range of environmental parameters the focus of their study was centred in the seasonal variability rather than in the interannual variability and, in particular the phytoplankton blooms rather than physical parameters. In this sense the re-analysis carried out in the present study of the instrumental time series collected by Clarke et al. (1988) is novel. The salinity and seawater time series suggest that Factory Cove, Borge Bay (**Fig. 2.1**) underwent a period of increasing salinity and seawater temperature range (especially during the austral summer months) from the early 1970s to the mid-late 1970s (**Fig. 4.20**); subsequently this trend reversed and the data show a period of freshening and reduced seawater temperature range until the early 1980s (**Fig. 4.20**). This was also accompanied by high primary production cycle from the early 1970s to the mid-late 1970s followed by a period of low primary production, with the exception of 1980, until the early 1980s (**Fig. 4.23**). It is worth noticing that the start of the low primary production period (i.e. 1978, **Fig. 4.23**) coincides with the change in trends in the salinity and seawater temperature time series (**Fig. 4.20**), although a negative trend in the chlorophyll time series was present already since 1974/75. Clarke et al. (1988) noticed the presence of these two periods of high and low chlorophyll concentration, although they could not find any direct correlation between the size of the bloom and the physical instrumental time series. Similarly in a later study, Clarke and Leakey (1996) found no relationship between the size of the microplankton bloom and ice duration, ice breakout and summer seawater temperature for the period 1988/94, although the authors found a significant correlation between the bloom size and the mean wind speed in November and January and an almost significant correlation with the mean wind speed in December and a significant positive relationship between the bloom size and the minimum seawater temperature from the previous winter, although the authors did not provide any explanation about the mechanism(s) driving this connection. Furthermore, Murphy et al. (1995) studied the long term interannual temporal variation in the sea-ice duration in the South Orkney Islands, concluding that circumpolar atmospheric and oceanic processes operating on a sub-decadal time scale were affecting the sea-ice extent. The authors also suggested a plus or minus one year offset between the atmospheric changes in the Southern Pacific and the ice behaviour at the South Orkney Islands (Murphy et al., 1995). This observation will become important when comparing the sclerochronologies developed from the *A. eightsii* specimens collected from the South Orkney Islands and the instrumental records, especially in the case of the climatic indices.

The comparison between the Clarke et al. (1988) instrumental seawater temperature record and the HadISST1 dataset (**Fig. 4.22**) offers some insights for the interpretation of the shell records, especially due to the limited availability of *in situ* environmental data. Collection of long-term year-round *in situ* instrumental data at Signy Station has ceased since Rothera started working as the main scientific station of the British Antarctic Survey (BAS). Due to current BAS research priorities, it is likely that the only long-term year-round instrumental measurements from the South Orkney Islands will be those collected by telemetric means. It is therefore crucial to understand the possible differences between the *in situ* instrumental records and the telemetric data series. It is worth noticing first that the HadISST1 data series used here is a region comprised between -62° -58° N latitude -47° W -43° W longitude box, with the South Orkney Islands centred in the box, and therefore the values from the HadISST1 data series are more representative of oceanic temperature values rather than coastal environmental conditions. This is likely the explanation for the difference between the temperature range (higher in the instrumental time series, **Fig. 4.22a**) and the average temperature (warmer in the telemetric time series, **Fig. 4.22b**) between both records (i.e. Clarke et al., 1998 *vs* HadISST1). Both records show a warming summer trend starting in 1973, however whereas the warming trend in the instrumental record ends in 1977, in the telemetric time series the warming trend plateaus during 1975/76 (**Fig. 4.22**). Subsequently both summer records show similar trends although the temperature rise during 1979 seems more pronounced in the HadISST1 time series and also the instrumental record shows a stronger cooling summer trend during 1980/81 and a stronger summer warming trend in 1982. (**Fig. 4.22**). This may be a reflection of the shallow coastal nature of the Clarke et al. (1988) data compared to the telemetric time series. An important feature of the telemetric SST time series (**Fig. 4.21**) is the significant cooling event, in all three time series (mean annual, summer and core winter) that occurred during the mid-1970s. Roman-Gonzalez et al. (2016) argued that the South Orkney Islands were affected by a cold oceanographic regime which had its origins in the driving environmental conditions that originated in the Weddell Polynya, which occurred between 1973 and 1976 (Gordon, 1982; Holland, 2001). The Weddell Polynya was a multi-annual sea-ice free region characterised by convective circulation associated with upwelling processes at the Maud Rise seamount (65°27’36.1”S, 2°57’8”E) that altered water column stratification (Gordon, 1982b; Holland, 2001). In addition, Gordon (1982) reported the presence of a “cold spot” under the sea surface which migrated westwards, in the direction of the South Orkney Islands, at an annual average drift rate of 1.3 cm sec^{-1}. This period is also framed within the 7-9 year cyclicity in the sea-ice highlighted by Murphy et al. (1995) ongoing since the mid-1960s (**Fig. 4.26**) and by intense phytoplankton bloom conditions (**Fig. 4.23**). Immediately after this cooling regime was characterised by general warming, both during the summer and especially during the core winter (**Fig. 4.21**), low chlorophyll levels (**Fig. 4.23**) and low fast-ice duration (**Fig. 4.26**). Climatic indices show that SAM underwent a period with a strong positive trend during the early 1970s (i.e. 1970/73), this trend reverse to a period dominated by SAM negative values from 1974/80 (**Fig. 4.28**); in addition, during the 1973/75 period strong El Niño conditions (i.e. 1973) were followed by two consecutive years of strong La Niña whereas 1976/78 was characterised by weak El Niño conditions (**Fig. 4.29**). Meredith et al. (2008b) investigated the impact of ENSO and SAM on the interannual variability of SST at South Georgia, situated north-east of the South Orkney Islands north of the Southern Antarctic Circumpolar Current Front (**Fig. 1.1**). Although the regions differ slightly, many of the results from their study are relevant to the South Orkney Islands and this study. The authors found that both ENSO and SAM play important roles in the SST anomalies at South Georgia, although over different time scales, being much shorter in the case of SAM (i.e. one month lag and via direct forcing) than in the case of ENSO (i.e. 5-6 months and via the action of meridional winds, Meredith et al., 2008b).

A comparison between the instrumental records from the South Orkney Islands and the WAP must be done with care since significant differences exist between the sites. For example, maximum water depth is significantly higher at the RaTS sampling site (approximately 500 m) than at the Factory Cove site (approximately 30 m); also, the Rothera Research Station is located at a higher latitude than Signy Research Station. Due to these reasons Ryder Bay shows a shorter summer season with a later start in comparison with Factory Cove and also (winter and summer) chlorophyll *a* levels are higher at Signy than at Rothera (Clarke et al., 2008).

Chapter V: Shell geochemistry

The use of chemical and isotopic composition analysis derived from calcareous skeletons is an established method in the study of past and present environmental conditions. However, understanding bivalve shell geochemistry is complex and is affected by biological processes that often confound the signals associated with environmental processes. Nonetheless, when the drivers regulating elemental or isotope incorporation into the shell matrix and the physico-chemical processes involved are understood, shell geochemistry offers very valuable information about the environmental conditions present during shell formation. The results and following discussion presented here constitute the first study of the annual and sub-annual variation of stable oxygen and carbon isotope geochemistry in the shells ($\delta^{18}O_{shell}$ and $\delta^{13}C_{shell}$) of *Aequiyoldia eightsii*.

Three separate experiments are considered in the chapter: i) high-resolution sampling, ii) low-resolution sampling and iii) lateral isotopic fractionation. The chapter is divided into study regions (i.e. South Orkney Islands and West Antarctic Peninsula). Subannual variability and seasonality in the stable oxygen and carbon isotope ratios were addressed in the high-resolution sampling; whereas the development of annually resolved stable isotope records was the main focus of the low-resolution sampling. In addition, the comparison between the records from both sampling strategies serves as a methodological calibration. Possible variability shell anatomical regions (i.e. anterior, ventral and posterior, **Fig. 1.9**) in the stable isotope oxygen and carbon ratios is addressed in the lateral isotopic fractionation experiment.

In addition, a comparison between the derived geochemical records and the instrumental records detailed in Chapter IV is also presented. For reference an example of a drilled *A. eightsii* shell is presented in **Fig. 5.1**.

Contrary to the usual practice, it was decided to present this chapter before the sclerochronology chapter (Chapter VI). This was because the particular methodology used to sample the specimens (c.f. section 2.8 in chapter II). Since the shells are drilled on the external surface and not on the sectioned profile, as is the case of other species such as those utilising *Glycymeris glycymeris* or *Arctica islandica* (e.g. Royer et al., 2013; Reynolds et al., 2017), the assignation of calendar years to the geochemical samples occurs *a posteriori*. In addition, the sclerochronology chapter (Chapter VI) will present a comparison of the shell growth record with the geochemical records and therefore these are presented in advance.

Specific hypothesis studied in this chapter are: i) $\delta^{18}O_{shell}$ and $\delta^{13}C_{shell}$ present variability along the life of the studied specimens, ii) A. eightsii shell precipitates in equilibrium with the environment, iii) the $\delta^{18}O_{shell}$ and $\delta^{13}C_{shell}$ variability reflects partly variations in the physical environment in which these animals lived, iv) there is no difference in the geochemical signature between the low resolution sampling and the equivalent samples of the high resolution sampling and v) there is no significant variability in the geochemical signature for a specific increment between anatomical parts of the shell.

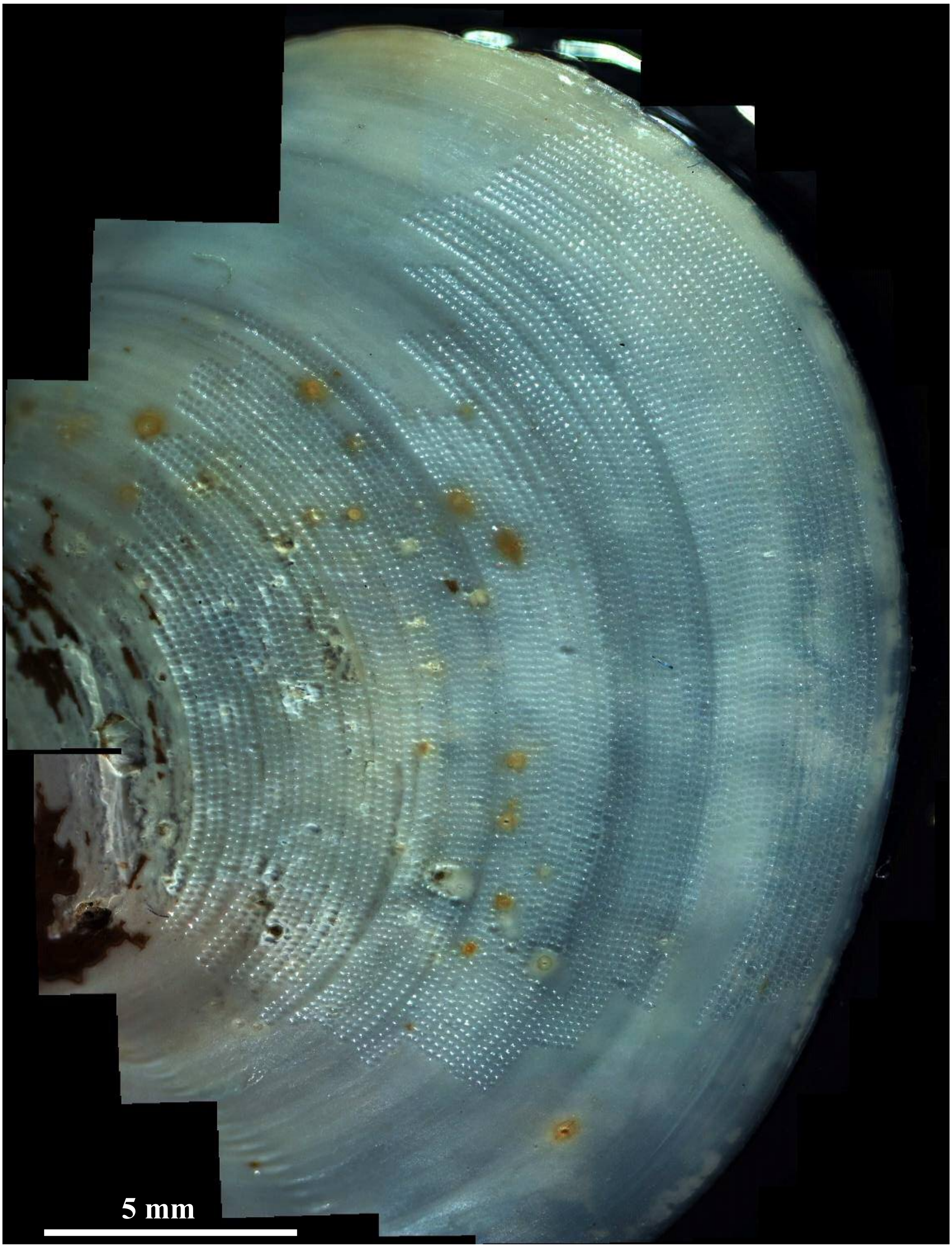
5 mm

Fig. 5.1 Microphotograph showing an example of an *A. eightsii* valve (specimen 15Ss) drilled for high-resolution geochemical analysis. Every dot drilled is approximately 150 µm in diameter (nearer the umbo drilling dots tend to be around 200 µm and nearer the margin tend to be around 110 µm in diameter). Every row of dots is considered a geochemical sample in the high-resolution sampling strategy.

5.1 South Orkney Islands

5.1.1 High-resolution sampling

High-resolution (i.e. sub-annual; **Fig. 2.6a**) geochemical records (i.e. $\delta^{18}O_{shell}$ and $\delta^{13}C_{shell}$) for the specimens 8804045, 191501025 and 192702003 are shown in **Fig. 5.2**, **Fig. 5.3** and **Fig. 5.4** respectively. For simplification of the text these specimens will be referred hereafter as 88Ss (1988 Signy shallow), 15Ss (1915 Signy shallow) and 27Sd (1927 Signy deep) respectively. The number of samples per annually-formed increment varied significantly as it depends on shell growth, which in turns is affected by the environment and biological factors. Overall the mean number of samples per annually-formed increment was 10 samples per increment ± 7 SD; however, there are significant differences (one-way ANOVA, $F_{1,29} = 13.124$, $p = 0.001$) between the shallow-collected specimens (88Ss and 15Ss; 7 samples increment^{-1} ± 5 SD) and specimen 27Sd (15 samples increment^{-1} ± 6 SD). This difference was expected considering the abnormal large size of specimen 27Sd (**Fig. 3.1**). In addition, the high-resolution records were averaged to produce single annual values calculated from the corresponding samples (**Fig. 5.5)**. The annually averaged $\delta^{18}O_{shell}$ records have greater variability than the $\delta^{13}C_{shell}$ records (**Fig. 5.5**). In addition, some samples presented a particularly high variability (e.g. specimen 15Ss samples 1903 and 1905; **Fig. 5.5**). Specimen 88Ss (**Fig. 5.2**) has an average of 3.85 ‰ ± 0.24 SD in the $\delta^{18}O_{shell}$ and 1.90 ‰ ± 0.29 SD in the $\delta^{13}C_{shell}$; specimen 15Ss (**Fig. 5.3**) has an average of 3.97 ‰ ± 0.27 SD in the $\delta^{18}O_{shell}$ and 1.63 ‰ ± 0.39 SD in the $\delta^{13}C_{shell}$ and specimen 27Sd (**Fig. 5.4**) has an average of 3.86 ‰ ± 0.15 SD in the $\delta^{18}O_{shell}$ and a significantly reduced average of 0.92 ‰ ± 0.29 SD in the $\delta^{13}C_{shell}$. All specimens show a trend towards lower $\delta^{18}O_{shell}$ and $\delta^{13}C_{shell}$ with ontogenetic age. The trends for specimen 88Ss (**Fig. 5.2**) have a slope of -0.005‰ per sample (i.e. approximately 150 µm apart) for $\delta^{18}O_{shell}$ and -0.004 ‰ per sample for $\delta^{13}C_{shell}$, the trends for specimen 15Ss (**Fig. 5.3**) have a slope of -0.008 ‰

per sample (also approximately 150 µm apart) for $\delta^{18}O_{shell}$ and -0.002 ‰ per sample for $\delta^{13}C_{shell}$; the trends for specimen 27Sd (**Fig. 5.4**) have a slope of -0.005 ‰ per sample (also approximately 150 µm apart) for $\delta^{18}O_{shell}$ and -0.005 ‰ per sample for $\delta^{13}C_{shell}$. Isotopic ranges for $\delta^{13}C_{shell}$ are 1.41 ‰ (88Ss), 1.52 ‰ (15Ss) and 1.21 ‰ (27Sd), and for $\delta^{18}O_{shell}$ they are 1.04 ‰ (88Ss), 0.99 ‰ (15Ss) and 0.58 ‰ (27Sd).

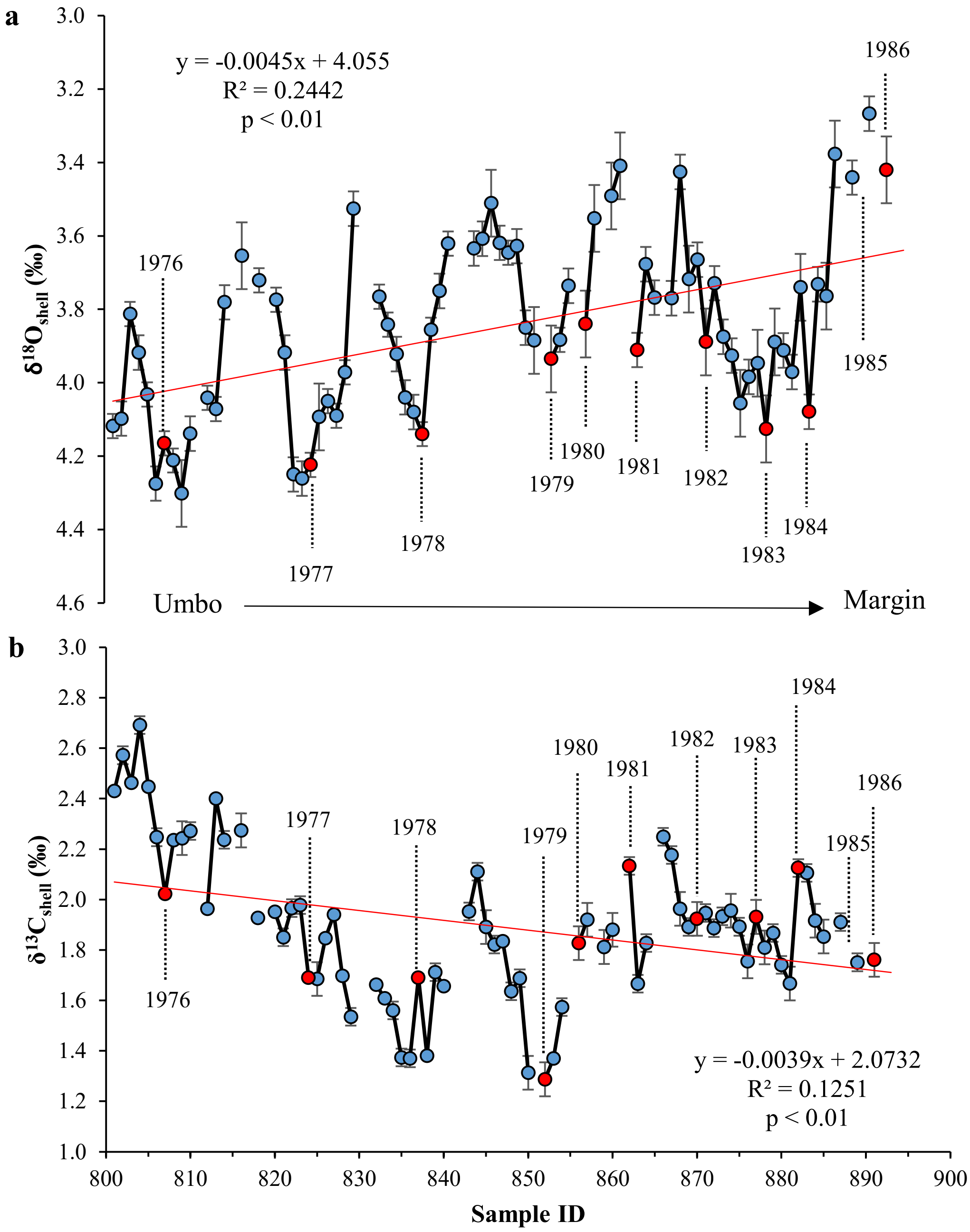

Fig. 5.2 Geochemical records of **a)** $\delta^{18}O_{shell}$ (‰ VPDB, note the inverted Y-axis) and **b)** $\delta^{13}C_{shell}$ (‰ VPDB) collected from specimen 88Ss (800 sample series). Drilling direction was from umbo towards the shell margin; this is indicated with an arrow. The first sample in each calendar

year is indicated with a red dot. The error bars represent the instrumental external precision. Linear regression lines (red line) were fitted to the data, regression equation and R^2 are also shown.

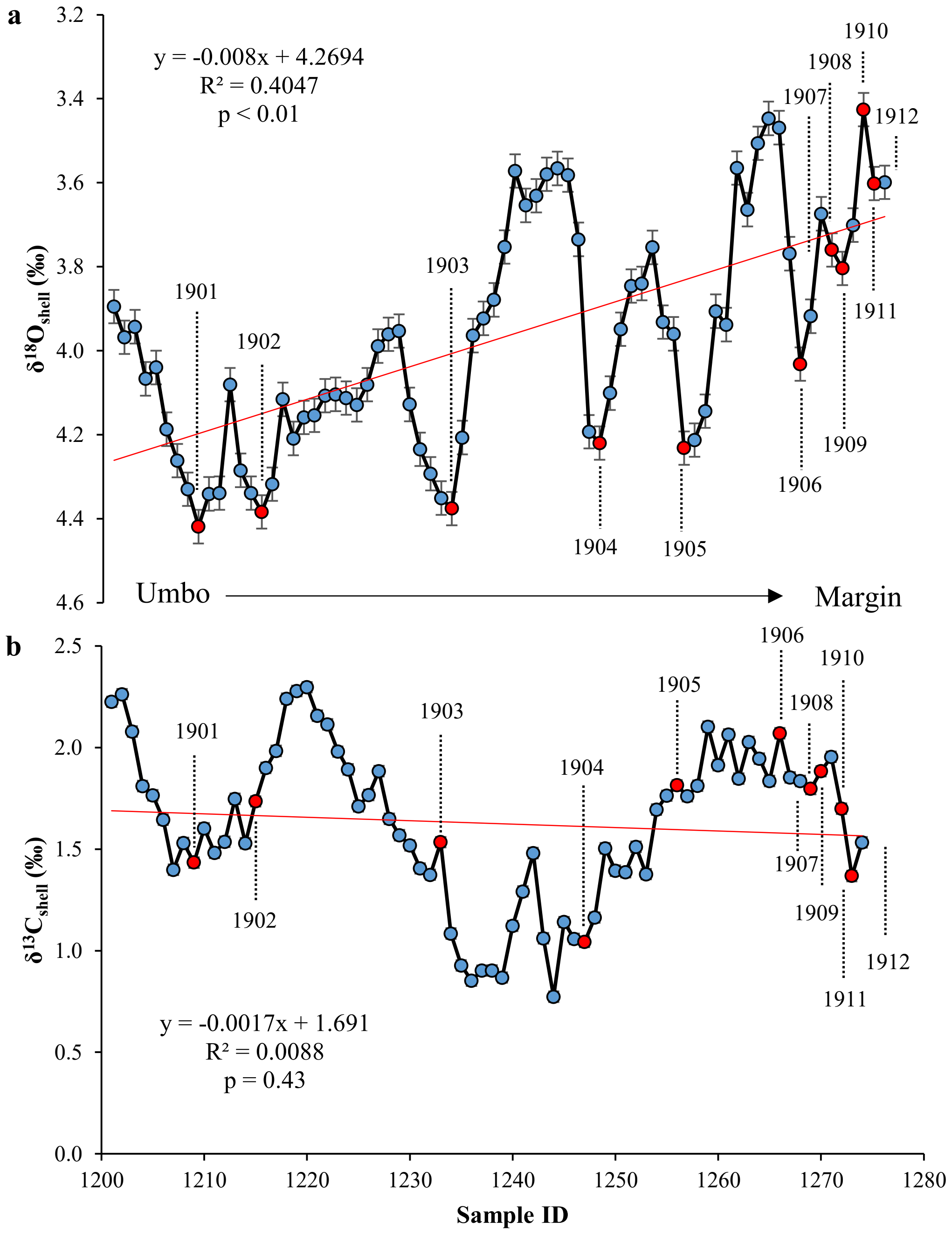

Fig. 5.3 Geochemical records of **a)** $\delta^{18}O_{shell}$ (‰ VPDB, note the inverted Y-axis) and **b)** $\delta^{13}C_{shell}$ (‰ VPDB) collected from specimen 15Ss (1200 sample series). Drilling direction was from umbo towards the shell margin; this is indicated with an arrow. The first sample in each calendar year is indicated with a red dot. The error bars represent the instrumental external precision in the case of the $\delta^{13}C_{shell}$, error bars are smaller than the size of the symbols used. Linear regression lines (red line) were fitted to the data, regression equation and R^2 are also shown.

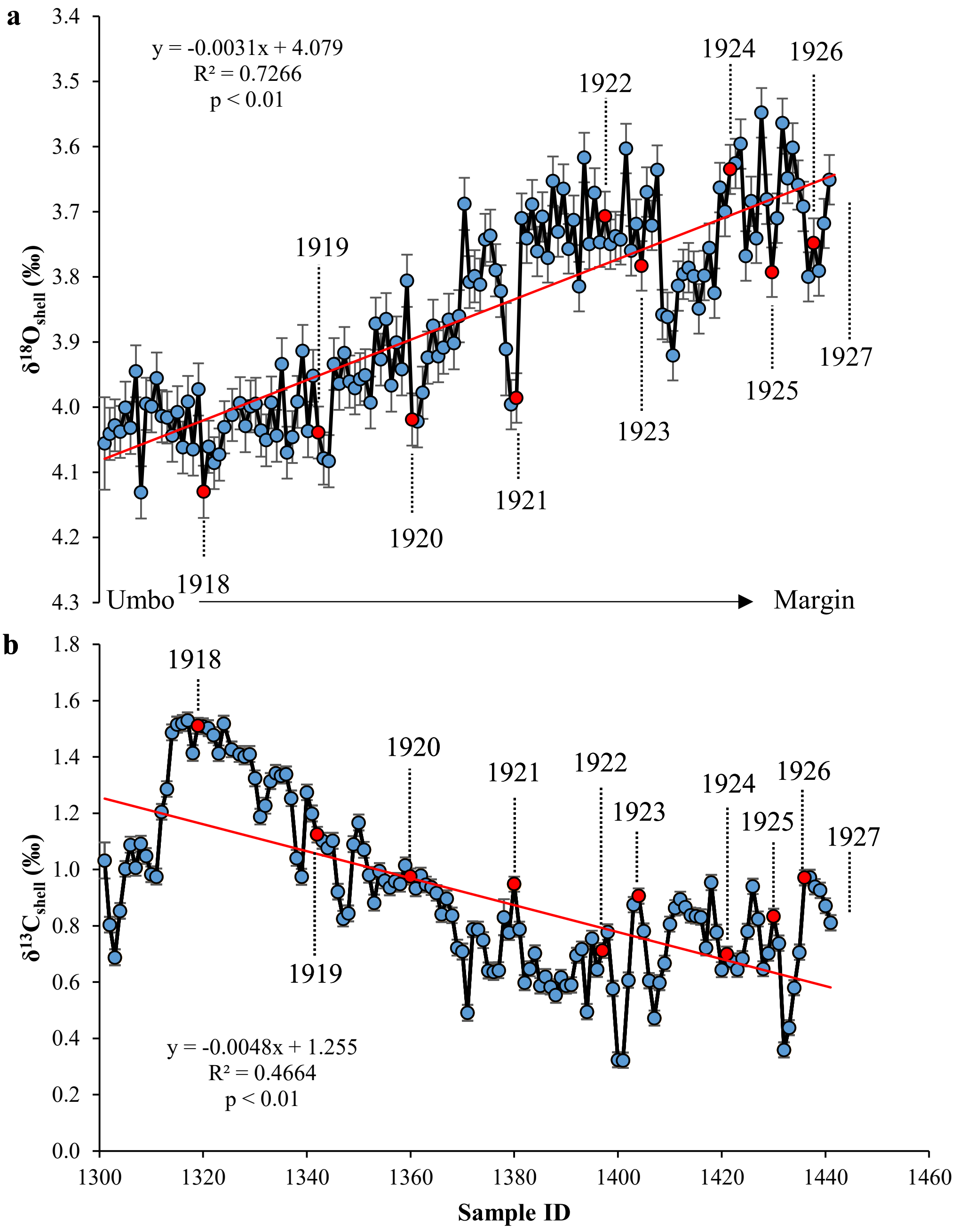

Fig. 5.4 Geochemical records of **a)** δ^{18}O$_{shell}$ (‰ VPDB, note the inverted Y-axis) and **b)** δ ^{13}C$_{shell}$ (‰ VPDB) collected from specimen 27Sd (1300 sample series). Drilling direction was from

umbo towards the shell margin; this is indicated with an arrow. The first sample in each calendar year is indicated with a red dot. The error bars represent the instrumental external precision. Linear regression lines (red line) were fitted to the data, regression equation and R^2 are also shown.

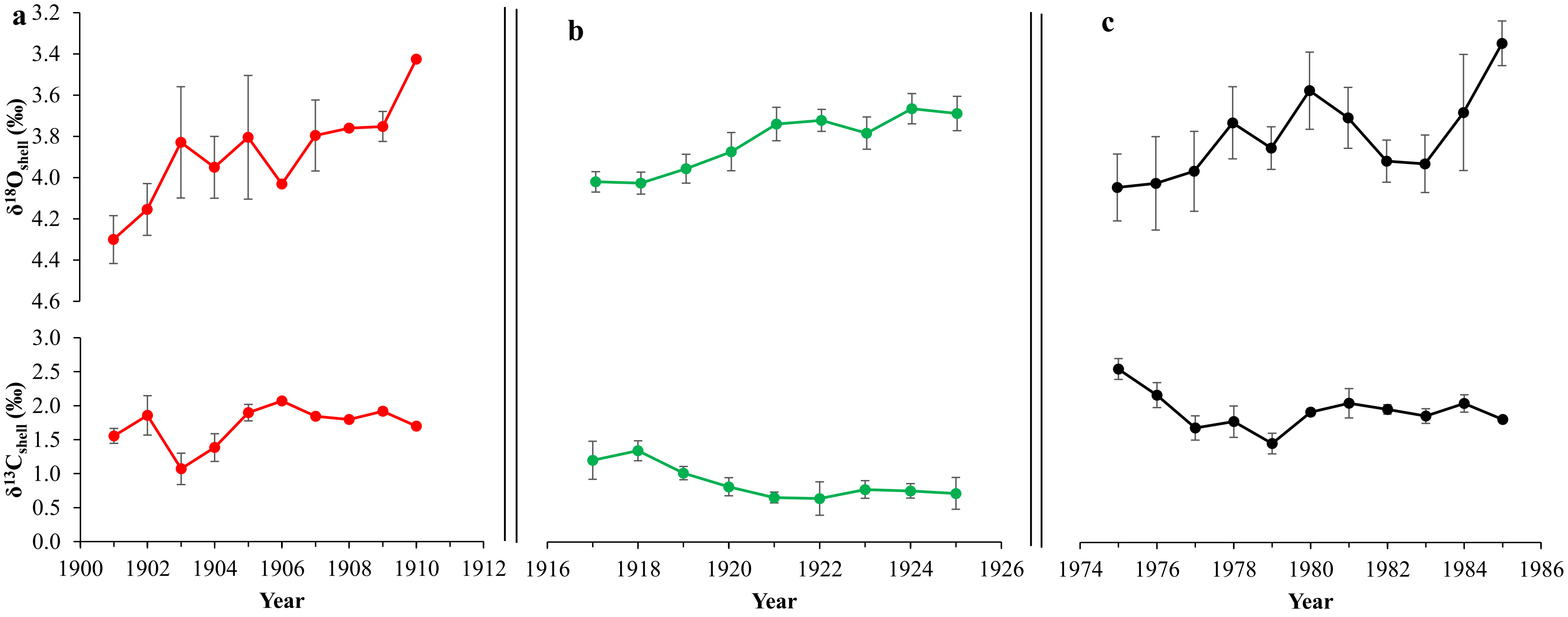

Fig. 5.5 Annual average calculated from the high-resolution sampling for **a)** $\delta^{18}O_{shell}$ (‰ VPDB, note the inverted Y-axis) and **b)** $\delta^{13}C_{shell}$ (‰ VPDB) from the specimens 15Ss (red), 27Sd (green) and 88Ss (black). The error bars show the standard deviation.

The $\delta^{18}O_{shell}$ records from the shallow-collected specimens 88Ss and 15Ss show a marked seasonal variation (0.43 ‰ yr $^{-1}$± 0.16 SD for the period 1975/83 and 0.43 ‰ yr $^{-1}$± 0.19 SD for the period 1900/06 respectively; **Fig. 5.2a** and **Fig. 5.3a**), whereas the $\delta^{18}O_{shell}$ record from the deeper-collected specimen 27Sd shows much less sub-annual variability (0.20 ‰ yr $^{-1}$± 0.06 SD for the period 1917/25, **Fig. 5.4a**). The 88Ss $\delta^{18}O_{shell}$ record (**Fig. 5.2a**) presents four distinct annual cycles (1975/78 from sample 801 to 852) and shows an average sub-annual variability of 0.43 ‰ ± 0.16 SD for the 1975/83 period. For the 1975/79 period, the isotopically highest part of the 88Ss $\delta^{18}O_{shell}$ record became progressively lower at an average rate of -0.11 ‰ yr^{-1} ± 0.08 SD, then between 1980 and 1981 it remained relatively stable (around 3.88 ‰ ± 0.04 SD) becoming particularly higher (+0.24 ‰) again during 1982 (**Fig. 5.2a**). Although there are subsequent gaps in the 88Ss $\delta^{18}O_{shell}$ record, the available data suggest that the $\delta^{18}O_{shell}$ became lower from 1984 (from sample 882; **Fig. 5.2a**). The lowest part of the sub-annual cycles also followed the same trend with the exception of 1979, which showed a particularly heavy value for the lowest part of the sub-annual cycle (**Fig. 5.2a**); excluding 1979, the lowest part of the sub-annual cycle became -0.16 ‰ ± 0.13 SD lower for the period 1975/1980 (**Fig. 5.2a**). The 15Ss $\delta^{18}O_{shell}$ record shows five sub-annual cycles from 1901 to 1905 (**Fig. 5.3a**). The 1901 $\delta^{18}O_{shell}$ cycle (from sample 1209 to 1215, **Fig. 5.3a**) is a short cycle (narrow increment) with one single sample (1212) significantly lower than the rest of the samples from the cycle; the 1902 $\delta^{18}O_{shell}$ cycle (from sample 1215 to 1233, **Fig. 5.3a**) presents a flat "bell shape" when compared to the other annual cycles in the record. The $\delta^{18}O_{shell}$ cycles from 1903 to 1906 present a bell shape and the 1906 $\delta^{18}O_{shell}$ cycle shows a trend towards lower $\delta^{18}O_{shell}$ values (**Fig. 5.3a**). Both, the lowest and the highest part of the sub-annual cycle remained relatively stable for the 1900/02 period (on average 3.98 ‰ ± 0.10 SD for the lowest part and 4.39 ‰ ± 0.02 SD for the highest part), subsequently the highest part of the sub-annual cycles became progressively lower (on average -0.12 ‰ yr $^{-1}$ ± 0.11 SD for the 1903/06 period) and although a similar trend was present in the lowest part of the sub-annual cycle this was more variable (**Fig. 5.3a**). In contrast to the previously analysed specimens, variability in the 27Sd $\delta^{18}O_{shell}$ record (**Fig. 5.4a**) is more difficult to describe as it presents less sub-annual variability making any shape in the annual cycles less distinguishable from the noise in the record. The samples comprising the year 1920 show the clearest sub-annual cycle in the record with a difference of 0.17 ‰ between the highest (i.e. sample 1380) and the lowest (i.e. sample 1370). The sub-annual variability is significantly lower (0.20 ‰ ± 0.06 SD for the period 1917/25, one-way ANOVA, $F_{1,23} = 17.052$, $p < 0.001$) than in the other specimens (0.44 ‰ ± 0.15 SD for the period 1975/83 and 0.43 ‰ ± 0.19 SD for the period 1900/06 for the specimens 88Ss and 15Ss respectively). A trend towards lower $\delta^{18}O_{shell}$ values is present in the lowest and the highest part of the record (**Fig. 5.4a**). A noticeable change in the position of the annually-formed growth line relative to the $\delta^{18}O_{shell}$ value in the subannual cycles is present after 1921 (**Fig. 5.4a**). Prior to 1921 the annually-formed growth line coincides with heavy $\delta^{18}O_{shell}$ values within the subannual cycle; whereas after 1921 this pattern becomes more irregular.

Although the $\delta^{13}C_{shell}$ records present an overall negative trend (on average -0.07 ‰ yr^{-1} ± 0.05 SD), the interannual variability between specimens is different and the $\delta^{13}C_{shell}$ sub-annual cycles are less marked than those in the $\delta^{18}O_{shell}$ record. In addition, the position of the growth line (i.e. line present at the end on an annually-formed increment) does not seem to correspond with either the highest or the lowest section of the annual isotope cycle, although it tends to be closer to the lowest part rather than to the highest part. The 88Ss $\delta^{13}C_{shell}$ record (**Fig. 5.2b**) shows a negative trend for the period 1977/80 (from sample 801 to 852; -0.02 ‰ per sample) and subsequently a slight positive trend (from sample 853 to 891; 0.003 ‰ per sample). Similarly, the 15Ss $\delta^{13}C_{shell}$ record (**Fig. 5.3b**) shows a negative trend at the beginning of the series for the period 1906/1908 (from sample 1201 to 1247; -0.02 ‰ per sample) and a subsequent positive trend (from sample 1248 to 1274, 0.01 ‰ per sample). In contrast to the shallow collected specimens, the 17Sd $\delta^{13}C_{shell}$ record (**Fig. 5.4b**) shows a strong positive trend for 1917 (from sample 1301 to 1318, 0.04 ‰ per sample), then a period (1918/20) with a negative trend (from sample 1319 to 1379, -0.01 ‰ per sample), following which the trend in the $\delta^{13}C_{shell}$ record becomes neutral for the period 1921/26 (from sample 1380 to 1441, 0.003 ‰ per sample).

Gaps in the geochemical records are due to insufficiently small samples of shell powder for stable isotope analysis. Samples near the edge of shell margin were not collected as the shell was very thin and curved, which broke easily under the pressure of the micromill drill bit. Therefore the last few years of growth (most recent) are not available in each geochemical record. The comparison between the high-resolution photographs of the drilled shells and the geochemical records shows that the annual growth lines coincide approximately with peaks (i.e. heavy values) in the $\delta^{18}O_{shell}$, although the highest $\delta^{18}O_{shell}$ value did not always coincide with the annual growth line. A comparison between the $\delta^{18}O_{shell}$ and $\delta^{13}C_{shell}$ is shown in **Fig. A5.1**; a variable positive trend is present in most of the specimens, although the regression slopes do not differ statistically (**Fig. 5.6** and **Fig. 5.7**).

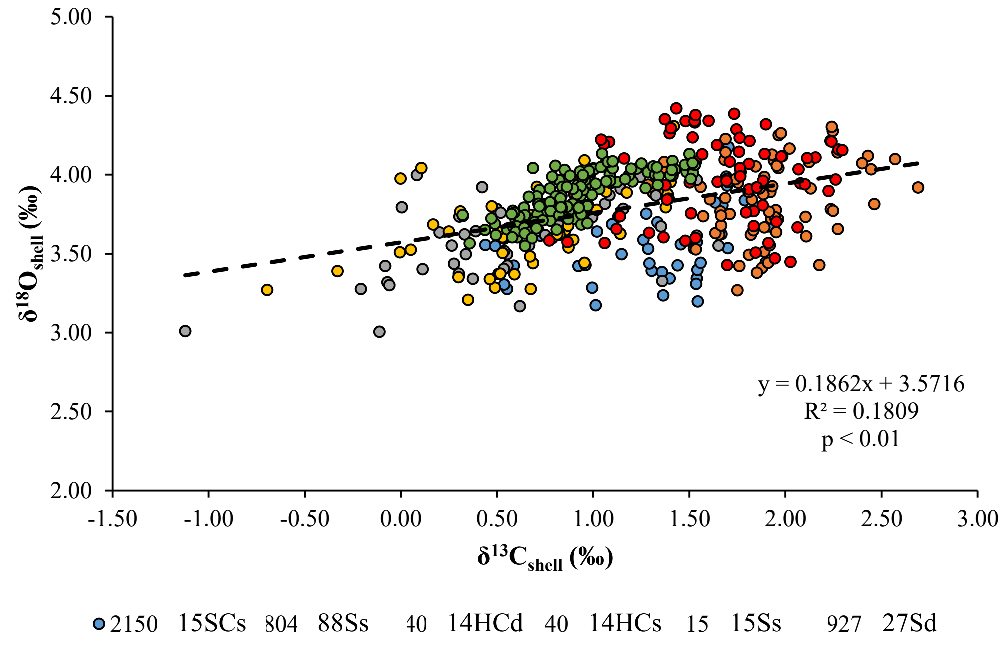

Fig. 5.6 Relationship between the $\delta^{18}O_{shell}$ (‰ VPDB) and the $\delta^{13}C_{shell}$ (‰ VPDB) of the high-resolution samples from the specimens from the South Orkney Islands (88Ss, 15Ss and 27Sd) and from the WAP (15SCs, 14HCd and 14HCs). The linear regression line (black dashed line) is also shown; the equation from the regression line and the R^2 are also provided.

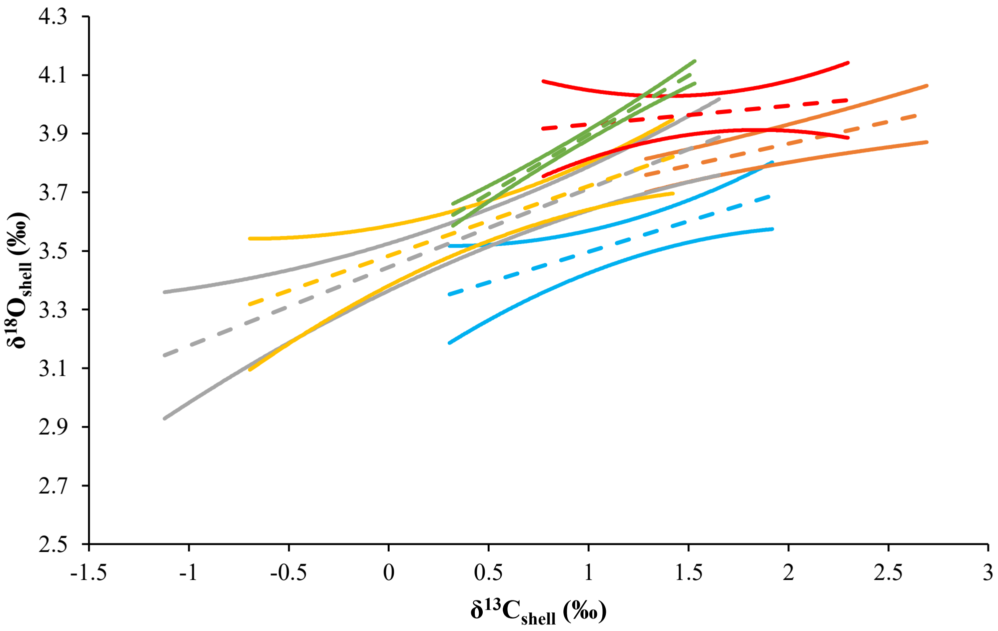

Fig. 5.7 Linear regressions between $\delta^{18}O_{shell}$ and $\delta^{13}C_{shell}$ (dashed lines) and 95 % confidence intervals (solid lines) for specimens: 15SCs (blue), 88Ss (orange), 14HCd (grey), 14HCs (yellow) 15Ss (red), 27Sd (green) based on the data shown in **Fig. 5.6**.

The temporal resolution of the high-resolution sampling varies between annually-formed increments (i.e. more geochemical samples were collected from wider increments than from narrow increments although both represent a full growing season), so that the slopes of the geochemical records are not directly comparable between increments or between specimens. However, if each sample is normalized with respect to time (i.e. shell growing season of five months, from November to March; based on a linear model of growth), the comparison between the trends becomes possible; these data are presented in **Fig. 5.8**. To avoid the introduction of artefact due to the inclusion of partial increments, the samples from partial increments were removed from the records. It can be seen that across the three time periods covered (1917/26 for 27Sd, 1900/10 for 15Ss and 1975/86 for 88Ss) there was a trend towards lower $\delta^{18}O_{shell}$ (**Fig. 5.8a**) and if the trend is averaged for the overall period (1917/86) this is -0.05 ‰ yr^{-1} ± 0.02 SD. The trends of the temporally normalized $\delta^{13}C_{shell}$ records are more varied (**Fig. 5.8b**), however the $\delta^{13}C_{shell}$ records have not been detrended and could include ontogenetic trends. The deep-collected specimen 27Sd shows the greatest trend towards lower $\delta^{13}C_{shell}$. The trends from the shallow collected specimens showed that the more modern specimen (88Ss) presented a trend towards lower $\delta^{13}C_{shell}$ whereas the older 15Ss presents a negligible positive trend; although 27Sd also presented a negative trend, as in 88Ss, this was more marked with increasing ontogenetic age (**Fig. 5.8b**).

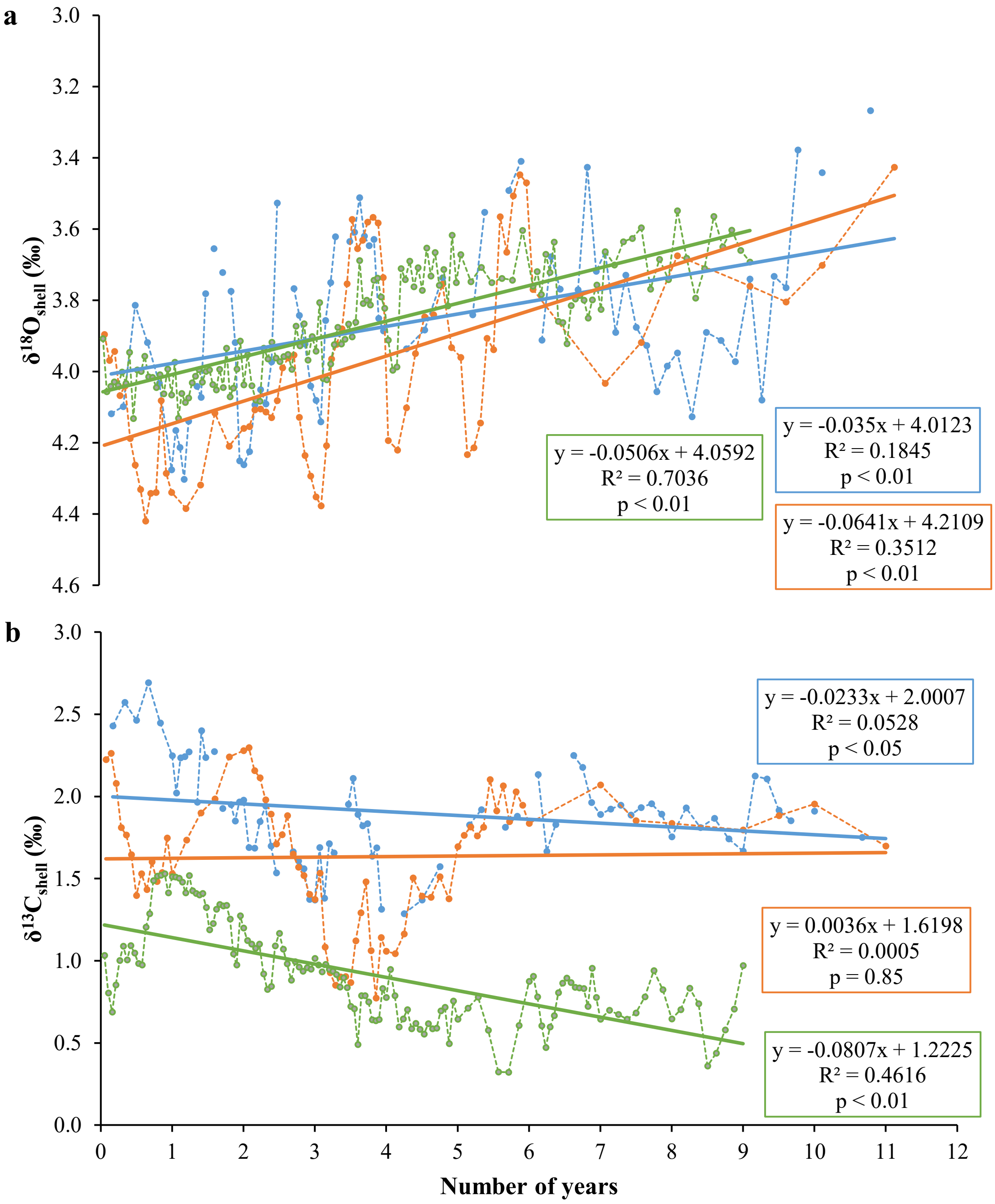

Fig. 5.8 Stable isotope records **a)** $\delta^{18}O_{shell}$ (‰ VPDB, note the inverted Y-axis) and **b)** $\delta^{13}C_{shell}$ (‰ VPDB) from the high-resolution sampling from the South Orkney Islands specimens: 88Ss (blue), 15Ss (orange) and 27Sd (green) after normalizing temporal distribution of samples. Linear

trends have been fitted to each series and the equation and R^2 of each regression line are also provided.

5.1.2 Low-resolution sampling

Low-resolution (i.e. annual) sampling results for specimens, 15Ss, 27Sd and 88Ss are shown in **Fig. 5.9a**, **Fig. 5.9b** and **Fig. 5.9c** respectively. It was possible to sample six annually-formed increments in specimen 88Ss (from 1977 to 1982, **Fig. 5.9c**), six annually-formed increments in specimen 15Ss (from 1905 to 1910, **Fig. 5.9a**) and nine annually-formed increments in specimen 27Sd (from 1917 to 1925, **Fig. 5.9b**). The 88Ss $\delta^{18}O$ record shows an average of 3.82 ‰ ± 0.15 SD and a significant change towards lower $\delta^{18}O_{shell}$ from 1979 to 1980 (**Fig. 5.9c**). The 88Ss $\delta^{13}C_{shell}$ record shows an average of 1.59 ‰ ± 0.27 SD and interannual reduced variability; a trend towards lower $\delta^{13}C_{shell}$ values from 1977/79 is present which then reverts towards higher $\delta^{13}C_{shell}$ values from 1979/1982 (**Fig. 5.9c**). The 15Ss $\delta^{18}O_{shell}$ record shows an average of 3.84 ‰ ± 0.20 SD and a change of state from heavy $\delta^{18}O_{shell}$ values (4.00 ‰ ± 0.08 SD on average) for the period 1900/2 to lower $\delta^{18}O_{shell}$ values (3.67 ‰ ± 0.105 SD on average) for the period 1903/1905 (**Fig. 5.9A**). The 15Ss $\delta^{13}C_{shell}$ record shows an average of 1.54 ‰ ± 0.30 SD and a slight trend towards higher $\delta^{13}C_{shell}$ values for the period 1900/02, then the trend changes towards lower $\delta^{13}C_{shell}$ values during 1902/03 (0.657 ‰ in difference) to revert afterwards to a trend towards higher $\delta^{13}C_{shell}$ value during 1903/05 (**Fig. 5.9a**). The 27Sd $\delta^{18}O_{shell}$ record shows an average of 3.88 ‰ ± 0.164 SD and a trend towards lower $\delta^{18}O_{shell}$ values in the entire record (0.41 ‰ difference between 1917 and 1925, **Fig. 5.9b**). The 27Sd $\delta^{13}C_{shell}$ record shows an average of 0.82 ‰ ± 0.28 SD and also a trend towards lower $\delta^{13}C_{shell}$ values in the entire record (0.85 ‰ difference between 1917 and 1925, **Fig. 5.9b**).

A comparison between the low-resolution sampling and the high-resolution sampling is presented in **Table A5.1** and **Fig. 5.10**. The low-resolution geochemical values (**Fig.**

5.9a, **Fig. 5.9b** and **Fig. 5.9c**) coincide with approximately the lowest part of the annual cycle of the equivalent samples from the high-resolution sampling (**Fig. 5.2**, **Fig. 5.3** and **Fig. 5.4**). The averages of the high-resolution sampling tend to be higher than the equivalent samples from the low-resolution sampling in the specimens 88Ss and 15Ss (**Table A5.1** and **Fig. 5.10**); 0.33 ‰ ± 0.09 SD ($\delta^{13}C_{shell}$) and 0.03 ‰ ± 0.16 SD ($\delta^{18}O_{shell}$) in the case of 88Ss, 0.08 ‰ ± 0.07 SD ($\delta^{13}C_{shell}$) and 0.16 ‰ ± 0.04 SD ($\delta^{18}O_{shell}$) in the case of 15Ss. The 27Sd $\delta^{18}O_{shell}$ record was the only case which showed lower isotopic values in the high-resolution sampling than in the low-resolution sampling (-0.08 ‰ ± 0.09 SD, **Fig. 5.10b**), the 27Sd $\delta^{13}C_{shell}$ records are very similar between them (0.01 ‰ ± 0.12 SD, **Fig. 5.10b**). The 88Ss $\delta^{18}O_{shell}$ record (**Fig. 5.10c**) showed lower values for 1979, 1981 and 1982 in the averaged high-resolution sampling than the equivalent years from the low-resolution sampling.

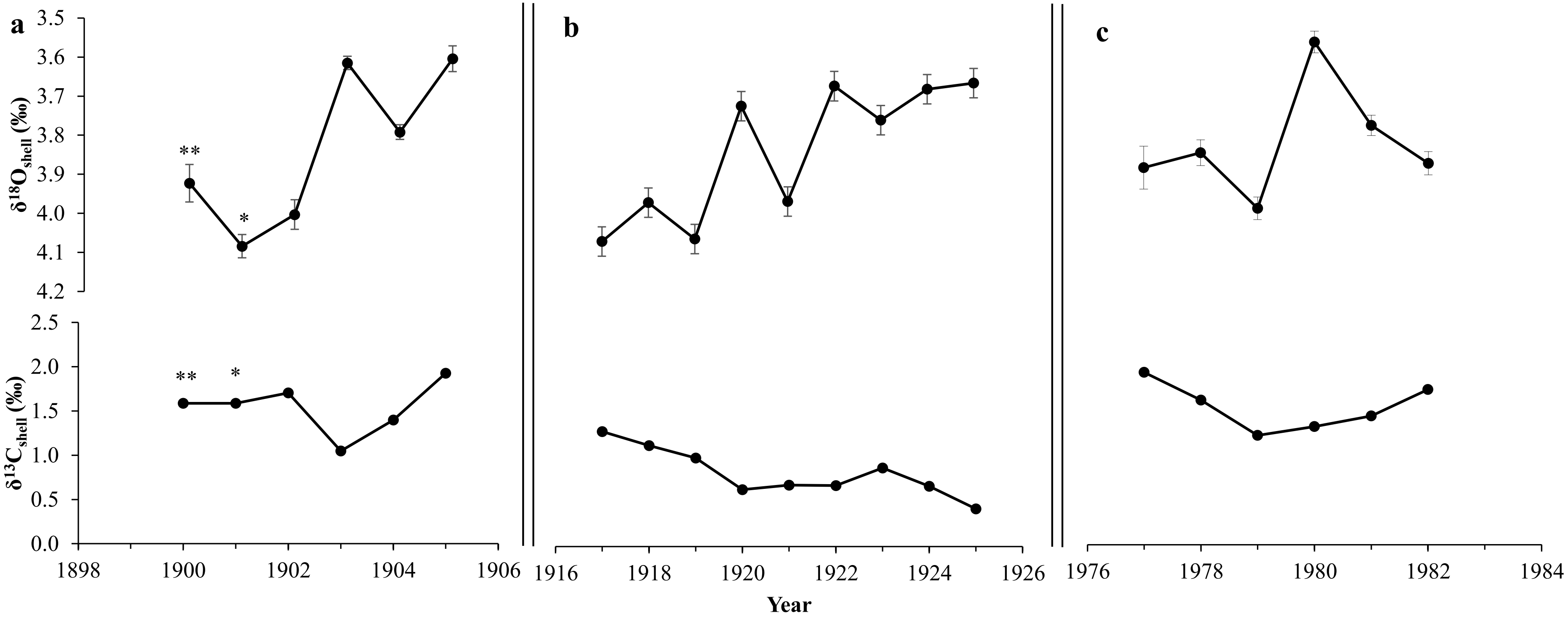

Fig. 5.9 Stable oxygen and carbon ($\delta^{18}O_{shell}$ and $\delta^{13}C_{shell}$ ‰ VPDB) records, note the inverted Y-axis in the $\delta^{18}O_{shell}$, from the low-resolution sampling collected from **a)** specimen 88Ss. The sample highlighted with an asterisk indicates that the sample incorporates the whole increment belong to 1901 and part of the 1900 increment. The sample highlighted with a double asterisk indicates that the sample contains the first half of 1900. **b)** specimen 15Ss and **c)** specimen 27Sd. The error bars represent the instrumental external precision in the case of the $\delta^{13}C_{shell}$, if error bars do not show it is because they are smaller than the symbol used.

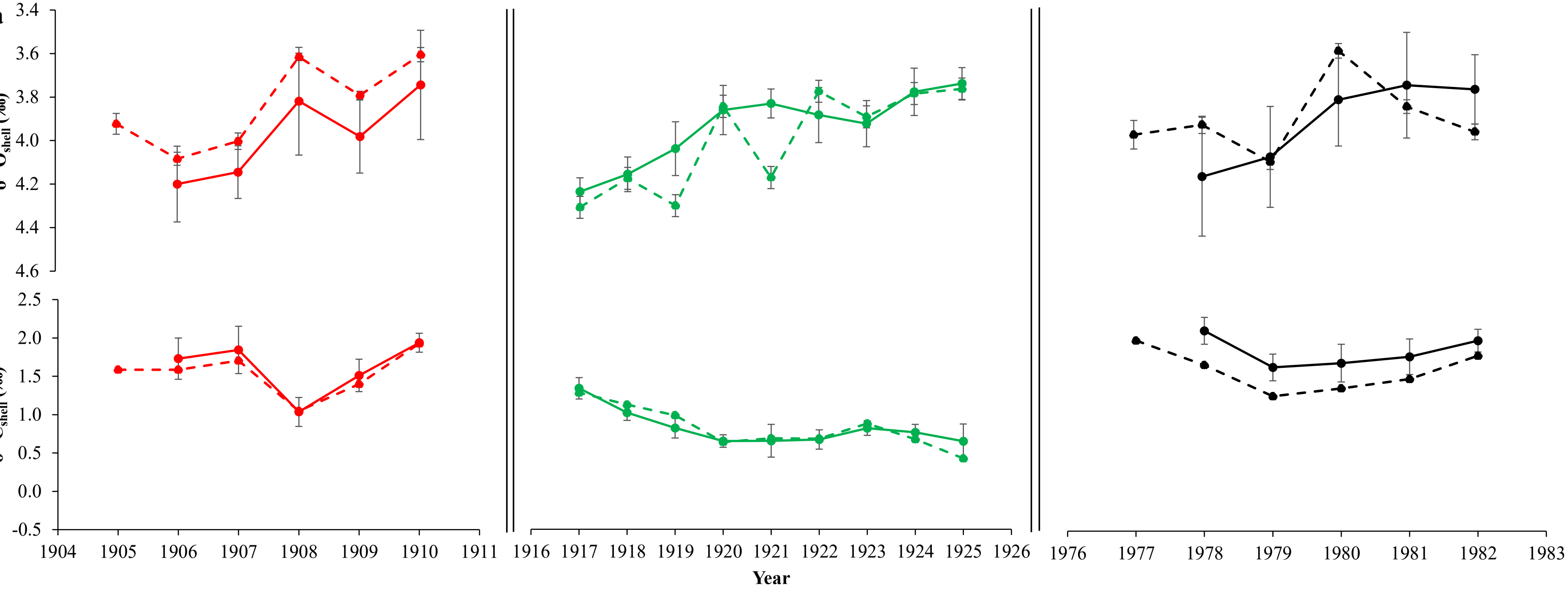

Fig. 5.10 Comparison of the **a)** $\delta^{18}O_{shell}$ (‰ VPDB, note the reversed Y-axis) and **b)** $\delta^{13}C_{shell}$ (‰ VPDB) for the high-resolution sampling (solid lines) and the low-resolution sampling (dashed lines) for specimens, 15Ss (red), 27Sd (green) and 88Ss (black). The error bars show the standard deviation.

5.1.3 Comparison with instrumental records

Only the most modern specimen (i.e. 88Ss) from those analysed covers a period for which there are instrumental environmental data available from the South Orkney Islands. A comparison between instrumental data (i.e. seawater temperature, chlorophyll concentration) extracted from Clarke et al. (1988) and $\delta^{13}C_{shell}$, $\delta^{18}O_{shell}$ records from specimen 88Ss are presented in **Fig. 5.11**. As no paired valve was available from specimen 88Ss (there was no paired valves for any of the specimens collected in 1988) it was not possible to carry out three way crossmatching calibration between the increments seen on the outer surface of the shell, the internal increments observable from a shell section and the geochemical records, although the geochemical records and the outer surface increments were successfully crossmatched. This lack of calibration between the outer surface and the internal shell increments can be a product of offsets in the temporal alignment due to the misidentification of increments. The comparison between the seawater temperature record and the $\delta^{18}O_{shell}$ records (**Fig. 5.11a**) shows apparent contradictory terms; from 1972 to 1978 summer peak seawater temperature rose, with summer peak seawater temperatures decreasing subsequently from 1978 to 1983 but the $\delta^{18}O_{shell}$ record shows a trend towards lower values for the 1976/81 period and a trend towards higher values for the 1981/84 period. In addition, the comparison between the chlorophyll concentration and the $\delta^{13}C_{shell}$ records (**Fig. 5.11b**), shows a strong negative trend in the chlorophyll concentration record from 1974 to 1979 whereas the $\delta^{13}C_{shell}$ record shows a strong negative trend from 1976 to 1978. On the other hand, if an offset of (minus) two years is artificially introduced in the geochemical data (**Fig. A5.2**), the trends in both the environmental record and the geochemical data coincide ($r = 0.62$, $p = 0.08$, $n = 9$, based on annual averages for a five month growing season from November to March). As a comparison the correlation calculated using the same temporal resolution but without the minus two year offset was r = 0.09, p = 0.84, n = 7 (**Fig. 5.11**). It is not possible to test whether there is indeed an offset in the geochemical data due to the lack of a sectioned profile from the 88Ss specimen; however even though the only valve available was drilled, it is still possible to section the specimen parallel to the maximum growth axis and the high-resolution geochemical sampling profile.

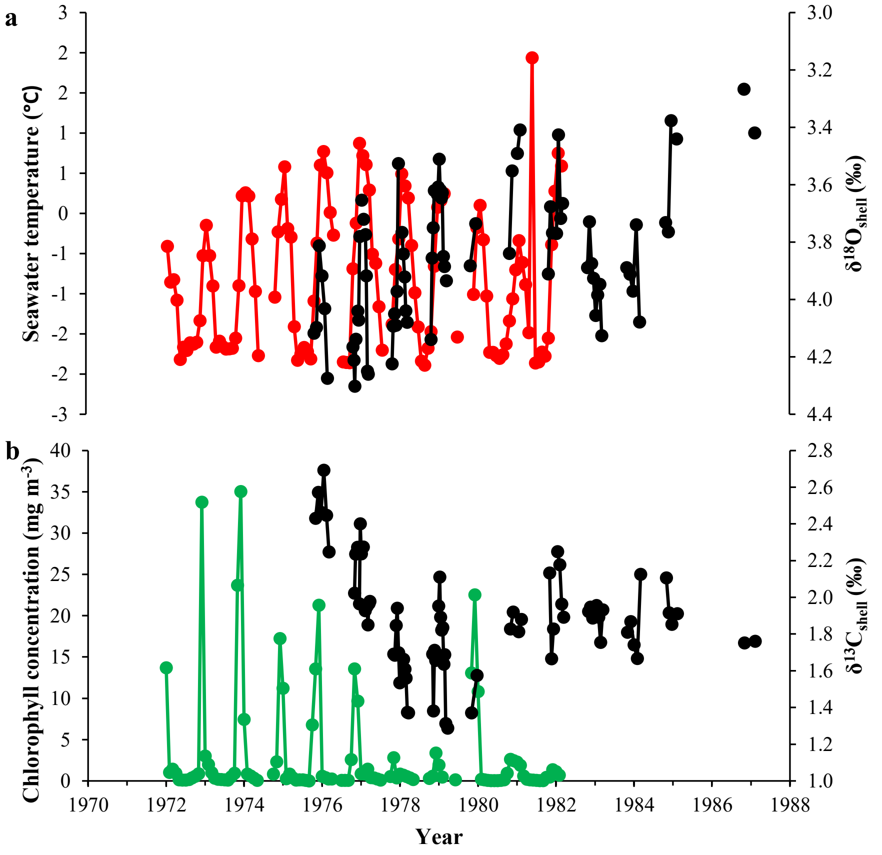

Fig. 5.11 Comparison between **a)** the seawater temperature (°C, red line, data extracted from Clarke et al., 1988) and the $\delta^{18}O_{shell}$ (‰ VPDB, black line, note the inverted Y-axis) from specimen 88Ss and **b)** chlorophyll concentration (mg m^{-3}, green line, data extracted from Clarke et al., 1988) and the $\delta^{13}C_{shell}$ (‰ VPDB, black line) from specimen 88Ss.

5.2 West Antarctic Peninsula

5.2.1 High-resolution sampling

The $\delta^{18}O_{shell}$ and the $\delta^{13}C_{shell}$ records of specimens 21504031, 21402010 and 21403025 are shown in **Fig. 5.12**, **Fig. 5.13** and **Fig 5.14** respectively. Additionally, in order to facilitate the visual comparison between the records, these have been compiled in **Fig. A5.3**. For simplification of the text these specimens will be referred hereafter as 15SCs (2015 South Cove shallow), 14HCd (2014 Hangar Cove deep) and 14HCs (2014 Hangar Cove shallow) respectively. Also, similar to the South Orkney Islands samples, a comparison between the $\delta^{18}O_{shell}$ and the $\delta^{13}C_{shell}$ is provided in **Fig. A5.1** and **Fig. 5.6**. The average number of samples per annually-formed increment was five samples increment^{-1} ± 3 SD, which is a similar average to that one from the shallow-collected specimens from the South Orkney Islands. The annually-formed growth line generally coincided with the highest portion of the sub-annual cycle, although there are a few exceptions. Sub-annual cycles in the $\delta^{18}O_{shell}$ records are present in all specimens, being particularly clear in specimen 15SCs (**Fig. 5.12a**) which presents five clear cycles.

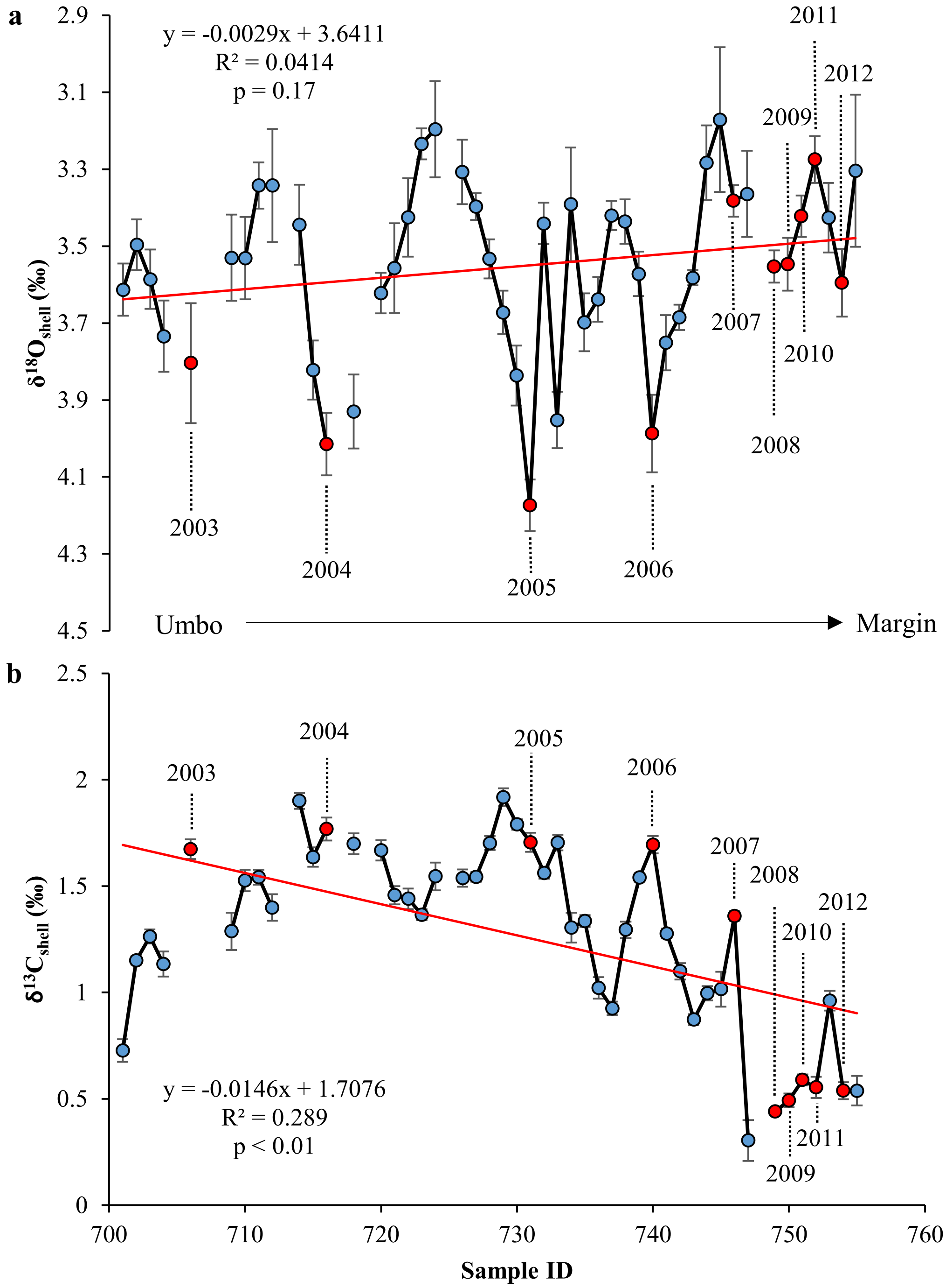
a
b
y = -0.0029x + 3.6411
R² = 0.0414
p = 0.17
δ18Oshell (‰)
2.9
3.1
3.3
3.5
3.7
3.9
4.1
4.3
4.5
2003
2004
2005
2006
2007
2008
2009
2010
2011
2012
Umbo
Margin
y = -0.0146x + 1.7076
R² = 0.289
p < 0.01
δ13Cshell (‰)
2.5
2
1.5
1
0.5
0
700
710
720
730
740
750
760
Sample ID

Fig. 5.12 Geochemical records of **a)** $\delta^{18}O_{shell}$ (‰ VPDB, note that the Y-axis has been inverted) and **b)** $\delta^{13}C_{shell}$ (‰ VPDB) collected from specimen 15SCs (700 series). Drilling direction was from the umbo towards the shell margin; this is indicated with an arrow. The first sample in each calendar year is indicated with a red dot. The error bars represent the instrumental external precision. Linear regression lines (red line) were fitted to the data, regression equation and R^2 are also shown.

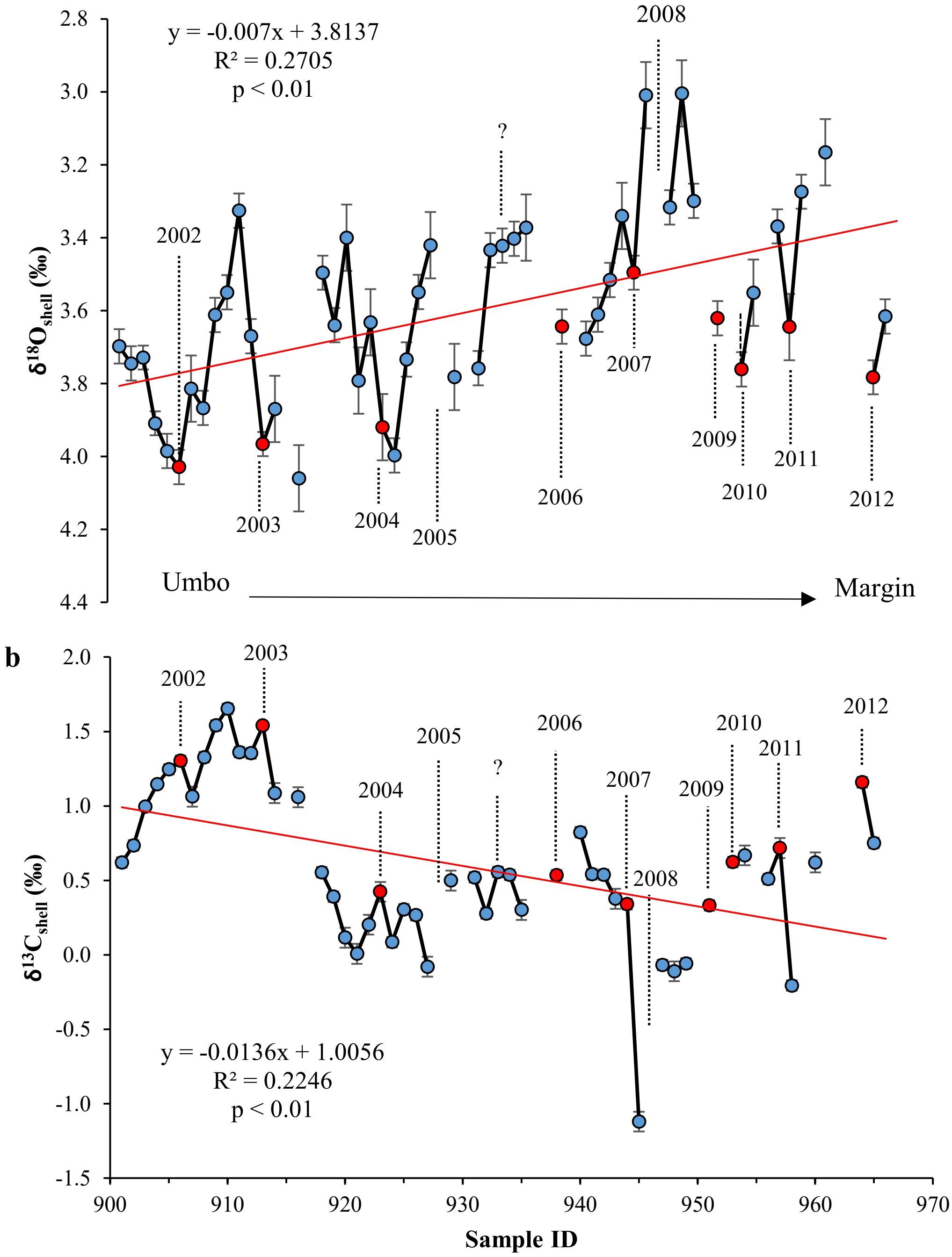
y = -0.007x + 3.8137
R² = 0.2705
p < 0.01
δ18Oshell (‰)
2.8
3.0
3.2
3.4
3.6
3.8
4.0
4.2
4.4
2002
2003
2004
2005
?
2006
2007
2008
2009
2010
2011
2012
Umbo
Margin
b
δ13Cshell (‰)
2.0
1.5
1.0
0.5
0.0
-0.5
-1.0
-1.5
2002
2003
2004
2005
?
2006
2007
2008
2009
2010
2011
2012
y = -0.0136x + 1.0056
R² = 0.2246
p < 0.01
900
910
920
930
940
950
960
970
Sample ID

Fig. 5.13 Geochemical records of **a)** $\delta^{18}O_{shell}$ (‰ VPDB, note the inverted Y-axis) and **b)** $\delta^{13}C_{shell}$ (‰ VPDB) collected from specimen 14HCd (900 sample series). Drilling direction was from the umbo towards the shell margin; this is indicated with an arrow. The first sample in each calendar year is indicated with a red dot. The error bars represent the instrumental external precision. The question mark indicates the position of faint increment which was not considered as an annually-formed growth check. Linear regression lines (red line) were fitted to the data, regression equation and R^2 are also shown.

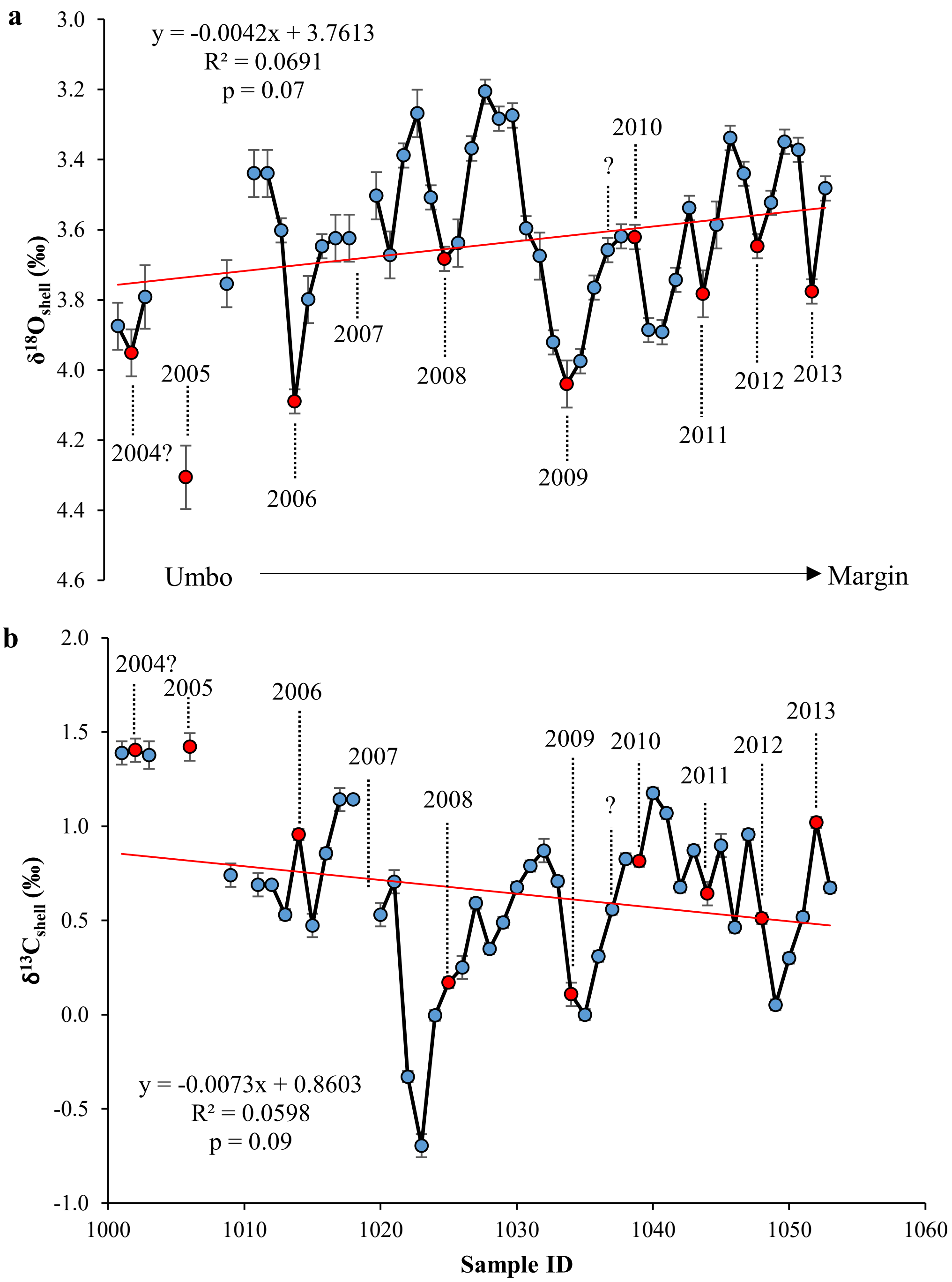
a
3.0
3.2
3.4
3.6
3.8
4.0
4.2
4.4
4.6
δ18Oshell (‰)
y = -0.0042x + 3.7613
R² = 0.0691
p = 0.07
2004?
2005
2006
2007
2008
2009
?
2010
2011
2012
2013
Umbo
Margin
b
2.0
1.5
1.0
0.5
0.0
-0.5
-1.0
δ13Cshell (‰)
2004?
2005
2006
2007
2008
2009
?
2010
2011
2012
2013
y = -0.0073x + 0.8603
R² = 0.0598
p = 0.09
1000
1010
1020
1030
1040
1050
1060
Sample ID

Fig. 5.14 Geochemical records of **a)** $\delta^{18}O_{shell}$ (‰ VPDB, note the inverted Y-axis) and **b)** $\delta^{13}C_{shell}$ (‰ VPDB) collected from specimen 14HCs (1000 sample series). Drilling direction was from the umbo towards the shell margin; this is indicated with an arrow. The first sample in each calendar year is indicated with a red dot. The error bars represent the instrumental external precision. The question mark indicates the position of a faint increment that was not considered as an annually-formed growth check. Linear regression lines (red line) were fitted to the data, regression equation and R^2 are also shown.

All the $\delta^{18}O_{shell}$ records show a varying trend towards lower $\delta^{18}O_{shell}$ with ontogenetic age: specimen 15SCs (**Fig. 5.12**) has a slope of -0.003 ‰ per sample (i.e. approximately 150 µm apart) in the $\delta^{18}O_{shell}$ record and -0.015 ‰ per sample (i.e. also approximately 150 µm apart) in the $\delta^{13}C_{shell}$ record; specimen 14HCd (**Fig. 5.13**) shows a trend of -0.01 ‰ per sample in the $\delta^{18}O_{shell}$ record and -0.01 ‰ per sample in the $\delta^{13}C_{shell}$ record and specimen 14HCs (**Fig. 5.14**) shows a slope of -0.004 ‰ per sample in the $\delta^{18}O_{shell}$ record and -0.01 ‰ per sample in the $\delta^{13}C_{shell}$ record. Specimen 15SCs (**Fig. 5.12**) shows an average of 3.55 ‰ ± 0.23 SD $\delta^{18}O_{shell}$ record and an average of 1.27 ‰ ± 0.43 SD in the $\delta^{13}C_{shell}$ record. Furthermore, the 15SCs $\delta^{18}O_{shell}$ record (**Fig. 5.12a**) shows a trend towards lower $\delta^{18}O_{shell}$ in the lowest part of the sub-annual cycle and a trend towards higher $\delta^{18}O_{shell}$ in the highest part of the sub-annual cycle, meaning an increasing total range in $\delta^{18}O_{shell}$, between sample 701 and 730 (i.e. 2003/05). The shift towards higher $\delta^{18}O_{shell}$ is especially marked during the year 2004/05, from 3.20 ‰ (sample 724, **Fig. 5.12a**) to 4.17 ‰ (sample 731, **Fig. 5.12a**). On average the sub-annual variability for the period 2002/06 is 0.55 ‰ ± 0.31 SD in the case of the $\delta^{18}O_{shell}$ record and 0.36 ‰ ± 0.13 SD in the case of the $\delta^{13}C_{shell}$ record, note that these were calculated using the undetrended data series (for both $\delta^{18}O_{shell}$ and $\delta^{13}C_{shell}$) and therefore any ontogenetic trend in the series can have an impact in the sub-annual variability. In addition, three samples (i.e. 733, 735 and 736) from the 2005 cycle appear to be unusually heavy (**Fig. 5.12a**) when compared with the $\delta^{18}O_{shell}$ variability from previous annual cycles. The presence of several gaps in the $\delta^{18}O_{shell}$ record from specimen 14HCd (**Fig. 5.13a**) impedes a clear visualization of many of the annual cycles in the

$\delta^{18}O_{shell}$ record. On average the 14HCd $\delta^{18}O_{shell}$ record is 3.61 ‰ ± 0.25 SD and the $\delta^{13}C_{shell}$ record is 0.60 ‰ ± 0.54 SD. Furthermore, the sub-annual variability for the period 2000/03 (note the shortness of the period considered as this is the only period with clear distinguishable sub-annual cycles) for the $\delta^{18}O_{shell}$ record is on average 0.43 ‰ ± 0.14 SD and 0.44 ‰ ± 0.23 SD for the $\delta^{13}C_{shell}$ record. The comparison between the 14HCd $\delta^{18}O_{shell}$ record (**Fig. 5.13a**) with the high-resolution photograph of the drilled shells shows that in several cases the annually-formed growth line did not coincide with the highest sample within an annual cycle (i.e. sample 913, 2002; sample 923, 2003; sample 933, 2005 and sample 938, 2006). No data are available for the years 2013 and 2014 as the outermost region of the margin was not sampled due to the fragility and reduced thickness of the shell in this section. Specimen 14HCs (**Fig. 5.14**) shows an average of 3.64 ‰ ± 0.24 SD in the $\delta^{18}O_{shell}$ record and 0.65 ‰ ± 0.44 SD in the $\delta^{13}C_{shell}$ record. Similar to 14HCd, the 2010 growth line (i.e. sample 1039) in the 14HCs $\delta^{18}O_{shell}$ record (**Fig. 5.14a**) does not coincide with highest $\delta^{18}O_{shell}$ value in the sub-annual cycle. Two prominent shifts towards higher $\delta^{18}O_{shell}$ are present in the record, the first during 2005/06 (from 3.43 ‰, sample 1012, to 4.09 ‰, sample 1014; **Fig. 5.14a**) and the second during the 2008/09 cycle (from 3.27 ‰, sample 1030 to 4.04 ‰, sample 1034; **Fig. 5.14a**). Few data are available for 2013 and no data for 2014 as the outermost section of the shell margin was not sampled completely due to the fragility and reduced thickness of the shell. Isotopic ranges for $\delta^{13}C_{shell}$ are 1.61 ‰ (15SCs), 2.77 ‰ (14HCd) and 2.12 ‰ (14HCs); and for $\delta^{18}O_{shell}$ 1.00 ‰ (15SCs), 1.06 ‰ (14HCd) and 1.10 ‰ (14HCs). The average of $\delta^{18}O_{shell}$ ranges (i.e. 1.05 ‰ ± 0.05 SD) differs significantly from the range of the $\delta^{18}O_{water}$ (0.71 ‰ for the period August 2001 to March 2015; see Chapter IV subsection 4.1.5 and **Fig. 4.18**) for the entire length of the record (i.e. including winter months) and differs even more if only the range of the $\delta^{18}O_{water}$ for *A. eightsii* growing season (i.e. Nov-Mar) is considered (0.54 ‰).

The $\delta^{13}C_{shell}$ records show more variability in their trends; the 15SCs $\delta^{13}C_{shell}$ record (**Fig. 5.12b**) shows a trend towards higher $\delta^{13}C_{shell}$ for three years (from sample 700 to 731; **Fig. 5.12b**) switching afterwards to a trend towards lower $\delta^{13}C_{shell}$ values. An abrupt change was also noticeable in 2007 when $\delta^{13}C_{shell}$ became significantly lower (**Fig. 5.12b**). The position of the growth line relative to the $\delta^{13}C_{shell}$ record also varied; whereas in 2006 (sample 740) and 2007 (sample 746) the growth line coincides with the highest $\delta^{13}C_{shell}$ value of the annual cycle, in 2004 (sample 716) and 2005 (sample 731) the growth line is immediately after a peak in the $\delta^{13}C_{shell}$ record (samples 714 and 729 respectively; **Fig. 5.12b**). The 14HCd $\delta^{13}C_{shell}$ record (**Fig. 5.13b**) shows a trend towards higher $\delta^{13}C_{shell}$ during 2001 and 2002 (from sample 900 to 913; **Fig. 5.13b**) switching to a trend towards lower $\delta^{13}C_{shell}$ values during 2003 (from sample 913 to 921; **Fig. 5.13b**); subsequently a slightly positive trend towards higher $\delta^{13}C_{shell}$ is apparent in the record. A noticeable shift towards lower $\delta^{13}C_{shell}$ is present during 2007 (**Fig. 5.13b**) from 0.34 ‰ (sample 944) to -1.12 ‰ (sample 945). A distinguishable, although faint, line was present in the portion of the shell formed during 2005 (sample 933, **Fig. 5.13b**) although it was regarded as a disturbance line. The 14HCs $\delta^{13}C_{shell}$ record shows a trend toward lower $\delta^{13}C_{shell}$ between 2004 and 2007 and a subtle trend towards higher $\delta^{13}C_{shell}$ afterwards (**Fig. 5.14b**). The position of the growth lines relative to the $\delta^{13}C_{shell}$ record is variable and no clear relationship between both can be established. The 2005/06 increment showed a trend towards lower $\delta^{13}C_{shell}$ values; however the growth check (sample 1014) did not coincide with the lower $\delta^{13}C_{shell}$ annual value (sample 1013). Other cases such as 2009/10 and 2012/13 there was a trend towards higher $\delta^{13}C_{shell}$ and the growth check coincided with the heavy $\delta^{13}C_{shell}$ values (samples 1039 and 1052; **Fig. 5.14b**).

The trends in $\delta^{18}O_{shell}$ and $\delta^{13}C_{shell}$ records show no clear relationship, although in nine out of 29 cases a minimum of $\delta^{18}O_{shell}$ coincided with a rise in $\delta^{13}C_{shell}$.

An analysis of the shell profiles of the sectioned shells revealed that specimen 15SCs has an ontogenetic age of 17 years (1999/2015), specimen 14HCd 16 years (1998/2014). No profile of specimen 14HCs was available, therefore only an estimation of 14 years based of the outer surface of the shell was possible (2000/14).

Similar to the South Orkney Islands specimens, the temporal scale of the high-resolution records have to be standardized before a comparison in the slope of the series can be made. The results after the temporal standardization was carried out, as described for the specimens from the South Orkney Islands, are shown in **Fig. 5.15**. All specimens show a similar trend towards lower $\delta^{18}O_{shell}$ (-0.03 ‰ ± 0.01 SD on average, **Fig. 5.15a**), being slightly more pronounced in specimen 14HCd. Trends in the $\delta^{13}C_{shell}$ record are also towards lower values although the slope varies (**Fig. 5.15b**), with specimen 15SCs having the strongest gradient. The $\delta^{13}C_{shell}$ records presented here for the South Orkney Islands have not been detrended and could include ontogenetic trends that may vary depending on the age of the specimen.

The annual averages of the high-resolution records of the WAP specimens are presented in **Fig. 5.16**. The $\delta^{18}O_{shell}$ records show similar trends and although there is no statistical differences between specimens (one-way ANOVA, $F_{2,30} = 2.426$, $p = 0.11$), the records from the Hangar Cove specimens (14HCd and 14HCs) show higher degree of correlation ($r = 0.71$, $p = 0.02$, $n = 10$) than any of those specimens with the South Cove specimen (15SCs; **Fig. 5.16a**). The shallow-collected specimens show lower values during 2007/08 which were preceded and followed higher isotopic values (**Fig. 5.16a**). The deep collected specimen 14HCd does not show particularly lower isotopic values for 2007/08, although the 2007 second lowest value from the entire record (**Fig. 5.16a**).

Similarly, the $\delta^{13}C_{shell}$ records show similar trends, which are also not statistically different (one-way ANOVA, $F_{2,30} = 2.916$, $p = 0.07$; **Fig. 5.16b**). Contrary to what shown in the $\delta^{18}O_{shell}$ records, a strong correlation between the shallow-collected specimens (15SCs and 14HCs; $r = 0.712$, $p = 0.02$, $n= 10$), instead of between sampling locations. Interestingly, the samples from 2007 in specimens 15SCs and 14HCd show a very large variability, represented in **Fig. 5.16b** as standard error. All $\delta^{13}C_{shell}$ records show a trend towards lower $\delta^{13}C_{shell}$ values from 2001/07 and a subsequent trend towards higher values (**Fig. 5.16b**); this is taking in consideration that ontogenetic trends may be present in the $\delta^{13}C_{shell}$ records and therefore such trends may change if the effect of ontogeny is to be removed.

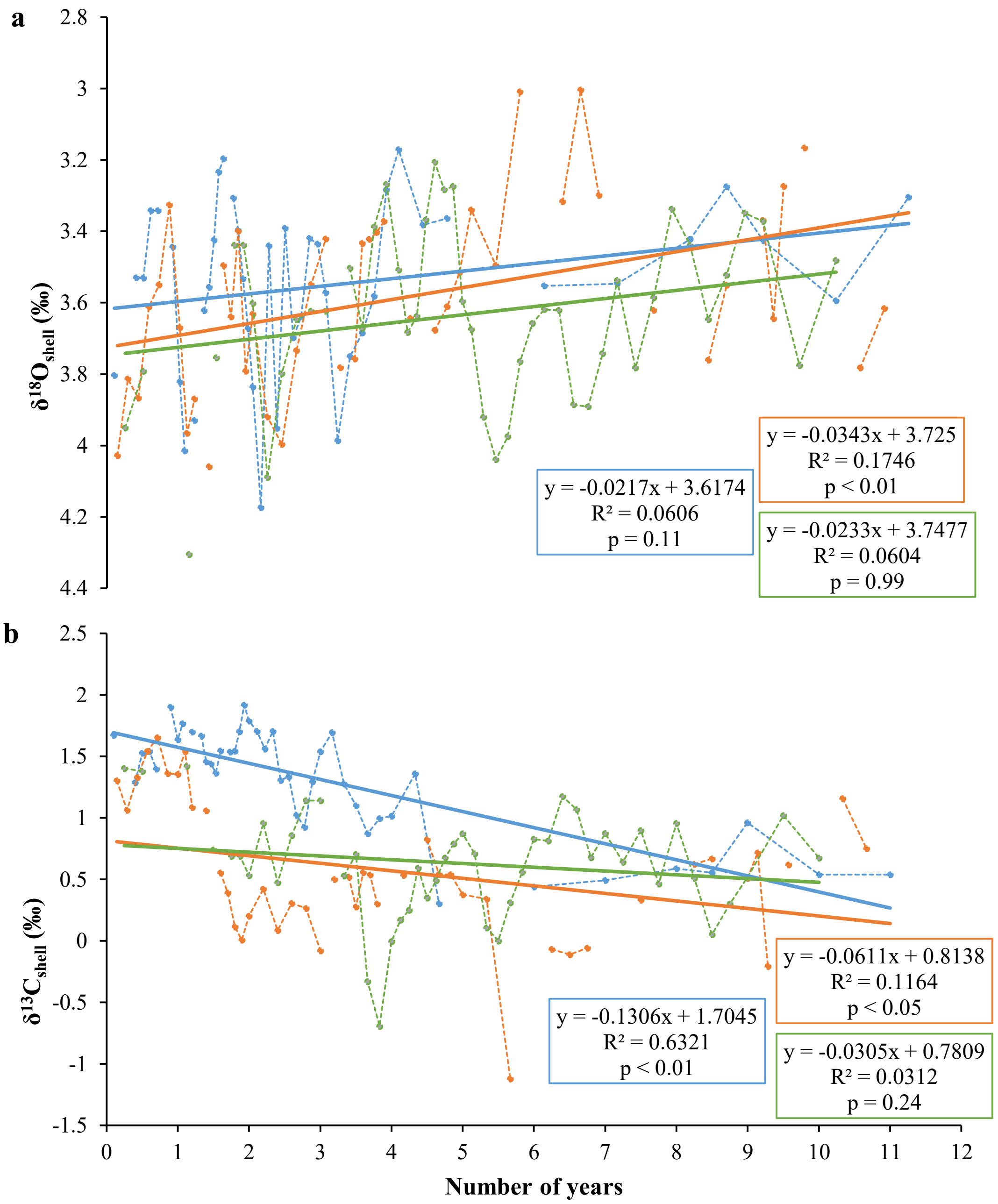

Fig. 5.15 Stable isotope records **a)** $\delta^{18}O_{shell}$ (‰ VPDB, note the inverted Y-axis) and **b)** $\delta^{13}C_{shell}$ (‰ VPDB) from the high-resolution sampling from the WAP specimens: 15SCs (blue), 14HCd

(orange) and 14HCs (green) after normalizing temporal distribution of samples. Linear trends have been fitted to each series and the equation and R^2 of each regression line are also provided.

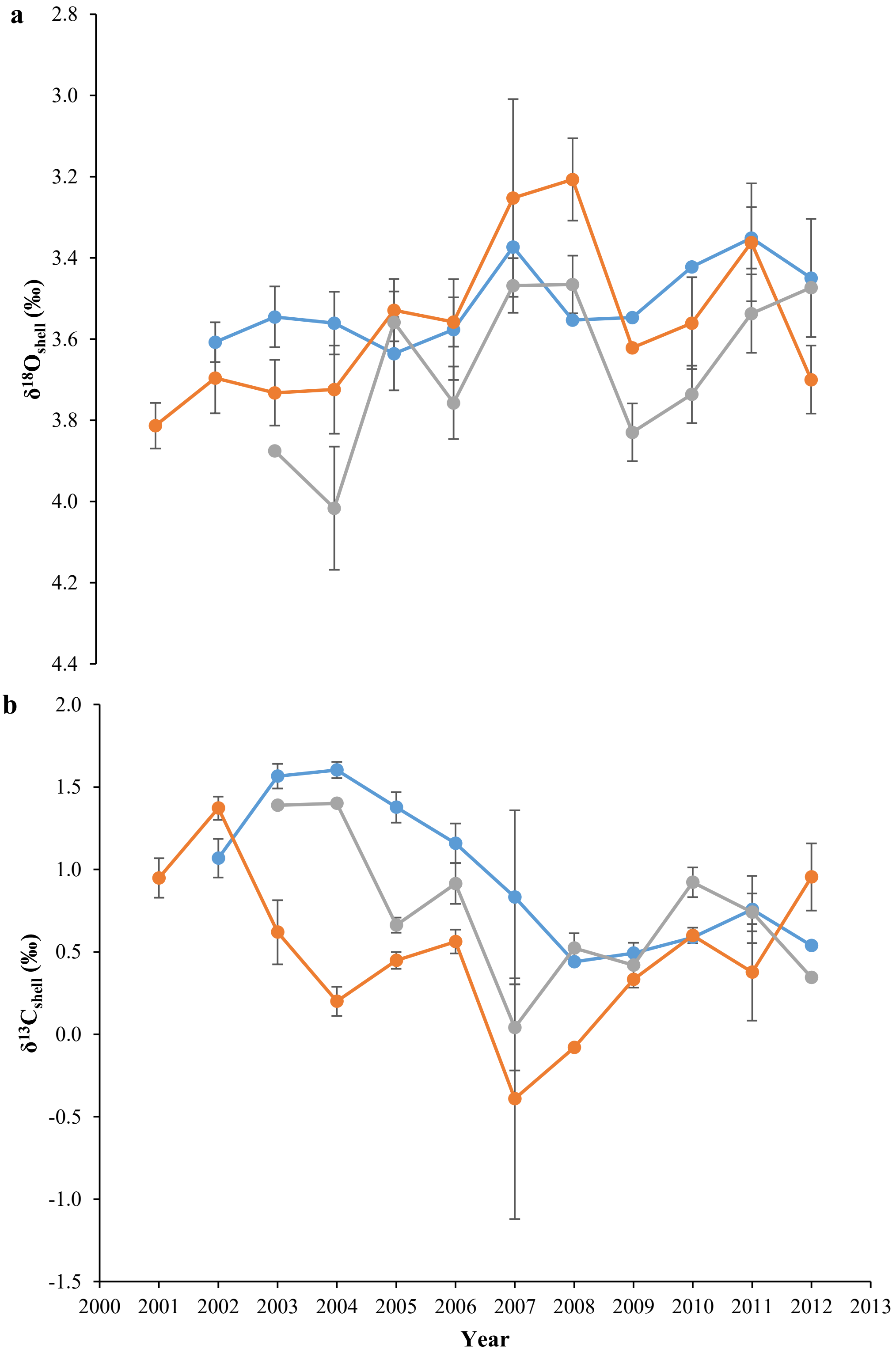
a
2.8
3.0
3.2
3.4
3.6
3.8
4.0
4.2
4.4
$\delta^{18}O_{shell}$ (‰)
b
2.0
1.5
1.0
0.5
0.0
-0.5
-1.0
-1.5
$\delta^{13}C_{shell}$ (‰)
2000
2001
2002
2003
2004
2005
2006
2007
2008
2009
2010
2011
2012
2013
Year

Fig. 5.16 Annual averages from the high-resolution geochemical sampling for **a)** $\delta^{18}O_{shell}$ (‰ VPDB; note the inverted Y-axis) and **b)** $\delta^{13}C_{shell}$ (‰ VPDB) for specimens 15SCs (blue), 14HCd (orange) and 14HCs (grey). The error bars represent the standard error.

5.2.2 Low-resolution sampling

The results of the low-resolution geochemical sampling from specimens 15SCs, 14HCd and 14HCs are presented in **Fig. 5.17a**, **Fig. 5.17b** and **Fig. 5.17c** respectively. For specimens 15SCs and 14HCd, only three annual samples were obtained, whereas for the specimen 14HCs seven annual samples were collected. For specimen 15SCs, a series of two narrow increments, corresponding to 2007/08, were incorporated along with the wider 2006 increment (**Fig. 5.17a**). In addition, specimen 15SCs shows an average of 3.48 ‰ ± 0.07 SD $\delta^{18}O_{shell}$ and 1.09 ‰ ± 0.27 SD $\delta^{13}C_{shell}$; the $\delta^{18}O_{shell}$ record (**Fig. 5.17a**) shows an increase in 2005 of 0.12 ‰ whereas the $\delta^{13}C_{shell}$ record (**Fig. 5.17a**) shows a trend towards lower $\delta^{13}C_{shell}$ from 2004 to 2008. Specimen 14HCd shows on average 3.42 ‰ ± 0.06 SD for $\delta^{18}O_{shell}$ and -0.06 ‰ ± 0.17 SD for $\delta^{13}C_{shell}$ (**Fig. 5.17b**). The $\delta^{18}O_{shell}$ record (**Fig. 5.17b**) shows a reduction between 2004 and 2005 of -0.13 ‰ whereas the $\delta^{13}C_{shell}$ record (**Fig. 5.17b**) shows negative $\delta^{13}C_{shell}$ values in 2004 and 2006 with a higher $\delta^{13}C_{shell}$ value in 2005 (0.27 ‰ in difference). Specimen 14HCs has the longest low-resolution geochemical record (**Fig. 5.17c**). There is a significant positive correlation between both geochemical records (i.e. $\delta^{18}O_{shell}$ and $\delta^{13}C_{shell}$; $r = 0.780$, $p < 0.05$, $n = 7$). The 14HCs $\delta^{18}O_{shell}$ record (**Fig. 5.17c**) is on average 3.43 ‰ ± 0.12 SD, and it shows a shift towards lower values during 2006/07 and during 2010/12. The 14HCs $\delta^{13}C_{shell}$ record (**Fig. 5.17c**) is on average 0.38 ‰ ± 0.46 SD and similarly to the $\delta^{18}O_{shell}$ record shows a shift towards lower values during 2006/07 and during 2010/12.

A comparison between the low-resolution sampling and the high-resolution sampling is presented in **Table A5.2** and **Fig. 5.18**. As for the South Orkney Islands (**Table A5.1**) the high-resolution averages of both geochemical indices tend to be higher than the geochemical values from the low-resolution sampling (**Fig. 5.18**). In the case of specimen 15SCs, the low-resolution geochemical values (**Fig. 5.17a**) coincide with the range of the lowest section of equivalent time frame in the high-resolution sampling (**Fig. 5.12**). It is noteworthy that the low-resolution sampling produced a lower $\delta^{13}C_{shell}$ value for 2004 (**Fig. 5.17a**) than any of the equivalent samples from the high-resolution sampling (**Fig. 5.12b**). Similarly, the low-resolution sampling from specimen 14HCd produced lower values (**Fig. 5.17b**) for both in the case of $\delta^{13}C_{shell}$ than those equivalent from the high-resolution sampling (**Fig. 5.13**). The low-resolution sampling from specimen 14HCs also produced lower values than any equivalent periods in the high-resolution sampling (**Fig. 5.13**): 2005, 2006, 2009, and 2010 for the $\delta^{18}O_{shell}$ and 2005, 2006 and 2010 in the case of $\delta^{13}C_{shell}$. In general there is good temporal agreement in the geochemical analysis from different specimens, with the exception of 2005 as specimen 15SCs shows higher $\delta^{13}C_{shell}$ whereas specimen 14HCd shows lower $\delta^{13}C_{shell}$ (**Fig. 5.18b**). The other discrepancy between the specimens can be seen the $\delta^{18}O_{shell}$ value from 2006 for specimen 15SCs (**Fig. 5.18b**) which is lower than the equivalent sample from specimen 14HCs.

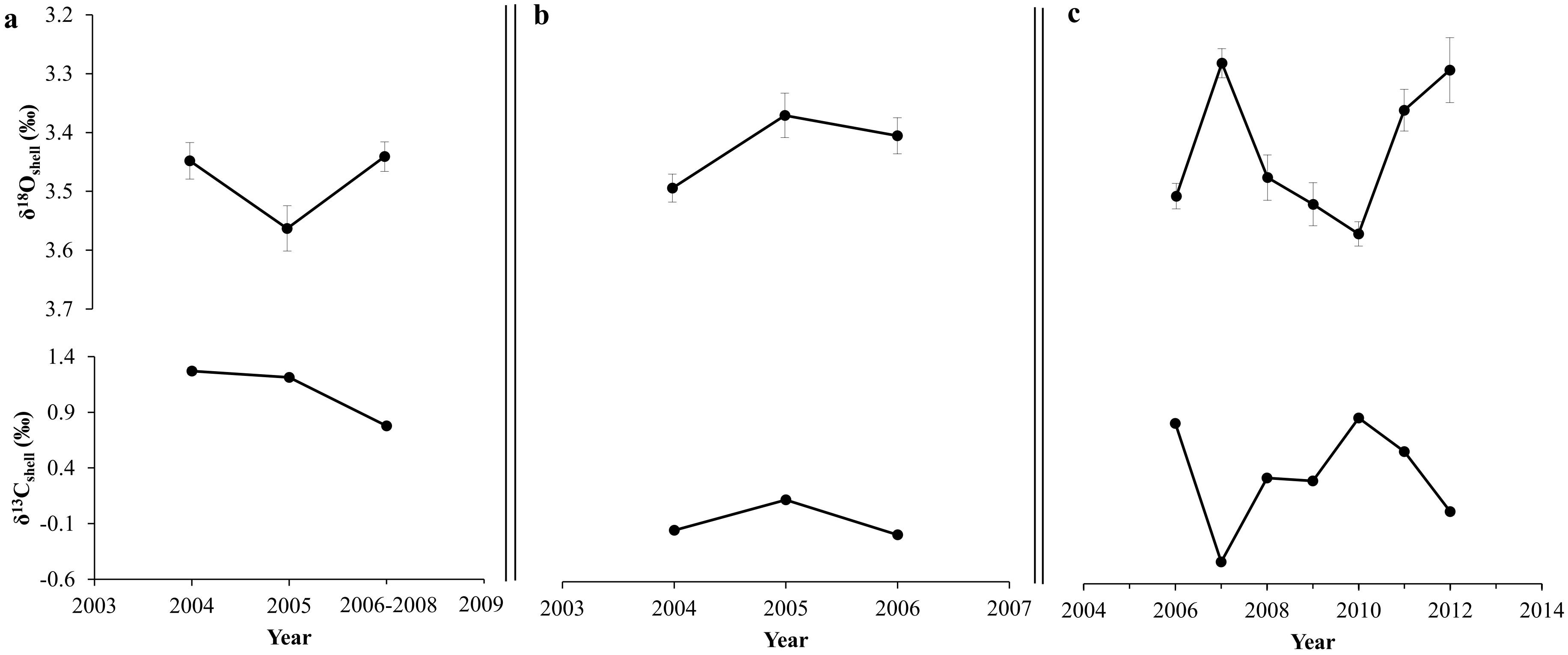

Fig. 5.17 Stable oxygen and carbon ($\delta^{18}O_{shell}$ and $\delta^{13}C_{shell}$ ‰ VPDB) records, note the inverted

Y-axis in the $\delta^{18}O_{shell}$, from the low-resolution sampling collected from **a)** specimen 15SCs, **b)** specimen 14HCd and **c)** specimen 14HCs. The error bars represent the instrumental external precision in the case of the $\delta^{13}C_{shell}$, if error bars do not show it is because they are smaller than

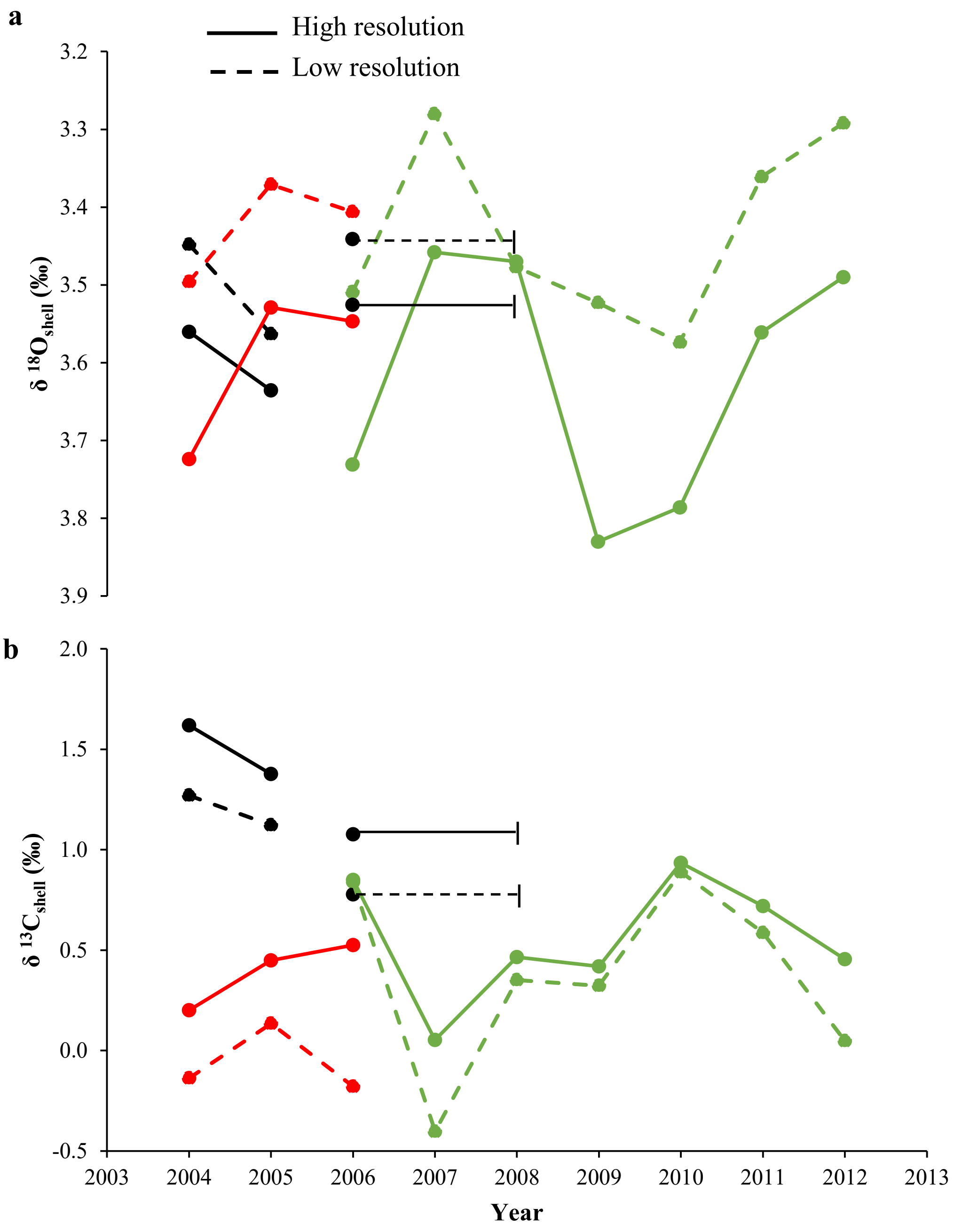

Fig. 5.18 Comparison of the **a)** $\delta^{18}O_{shell}$ (‰ VPDB, note the reversed Y-axis) and **b)** $\delta^{13}C_{shell}$ (‰ VPDB) for the high-resolution sampling (solid lines) and the low-resolution sampling (dashed

lines) for specimens 15SCs (black), 14HCd (red) and 14HCs (green). The horizontal errors bars in the 15SCs series indicate that the geochemical sample spanned over three annually-formed increments (2006/08, cf. **Fig. 5.17a**), the measurement value was placed in 2006 since 2007 and 2008 increments were much narrower compared to 2006 increment.

5.2.3 Comparison with instrumental records

The comparison between the $\delta^{13}C_{shell}$ and the instrumental chlorophyll concentration (see **Fig. 4.12**) record averaged at 15 m water depth is shown in **Fig. 5.19**. If averaged between shells the $\delta^{13}C_{shell}$ changes from 1.07 ‰ ± 0.51 SD prior to 2007/08 to 0.47 ‰ ± 0.45 SD after 2007/08 coincident with the change from a high primary production state to a low primary production state (see Chapter IV). A comparison between the $\delta^{18}O_{shell}$ and the instrumental $\delta^{18}O_{water}$ records is provided in **Fig. 5.20a**. This comparison highlighted a difference in range between the $\delta^{18}O_{shell}$ records (0.43 ‰ ± 0.20 SD; average of the annual ranges of specimens: 15SCs, 14HCs and 14HCd) and the $\delta^{18}O_{water}$ record (0.55 ‰ ± 0.28 SD for August-July for the period 2002/14 and 0.27 ‰ ± 0.17 SD when only November-March for the period 2002/15; calculations carried out after conversion of $\delta^{18}O_{water}$ values from SMOW to VPDB scale). This difference can also be appreciated in the estimated temperatures calculated using the Grossman and Ku (1986) equation adapted by Dettman et al. (1999; $T\,°C = 20.6 - 4.34 \times (\delta^{18}O_{ar} - (\delta^{18}O_{w} - 0.27))$) using a fixed $\delta^{18}O_{water}$ value calculated as an average between November and March for the length of the record (**Fig. 5.20b**). The estimated temperatures are clearly overestimating the maximum summer seawater temperatures (**Fig. 5.20b**). An analysis was carried out to determine the theoretical $\delta^{18}O_{shell}$ using instrumental data ($\delta^{18}O_{water}$ and seawater temperature) from the RaTS dataset; a synthetic $\delta^{18}O_{shell}$ (hereafter $\delta^{18}O_{syn}$) was calculated after rearranging the Grossman and Ku (1986) equation in order to calculate $\delta^{18}O_{syn}$, then the term $\delta^{18}O_{water}$ was substituted for the mixing line equation ($\delta^{18}O_{water} = 0.2726 \times \text{Salinity} - 9.7475$; **Fig. 4.17**) derived from the instrumental record and monthly measurements of salinity and seawater temperatures were used to calculate $\delta^{18}O_{syn}$. An offset of 0.57 ‰ was found between the average instrumental $\delta^{18}O_{shell}$ (3.60 ‰ ± 0.24 SD) and the average $\delta^{18}O_{syn}$ (4.17 ‰ ± 0.27 SD). Subsequently, three scenarios were considered, i) where the offset between $\delta^{18}O_{shell}$ and $\delta^{18}O_{water}$ is due exclusively to differences in salinity, which was artificially modified, and the instrumental seawater temperature measurements are left unmodified ii) where the offset is due exclusively to difference in seawater temperature, which is artificially modified, and instrumental salinity measurements are left unmodified iii) where the offset is due to a combination of seawater temperature and salinity differences, both measurements are artificially modified. Following this the salinity and temperature instrumental measurements were adjusted accordingly in order to obtain a $\delta^{18}O_{syn}$ record, which presents the same average as the instrumental $\delta^{18}O_{shell}$ record. In the first scenario (i.e. only due solely to salinity differences) it was found that seawater had to be freshened by 2.05 (**Fig. 5.21a**), in the second scenario (i.e. only due exclusively to seawater temperature differences) it was found that seawater temperature has to be 2.45 °C warmer (**Fig. 5.21b**). These analyses also provide an estimation in the same $\delta^{18}O_{shell}$ (i.e. VPDB) of the offset between the expected $\delta^{18}O_{shell}$ (i.e. synthetic) and the instrumental $\delta^{18}O_{shell}$, which is approximately 0.57 ‰. VPDB. For the third scenario the co-variability between instrumental seawater temperature and salinity was determined by applying a linear regression to the instrumental data series (**Fig. A5.4**); the relationship is that for each degree (°C) to warm (cool) the seawater, the salinity has to be lowered (increased) by 0.7. The results under this scenario are that in order to correct the offset, seawater temperature has to be 1.3 °C warmer and salinity has to be 0.91 fresher (**Fig. 5.21c**).

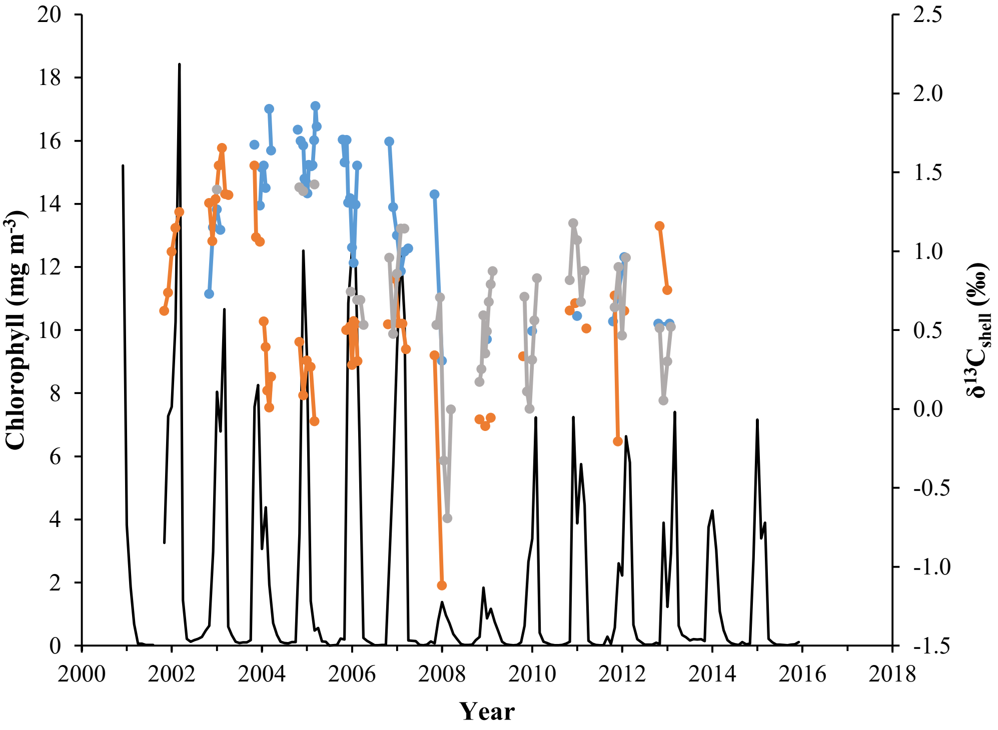

Fig. 5.19 Comparison between chlorophyll concentration (mg m^{-3}) at the RaTS site averaged for the top 15 m of the water column and the $\delta^{13}C_{shell}$ (‰ VPDB) of specimens: 15SCs (blue), 14HCd (orange) and 14HCs (grey).

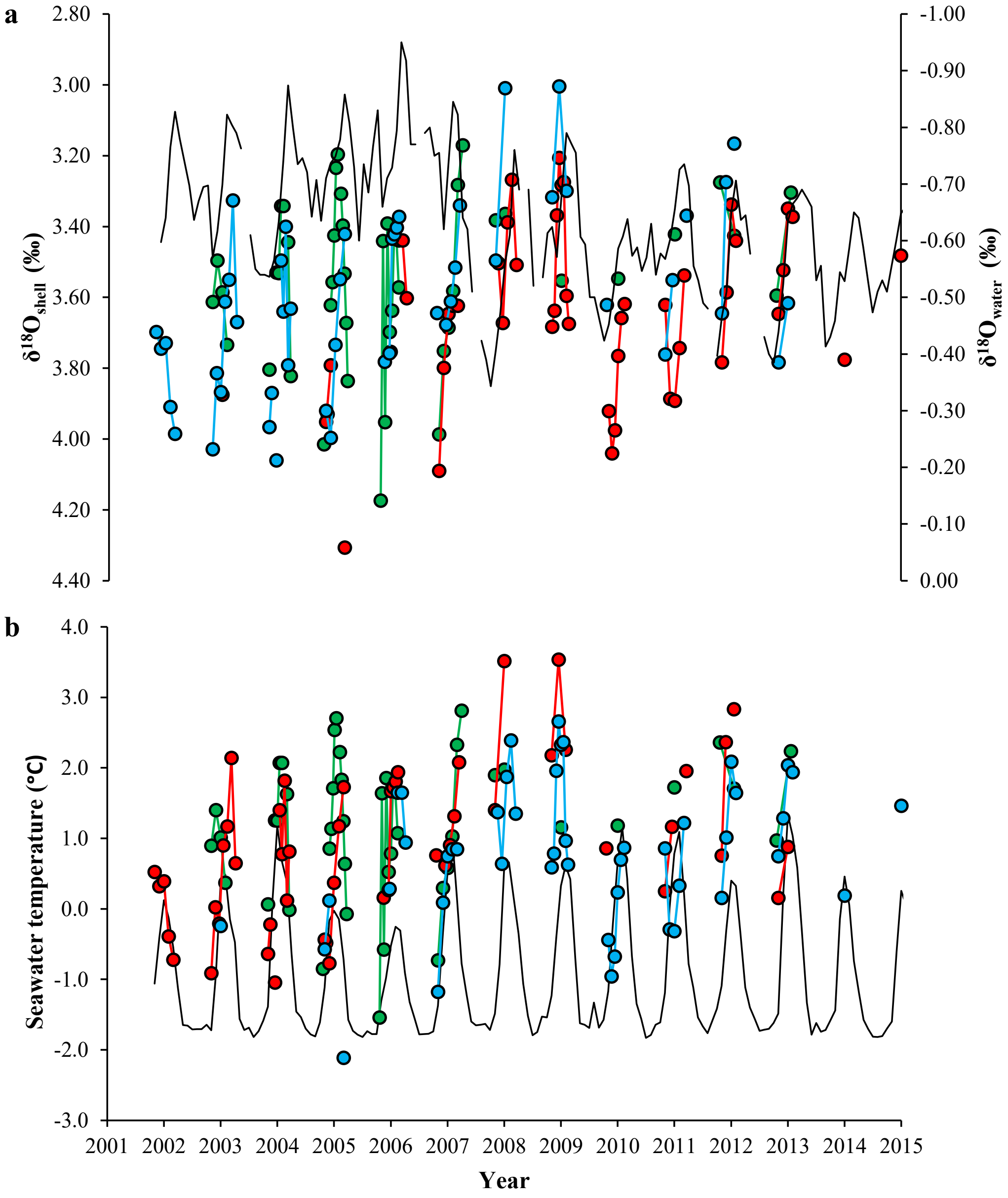

Fig. 5.20 a) Comparison between the instrumental δ^{18}O$_{\text{water}}$ (‰ SMOW, solid black line) and the δ^{18}O$_{\text{shell}}$ (‰ VPDB) measurements of specimens 14HCd (blue dots), 15SCs (green dots) and 14HCs (red dots). Note the reverse Y-axis and the difference in the range covered **b)** Instrumental seawater temperatures (solid black line) and estimated seawater temperatures from the shell carbonate samples calculated using the modified Grossman and Ku (1986) relationship between

$\delta^{18}O_{water}$ and biogenic aragonite $\delta^{18}O$ (Dettman et al., 1999) using a fixed average $\delta^{18}O_{water}$ between November and March (i.e. shell growing season).

a

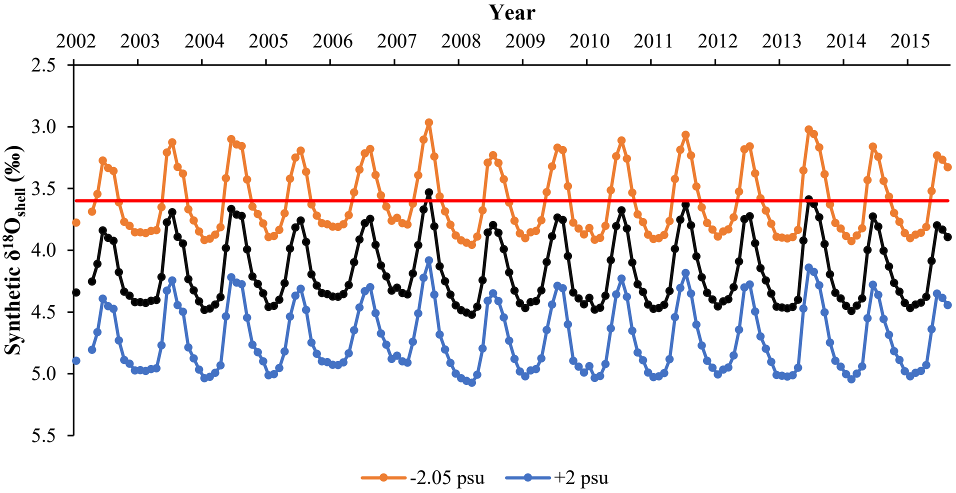
Year
2002
2003
2004
2005
2006
2007
2008
2009
2010
2011
2012
2013
2014
2015
2.5
3.0
3.5
4.0
4.5
5.0
5.5
Synthetic δ18Oshell (‰)
-2.05 psu
+2 psu

b

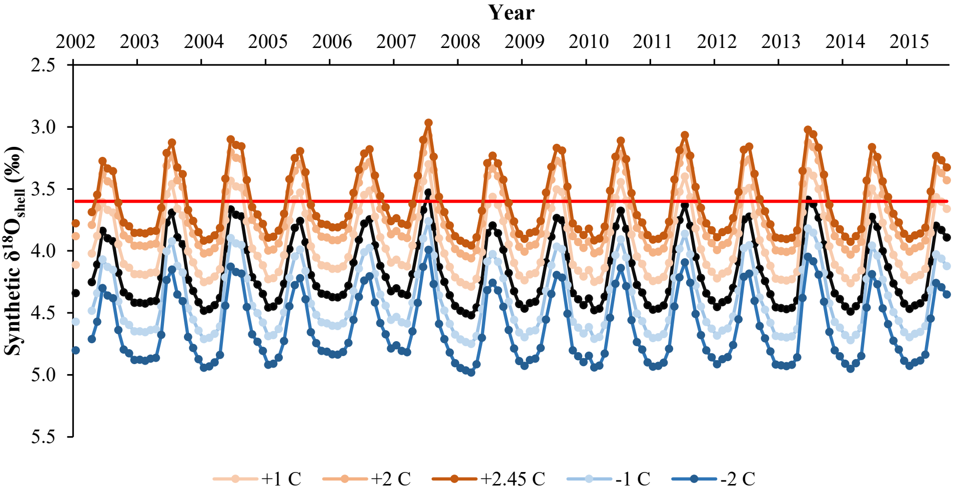
Year
2002
2003
2004
2005
2006
2007
2008
2009
2010
2011
2012
2013
2014
2015
2.5
3.0
3.5
4.0
4.5
5.0
5.5
Synthetic δ18Oshell (‰)
+1 C
+2 C
+2.45 C
-1 C
-2 C

c

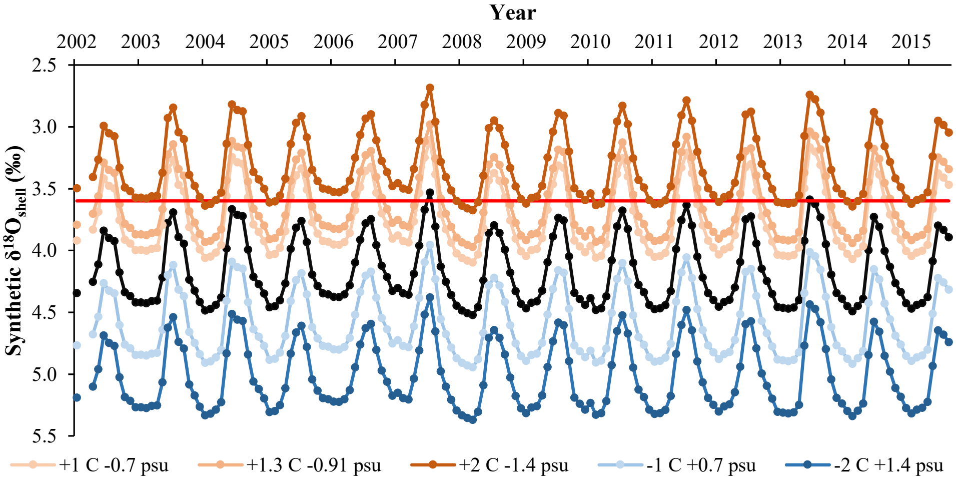
Year
2002
2003
2004
2005
2006
2007
2008
2009
2010
2011
2012
2013
2014
2015
2.5
3.0
3.5
4.0
4.5
5.0
5.5
Synthetic δ18Oshell (‰)
+1 C -0.7 psu
+1.3 C -0.91 psu
+2 C -1.4 psu
-1 C +0.7 psu
-2 C +1.4 psu

Fig. 5.21 Results from the $\delta^{18}O_{syn}$ (‰ VPDB, note the inverted Y-axis), derived from the modified Grossman and Ku (1986) by Dettman et al. (1999) equation, analysis showing different **a)** salinity scenarios, **b)** temperature scenarios and **c)** a combination of temperature and salinity changes. In all plots, the black line represents the $\delta^{18}O_{syn}$ with no artificial temperature and/or salinity changes, the solid red line represents the instrumental average $\delta\ ^{18}O_{shell}$ determined in the geochemical analysis (i.e. 3.599 ‰). For the artificial changes applied in the different scenarios refer to the pertinent legend. Colour grading indicate shifts towards warmer (red) and cooler (blue) seawater temperature.

5.3 Lateral isotopic fractionation

This section covers the results of the lateral isotopic fractionation study of $\delta^{18}O_{shell}$ and $\delta^{13}C_{shell}$ of *A. eightsii*. Geochemical differences between the anterior, ventral and posterior part of the shell were studied (c.f. Chapter II section 2.8).

Three independent valves were drilled for this analysis: specimen 21504010 (collected from approximately 15 m water depth from South Cove, Ryder Bay, West Antarctic Peninsula (WAP), in February 2015), specimen 8804034 (collected from approximately 8 m water depth at Factory Cove, Signy Island, South Orkney Islands, in April 1988) and specimen 191501036 (collected from approximately 11 m water depth at Signy Island, South Orkney Islands, in 1915). Geochemical analysis results ($\delta^{18}O_{shell}$ and $\delta^{13}C_{shell}$) for the specimens 21504010, 8804034 and 191501036 are shown in **Fig. 5.22**, **Fig. 5.23** and **Fig. 5.24** respectively.

Specimen 21504010 (**Fig. 5.22**) shows differences between anatomical parts of the shell (i.e. anterior, ventral and posterior) in both the $\delta^{18}O_{shell}$ and $\delta^{13}C_{shell}$ from three independent increments located near the umbo, in the mid-section of the shell and near the margin (shell rim). The average $\delta^{18}O_{shell}$ of the increments sampled (from umbo towards margin, **Fig. 2.6c**) are 3.78 ‰ ± 0.12 SD, 3.66 ‰ ± 0.12 SD and 3.69 ‰ ± 0.21 SD and in the case of the $\delta^{13}C_{shell}$ are 1.38 ‰ ± 0.11 SD, 1.72 ‰ ± 0.11 SD and 1.30 ‰ ± 0.32 SD. These results indicate that the margin section has a higher variability between sampling transects than the umbo or the middle sections (**Fig. 5.22**). In the $\delta^{18}O_{shell}$ records, the anterior sample normally presents the lowest geochemical values with the exception of the margin section, which the lowest value was in the anterior part of the shell, and in all transects the highest geochemical value corresponded with the ventral sample (**Fig. 5.22a**, see **Fig. 2.6c** for reference). On the other hand in the $\delta^{13}C_{shell}$ record the posterior sample tends to be geochemically heavy and the anterior sample significantly lower (**Fig. 5.22b**). In addition, the ventral transect shows large variability relative to the other two anatomical parts, slightly higher in the case of the umbo section, slightly lower in the middle section and significantly higher in the margin section (**Fig. 5.22b**). Additionally the ventral transect (**Fig. 2.6c**) presented a higher $\delta^{18}O_{shell}$ value (0.25 ‰ ± 0.10 SD; **Fig. 5.22a**) than the anterior and posterior transect. For $\delta^{13}C_{shell}$, the anterior part of the shell has consistently lower $\delta^{13}C_{shell}$ values (-0.28 ‰ ± 0.02 SD on average) than the posterior or ventral parts and no clear pattern was present between the anterior and the ventral part.

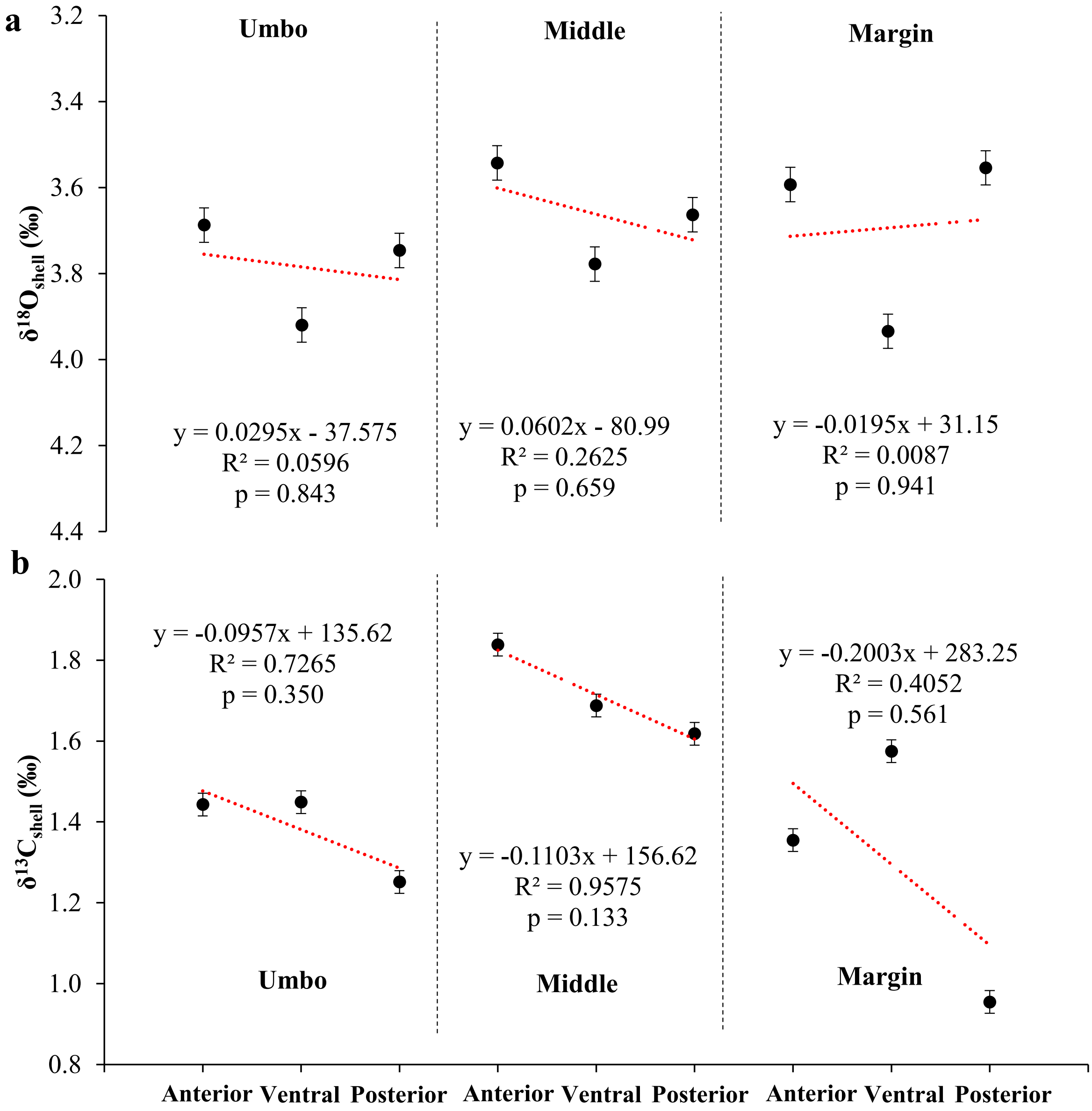

Fig. 5.22 Stable isotope results from the lateral fractionation analysis **a)** $\delta^{18}O_{shell}$ (‰ VPDB, note the inverted Y-axis) and **b)** $\delta^{13}C_{shell}$ (‰ VPDB) collected from specimen 21504010 in relation to the anatomical parts of the shell (from left to right: anterior, ventral and posterior). The graphs have been divided into Umbo, Middle and Margin indicating the relative position of the drilled increment. All samples (black dots) within each section (Umbo, Middle and Margin) belong to the same increment. The first dot of each section represents the anterior part of the shell, the middle

dot represents the ventral part of the shell and the third dot represents the posterior part of the shell. A linear trend (red dotted line) was fit to each set of samples; the equation defining the trend line and R^2 are also provided. The error bars indicate the analytical external precision.

Specimen 8804034 has an average $\delta^{18}O_{shell}$ of 3.65 ‰ ± 0.03 SD and an average $\delta^{13}C_{shell}$ of 1.62 ‰ ± 0.15 SD (**Fig. 5.23**). As for specimen 2150410, specimen 8804034 shows a subtle trend towards lower $\delta^{18}O_{shell}$ from the posterior part (**Fig. 2.6c**) of the shell towards the anterior part of the shell (**Fig. 5.23a**); however, it shows a trend towards lower $\delta^{13}C_{shell}$ (**Fig. 5.23b**). In addition, ventral position does not present any significant difference in the $\delta^{18}O_{shell}$, as seen in specimen 21504010, when compared to the anterior and posterior transects (**Fig. 2.6c**). Specimen 8804034 shows a similar $\delta^{13}C_{shell}$ trend (-0.14, **Fig. 5.23b**) when compared to the middle increments from specimen 21504010 (-0.11, **Fig. 5.22b**).

Specimen 191501036 shows an average $\delta^{18}O_{shell}$ of 3.93 ‰ ± 0.07 SD and an average $\delta^{13}C_{shell}$ of 1.80 ‰ ± 0.06 SD (**Fig. 5.24**). Similar to 8804034, although more subtle, specimen 191501036 shows a trend towards lower $\delta^{13}C_{shell}$ from the posterior part towards the anterior part of the shell (**Fig. 2.6c**). On the contrary, specimen 191501036 presents a subtle trend towards higher $\delta^{18}O_{shell}$ from the posterior towards the anterior part of the shell (**Fig. 2.6c**). Also contrary to specimens 21504010 and 8804034, the ventral position shows a slightly lower $\delta^{18}O_{shell}$ value (-0.11 ‰ ± 0.06 SD) than the anterior and posterior positions (**Fig. 5.24a** and **Fig. 2.6c** for reference of the sampling positions).

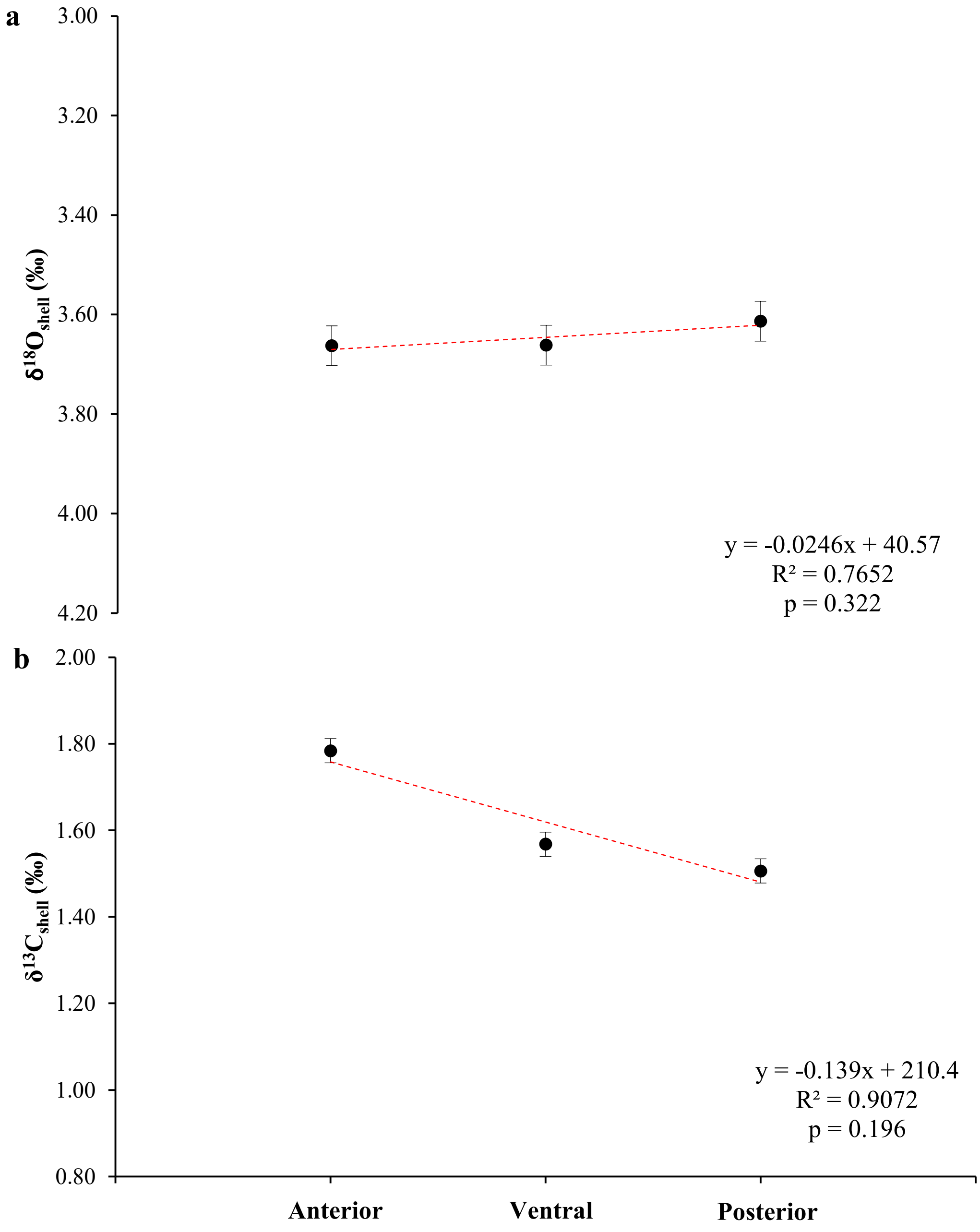

Fig. 5.23 Geochemical results **a)** $\delta^{18}O_{shell}$ (‰ VPDB, note the inverted Y-axis) and **b)** $\delta^{13}C_{shell}$ (‰ VPDB) collected from a mid-section increment of the specimen 8804034 in relation to the

anatomical parts of the shell (anterior, ventral and posterior). These samples were drilled in the middle section of the shell. The first dot of the series represents the anterior part of the shell, the middle dot represents the ventral part of the shell and the third dot represents the posterior part of the shell. A linear trend (red dotted line) was fit to each set of samples, the equation defining the trend line and R^2 are also provided. The error bars represent the instrumental external precision.

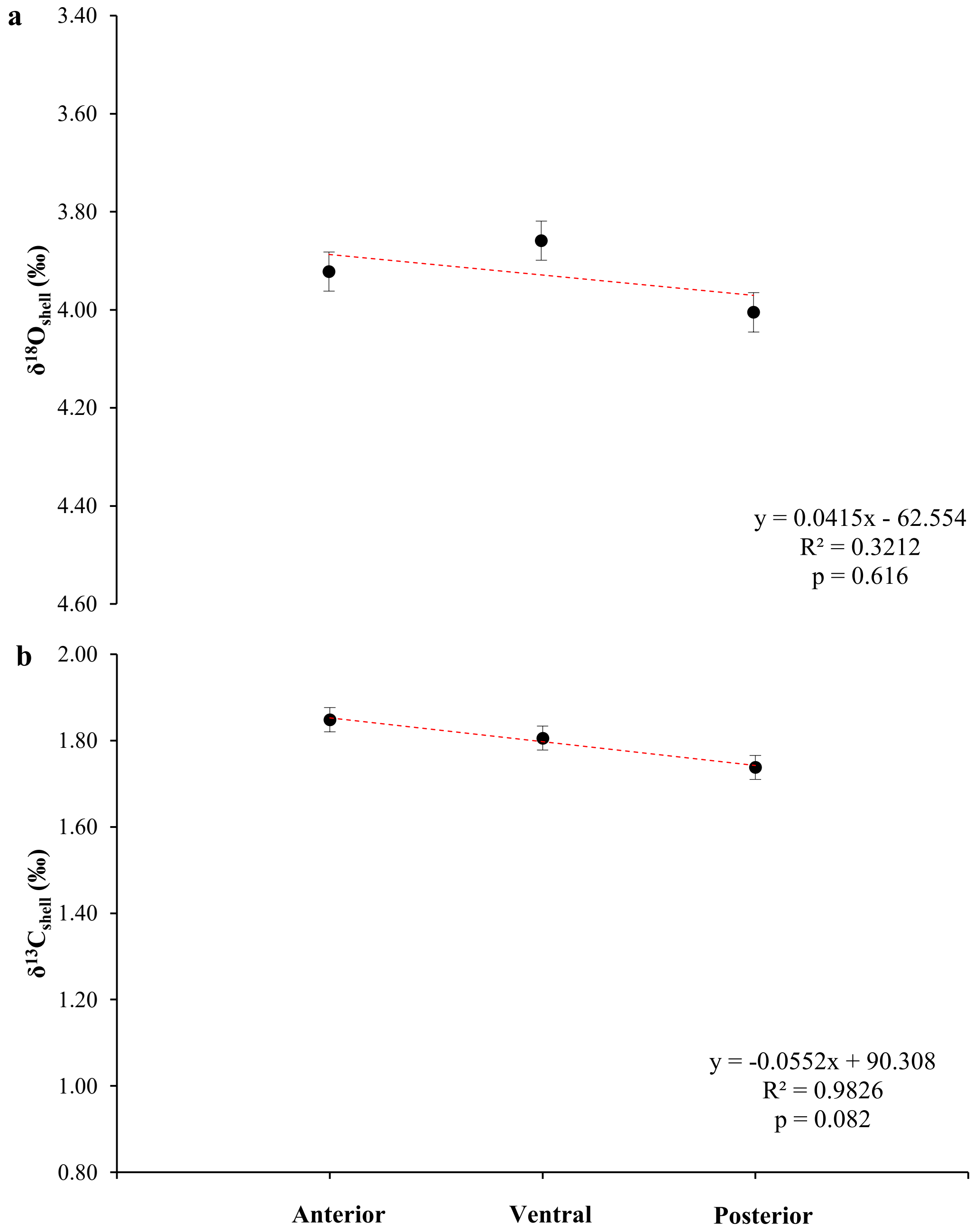

Fig. 5.24 Geochemical results **a)** $\delta^{18}O_{shell}$ (‰ VPDB, note the inverted Y-axis) and **b)** $\delta^{13}C_{shell}$ (‰ VPDB) collected from a mid-section increment of the specimen 191501036 in relation to the

anatomical parts of the shell (anterior, ventral and posterior). These samples were drilled in the Middle section of the shell. The first dot of the series represents the anterior part of the shell, the middle dot represents the ventral part of the shell and the third dot represents the posterior part of the shell. A linear trend (red dotted line) was fit to each set of samples, the equation defining the trend line and R^2 are also provided. The error bars represent the instrumental external precision.

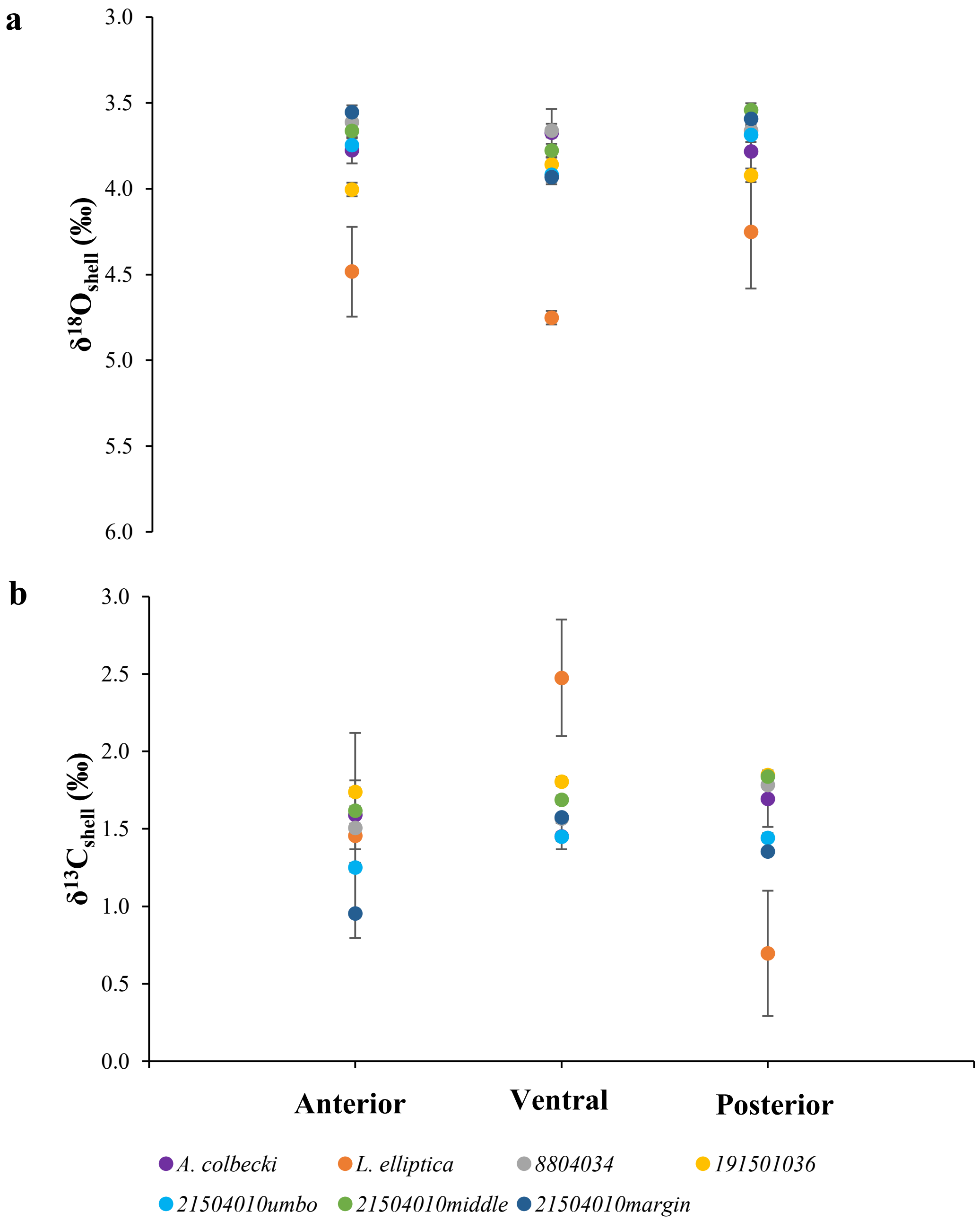

Fig. 5.25 Averaged **a)** $\delta^{18}O_{shell}$ (‰ VPDB) and **b)** $\delta^{13}C_{shell}$ (‰ VPDB) from *A. colbecki* and *L. elliptica* from samples (data extracted from Barrera et al., 1990, 1994) and the three *A. eightsii* specimens (8804034, 191501036 and 21504010) sampled for the lateral fractionation study.

Samples have been divided according to the anatomical part of the shell from which they were collected (i.e. anterior, ventral and posterior). The error bars for *A. colbecki* and *L. elliptica* represent the standard deviation and instrumental precision for *A. eightsii* samples.

A comparison between stable isotope values from *A. colbecki* and *L. elliptica* collected by Barrera et al. (1990, 1994; data extracted from the publications) and the measurements from the *A. eightsii* lateral fractionation experiment are provided in **Fig. 5.25**. It can be observed that the *A. eightsii* specimens are more similar to the *A. colbecki* samples than either to the *L. elliptica* samples, this is confirmed statistically by a one-way ANOVA and Fisher's LSD tests for $\delta^{18}O_{shell}$ (**Table A5.3**) whereas for $\delta^{13}C_{shell}$ no difference was found between species (one-way ANOVA, $F_{(2,18)} = 0.007$, $p = 0.993$). In addition, Kruskal-Wallis H tests showed that there are no differences in $\delta^{18}O_{shell}$ or $\delta^{13}C_{shell}$ between the different anatomical positions (i.e. anterior, ventral and posterior, **Fig. 2.6c**) irrespective of the species (*A. eightsii*, *L. elliptica* and *A. colbecki*), $\chi^2(2) = 1.320$, $p = 0.517$ for $\delta^{18}O_{shell}$ $\chi^2(2) = 1.811$, $p = 0.404$ for $\delta^{13}C_{shell}$. The similarities in the geochemical values, according to the anatomical position of the shell, between the different species suggest that the observed lateral fractionation is related to biological drivers of shell growth and is not caused by an artefact from the sampling techniques used for *A. eightsii*.

5.4 Discussion

The form of the sub-annual stable isotope records (especially the $\delta^{18}O_{shell}$ records) offers some insight into the *A. eightsii* growing season. The position of the annually-formed increment line generally coincided with isotopically heavy $\delta^{18}O_{shell}$ values, although in many cases the growth check did not coincide with the highest $\delta^{18}O_{shell}$ sub-annual sample (**Fig. 5.2a**, **5.3a**, **5.4a**, **5.12a**, **5.13a** and **5.14a**). The position of the annually-formed growth lines in the temperate bivalve *Arctica islandica* did also not coincide with the highest $\delta^{18}O_{shell}$ value within a subannual cycle (Weidman and Kyger, 1994;

Witbaard et al., 1994); and coincided with the time of annual bottom seawater temperature maxima. Similarly, specimens of the bivalve *Glycymeris bimaculata* collected in the Adriatic Sea showed the annually-formed growth lines subsequent to the $\delta^{18}O_{shell}$ maxima within the subannual cycle (Bušelić et al., 2015). The relative position of the annually-formed growth line with the subannual $\delta^{13}C_{shell}$ values also showed large variability; although generally the growth line tended to coincide with high $\delta^{13}C_{shell}$ values within the subannual cycle (**Fig. 5.2b**, **5.3b**, **5.4b**, **5.12b**, **5.13b** and **5.14b**). In the case of $\delta^{13}C_{shell}$, Witbaard et al. (1994) showed that in *A. islandica* from the North Sea the growth lines coincided with the annual $\delta^{13}C_{shell}$ minima or were immediately prior to the minima. Whereas in *G. bimaculata* the growth line coincided with the $\delta^{13}C_{shell}$ minima or immediately after the minima (Bušelić et al., 2015). The high-resolution stable isotope records of *A. eightsii* showed similar results to these species for $\delta^{18}O_{shell}$; however, the growth line coincided with high $\delta^{13}C_{shell}$ values contrary to *A. islandica* and *G. bimaculata*. This characteristic may be due to differences between temperate and Antarctic shallow marine environments. Brey and Mackensen (1997) showed similar $\delta^{18}O_{shell}$ and $\delta^{13}C_{shell}$ patterns to those from *A. eightsii* in the Antarctic bivalve *Laternula elliptica*, although the low-resolution of their records prevents a more detailed comparison.

The comparison between the high-resolution and the low-resolution geochemical sampling offer an opportunity to validate this new approach (i.e. sampling from the outer surface instead from the sectioned profile) of sampling thin mollusc shell on their external surface. In most cases the low-resolution sampling value matched with the average of the equivalent temporal samples from the high-resolution sampling (**Fig. 5.10** and **Fig. 5.18**). The offset between both records (i.e. low-resolution sampling and averaged high-resolution sampling) of lower isotopic values in the low-resolution sampling can be explained in terms of lateral fractionation, based on the results from the lateral fractionation experiment, as the low-resolution sampling was collected from a transect close to either the anterior or posterior part of the shell whereas the high-resolution sampling was collected from the ventral region of the shell (further discussion below when considering the lateral fractionation results). Alternatively, the offset could be due to a systematic bias associated with the drilling technique, caused by the internal shell structure (e.g. thinning of the outer shell layer at the posterior and anterior part of the shell). Furthermore, the presence of a few discrepancies between equivalent samples from both sampling strategies (e.g. **Fig. 5.10a**) suggest that the technique is not free from technical issues and can be refined further. Some possible explanations for these discrepancies are: i) missing samples from the high-resolution record due to the low amount of powder collected can potentially bias the average value, ii) incorporation of more than one increment in the low-resolution sampling due to outer shell layer thinning in the anterior and posterior region of the shell and iii) the presence of orange dot inclusions (**Fig. 3.3** and **Fig. 3.4**) on the outer shell surface which may have an effect on the geochemical signature of the shell carbonate; however especial care was paid not to include material from the orange dots. If some of these dots were sampled by mistake in any of the records it could potentially affect the geochemical signature. If these dots are the early stages of chemical dissolution of the shell after the periostracum was damaged, there could be fractionation processes affecting the geochemical signature of the carbonates in these regions.

The current *A. eightsii* $\delta^{13}C_{shell}$ records add to the existing literature on ontogenetic trends in $\delta^{13}C_{shell}$ in bivalve molluscs (e.g. Jones, 1983; Brey and Mackensen, 1997; Elliot et al., 2003; Lorrain et al., 2004; Gillikin et al., 2005; Schöne et al., 2005; Gillikin et al., 2006; Schöne et al., 2011). The different studies suggest the presence of negative (Jones et al., 1983; Lorrain et al., 2004), positive (Brey and Mackensen, 1997; Gillikin et al., 2005), negligible/non-existent (Schöne et al., 2005, 2011) or even limited to early years of growth (Butler et al., 2011) trends in the $\delta^{13}C_{shell}$ record. These studies were based on different bivalve species (e.g. *A. islandica*, *Mytilus edulis*, *Spisula solidissima*). Although results from different studies of *A. islandica* were consistent in showing a negligible/non-existent trend or limited to the early years of growth (Schöne et al. 2005, 2011; Butler et al., 2011), it seems likely there is a species-specific $\delta^{13}C_{shell}$ age relationship. In general terms, *A. eightsii* seems to show a negative trend in the $\delta^{13}C_{shell}$ record with ontogenetic age (**Fig. 5.8b** and **Fig. 5.15b**) in contrast to the other Antarctic bivalve studied to date, *L. elliptica*, which presented a positive trend in the $\delta^{13}C_{shell}$ record (Brey and Mackensen, 1997); however, it has to be noted that it is likely that ontogenetic trends are present in the $\delta^{13}C_{shell}$ records.

Several biological, ecological and physical processes can be affect the $\delta^{13}C_{shell}$. Some of these include the dissolved inorganic carbon (DIC) in the seawater in which the shell was formed ($\delta^{13}C_{DIC}$), the carbon signature from the food sources that the animal uses ($\delta^{13}C_{food}$; Keith et al., 1964; Gillikin et al., 2007; McConnaughey and Gillikin, 2008; Owen et al., 2008). The $\delta^{13}C_{DIC}$ is affected by photosynthetic activity as light carbon (i.e. ^{12}C) is preferentially removed from the inorganic carbon pool; this makes $\delta^{13}C_{shell}$ a potential proxy for primary production (McKenzie, 1985; Krantz et al., 1987; Gillikin et al., 2006). In the WAP specimens, the drop from the average $\delta^{13}C_{shell}$ prior to 2007/08 when compared to the period after 2007/08 (**Fig. 5.19**) is coincident with a change of state at Ryder Bay from high ice concentration, shallow mixing and high primary production to low ice concentration, deep mixing and low primary production (Venables et al., 2013; also see Chapter III), which suggests that the $\delta^{13}C_{shell}$ records are capturing this change of state. In addition the $\delta^{13}C_{shell}$ of all the specimens showed a significant change towards lower $\delta^{13}C_{shell}$ (-1.31 ‰ ± 0.22 SD) during 2007/08 (**Fig. 5.12b**, **Fig 5.13b** and **Fig. 5.14b**). Interestingly, low levels of chlorophyll concentration remained during 2008/09, however the $\delta^{13}C_{shell}$ shows higher values than when compared to the drop from 2007/08 (**Fig. 5.19**). One difference with 2007/08 can be found in the sea-ice concentration, during 2007/08 sea-ice did not last long and broke up at Ryder Bay during August-September (**Fig. 4.16**), when there was no sea ice present, whereas during 2008/09 the sea ice was present continuously from July to September. Phytoplankton depends heavily on sea ice as it influences stratification in the water column (e.g. Dierssen et al., 2002) and although suspended chlorophyll levels remained low, the presence of the continuous sea ice could have had an effect in the $\delta^{13}C_{shell}$. *A. eightsii* is believed to be able to grow even under reduced phytoplankton conditions by utilising the local benthic microalgae (Peck et al., 2000), which depends at least partly on the sea-ice cover (Gilbert, 1991). The suspended chlorophyll dataset from RaTS is more likely to reflect the phytoplankton blooms rather than the benthic microalgae blooms and a combination of both may reflect better the $\delta^{13}C_{shell}$ variability.

For understanding the $\delta^{13}C_{shell}$ records and their interannual variability it is also important to understand the feeding mechanisms and food sources of *A. eightsii*. Deposit feeding and filter feeding have been proposed to be the principal feeding mechanisms of *A. eightsii* (Davenport, 1988). Under close examination in controlled aquarium conditions, *A. eightsii* collected the organic matter on the sediment surface by extending the palp proboscides, leaving no noticeable marks on the surface substratum (Davenport, 1988), which suggests that no or little organic matter from within the sediment is ingested by *A. eightsii*. In addition, during the observation of the *A. eightsii* ventilation rhythms it was noticed the ingestion of diatoms through the inhalant syphon or alternatively by backflushing through the exhalant syphon (Davenport, 1988). If the sole food source of the species considered comes from filtering phytoplankton, the $\delta^{13}C_{shell}$ should in principle reflect phytoplankton activity (Krantz et al., 1987). Shifts in diatom species composition at Ryder Bay have been found to have a significant effect on the stable carbon isotopic signature of the particulate organic carbon ($\delta^{13}C_{POC}$; 4 ‰

increase), although this was not fully exported to the deposited POC (Henley et al., 2012). However, the dual feeding mechanism of *A. eightsii* could potentially have an effect on the $\delta^{13}C_{shell}$ signature depending on the food source (suspended planktonic, deposited planktonic or benthic microalgae) as well as possible fractionation processes that may occur after phytoplankton deposition.

5.4.1 South Orkney Islands

The comparison of the trends in the temporally normalized geochemical records (**Fig. 5.8** and **Fig. 5.15**) also offers an insight into how the shallow and deep coastal environments of the South Orkney Islands have been changing for almost a century. Comparing the trends of specimens 15Ss and 27Sd, which are more closely related in the temporal frame, shows that the shallow-collected specimen (15Ss) presents a slightly more rapid change (-0.06 ‰ yr^{-1}) towards lower $\delta^{18}O_{shell}$ for a similar period of time than the deep-collected 27Sd specimen (-0.05 ‰ yr^{-1}; **Fig. 5.8a**). This is expected as shallow environments react more rapidly to environmental changes than deeper environments (e.g. Meredith et al., 2008a; Scourse et al., 2012; Venables and Meredith, 2014). A much more significant difference between these two specimens can be observed in the $\delta^{13}C_{shell}$ records (**Fig. 5.8b**); although taking into consideration that ontogenetic trends may be affecting the $\delta^{13}C_{shell}$ records, the deep-collected 27Sd presents a more pronounced shift towards lower $\delta^{13}C_{shell}$ (-0.08 ‰ yr^{-1}) than the shallow-collected 15Ss specimen (0.004 ‰ yr^{-1}). Furthermore, if only the shallow-collected specimens (15Ss in orange and 88Ss in blue) are considered the more modern specimen (88Ss) presents a reduced trend (i.e. approximately half, -0.04 ‰ yr^{-1}) towards lower $\delta^{18}O_{shell}$ than the one from the older specimen (15Ss, -0.06 ‰ yr^{-1}; **Fig. 5.8a**); however the 88004045 specimen presents a stronger trend towards lower $\delta^{13}C_{shell}$ (-0.02 ‰ yr^{-1}) than the 15Ss specimen (0.004 ‰ yr^{-1}, **Fig. 5.8b**). Both these shallow-collected specimens present more similar $\delta^{13}C_{shell}$ trends between them than compared with the deep-collected 27Sd specimen. Based on these results it is likely that the processes driving $\delta^{18}O_{shell}$ variability (i.e. biological and/or environmental) are fairly constant for the periods considered (i.e. 1900/10, 1917/25 and 1975/85) in the South Orkney Island specimens, as they present similar trends independent from the time frame and/or depth. The processes driving changes in the $\delta^{13}C_{shell}$ seem to be affecting the deep-collected specimen more than the shallow-collected specimens, although this assumes that no ontogenetic trend is affecting the $\delta^{13}C_{shell}$ records or that the ontogenetic trend is similar between them.

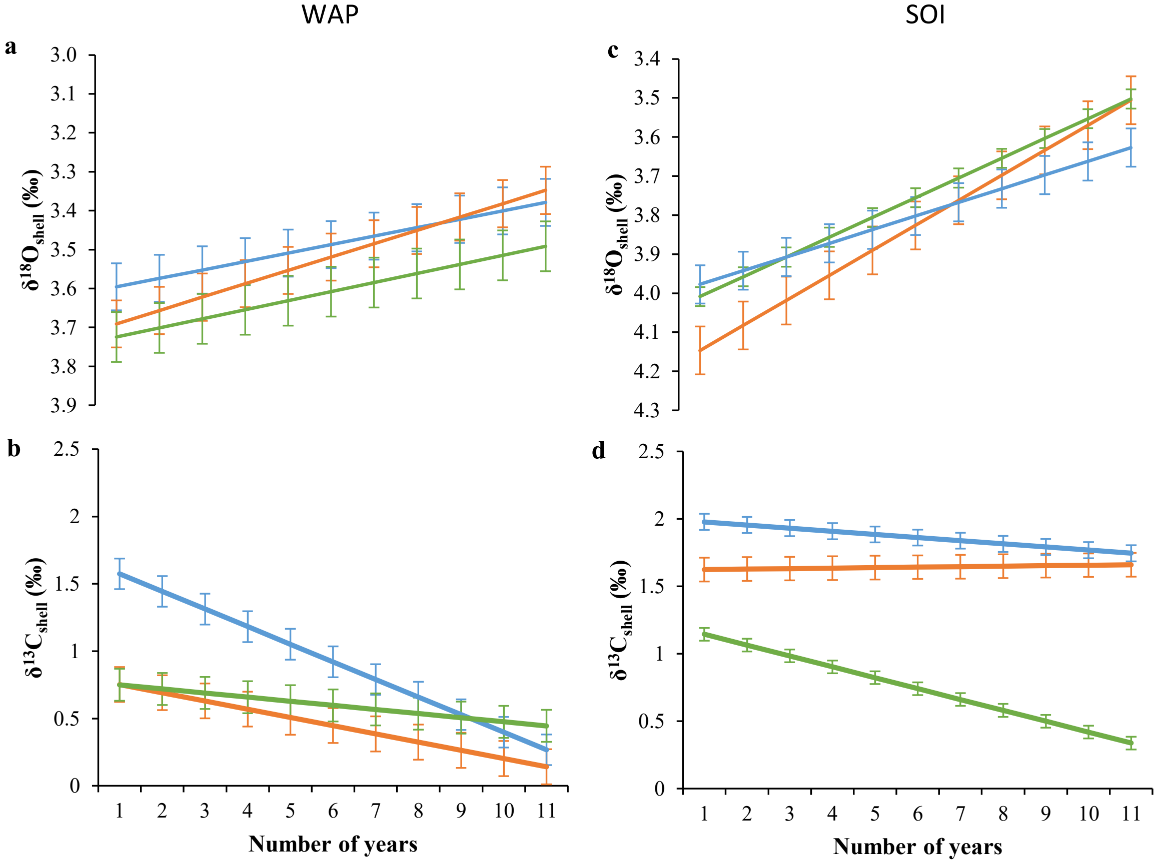

Fig. 5.26 Regression slopes between the $\delta^{18}O_{shell}$ (‰), $\delta^{13}C_{shell}$ (‰) and number of ontogenetic years as displayed in Fig. A5.4 and Fig. A5.6 for the West Antarctic Peninsula (WAP) specimens

a) and **b)** 15SCs (blue), 14HCd (orange) and 14HCs (green) and for the South Orkney Islands (SOI) specimens **c)** and **d)** 88Ss (blue), 15Ss (orange) and 27Sd (green).

In addition, the comparison of the temporally normalized trends of the geochemical records between the specimens from the South Orkney Islands (**Fig. 5.8**) and from the WAP (**Fig. 5.15**) allows a latitudinal comparison between these two locations (**Fig. 5.26**). The slopes of the $\delta^{18}O_{shell}$ records from the South Orkney Islands specimens (**Fig. 5.8a** and **Fig. 5.26c**) were higher than any of the slopes from the $\delta^{18}O_{shell}$ records from the WAP (**Fig. 5.15a** and **Fig. 5.26a**). This could indicate that the processes driving $\delta^{18}O_{shell}$ change are acting more strongly at the South Orkney Islands as latitude environmental gradients are expected (Vaughan et al., 2003; Barnes et al., 2006; Meredith et al., 2008a; Stammerjohn et al., 2008a; Murphy et al., 2013); or alternatively, it could indicate that both regions are affected differently by the climatic drivers (Meredith and King, 2005; Cook et al., 2016). The $\delta^{13}C_{shell}$ records of the WAP present a more negative trend (-0.07 ‰ yr^{-1} ± 0.05 SD) than the South Orkney Islands specimens (-0.03 ‰ yr^{-1} ± 0.04 SD), although this difference is not statistically significant. This difference is even greater when only the shallow-collected specimens from the South Orkney Islands are compared (-0.01 ‰ yr^{-1} ± 0.02 SD) with the WAP specimens (all shallow-collected). This indicates that the processes affecting the $\delta^{13}C_{shell}$ are acting more strongly in recent times (i.e. 2001/13) on the WAP than in the earlier time frames (i.e. 1900/10, 1917/25 and 1975/85) from the South Orkney Islands specimens, with the limitation that there is a possibility that ontogenetic trends may be affecting the $\delta^{13}C_{shell}$ records.

The reduced variability in the $\delta^{18}O_{shell}$ and reduced average $\delta^{13}C_{shell}$ present in the deep-collected specimen (27Sd, **Fig. 5.4**), when compared to the shallow-collected (**Fig. 5.2** and **Fig. 5.3**) specimens, was expected and emphasises the differences between both environments. Surface waters around the South Orkney Islands experience a marked seasonal change; seawater temperature in Factory Cove varies between 0 and 2 °C in the summer and lower than -1.5 °C during winter, chlorophyll concentration can reach up to 50 mg m^{-3} during the summer whereas mean minimum levels during winter are about 0.2 mg m^{-3} (Clarke et al., 1988; Clarke and Leakey, 1996). In addition, the seasonal formation of sea-ice during austral winter, which presents high interannual variability, causes further environmental changes in the seawater salinity and water column stability (Clarke et al., 1988; Murphy et al., 1995; Barnes et al., 2006). The duration of fast-ice can have additional effect on the local benthic environments since it can protect against iceberg scouring, which has been reported to have significant effects at Factory Cove (Peck et al., 1999; Smale et al., 2007). Instrumental physical data from deeper section of the water column from the South Orkney Islands is very limited; the use of a Conductivity–Temperature–Depth/Satellite-Relay Data Logger (CTD–SRDL) attached to a southern elephant sea (*Mirounga leonine*) provided some valuable information about the hydrographic variability over a period over more than eight months in the waters around the South Orkney Islands (Meredith et al., 2011). At 300 m depth, approximately from where specimen 27Sd was collected, seawater temperature and salinity show higher values due to the present of the Warm Deep Water (Meredith et al., 2011). At this depth seasonal sea-ice has little to no effect as the mean sea-ice thickness for Factory Cove has been reported to vary from 0.3 to 1.23 m (Murphy et al., 1995). Chlorophyll levels are also expected to be minimal, although no chlorophyll concentration data at this depth is available. Regarding the differences between the $\delta^{18}O_{shell}$ records, both seawater temperature and salinity seasonal changes are more variable in shallow waters than at depth, therefore it is also expected that a $\delta^{18}O_{water}$ record developed at a similar depth will have less variability. It is also worth noting that all three specimens present very similar average, maximum and minimum $\delta^{18}O_{shell}$ values, which suggests that, even with the difference in depth, all three specimens grew in the same water mass. Regarding the differences between the $\delta^{13}C_{shell}$ records, the reduced average, maximum and minimum $\delta^{13}C_{shell}$ values of the deep-collected specimen 27Sd, suggest a much reduced (i.e. approximately half of that from shallow depth) photosynthetic activity in the deeper water where specimen 27Sd grew. However, this is still a higher than expected value if only phytoplankton is taken account of for $\delta^{13}C_{shell}$ values since chlorophyll concentrations at 320 m water depth, from where specimen 27Sd was collected (c.f. Chapter II section 2.1), is to be expected only a very small fraction of that found in shallow waters.

The comparison of specimen 88Ss with the South Orkney Islands instrumental environmental records (**Fig. 5.11** and **Fig. 5.8**) is crucial as it serves as a calibration for the specimens for which no instrumental record available. Based on this comparison there is a possibility that a two-year offset is present in the geochemical records, although this cannot be confirmed since the only valve available from this specimen is sectioned. This should be prioritised in future work with the specimens from the South Orkney Islands.

If further analyses demonstrate that there is a two-year offset in the geochemical record from the 88Ss specimen, the stable isotope profiles seem to reflect the environmental conditions (i.e. seawater temperature and chlorophyll concentration) present at that time in the coastal waters from the South Orkney Islands. The instrumental record was developed by Clarke et al. (1988) from measurements carried out at the same location (i.e. Borge Bay) where the *A. eightsii* specimens used in this study were collected and therefore, in theory, the geochemical records should be representative for the local environmental conditions. The negative seawater temperature trend during the 1977/81 period coincided with a freshening of the coastal waters at Borge Bay (**Fig. 4.20**) and therefore the $\delta^{18}O_{shell}$ records should register a shift towards lower values at this time.

Even though the $\delta^{13}C_{shell}$ record presents a negative trend, which coincides with the negative trend in the chlorophyll concentration record if the two-year offset is introduced (**Fig. A5.2b**), the record does not seem to capture the collapse of the phytoplankton stock in 1978/79 and 1981/82 as the $\delta^{13}C_{shell}$ record shifts towards higher values after the minimum in 1978 and remains relatively constant after that (**Fig. A5.2b**). This characteristic of the $\delta^{13}C_{shell}$ record, assuming the two-year offset, indicates that other factors are controlling $\delta^{13}C_{shell}$ which are masking the primary production signal in the $\delta^{13}C_{shell}$ record. This is also similar to the observation from the WAP samples (**Fig. 5.19**) where after a collapse during 2007/08 the $\delta^{13}C_{shell}$ showed a significant shift towards lower values but then during the next summer season (2008/09), when chlorophyll concentration remained at very low levels, $\delta^{13}C_{shell}$ showed a shift towards higher values. This reflects the current poor understanding of how *A. eightsii* $\delta^{13}C_{shell}$ is affected by environmental conditions although it seems to represent, in general terms, primary productivity. A possible explanation for the shift towards higher $\delta^{13}C_{shell}$ values in 2008/09 after the collapse of the chlorophyll stocks in 2007/08 when the chlorophyll levels remained low is that the increased iceberg scouring that Ryder Bay experienced following 2007 (Barnes and Souster, 2011b) remobilized a significant amount of nutrients into the water column that were previously locked into the soft sediments.

5.4.2 West Antarctic Peninsula

The use of combined oceanographic proxies such as $\delta^{18}O_{water}$ and salinity for surface waters has the advantage that whilst salinity is greatly affected by sea-ice formation processes, $\delta^{18}O_{water}$ is only marginally affected; this can be used for instance to distinguish sea-ice melt from meteoric freshwater input (e.g. Meredith et al., 2008a).

The comparison between the averaged high-resolution record and the low-resolution records (**Fig. 5.18**) provides several advantages. It allows a validation between the two methods and it also provides further insight in the lateral isotopic fractionation, as the low-resolution sampling was taken from either the anterior or the posterior part of the shell running parallel to the high-resolution sampling (**Fig. 2.6**). When the high and low-resolution sampling strategies were compared an offset (low-resolution having lower isotopic values) between both records was present, although they presented similar trends (**Fig. 5.10** and **Fig. 5.18**). In the discussion of these results it was argued that one of the reasons of the offset could be lateral fractionation in the low-resolution sampling since the sampling transect was adjacent (either to the anterior or posterior region of the shell) to the high-resolution sampling. The results of the lateral isotopic fractionation in *A. eightsii* showed that anterior and posterior parts have a lower intra-increment isotopic signature compared with the ventral part of the shell (**Fig. 5.22**, **Fig. 5.23**, **Fig. 5.24** and **Fig. 5.25**), which points to lateral fractionation, at least in part, as the cause of the offset between the high and the low-resolution records.

Specimens 14HCs and 14HCd were both collected from Hangar Cove although at different water depths, approximately 15 m and approximately 30 m respectively, whereas the specimen 15SCs was collected from South Cove from a depth approximately 15 m (**Fig. 5.18**). If only the specimens from Hangar Cove (14HCs and 14HCd, **Fig. 5.18**) are considered the offset in both geochemical records between both specimens is apparent and can be determined as 0.14 ‰ ± 0.10 SD for $\delta^{18}O_{shell}$ and -0.08 ‰ ± 0.20 SD for $\delta^{13}C_{shell}$. The $\delta^{18}O_{shell}$ data appear to indicate that the deep collected specimen (14HCd) was growing in an environment which either was warmer or fresher or a combination of both than the shallow collected specimen as a difference of 0.18 ‰ was present between the high-resolution records and a difference of 0.10 ‰ was present between the low-resolution records. The sequentially averaged depth temperature (**Fig. 4.2**) and salinity profiles (**Fig. 4.9**) indicate that whereas seawater temperature decreased with depth, salinity increased with water depth, indicating that the differences in the $\delta^{18}O_{shell}$ high and low-resolution records between the shallow and deep collected specimens is due solely to salinity differences between the two environments. In addition, the offset between the high and the low-resolution records in both specimens seems to remain relatively constant (0.19 ‰ ± 0.10 SD for the specimen 14HCs and 0.18 ‰ ± 0.05 SD for the specimen 14HCd), which permits an easy correction and alignment between the geochemical records from both specimens (**Fig. 5.18a**). The specimen collected from South Cove (15SCs) cannot be directly compared with the contemporary 14HCd specimen from Hangar Cove due to the difference in depth. Regarding the offset between the high and the low-resolution records, the 15SCs specimen presents a smaller offset (0.09 ‰ ± 0.02) than that from the Hangar Cove specimens (**Fig. 5.18a**). In the case of specimen 15SCs, it is difficult to determine whether the 2006/08 sample is more representative of any particular year. However, the increment corresponding to 2006 was wider in comparison with 2007/08 (see number of samples per year in **Fig. 5.12**) and accordingly more material was available from that increment into the mixed powder; therefore the isotopic value should be more representative of 2006 (**Fig. 5.18**).

An offset between the high and low-resolution records of the $\delta^{13}C_{shell}$ records of the Hangar Cove specimens (14HCs and 4HCd; **Fig. 5.18b**) is present as was the case in the $\delta^{18}O_{shell}$ records. However, in contrast to $\delta^{18}O_{shell}$ where the offset between the paired high and low-resolution records from both specimens was relatively constant, the offset between the high-resolution $\delta^{13}C_{shell}$ records is much lower (0.33 ‰) than the offset between the $\delta^{13}C_{shell}$ low-resolution records (1.02 ‰, **Fig. 5.18b**). This is mainly due to the samples from 2006 in specimen 14HCd, which present lower low-resolution sample or a higher high-resolution average. A gap in the high-resolution sampling of specimen 14HCd in 2006 is present (**Fig. 5.13**); this has the potential to bias the high-resolution average for that particular year and therefore introduce an artefact in the record. If a comparison with other annual $\delta^{13}C_{shell}$ cycles from the specimen 14HCd is made, it can be observed that the second sample (the one missing in 2006) present typically a lower

$\delta^{13}C_{shell}$ signature when compared to the first sample of any annual cycle (**Fig. 5.13**). If this is considered to be the case in 2006, it can be determined that the artefact is present in the high-resolution average, which presents a higher $\delta^{13}C_{shell}$ value than it should be, and that the low-resolution sample should in theory represent a more faithful representation of the environmental conditions (**Fig. 5.18b**). In addition it can also be seen that specimen 14HCd shows a lower average $\delta^{13}C_{shell}$ value than the sh9allower specimen 14HCs; which was expected as chlorophyll concentration decreases with depth (**Fig. 4.14**).

The most obvious difference found in this study between the average $\delta^{18}O_{shell}$ and the average $\delta^{18}O_{water}$ (approximately 0.57 ‰ VPDB) is one example of the complexity of the system. The analysis of three different scenarios based on $\delta^{18}O_{syn}$ offer some possible explanations to the presence of this offset between the $\delta^{18}O$ records. Dierssen et al. (2002) undertook an experiment at Anvers Island, WAP in which they compared near shore oceanographic parameters with an offshore (3.7 km offshore) station and found that the near shore station showed salinity approximately 0.2 lower than the offshore station and that in general the offshore station presented an elevated seawater temperature compared to the nearshore station. The authors also reported that although the average salinity was 33.2 psu the presence of a surface freshwater lens, which extended from a few meters down to 50 m, could lower the salinity to 30.5 psu (Dierssen et al., 2002). In the present study, under the scenario where only the salinity was modified (i.e. lowered, **Fig. 5.21a**), two different possibilities can be considered. First, as *A. eightsii* specimens were collected much closer to the coast than the location of the RaTS sampling station, meltwater runoff may affect more directly coastal seawater than the well-mixed seawater at the RaTS sampling point (i.e. inner bay). Also the greater range in the $\delta^{18}O_{shell}$ record when compared to the $\delta^{18}O_{water}$ record could be explained as coastal seawater being affected more strongly and directly by the meltwater runoff that is characterized by a depleted $\delta^{18}O$ signature. Potter and Paren (1985, in Meredith et al., 2008a) reported a $\delta^{18}O_{water}$ value of around -20 ‰ for the direct ice flux into the end of George VI ice shelf, which calves to Marguerite Bay (immediately located south of Ryder Bay; **Fig. 1.4**), and -13 ‰ in the direct accumulation of precipitation in the northern part of the ice shelf. A second possibility may be that due to the close location to the coast the local *A. eightsii* populations may have been located in the trajectory of a low salinity current under the influence of meltwater runoff from land. Alternatively, under the scenario where only temperature was modified (i.e. increased, **Fig. 5.21b**) differences in mixing between coastal and inner bay seawater (i.e. RaTS site) could be a reason for this temperature difference through intense irradiation of coastal seawater. In addition, it can be argued that the greater range in the $\delta^{18}O_{shell}$ record when compared to the $\delta^{18}O_{water}$ record is caused by coastal seawater experiencing a greater temperature variability. The same arguments can be applied to the third scenario, where seawater temperature and salinity were modified (**Fig. 5.21c**). This last experiment where seawater temperature and salinity were both modified has to be considered carefully due to the great variability present in the relationship between seawater temperature and salinity (**Fig. A5.4**) as the rate to which seawater temperature and salinity change co-dependently can vary significantly. In addition, an alternative hypothesis for the difference between the average $\delta^{18}O_{shell}$ and the average $\delta^{18}O_{water}$ could be difference in calcification sensitivity in *A. eightsii* with respect to the modified Grossman and Ku (1986) equation by Dettman et al. (1999). This could be due for instance to the great difference in seawater temperatures between the Dettman et al. (1999) study and the temperatures occurring during *A. eightsii* growing season.

The comparison of the trends of the temporally normalized geochemical records (**Fig. 5.26**) offers additional insights into the very local differences between sites. Whereas specimen 15SCs (blue) was collected in South Cove (i.e. located on the inner side of

Rothera Point at Ryder Bay, **Fig. 2.1b**) from approximately 15 m water depth, the specimens 14HCs (green) and 14HCd (orange) were collected at Hangar Cove (i.e. located in the outer side of Rothera Point, **Fig. 2.1b**) from approximately 15 and 30 m respectively. If only the shallow specimens are considered, it can be seen that the $\delta^{18}O_{shell}$ data show very similar slopes but with an offset toward lower $\delta^{18}O_{shell}$ in the case of the South Cove specimen (blue, **Fig. 5.15a**). This suggests that both shallow environments are subjected to the same regional climatic trends of either warming, freshening or a combination of both; in addition it also suggests that South Cove experiences either warmer, fresher, or a combination of both, local conditions when compared to the other side of Rothera Point (i.e. Hangar Cove). It was already shown in Chapter IV that surface waters of Ryder Bay have been freshening, with the exception of 2006/08 (**Fig. 4.9**) and warming, especially during the austral summer season (**Fig. 4.3**). Therefore, the trend towards lower $\delta^{18}O_{shell}$ values in the WAP specimens is likely due a combination of these processes. Local topography and oceanography can have a significant effect in the canalization of meltwater runoff as well as mixing conditions with coastal oceanic waters that may explain the difference between both sites. On the other hand, if only the specimens from Hangar Cove are considered (14HCs in green and 14HCd in orange, **Fig. 5.26a**) differences over depth within site can be investigated. The different trends in the $\delta^{18}O_{shell}$ could be interpret as either the deep Hangar Cove site being affected preferentially by either warming, freshening or a combination of both relative to the shallow site or that the shallow Hangar Cove site is being affected preferentially by either cooling, salinification or a combination of both relative to the deep site. As both records start at similar calendar dates (2003 in the case of the shallow-collected 14HCs specimen and 2001 in the case of the deep-collected 14HCd specimen) either of the described possible scenarios is equally feasible. Sequentially averaged salinity profiles for the RaTS site (**Fig. 4.9**) indicate that the top 25 m of the water column was becoming more homogenous (i.e. salinity profiles between the top 5 m and the 25 m are more tightly grouped) from 2004 to 2010 and considering that the spacing between the top 25 m average salinity and the top 50 m average salinity remained relatively constant, can be interpreted as the top 25 m of the water column presenting a relatively higher salinity compared to the period prior to 2004 or after 2009. If the oceanographic conditions present at the RaTS site can be extrapolated to Hangar Cove this could offer an explanation for the difference in the $\delta^{18}O_{shell}$ between the shallow and the deep collected specimens.

On the other hand, regarding the $\delta^{13}C_{shell}$ records and considering only the shallow-collected specimens, the South Cove specimen (blue) shows a significantly more negative trend and a higher $\delta^{13}C_{shell}$ value for most of the record than the shallow Hangar Cove (green) specimen (**Fig. 5.26b**). If only the specimens from Hangar Cove are considered, the deep-collected specimen (orange) presents a more negative trend to that from the shallow-collected specimen (green) and both show a very similar average $\delta^{13}C_{shell}$. Sequentially averaged chlorophyll concentration data across the water column (**Fig. 4.13**) in 2003/04 and 2006/07 shows mixed a condition for the period concerned (i.e. 2001 onwards), for the top 15 m of the water column (grey) a relatively lower chlorophyll concentration, compared to the top 25 m of the water column (medium blue). On the other hand, during the periods 2004/05 and 2011/13 the top 15 m of the water column had a relatively higher chlorophyll concentration than the top 25 m of the water column (**Fig. 4.13**). Based on the sequentially averaged chlorophyll concentration profiles it is difficult to determine whether the difference in $\delta^{13}C_{shell}$ trends between Hangar Cove shallow-collected and the deep-collected specimens is due to environmental processes or it is due solely to ontogenetic trends in the data or even due to natural variability in the $\delta^{13}C_{shell}$. Chlorophyll concentration varies rapidly across water depth (**Fig. 4.14**) and even though there are significant differences between 15 m water depth and 30 m water depth (a difference of approximately 2 to 2.5 mg m^{-3} of chlorophyll) there may not strong enough to affect the $\delta^{13}C_{shell}$. In order to determine the relationship between the $\delta^{13}C_{shell}$ and water depth a comparison between contemporary specimens collected from shallow waters (i.e. approximately 15 to 20 water depth) and from deep waters (i.e. more than 90 m water depth), where chlorophyll concentration is minimal, could offer much more insight into this relationship. Similar to what was found in the South Orkney Islands specimens, the deep collected specimen is expected to show a lower $\delta^{13}C_{shell}$ average compared to the shallow collected specimen (**Fig. 5.8b** and **Fig. 5.26d**); however, as the specimens from the South Orkney Islands were not contemporary with modern chlorophyll records, the relationship between $\delta^{13}C_{shell}$ and water depth cannot be fully investigated.

5.4.3 Stable isotope lateral fractionation

In addition to the multiple environmental processes affecting the isotopic fractionation and equilibrium, biological process can affect isotope fractionation during shell formation. Although more detailed work is required in order to confirm that the sole cause of the intra-increment differences in the $\delta^{18}O_{shell}$ and $\delta^{13}C_{shell}$ data reported in **Fig. 5.22**, **Fig. 5.23** and **Fig. 5.24** is the due to the action of biological processes and not an artefact caused by the sampling methodology, these preliminary results highlight the importance of understanding isotope fractionation with shell growth in *A. eightsii*, or in any other species used for sclerochronological analysis. There has been no investigation assessing how the different layers in *A. eightsii* shell vary laterally in thickness, therefore it could be hypothesised that lateral portions of the shell (anterior and posterior, **Fig. 2.6c**) have a reduced thickness. If this possible explanation proves to be the case, sampling artefacts could be introduced when sampling in the lateral portions of the shell, especially closer to the shell margin where increments are narrower and present a tighter distribution. Barrera et al. (1990, 1994) carried out more detailed experiments to assess lateral fractionation in Antarctic mollusc bivalves *Adamussium colbecki* and *L. elliptica*.

In the case of *A. colbecki* the authors found that, besides a sample adjacent to the umbo, there were a good agreement in the $\delta^{18}O_{shell}$ measurements (3.78 ‰ ± 0.16 SD on average) along the margin and that there was no clear trend between the $\delta^{18}O_{shell}$ record and ontogenetic age along a sampled transect on the external surface of the shell following the maximum growth axis (Barrera et al., 1990). In addition, the authors found that the $\delta^{18}O_{shell}$ values were in agreement to the estimated $\delta^{18}O_{water}$ (i.e. precipitation close to equilibrium) derived from the Shackleton (1974) palaeotemperature equation, as no $\delta^{18}O_{water}$ instrumental measurements were available. Similarly, Barrera et al. (1994) found, using similar methods, that *L. elliptica* shell showed $\delta^{18}O_{shell}$ close to equilibrium with ambient water and that there were significant differences between the anterior, ventral and posterior regions in both $\delta^{18}O_{shell}$ and $\delta^{13}C_{shell}$. The authors also reported $\delta^{18}O_{shell}$ enrichment in the aragonite *L. elliptica* shell (4.50 ‰ on average) when compared to a contemporary calcite specimen of *A. colbecki* (3.52 ‰ on average). Average values of $\delta^{18}O_{shell}$ from *A. eightsii* for the South Orkney Islands and for the WAP at Rothera are in between the values reported by Barrera et al. (1990, 1994) for *L. elliptica* and *A. colbecki* (3.60 ‰ ± 0.24 SD for the WAP specimens, 3.89 ‰ ± 0.21 SD for all the South Orkney Islands specimen and 3.91 ‰ ± 0.26 SD for only the shallow-collected specimens). Although it is impossible to determine at the present if this difference in the average $\delta^{18}O_{shell}$ is due to differences between species, as no contemporary specimens from other species were collected, this should be easy to test as *L. elliptica* is also found at Ryder Bay (Harper et al., 2012; Morley et al., 2012). This study could also determine if only *A. eightsii* presents such an offset between $\delta^{18}O_{shell}$ and $\delta^{18}O_{water}$ or if this is due to local oceanographic conditions where the bivalve populations live. Barrera et al. (1994) pointed out that hyposaline freshwater lenses were observed at McMurdo Sound (i.e. their collection site) extending to 6 m water depth and as their specimens were collected well below this depth (30 m for *L. elliptica* and 15 m for *A. colbecki*) they were not affected by these extreme seasonal changes. Similar hyposaline lenses have been reported in Ryder Bay, Barnes and Brockington (2003) reported hyposaline lenses in the top 10 m of the water column that could reduce the salinity by 1.0 psu at the height of the austral summer. Some of the *A. eightsii* specimens collected for this research were found in very shallow areas and therefore could be affected by these seasonal hyposaline lenses, which could have an effect in the shell stable isotope fractionation and even on shell growth as an environmental stressor.

5.5 Appendix – Tables and figures

Table A5.1 Comparison of the geochemical values of the $\delta^{13}C_{shell}$ (‰ VPDB) and $\delta^{18}O_{shell}$ (‰ VPDB) collected from the specimens 88Ss, 15Ss and 27Sd from the low-resolution sampling (± the external precision) and from the high-resolution sampling (± standard deviation).

		Low-resolution		**High-resolution**	
Specimen ID	**Year**	**$\delta^{13}C_{shell}$**	**$\delta^{18}O_{shell}$**	**$\delta^{13}C_{shell}$**	**$\delta^{18}O_{shell}$**
88Ss	1977	1.984 ± 0.026	3.879 ± 0.055		
88Ss	1978	1.664 ± 0.015	3.841 ± 0.033	2.112 ± 0.175	4.040 ± 0.228
88Ss	1979	1.258 ± 0.026	3.983 ± 0.029	1.634 ± 0.174	3.964 ± 0.194
88Ss	1980	1.360 ± 0.019	3.557 ± 0.028	1.690 ± 0.246	3.745 ± 0.177
88Ss	1981	1.482 ± 0.017	3.771 ± 0.026	1.773 ± 0.233	3.689 ± 0.203
88Ss	1982	1.786 ± 0.017	3.868 ± 0.030	1.983 ± 0.149	3.705 ± 0.133
15Ss	1905	1.586 ± 0.023	3.923 ± 0.048		
15Ss	1906	1.586 ± 0.027	4.084 ± 0.030	1.730 ± 0.269	4.200 ± 0.174
15Ss	1907	1.704 ± 0.011	4.003 ± 0.038	1.844 ± 0.308	4.145 ± 0.121
15Ss	1908	1.047 ± 0.017	3.615 ± 0.017	1.036 ± 0.189	3.819 ± 0.248
15Ss	1909	1.398 ± 0.020	3.792 ± 0.019	1.512 ± 0.211	3.981 ± 0.168
15Ss	1910	1.926 ± 0.021	3.605 ± 0.033	1.938 ± 0.123	3.744 ± 0.251
27Sd	1925	0.411 ± 0.027	3.665 ± 0.038	0.632 ± 0.222	3.646 ± 0.055
27Sd	1924	0.658 ± 0.027	3.681 ± 0.038	0.748 ± 0.102	3.675 ± 0.082
27Sd	1923	0.860 ± 0.027	3.761 ± 0.038	0.800 ± 0.092	3.785 ± 0.080
27Sd	1922	0.666 ± 0.027	3.673 ± 0.038	0.655 ± 0.125	3.755 ± 0.095
27Sd	1921	0.670 ± 0.027	3.971 ± 0.038	0.638 ± 0.211	3.715 ± 0.050
27Sd	1920	0.622 ± 0.027	3.725 ± 0.038	0.636 ± 0.080	3.738 ± 0.085
27Sd	1919	0.966 ± 0.027	4.068 ± 0.038	0.803 ± 0.129	3.871 ± 0.093

27Sd	1918	1.103 ± 0.027	3.974 ± 0.038	1.000 ± 0.100	3.960 ± 0.060
27Sd	1917	1.256 ± 0.027	4.074 ± 0.038	1.313 ± 0.138	4.020 ± 0.047

Table A5.2 Comparison of the geochemical values of the $\delta^{13}C_{shell}$ (‰ VPDB) and $\delta^{18}O_{shell}$ (‰ VPDB) collected from the specimens 15SCs, 14HCd and 14HCs from the low-resolution sampling (± the external precision) and from the high-resolution sampling (± standard deviation).

		Low-resolution		**High-resolution**	
Specimen ID	**Year**	$\delta^{13}C_{shell}$	$\delta^{18}O_{shell}$	$\delta^{13}C_{shell}$	$\delta^{18}O_{shell}$
15SCs	2004	1.271 ± 0.031	3.448 ± 0.031	1.619 ± 0.164	3.560 ± 0.267
15SCs	2005	1.123 ± 0.017	3.563 ± 0.038	1.377 ± 0.278	3.636 ± 0.270
15SCs	2006	0.778 ± 0.017	3.441 ± 0.025	1.077 ± 0.405	3.526 ± 0.274
14HCd	2004	-0.138 ± 0.016	3.496 ± 0.024	0.200 ± 0.198	3.724 ± 0.243
14HCd	2005	0.134 ± 0.017	3.371 ± 0.038	0.449 ± 0.125	3.529 ± 0.188
14HCd	2006	-0.179 ± 0.025	3.406 ± 0.031	0.525 ± 0.171	3.547 ± 0.124
14HCs	2006	0.840 ± 0.013	3.509 ± 0.022	0.850 ± 0.292	3.731 ± 0.190
14HCs	2007	-0.403 ± 0.015	3.280 ± 0.025	0.053 ± 0.673	3.458 ± 0.172
14HCs	2008	0.351 ± 0.018	3.477 ± 0.039	0.465 ± 0.295	3.470 ± 0.189
14HCs	2009	0.323 ± 0.017	3.523 ± 0.037	0.419 ± 0.333	3.830 ± 0.174
14HCs	2010	0.889 ± 0.023	3.574 ± 0.021	0.934 ± 0.229	3.786 ± 0.128
14HCs	2011	0.587 ± 0.027	3.361 ± 0.036	0.719 ± 0.206	3.561 ± 0.183
14HCs	2012	0.048 ± 0.030	3.292 ± 0.056	0.455 ± 0.384	3.490 ± 0.127

Table A5.3 One-way ANOVA and Fisher's LSD test results comparing differences in lateral $\delta^{18}O_{shell}$ fractionation between species (*A. eightsii*, *L. elliptica* and *A. colbecki*) using the data displayed in **Fig. 5.30**.

	Sum of Squares	df	Mean Square	F	Sig.
Between Groups	1.456	2	.728	28.908	.000
Within Groups	.453	18	.025		
Total	1.910	20			

Multiple Comparisons (Fisher' LSD test)

The mean difference is significant at the 0.05 level.

(I) species	(J) species	Mean Difference (I-J)	Std. Error	Sig.	95 % Confidence Interval	
					Lower Bound	Upper Bound
L. elliptica	A. eightsii	.75296*	.10038	.000	.5421	.9638
	A. colbecki	.75067*	.12959	.000	.4784	1.0229
A. eightsii	L. elliptica	-.75296*	.10038	.000	-.9638	-.5421
	A. colbecki	-.00229	.10038	.982	-.2132	.2086
A. colbecki	L. elliptica	-.75067*	.12959	.000	-1.0229	-.4784
	A. eightsii	.00229	.10038	.982	-.2086	.2132

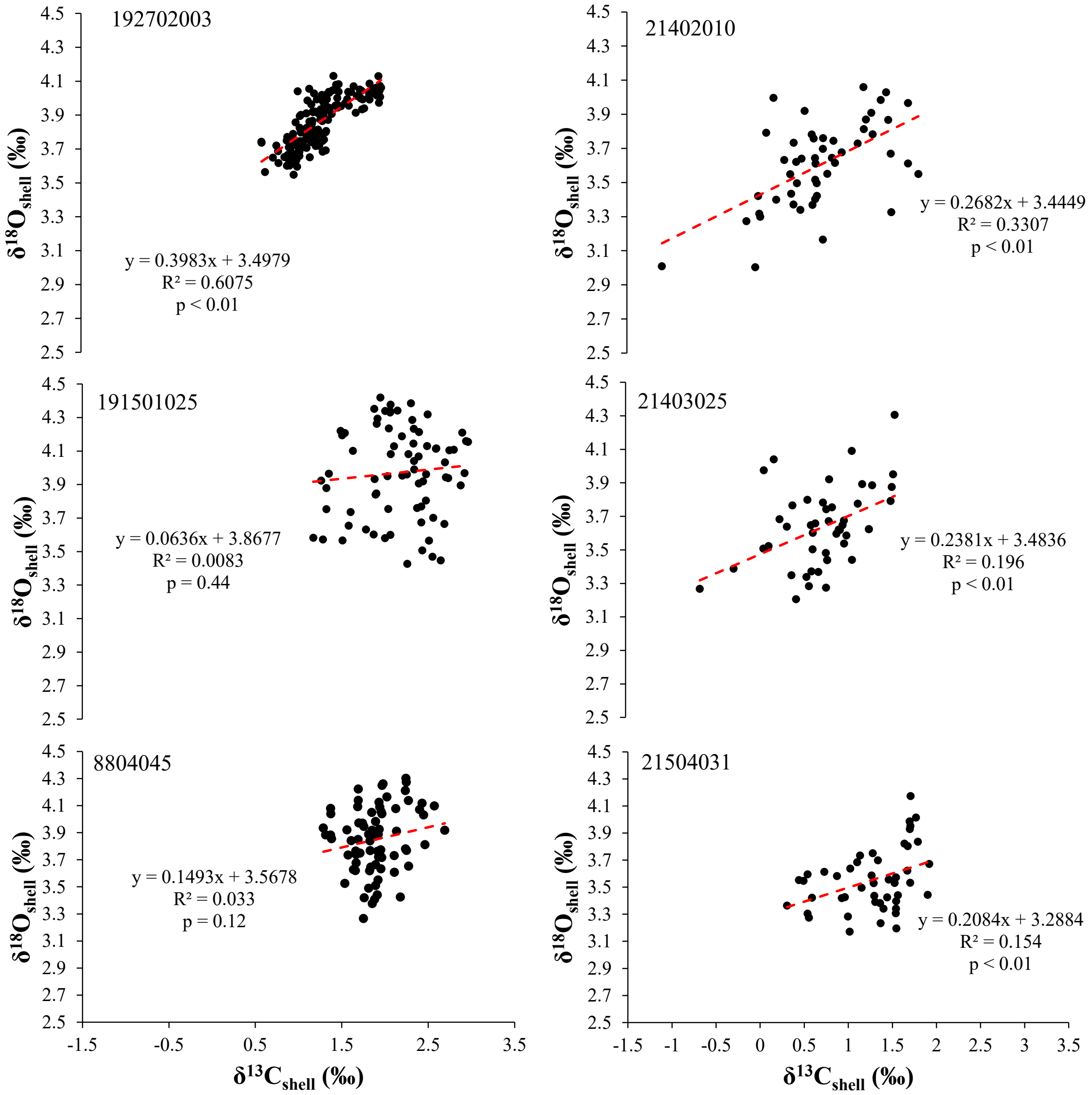

Fig. A5.1 Relationship between $\delta^{13}C_{shell}$ (‰ VPDB) and $\delta^{18}O_{shell}$ (‰ VPDB) of the high-resolution drilled samples. On the left column specimens from the South Orkney Islands and on the right column specimens from the WAP. A linear trend (dashed red line) was fitted to the datasets; the equation of the trend and the R^2 are shown in the inset.

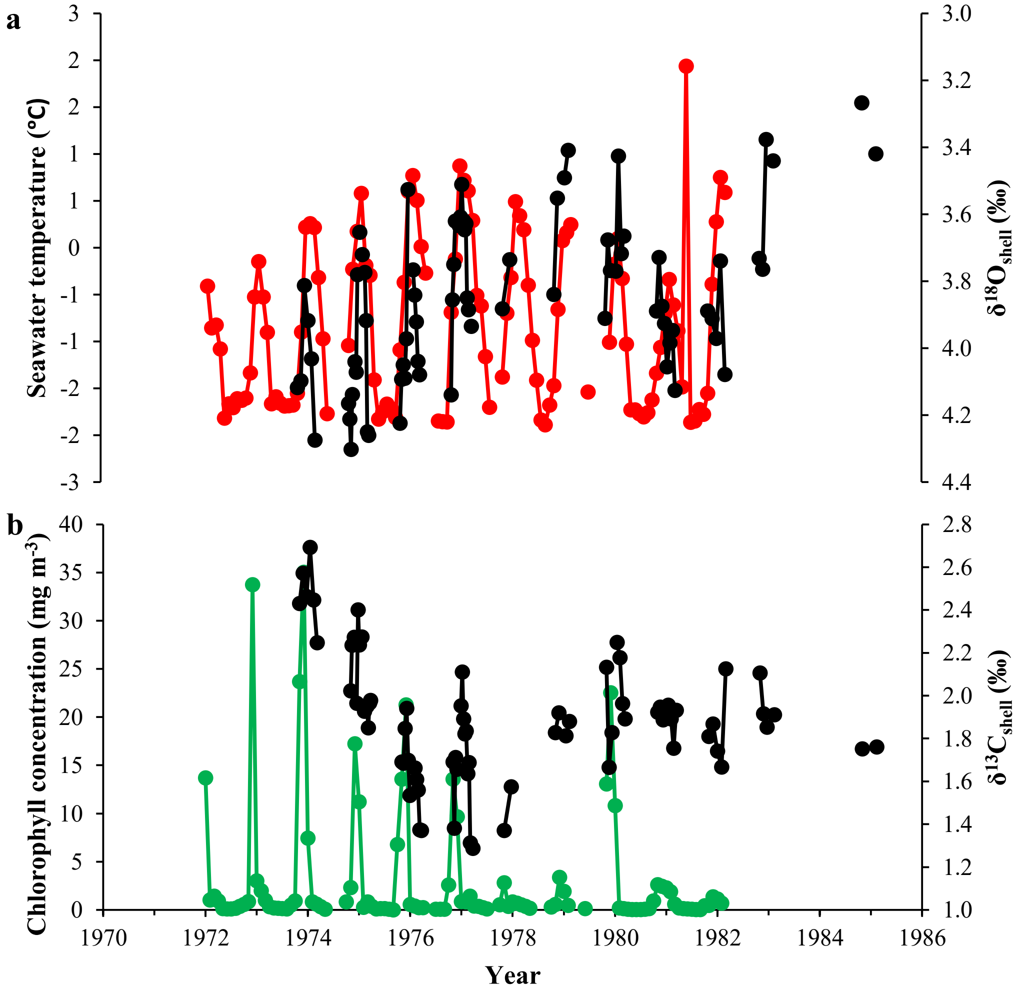

Fig. A5.2 Comparison between **a)** the seawater temperature (°C, red line, data extracted from *Clarke et al., 1*988) and the $\delta^{18}O_{shell}$ (‰ VPDB, note the inverted Y-axis) from the specimen 88Ss and **b)** chlorophyll concentration (mg m^{-3}, green line, data extracted from Clarke et al., 1988) and the $\delta^{13}C_{shell}$ (‰ VPDB) from the specimen 88Ss. In comparison to **Fig. 5.13** an offset of two years has been introduced artificially in both geochemical records.

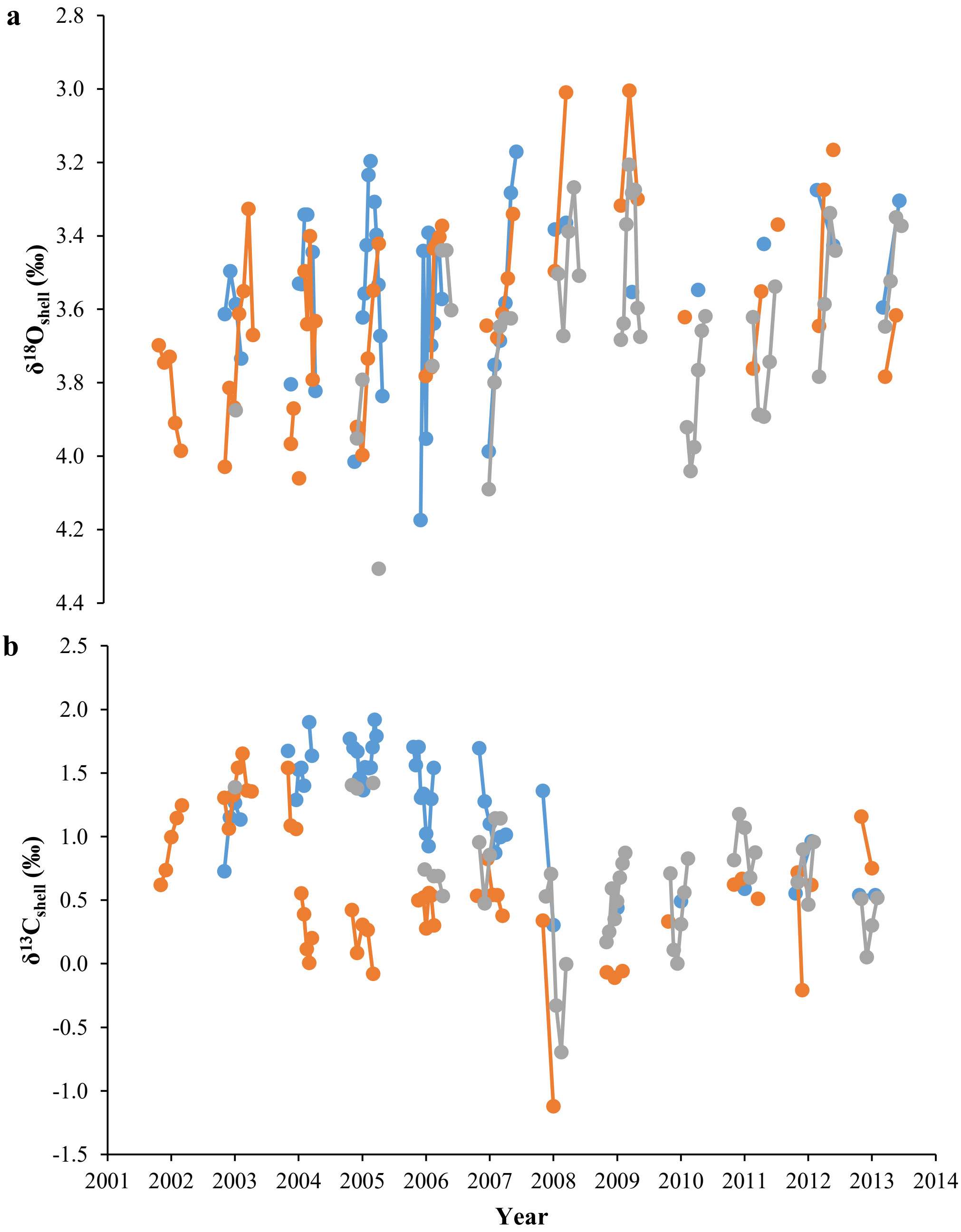

Fig. A5.3 Combination of **a)** $\delta^{18}O_{shell}$ records (‰ VPDB, note the inverted Y-axis) and **b)** $\delta^{13}C_{shell}$ records (‰ VPDB) for specimens 15SCs (blue), 14HCd (orange) and 14HCs (grey).

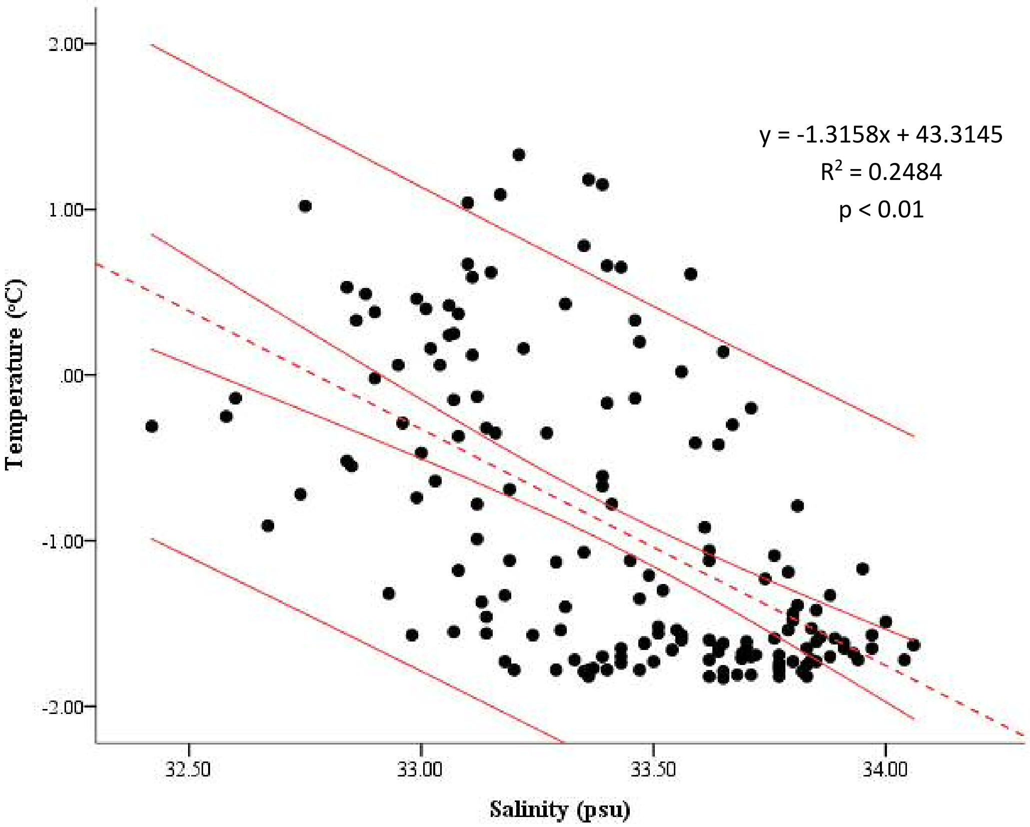

Fig. A5.4 Relationship between temperature and salinity for the top 15 m of the water column at the RaTS site. A linear trend (red dashed line) was fitted to the data; 95 % confidence intervals and 95 % prediction intervals (red solid lines), regression equation and R^2 are also provided.

Chapter VI: Sclerochronologies

In this chapter the chronologies, negative exponential (NE) and regional curve standardization (RCS) detrending results for each sampling location are presented. Intra- and inter-location comparisons are presented if a sufficient temporal overlap between local chronologies was present. In addition, comparisons between the chronologies and the instrumental and geochemical records are also provided.

This chapter is divided into three sections, the first two covering results for the two major studied regions: West Antarctic Peninsula (South Cove, Hangar Cove, Back Bay and Troval) and Signy Island, South Orkney Islands. Last, a discussion of the results from each sampling location is provided. For reference on the specific location of the study sites see **Fig. 2.1 (**Chapter II). A list of the specimens used to construct the different chronologies can be found in **Table A6.1.**

Specific hypothesis tested in this chapter are: i) specimens from each location present a common growth pattern, ii) this common growth pattern is related to the variability of the physical environment and iii) nearby locations present the same environmental controls on shell growth.

6.1 West Antarctic Peninsula

6.1.1 South Cove

The South Cove master ARSTAN chronologies (NE and RCS) were constructed by crossdating 11 specimens (**Fig. 6.1**). The average lifespan of the specimens incorporated into the chronology is 17 years and the longest-lived specimen is 21 years. The master chronology spans a period of 21 years, from 1995 to 2015 and it is characterised by alternating years of rapid (e.g. 2002, 2005, 2009, 2011 and 2014; **Fig. 6.1a**) and reduced shell growth (e.g. 2003, 2007 and 2013; **Fig. 6.1a**). In addition, between 2004 and 2007 the population at South Cove shows a trend towards reduced shell growth, which is followed by a trend towards rapid shell growth until 2009 (**Fig. 6.1a**). Both chronologies show high Expressed Population Signal (EPS) values for most of the period between 2003 and 2014; however a drop in the EPS is noticeable in 2011 (**Fig. 6.1b**), which is more pronounced in the RCS-chronology than in the NE-chronology. Autocorrelation indices for the South Cove chronology are provided in **Fig. A6.1a**; the chronology shows no autocorrelation for ten-year lags, although partial autocorrelation coefficients are close to significance at four-year lag (**Fig. A6.1a**).

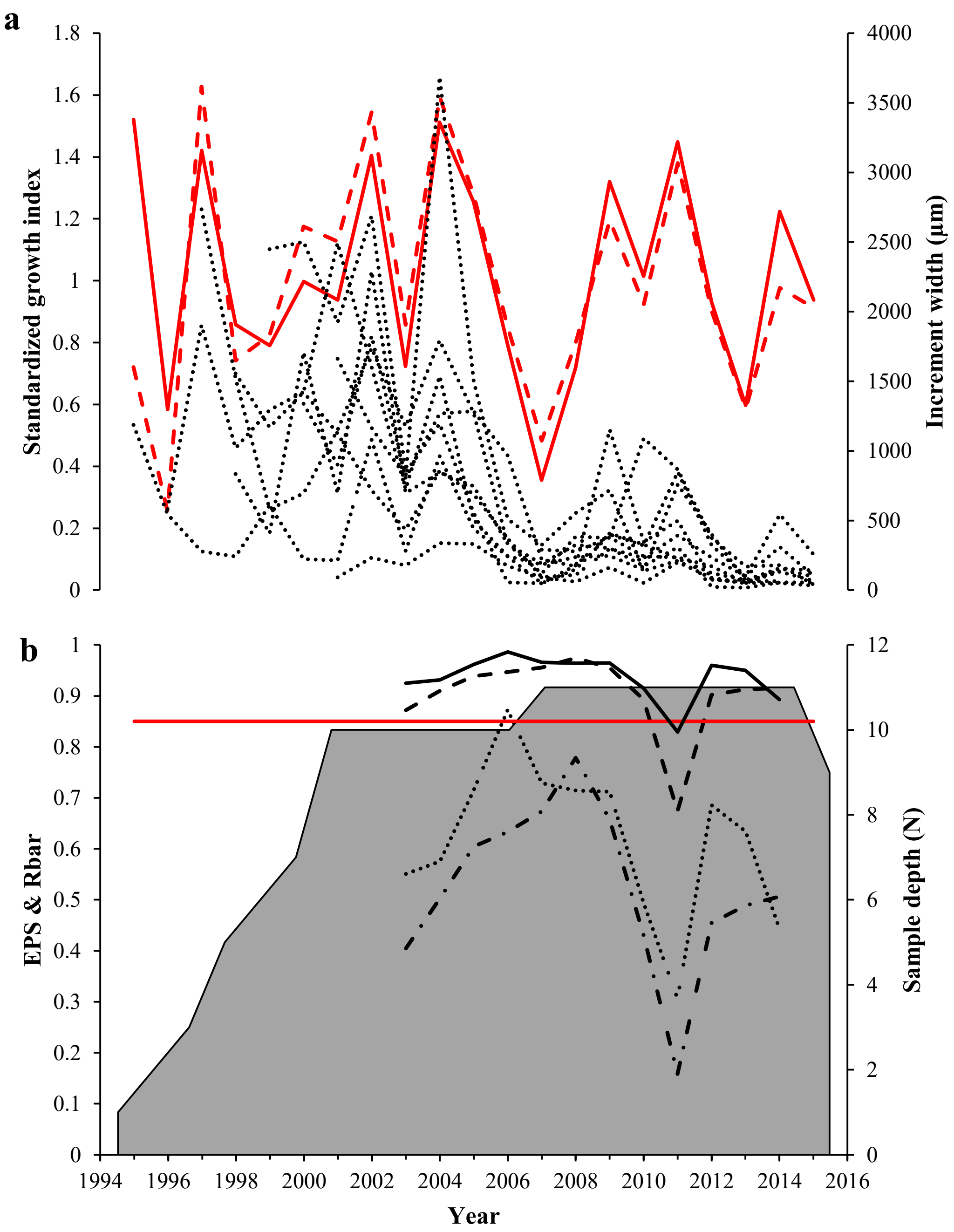

Fig. 6.1 a) South Cove NE-chronology (solid red line, primary Y-axis) and RCS-chronology (dashed red line) and the individual undetrended growth histories (dotted black lines, secondary

Y-axis) of the specimens used for constructing the master chronologies **b)** EPS from the NE-chronology (solid black line), EPS from the RCS-chronology (dashed black line), Rbar of the NE-chronology (dotted black line) and of the RCS-chronology (dashed-dotted black line) and sample depth (N) as a grey shaded area, the EPS = 0.85 threshold suggested by (Wigley et al., 1984) is represented with a solid red line.

6.1.2 Hangar Cove

Hangar Cove master ARSTAN chronologies (NE and RCS; **Fig. 6.2**) were successfully constructed by crossdating 16 specimens (nine collected at around 25-30 m water depth and seven collected at 15 m water depth).

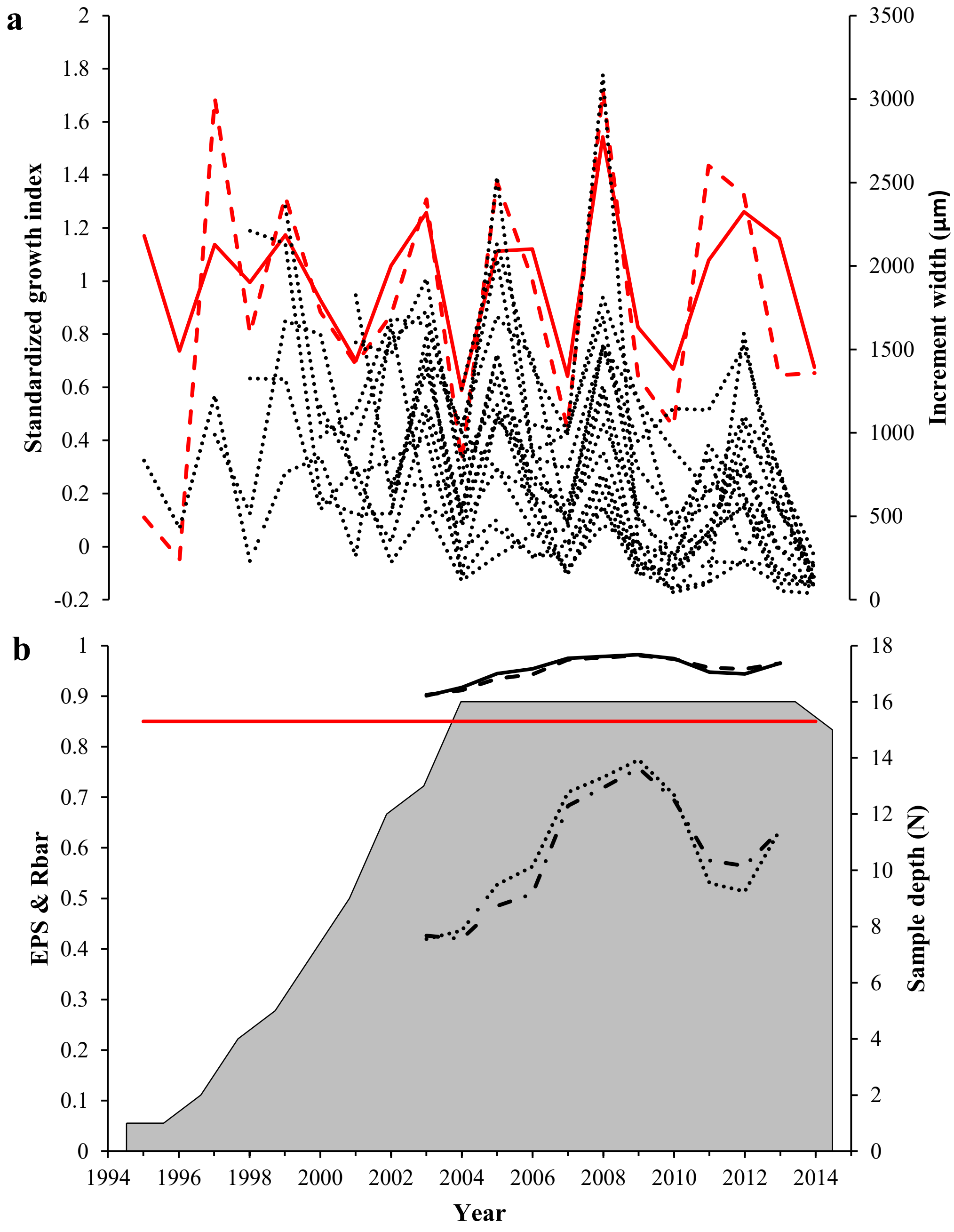

Fig. 6.2 a) Hangar Cove NE-chronology (solid red line, primary Y-axis) and RCS-chronology (dashed red line) and the individual undetrended growth histories (dotted black lines, secondary Y-axis) of the specimens used for constructing the master chronologies **b)** EPS from the NE-

chronology (solid black line), EPS from the RCS-chronology (dashed black line), Rbar of the NE-chronology (dotted black line) and of the RCS-chronology (dashed-dotted black line) and sample depth (N) as a grey shaded area, the EPS = 0.85 threshold suggested by (Wigley et al., 1984) is represented with a solid red line.

The average lifespan of the specimens incorporated into the chronologies was 14 years and the longest-lived specimen was 20 years; however only four specimens were older than 15 years. The chronologies are characterised by alternating multiannual periods of rapid growth (e.g. 2002/03, 2005/06, 2009, 2011/12; **Fig. 6.2a**) and reduced growth (e.g. 2004, 2008, 2009/10, 2013/14; **Fig. 6.2a**). These cycles present a three year period between 2001 and 2010 and a four year period in the case of the NE-chronology (three in the case of the RCS-chronology) between 2010 and 2014 (**Fig. 6.2a**). Both chronologies are robust (EPS > 0.85) for a period of eleven years (2003/13, **Fig. 6.2b**) indicated by the EPS value (on average EPS = 0.95 for the 2003/13 period). Prior to 2003 too few long-lived specimens remain in the chronologies and therefore the EPS is predictably much lower than 0.85. The chronologies present a high degree of correlation (Pearson's product-moment correlation, $r = 0.71$, $p < 0.01$, $n = 20$); however some differences can be identified between them in the robust period of the chronologies (2006, 2011 and 2013; **Fig 6.2a**). Autocorrelation indices for the Hangar Cove chronology are provided in **Fig. A6.1b;** the chronology shows no autocorrelation for ten-year lags, although partial autocorrelation coefficients are significant at two-year lag.

6.1.3 Back Bay, Lagoon Island

Back Bay master ARSTAN chronologies (NE and RCS) were constructed by crossdating a total of 11 specimens (**Fig. 6.3a**). The average lifespan of the specimens incorporated into the chronologies was 15 years and the longest-lived specimen was 20 years. The EPS of both chronologies becomes lower than the 0.85 threshold for the most recent part (from 2009 to present) of the chronologies, whereas the period 2003/09 shows EPS values higher than 0.85. The EPS of the RCS-chronology shows lower values than the equivalent from the NE-chronology (**Fig. 6.3b**). During this period (2009/15) the specimens presented an unusually high frequency of disturbance lines and short increments. Autocorrelation indices for the Back Bay chronology are provided in **Fig. A6.1c;** the chronology shows no autocorrelation for ten-year lags.

The chronologies show little shell growth variability between 2011 and 2015, prior to that period two cycles of low/high/low shell growth are present (2003/07 and 2007/11, **Fig. 6.3a**), 2007 being a year of particularly reduced shell growth and 2004 and 2008 years of particularly enhanced shell growth (**Fig. 6.3a**).

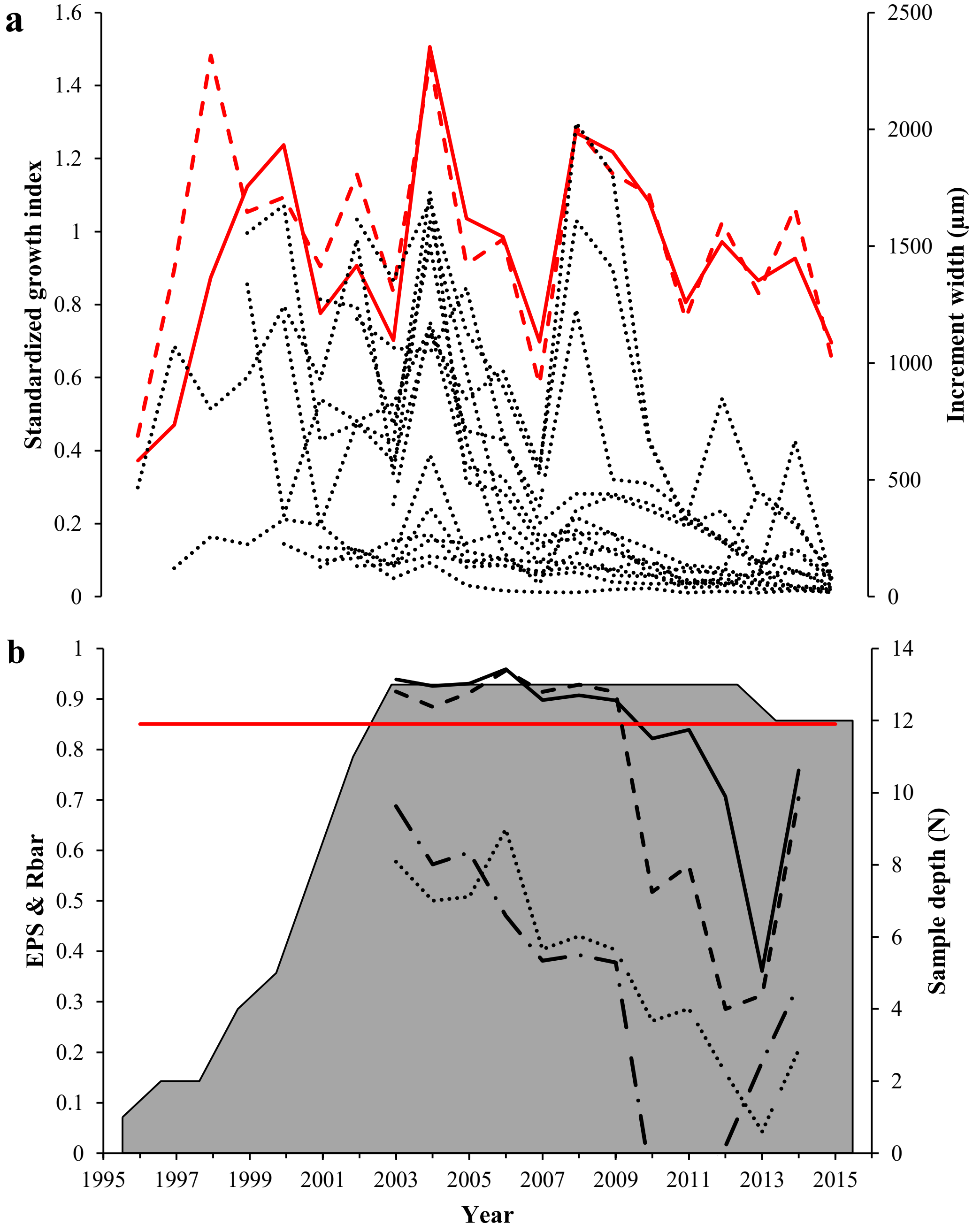

Fig. 6.3 a) Back Bay NE-chronology (solid red line, primary Y-axis) and RCS-chronology (dashed red line) and the individual undetrended growth histories (dotted black lines, right Y-axis) of the specimens used for constructing the master chronologies **b)** EPS from the NE-chronology

(solid black line), EPS from the RCS-chronology (dashed black line), Rbar of the NE-chronology (dotted black line) and of the RCS-chronology (dashed-dotted black line) and sample depth (N) as a grey shaded area, the EPS = 0.85 threshold suggested by (Wigley et al., 1984) is represented with a solid red line.

The sample depth of the chronologies is higher (up to 13, **Fig. 6.3b**) than the number of crossmatched specimens; this is due to the fact that for some specimens growth increment series from both the margin and the umbo were used in the chronology. Specimens from Back Bay are characterised by a high frequency of disturbance lines (i.e. growth checks normally adjacent to the annually-formed growth mark, **Fig. 6.4**) in the dark section of the annual increment in the hinge plate.

The chronologies were very similar (Pearson's product-moment correlation, $r = 0.76$, $p < 0.01$, $n = 20$), although some differences can be identified both in terms of trends (e.g. 2005 and 2009, **Fig. 6.3a**) and in terms of range (e.g. 2002 and 2014, **Fig. 6.3a**)

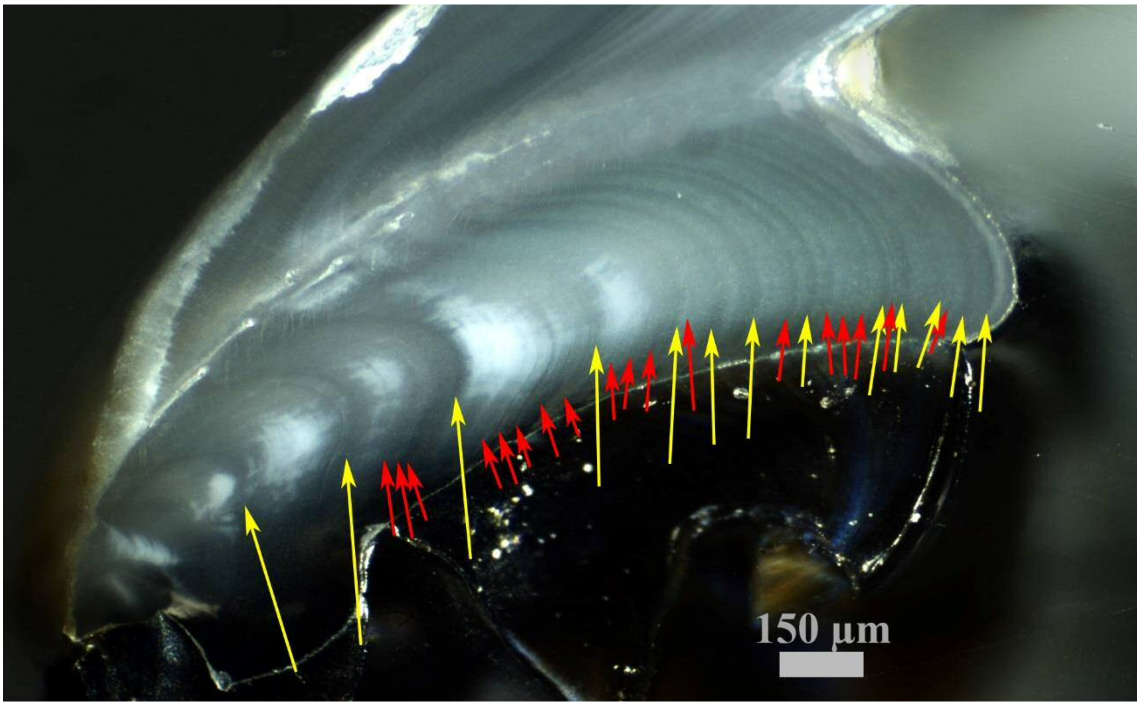

Fig. 6.4 Microphotograph of the hinge plate of a *A. eightsii* specimen collected from Back Bay showing some examples of annually formed increments (yellow arrows) and some doublets marks (red arrows). A scale bar is also included.

6.1.4 Trolval Island

It was not possible to construct a robust master chronology from Trolval. This was because there was a high presence of disturbance marks and frequent faint increments (**Fig. 6.5**), preventing the correct identification of the population common growth pattern. The growth histories of specimens are presented in **Fig. 6.6**. The average lifespan of the Trolval specimens was 18 years and the longest-lived specimen was 28 years; however, as these specimens have not been crossmatched there is the possibility of substantial error in the age determination.

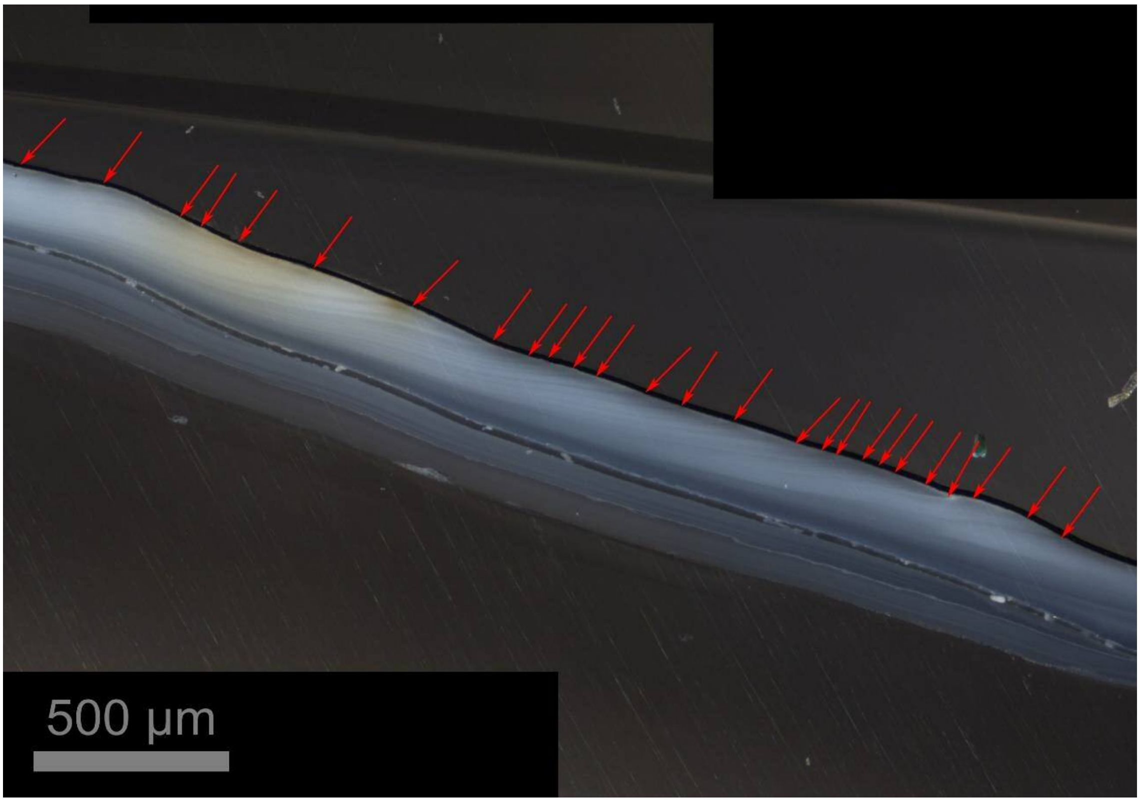

Fig. 6.5 Microphotograph of a section of an *A. eightsii* shell collected from Trolval (specimen 21401001) showing the presence of multiple markings in the shell (red arrows). Scale bar is also shown.

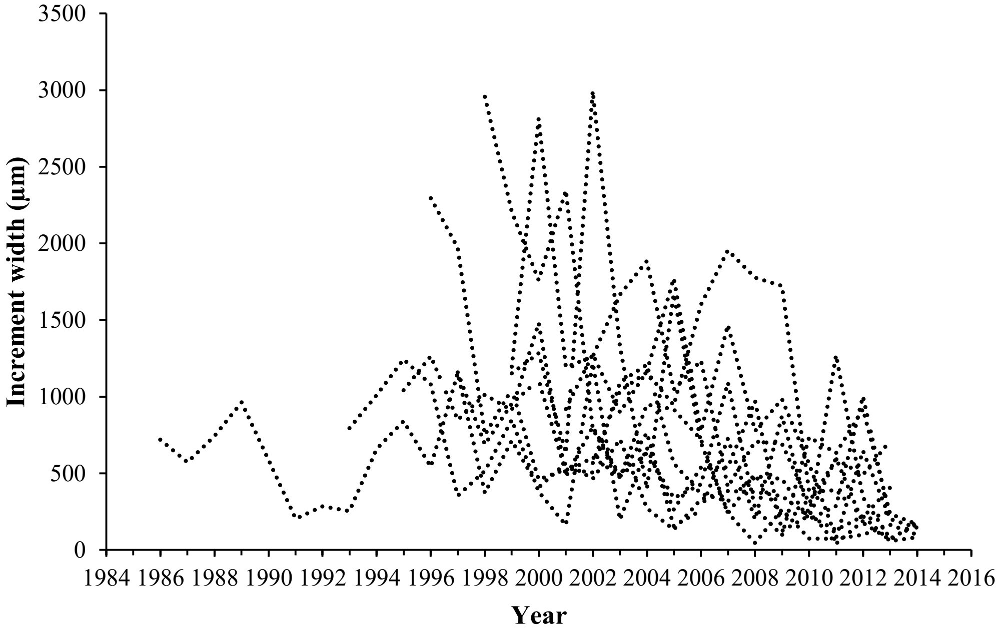

Fig. 6.6 Individual undetrended growth histories (dotted lines) of ten *A. eightsii* specimens collected from Trolval.

6.1.5 Comparison between master chronologies

The comparison between the master NE-chronologies showed differences between the inner Ryder Bay locations (i.e. South Cove and Back Bay) and the outer Ryder Bay location (i.e. Hangar Cove, **Fig. 6.7)**. South Cove and Back Bay master chronologies showed similar growth patterns, although not statistically significant (Pearson's product-moment correlation, $r = 0.29$, $R^2 = 0.09$, $n = 20$, $p = 0.21$), whereas neither the South Cove master chronology nor the Back Bay master chronology showed similarities with Hangar Cove master chronology (South Cove *vs.* Hangar Cove, $r = -0.07$, $R^2 = 0.004$, $n = 20$, $p = 0.78$; Back Bay *vs.* Hangar Cove, $r = 0.02$, $R^2 < 0.001$, $n = 19$, $p = 0.94$). However further analysis shows that the chronologies are not statistically different from each other (one-way ANOVA, $F_{2,59} = 0.5$, $p = 0.61$).

A noticeable point of disagreement between the inner Ryder Bay master NE-chronologies (i.e. South Cove and Back Bay) and the Hangar Cove master NE-chronology occurs in 2004 (**Fig. 6.7**), when the South Cove and Back Bay master chronologies show increased shell growth whereas the Hangar Cove master chronology shows a marked decreased shell growth. Within Ryder Bay the period between 2008 and 2011 shows a degree of disagreement between the master chronologies, most noticeable in 2011 when the South Cove master chronology shows increased shell growth but the Back Bay master chronology shows reduced shell growth. On the other hand, all three master chronologies show a period, between 2005 and 2008, which was characterised by markedly reduced shell growth (2006/07) preceded and followed by period of increased shell growth (2005/06 and 2008 respectively; **Fig. 6.7**).

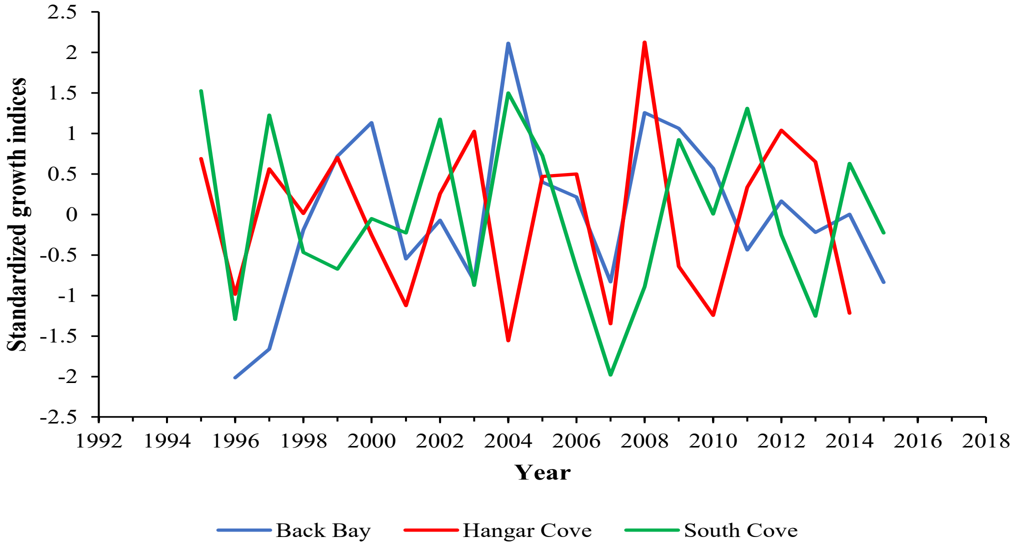

Fig. 6.7 Comparison between the master NE-chronologies from South Cove (solid green line), Back Bay (solid blue line), and Hangar Cove (solid red line).

a

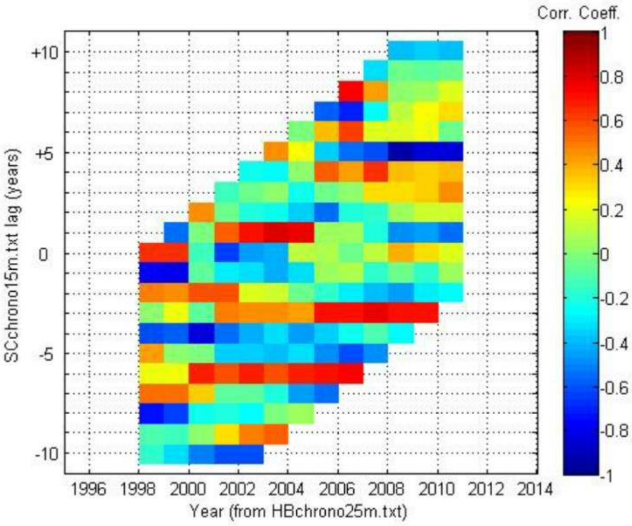
Corr. Coeff.
1
0.8
0.6
0.4
0.2
0
-0.2
-0.4
-0.6
-0.8
-1
+10
+5
0
-5
-10
SCchrono15m.txt lag (years)
1996
1998
2000
2002
2004
2006
2008
2010
2012
2014
Year (from HBchrono25m.txt)

b

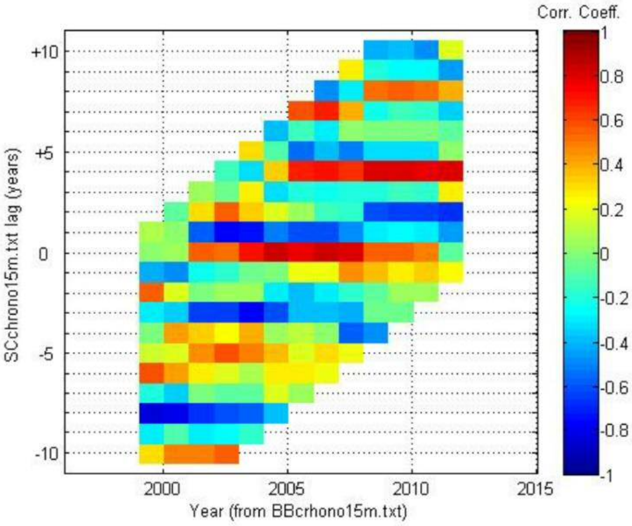
Corr. Coeff.
1
0.8
0.6
0.4
0.2
0
-0.2
-0.4
-0.6
-0.8
-1
+10
+5
0
-5
-10
SCchrono15m.txt lag (years)
2000
2005
2010
2015
Year (from BBcrhono15m.txt)

c

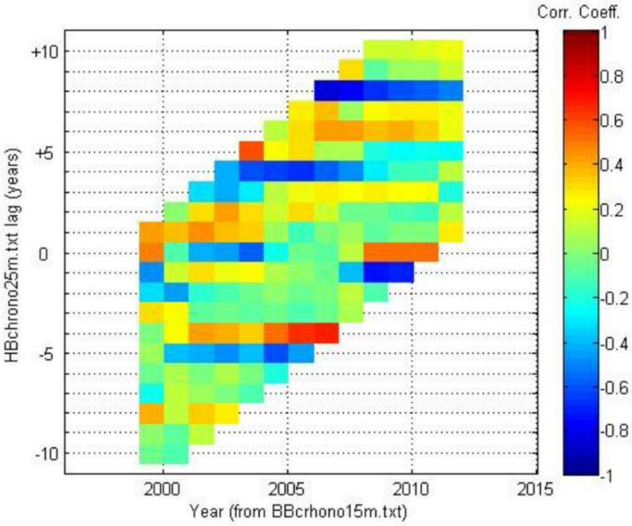
Corr. Coeff.
1
0.8
0.6
0.4
0.2
0
-0.2
-0.4
-0.6
-0.8
-1
+10
+5
0
-5
-10
HBchrono25m.txt lag (years)
2000
2005
2010
2015
Year (from BBcrhono15m.txt)

Fig. 6.8 SHELLCORR graphical output showing running lagged correlations in a seven year window between the negative exponential chronologies from **a)** South Cove and Hangar Cove, **b)** South Cove and Back Bay and **c)** Hangar Cove and Back Bay. The coloured scale indicates the Pearson's product-moment correlation (r) with warm colours indicating positive correlation, cold colours indicating negative correlations and greens for no correlation. Primary Y-axis indicates the lag between the series in years.

In addition, a comparison between the chronologies using lagged running correlations shows a possible lag between the South Cove chronology and Hangar Cove chronology at minus four-year lag and possibly the presence of an offset between the chronologies around 2001/02 (**Fig. 6.8a**). A similar comparison between the South Cove NE-chronology and the Back Bay NE-chronology shows a moderately positive correlation at zero-year lag (**Fig. 6.8b**) and also a moderately positive correlation at plus four-year lag. A comparison between the Hangar Cove NE-chronology and the Back Bay NE-chronology shows little or no correlation between them (**Fig. 6.8c**).

6.1.6 Comparison with instrumental records

This subsection covers a comparison between the South Cove and Hangar Cove NE-chronologies and the instrumental records available from the RaTS program (c.f. section 4.1., chapter IV). The Back Bay chronology was not compared with the instrumental records since a significant part of the chronology is not robust (i.e. from 2009 to 2014, **Fig. 6.3**). The South Cove chronology is compared with environmental parameters belonging to the upper 15 m of the water column and to the 15 m water depth measurements, since the specimens collected were collected from around 15 m water depth; whereas the Hangar Cove chronology is compared with environmental parameters belonging to the upper 25 m of the water column and to the 25 m water depth measurements, since specimens from Hangar Cove were collected around that water depth.

Correlations between the South Cove NE-chronology and Hangar Cove NE-chronology with, respectively, the monthly averaged seawater instrumental temperature record for the upper 15 m and for the upper 25 m of the water column are presented in **Table 6.1**. The monthly Pearson's production-moment correlation coefficients do not show any seasonal pattern of correlation and none of the correlations are statistically significant. These coefficients were subsequently used to weight the seawater temperature records.

Table 6.1 Pearson's product-moment correlation (r) of the NE-chronologies from South Cove and Hangar Cove and the monthly averaged seawater temperature records for the upper 15 m and upper 25 m of the water column from the RaTS dataset.

Location / Month	**Jan**	**Feb**	**Mar**	**Apr**	**May**	**Jun**	**Jul**	**Aug**	**Sep**	**Oct**	**Nov**	**Dec**
South Cove	0.04	-0.24	-0.16	-0.40	-0.36	-0.06	-0.16	0.07	-0.22	0.23	0.20	-0.09
Hangar Cove	-0.20	-0.11	-0.22	0.12	0.08	0.02	-0.20	-0.14	0.33	0.27	-0.12	0.06

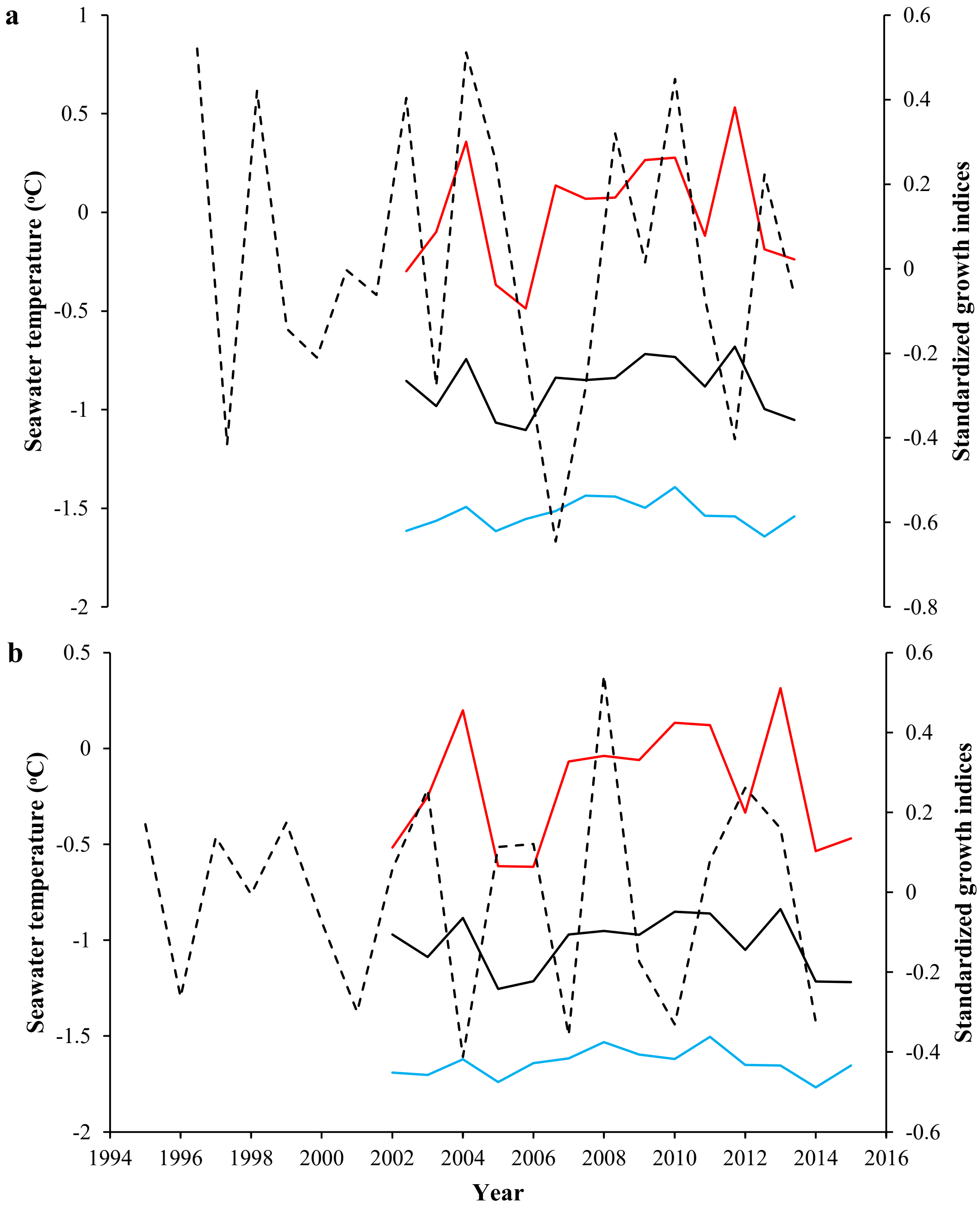

Fig. 6.9 Comparison between the **a)** South Cove NE-chronology (dashed black line) with the mean summer (December-April, red line), mean annual (August-July, black solid line) and mean winter (May-November, blue line) temperature records for the upper 15 m of the water column

from the RaTS program **b)** Hangar Cove NE-chronology (dashed black line) with the mean summer (December-April, red line), mean annual (August-July, black solid line) and mean winter (May-November, blue line) temperature records for the upper 25 m of the water column from the RaTS program.

A comparison between the NE-chronologies and the instrumental temperature records for the upper 15m and upper 25 m of the water column is shown in **Fig. 6.9**. The South Cove chronology shows no correlation (Pearson's product-moment correlation) with any of the temperature records averaged over the upper 15 m of the water column (**Fig. 6.9a**): weighted mean annual (August-July; $r = 0.07$, $p = 0.80$, $n = 15$), summer (December-April; $r = -0.08$, $p = 0.77$, $n = 15$) and winter (May-November; $r = 0.03$, $p = 0.91$, $n = 14$); neither did the Hangar Cove chronology with any of the temperature records averaged over the upper 25 m of the water column (**Fig. 6.9b**): weighted mean annual ($r = -0.07$, $p = 0.74$, $n = 14$), summer ($r = -0.15$, $p = 0.61$, $n = 14$) and winter ($r = 0.17$, $p = 0.59$, $n = 13$). In South Cove, the chronology shows periods of low shell growth during years of increased seawater temperature (e.g. 2007, 2009 and 2012, **Fig. 6.9a**), however during 2004 when increased seawater temperatures were present the chronology shows enhanced shell growth (**Fig. 6.9a**). In Hangar Cove, during the period of reduced seawater temperature between 2004 and 2007 the local *A. eightsii* population showed enhanced shell growth as was also the case during 2012 (**Fig. 6.9b**); whilst during years of increased seawater temperature (e.g. 2004, 2010 and 2013) the *A. eightsii* population showed reduced shell growth (**Fig. 6.9b**). Additional comparisons between the NE-chronologies with the temperature records measured at 15 m and 25 m water depth (for South Cove and Hangar Cove respectively) does not show any significant correlation (**Table 6.2**).

Table 6.2 Pearson's product-moment correlations between the Hangar Cove and South Cove NE-chronologies and the annual (August-July), summer (December-April), winter (May-November) and core winter (July-September) sea-surface temperature (SST) records from the RaTS dataset.

	Annual SST	**Summer SST**	**Winter SST**	**Core Winter SST**
South Cove	r = -0.09, p = 0.74, n = 17	r = -0.13, p = 0.62, n = 18	r = -0.10, p = 0.70, n = 18	r = -0.11, p = 0.67, n = 18
Hangar Cove	r = -0.25, p = 0.36, n = 16	r = -0.15, p = 0.58, n = 17	r < -0.01, p = 1.00, n = 17	r = -0.03, p = 0.92, n = 17

a

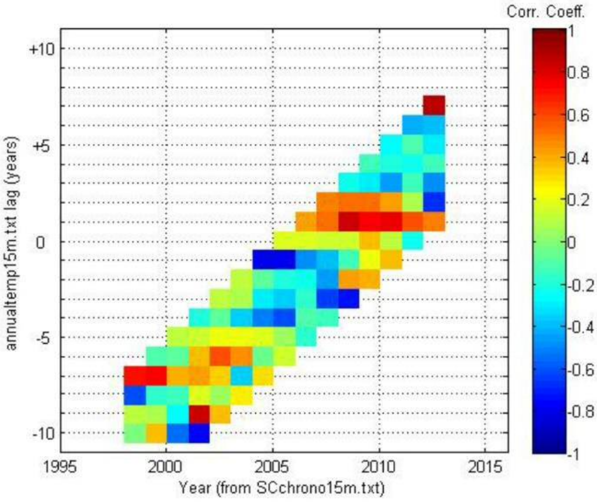
Corr. Coeff.
annualtemp15m.txt lag (years)
+10
+5
0
-5
-10
1995
2000
2005
2010
2015
Year (from SCchrono15m.txt)
1
0.8
0.6
0.4
0.2
0
-0.2
-0.4
-0.6
-0.8
-1

b

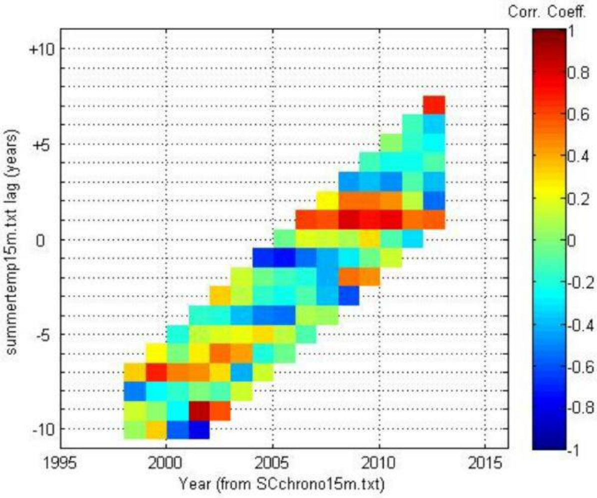
Corr. Coeff.
summertemp15m.txt lag (years)
+10
+5
0
-5
-10
1995
2000
2005
2010
2015
Year (from SCchrono15m.txt)
1
0.8
0.6
0.4
0.2
0
-0.2
-0.4
-0.6
-0.8
-1

c

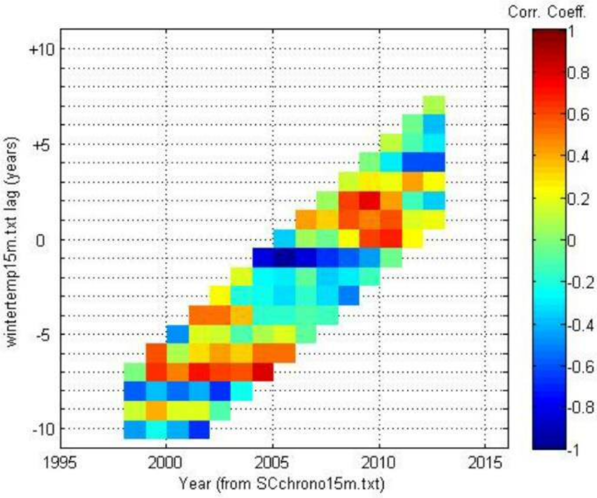
Corr. Coeff.
wintertemp15m.txt lag (years)
+10
+5
0
-5
-10
1995
2000
2005
2010
2015
Year (from SCchrono15m.txt)
1
0.8
0.6
0.4
0.2
0
-0.2
-0.4
-0.6
-0.8
-1

Fig. 6.10 SHELLCORR output showing lagged running correlations between the South Cove NE-chronology and weighted mean **a)** annual (August-July), **b)** summer (December-April) and **c)** winter (May-November) seawater temperature records for the upper 15 m of the water column. The coloured scale indicates the Pearson's product-moment correlation (r) with warm colours indicating positive correlation, cold colours indicating negative correlations and greens for no correlation. Primary Y-axis indicates the lag between the series in years.

a

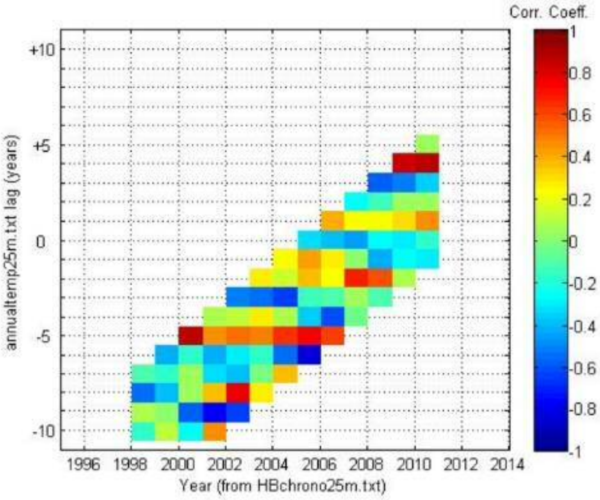
Corr. Coeff.
1
0.8
0.6
0.4
0.2
0
-0.2
-0.4
-0.6
-0.8
-1
+10
+5
0
-5
-10
annualtemp25m.txt lag (years)
1996
1998
2000
2002
2004
2006
2008
2010
2012
2014
Year (from HBchrono25m.txt)

b

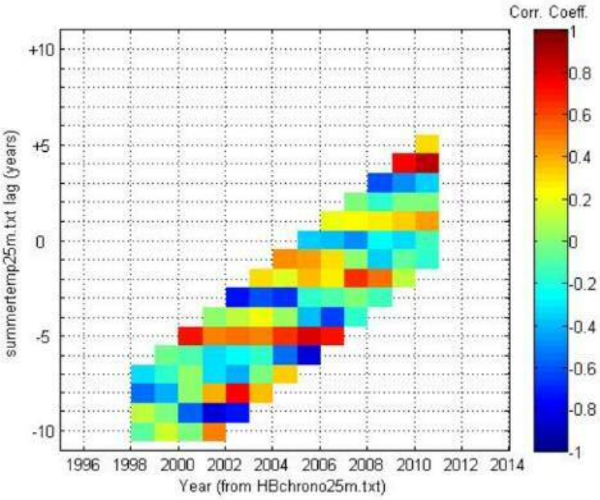
Corr. Coeff.
1
0.8
0.6
0.4
0.2
0
-0.2
-0.4
-0.6
-0.8
-1
+10
+5
0
-5
-10
summertemp25m.txt lag (years)
1996
1998
2000
2002
2004
2006
2008
2010
2012
2014
Year (from HBchrono25m.txt)

c

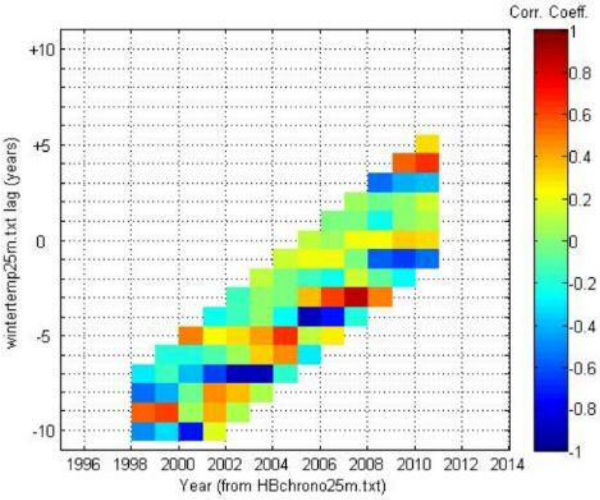
Corr. Coeff.
1
0.8
0.6
0.4
0.2
0
-0.2
-0.4
-0.6
-0.8
-1
+10
+5
0
-5
-10
wintertemp25m.txt lag (years)
1996
1998
2000
2002
2004
2006
2008
2010
2012
2014
Year (from HBchrono25m.txt)

Fig. 6.11 SHELLCORR output showing lagged running correlations between the Hangar Cove NE-chronology and weighted mean **a)** annual (August-July), **b)** summer (December-April) and **c)** winter (May-November) seawater temperature records for the upper 25 m of the water column. The coloured scale indicates the Pearson's product-moment correlation (r) with warm colours indicating positive correlation, cold colours indicating negative correlations and greens for no correlation. Primary Y-axis indicates the lag between the series in years.

Running lagged correlations between the South Cove and the Hangar Cove NE-chronologies weighted mean annual (August-July), summer (December-April) and winter (May-November) seawater temperature are provided in **Fig. 6.10** and **Fig. 6.11** respectively. The South Cove NE-chronology shows a strong positive correlation at plus one-year lag (NE-chronology lagging) with the weighted mean annual (**Fig. 6.10a**) and mean summer (**Fig. 6.10b**) seawater temperature and a strong negative correlation at minus one-year lag with the weighted mean winter temperature (**Fig. 6.10c**). In the Hangar Cove NE-chronology no apparent correlation is present, beside a positive correlation at minus five-year lag, with the weighted mean annual (**Fig. 6.11a**) and summer (**Fig. 6.11b**) seawater temperature records. Running lagged correlations between the Hangar Cove NE-chronology and the weighted mean winter seawater temperature record do not show any significant correlation, either positive or negative, for the plus/minus ten-year lag considered.

A comparison between the South Cove and Hangar Cove NE-chronologies with the respective chlorophyll concentration records (upper 15 m of the water column for South Cove chronology and upper 25 m of the water column for the Hangar Cove chronology) is presented in **Fig. 6.12**. Neither the South Cove chronology exhibit any clear relationship with the chlorophyll concentration record for the top 15 m of the water column ($r = -0.05$, $p = 0.85$, $n = 17$; **Fig. 6.12a**) nor the Hangar Cove chronology with the chlorophyll concentration record for the upper 25 m of the water column at the RaTS site ($r = -0.17$, $p = 0.53$, $n = 16$; **Fig. 6.12b**). In order to check whether there was any offset between the chronologies and their respective chlorophyll record, a SHELLCORR plot showing the lagged running correlations was generated (**Fig. 6.13**). South Cove chronology shows a strong negative correlation with the chlorophyll record at minus one-year lag and a relatively strong positive correlation at plus two year lag (**Fig. 6.13a**). In the Hangar Cove chronology there is no apparent lagged correlation with the chlorophyll record (**Fig. 6.13b**).

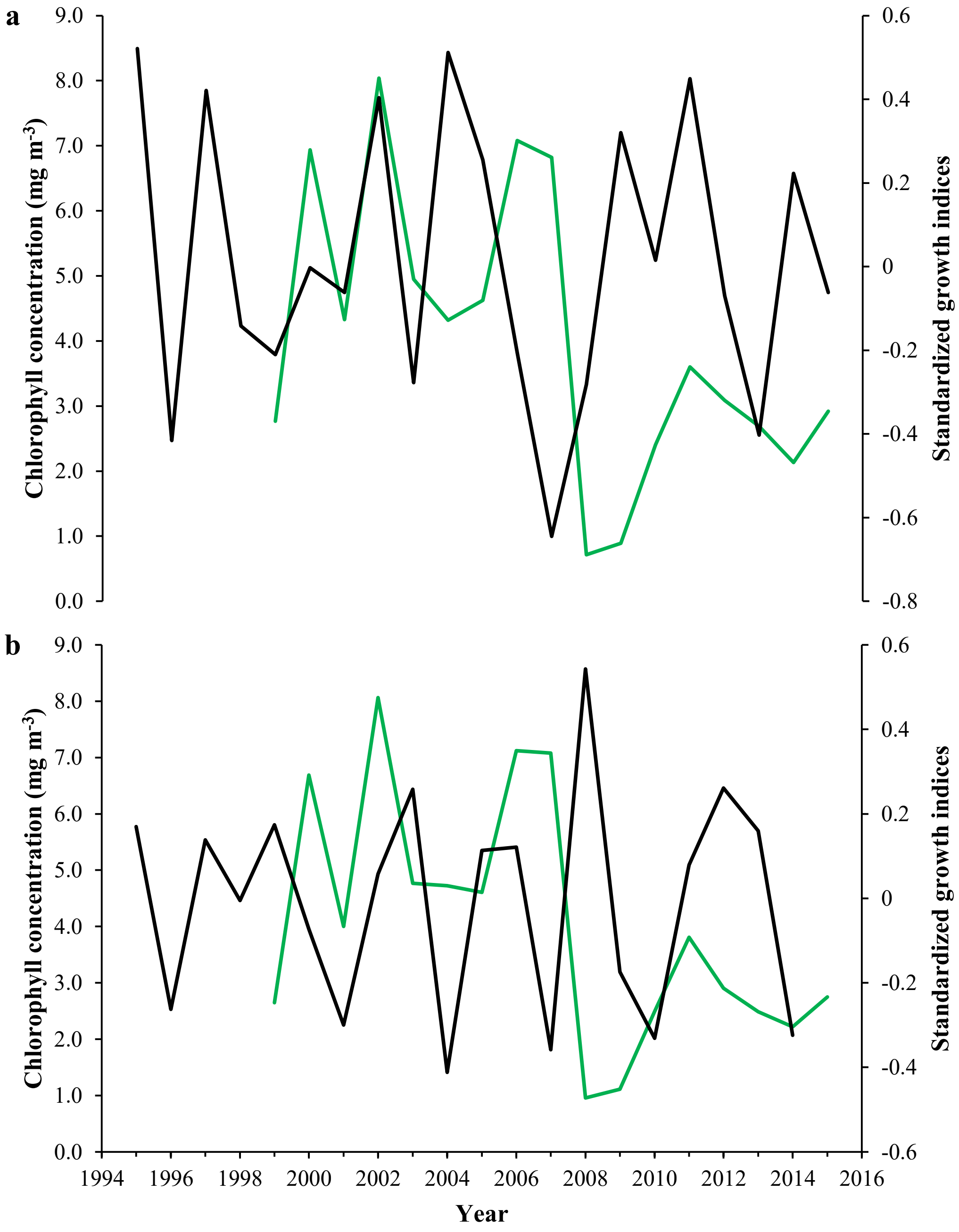

Fig. 6.12 Comparison between the **a)** South Cove NE-chronology (solid black line) and the chlorophyll concentration for the upper 15 m of the water column averaged between November and April (green line) **b)** Hangar Cove NE-chronology (solid black line) and the chlorophyll

concentration for the upper 25 m of the water column (green line) averaged between November and April.

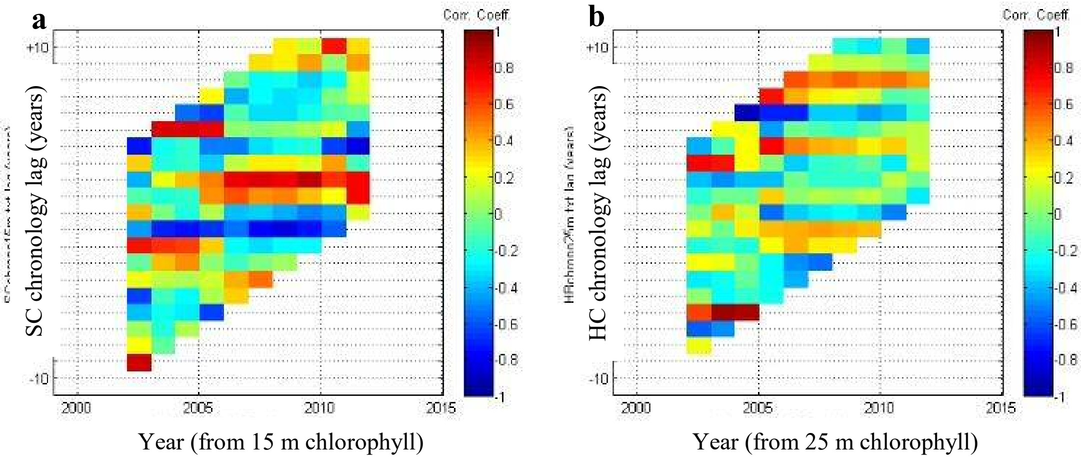

Fig. 6.13 Graphical output from SHELLCORR showing running lagged correlations, based on a seven year window, between the **a)** South Cove NE-chronology and the chlorophyll concentration record for the upper 15 m of the water column and **b)** Hangar Cove NE-chronology and the chlorophyll concentration record for the upper 25 m of the water column. The coloured scale indicates the Pearson's product-moment correlation (r) with warm colours indicating positive correlation, cold colours indicating negative correlations and greens for no correlation. Primary Y-axis indicates the lag between the series in years.

A comparison between the South Cove and Hangar Cove chronologies and fast-ice duration from the RaTS program is provided in **Fig. 6.14**. The South Cove chronology and the fast-ice duration record have a significant positive correlation ($r = 0.47$, $p < 0.05$, $n = 19$; **Fig. 6.14a**), although an offset is evident between the records in 2003/04 and 2004/05 (**Fig. 6.14a**). On the other hand, even though it appears there is a high visual similarity between the Hangar Cove chronology and the fast-ice duration record, the correlation is not significant ($r = 0.28$, $p = 0.26$, $n = 18$).

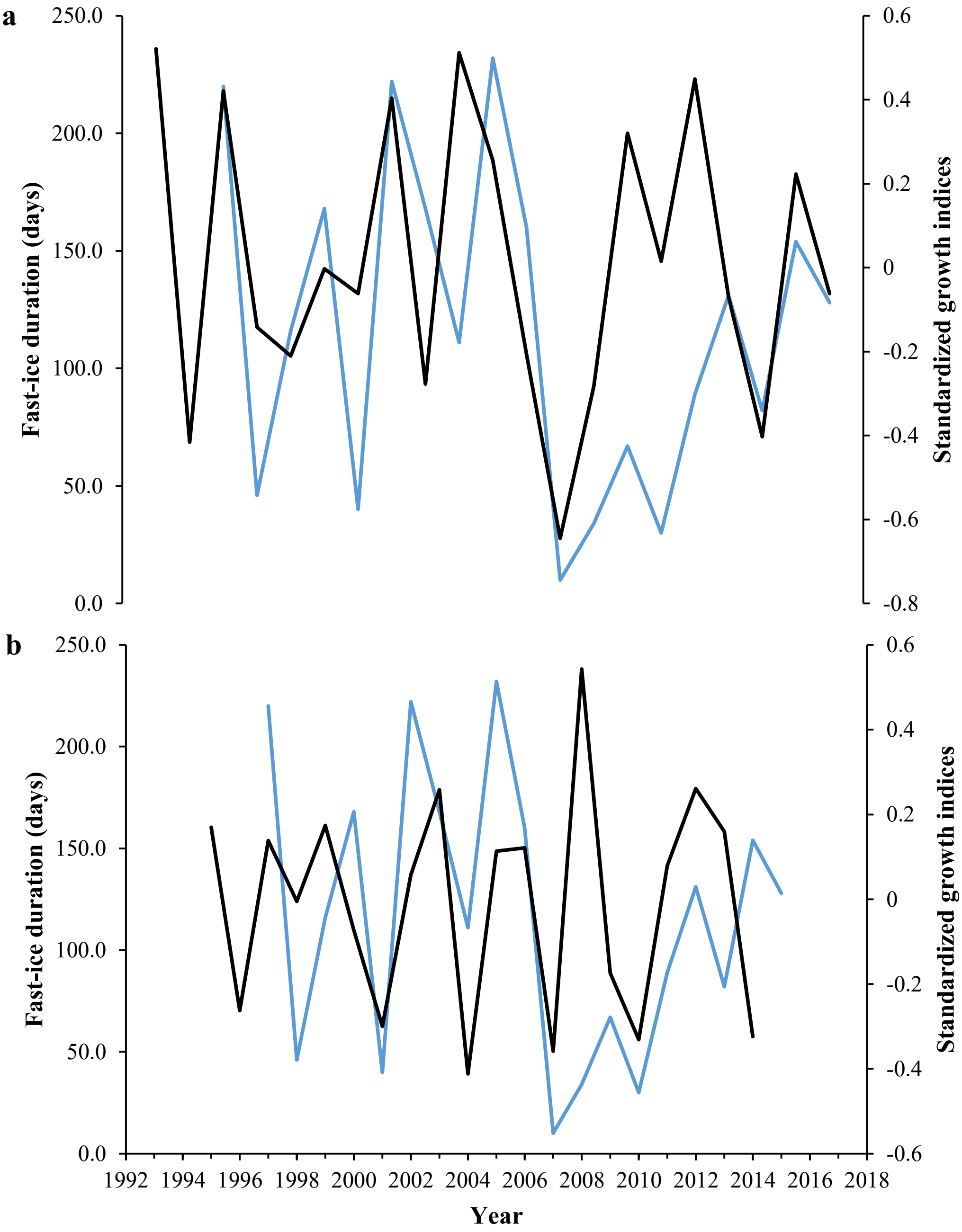

Fig. 6.14 Comparison between the **a)** South Cove NE-chronology (solid black line) and the fast-ice duration record from the RaTS program (blue line) **b)** Hangar Cove NE-chronology (solid black line) and the fast-ice duration record from the RaTS program (blue line).

Running lagged correlations between the South Cove and the Hangar Cove NE-chronologies and the fast-ice duration record are provided in **Fig. 6.15**. The South Cove NE-chronology shows a moderate positive correlation at minus one-year lag centred in 2005/06 (**Fig. 6.15a**); whereas the Hangar Cove NE-chronology shows no correlation between 2005/11 and the fast-ice duration record at zero-year lag (**Fig. 6.1** and **Fig. 6.14b**) although prior to 2(the positive correlation becomes strc r (**Fig. 6.15b** and **Fig. 6.14b**). The Ha r Cove NE-chronology also shows strc ɔositive correlations at plus/minus three ar lag (especially at plus three-year lag, . .g. 6.15b**).

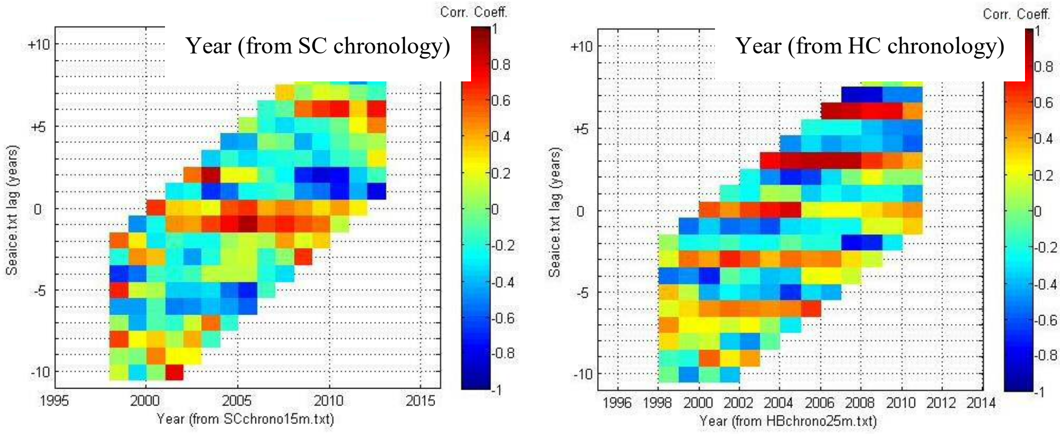

Fig. 6.15 Graphical output from SHELLCORR showing running lagged correlations, based on a seven year window, between the fast-ice duration record and **a)** South Cove (SC) NE-chronology and **b)** Hangar Cove (HC) NE-chronology. The coloured scale indicates the Pearson's product-moment correlation (r) with warm colours indicating positive correlation, cold colours indicating negative correlations and greens for no correlation. Primary Y-axis indicates the lag between the series in years.

A comparison between the Hangar Cove chronology and the South Cove chronology with the geochemical records extracted from specimens collected in each location is provided in **Fig. 6.16** and **Fig. 6.17** respectively. The Hangar Cove NE-chronology shows little agreement between the two available isotope records (**Fig. 6.16**); correlations between shell growth and the averaged $\delta^{18}O_{shell}$ (‰) records from the high-resolution geochemical sampling show negative relationship, however not significant (r = -0.43, p = 0.21, n = 10 for specimen 21403025 and r = -0.26, p = 0.42, n = 12 for specimen 21402010). The shell growth and the $\delta^{13}C_{shell}$ (‰) records showed no apparent correlation (r = -0.05, p = 0.88, n = 10 for specimen 21403025 and r = -0.12, p = 0.72, n = 12 for specimen 21402010). Similarly, the South Cove chronology shows little correlation with the averaged isotope records from specimen 21405031 (r = 0.26, p = 0.44, n = 11 for $\delta^{18}O_{shell}$ and r = 0.18, p = 0.60, n = 11 for $\delta^{13}C_{shell}$; **Fig. 6.17**). Although there is no correlation between the chronologies and the geochemical records, it is notable that during 2007/08, when the phytoplankton bloom in Ryder Bay collapsed (c.f. section 4.1.2 and **Fig. 4.12**) the shell growth indices and the $\delta^{13}C_{shell}$ records show minimum values or negative trends (**Fig. 6.16b** and **Fig. 6.17b**). This is somewhat difficult to confirm in the 21405031 $\delta^{13}C_{shell}$ record since the average value for 2007 contains large variability (**Fig. 6.17b**). In addition, since these geochemical records derive from single specimens, ontogenetic trends may be present in the data series, especially in the case of $\delta^{13}C_{shell}$.

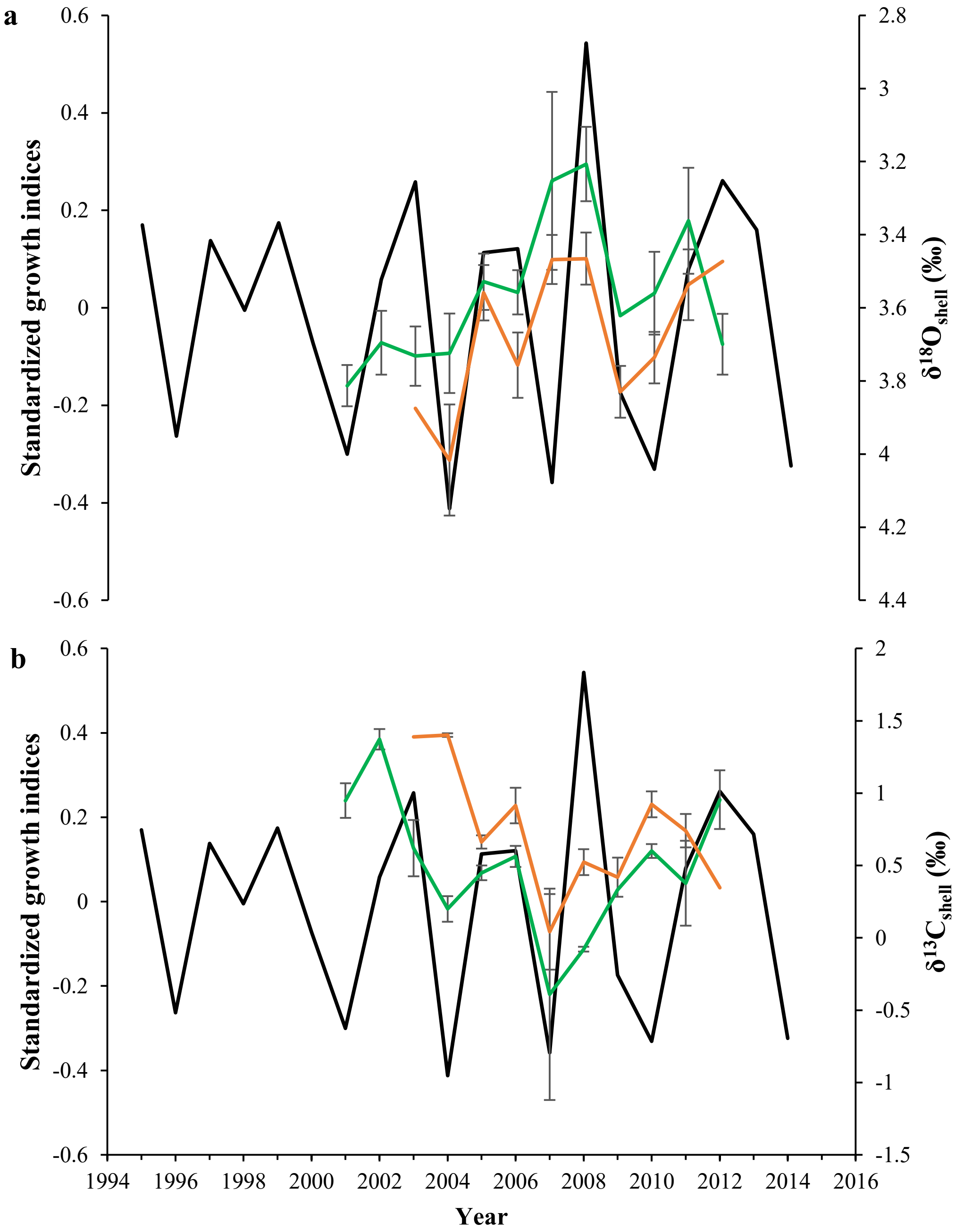

Fig. 6.16 Comparison between the Hangar Cove chronology (black line) and annual average from the high-resolution geochemical sampling for **a)** $\delta^{18}O_{shell}$ (‰, VPDB), note the inverted

secondary Y-axis and **b)** δ^{13}C$_{shell}$ (‰, VPDB) collected from the specimens 21403025 (orange line) and 21402010 (green line). Error bars represent the standard error.

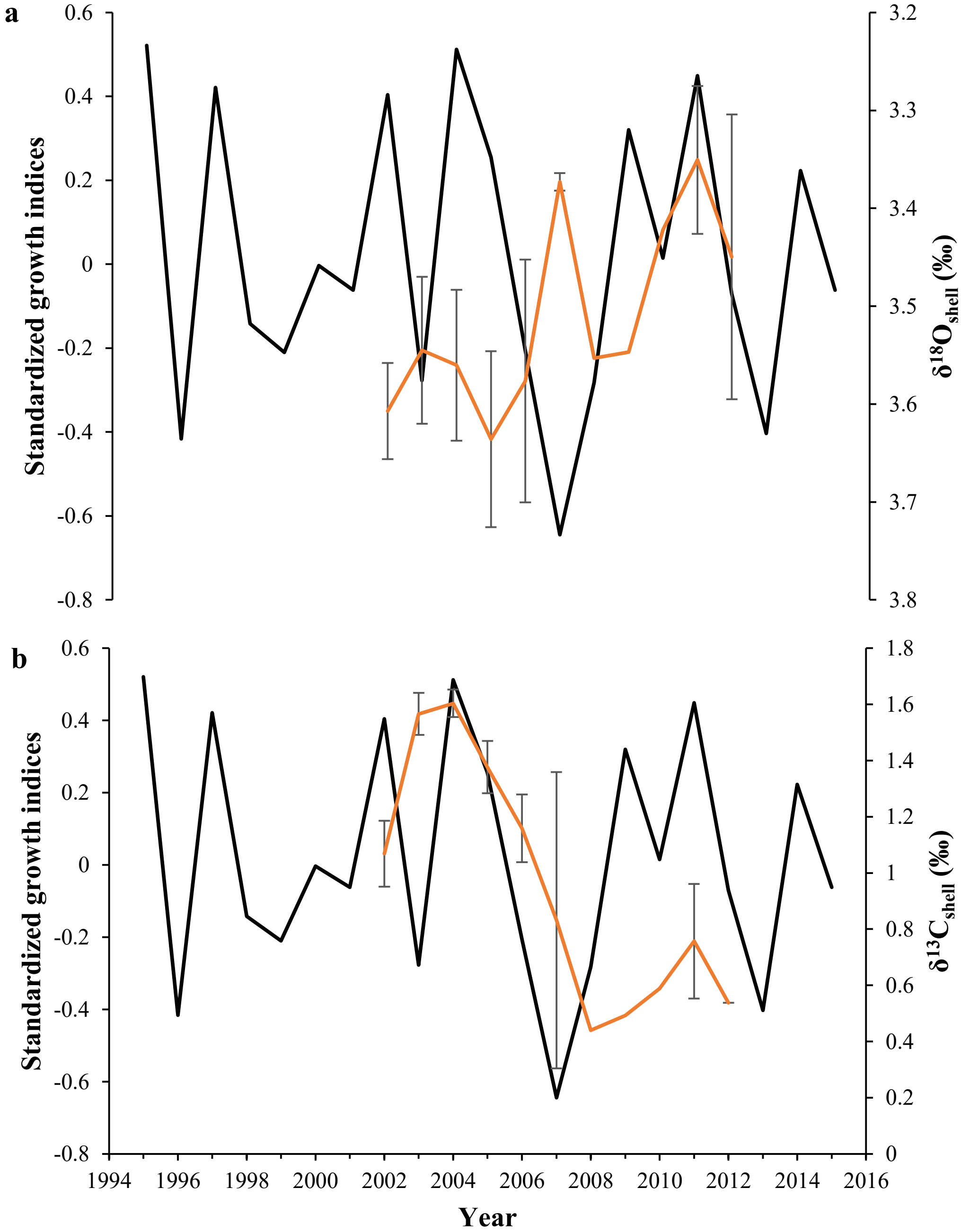

Fig. 6.17 Comparison between the South Cove chronology (black line) and annual average from the high-resolution geochemical sampling for **a)** $\delta^{18}O_{shell}$ (‰, VPDB), note the inverted secondary Y-axis and **b)** $\delta^{13}C_{shell}$ (‰, VPDB) collected from specimen 21405031(orange line). Error bars represent the standard error.

The comparison between the South Cove and Hangar Cove NE-chronologies and the climatic indices showed further differences between the sites. Correlations between the chronologies, the bimonthly Multivariate El Niño Southern Oscillation (ENSO) Index (MEI) values and the monthly Southern Annular Mode (SAM) values are shown in **Table 6.3**. When the entire length of the overlap between the series is considered, the South Cove chronology presents stronger correlations, although not significant, with MEI between May-June and November-December (1995/2015 period), whereas the Hangar Cove chronology appears to show no correlation with MEI (1995/2014 period; **Table 6.3**). When only the robust part of the chronologies are considered, the Hagar Cove chronology shows stronger negative correlations, although not significant, with the MEI values for the period between December-January and April-May; for the South Cove chronology, correlation coefficients become weaker for the period between May-June and November-December (**Table 6.3**). Temporal lags between the MEI and South Cove chronology were studied by averaging MEI values for four, seven months and a year prior to the *A. eightsii* growth season (i.e. November-March) and for the period between May-June and August-September (as this period shows the stronger positive correlation coefficients). As expected based on the monthly correlations coefficients, the Hangar Cove chronology did not show any correlation with the lagged averaged MEI for any of the temporal lags (data not shown). On the other hand, the South Cove chronology showed moderate correlations, although not statistically significant, with the four month lag (JA-SO, $r = 0.41$, $p = 0.07$, $n = 20$), the seven-month lag (AM-SO, $r = 0.43$, $p = 0.06$, $n = 20$) and the strongest with the MJ-AS period ($r = 0.44$, $p = 0.06$, $n = 20$), although the correlation dropped with a one-year lag (ON-SO; **Table 6.4**). In addition, the relationship between the averaged MEI for the MJ-AS period and the

South Cove chronology shows a reduction in correlation based on a five year running window (**Fig. 6.13**).

Table 6.3 Correlations between the Hangar Cove (HC) and South Cove (SC) NE-chronologies, the bimonthly values of the MEI and the monthly values of the SAM. The periods 2003/15 (SC chronology) and 2003/14 (HC chronology) correspond with the periods when the chronologies are robust and the periods 1995/2015 (SC chronology) and 1995/2014 (HC chronology) are the maximum overlap with the climatic records.

MEI	**Period**	**DJ**	**JF**	**FM**	**MA**	**AM**	**MJ**	**JJ**	**JA**	**AS**	**SO**	**ON**	**ND**
HC	1995/2014	-0.18	-0.21	-0.19	-0.18	-0.18	0.14	0.16	0.09	0.17	0.14	0.08	0.04
	2003/2014	-0.41	-0.45	-0.39	-0.43	-0.52	0.03	0.11	0.03	0.15	0.11	0.03	-0.01
SC	1995/2015	-0.11	-0.04	-0.01	0.08	0.28	0.38	0.40	0.37	0.34	0.30	0.31	0.34
	2003/2015	-0.37	-0.17	-0.09	-0.04	0.22	0.24	0.26	0.22	0.18	0.13	0.17	0.19
SAM	**Period**	**Jan**	**Feb**	**Mar**	**Apr**	**May**	**Jun**	**Jul**	**Aug**	**Sep**	**Oct**	**Nov**	**Dec**
HC	1995/2014	0.30	0.32	-0.05	0.03	0.28	0.03	-0.04	0.12	0.15	-0.10	-0.04	-0.06
	2003/2014	0.29	0.21	0.13	0.10	0.26	0.03	0.02	-0.02	0.03	0.07	-0.05	-0.20
SC	1995/2015	0.34	-0.07	-0.27	0.19	-0.06	0.11	-0.13	0.11	0.36	-0.34	-0.28	-0.13
	2003/2015	0.26	-0.31	-0.13	0.39	-0.05	0.13	0.13	0.06	0.33	0.16	-0.34	-0.16

The monthly comparison between the chronologies and the SAM provided a less clear pattern of correlation for either the entire length of the overlap between the series or the period when the chronologies are robust (**Table 6.3**). In addition, the lagged correlations (three, six and twelve months and the June-September period) did not show any apparent correlation with chronologies (data not shown).

Table 6.4 Correlations between the Hangar Cove (period considered 1995/2014) and South Cove (period considered 1995/2015) NE-chronologies and lagged averages of the MEI.

Lag	Averaged period	South Cove	Hangar Cove
4 months	Aug-Oct	0.41	0.15
7 months	May-Oct	0.43	0.12
12 months	Nov-Oct	0.22	-0.02
-	May-Sep	0.44	0.16

6.2 South Orkney Islands

6.2.1 1915 A. Bennett collection

Master chronologies (NE and RCS) were successfully constructed using 15 specimens from the 1915 A. Bennett collection (**Fig. 6.18a**). The average lifespan of the specimens incorporated into the chronology was 13 years and the longest-lived specimen was 22 years. The NE-chronology is robust (EPS > 0.85) for a period of ten years (1906/15, **Fig. 6.18b**); the RSC-chronology is also robust for ten years although over a slightly different period (1905/14, **Fig. 6.18b**), with the EPS falling significantly prior to 1904 due to the lack of long-lived specimens. The chronologies show alternating period of rapid growth (e.g. 1905, 1907, 1909 and 1912; **Fig. 6.18a**) and reduced growth (e.g. 1906, 1908, 1910/11 and 1913; **Fig. 6.18a**). The chronologies showed a high degree of similarity (r = 0.90, p < 0.01, n = 22), although some differences can be appreciated in the most recent part of the chronology (1915/14, **Fig. 6.18a**). Autocorrelation indices for the AB1915 chronology are provided in **Fig. A6.1d;** the chronology shows autocorrelation at one-year lag and also significant partial autocorrelations at one and at four-year lags.

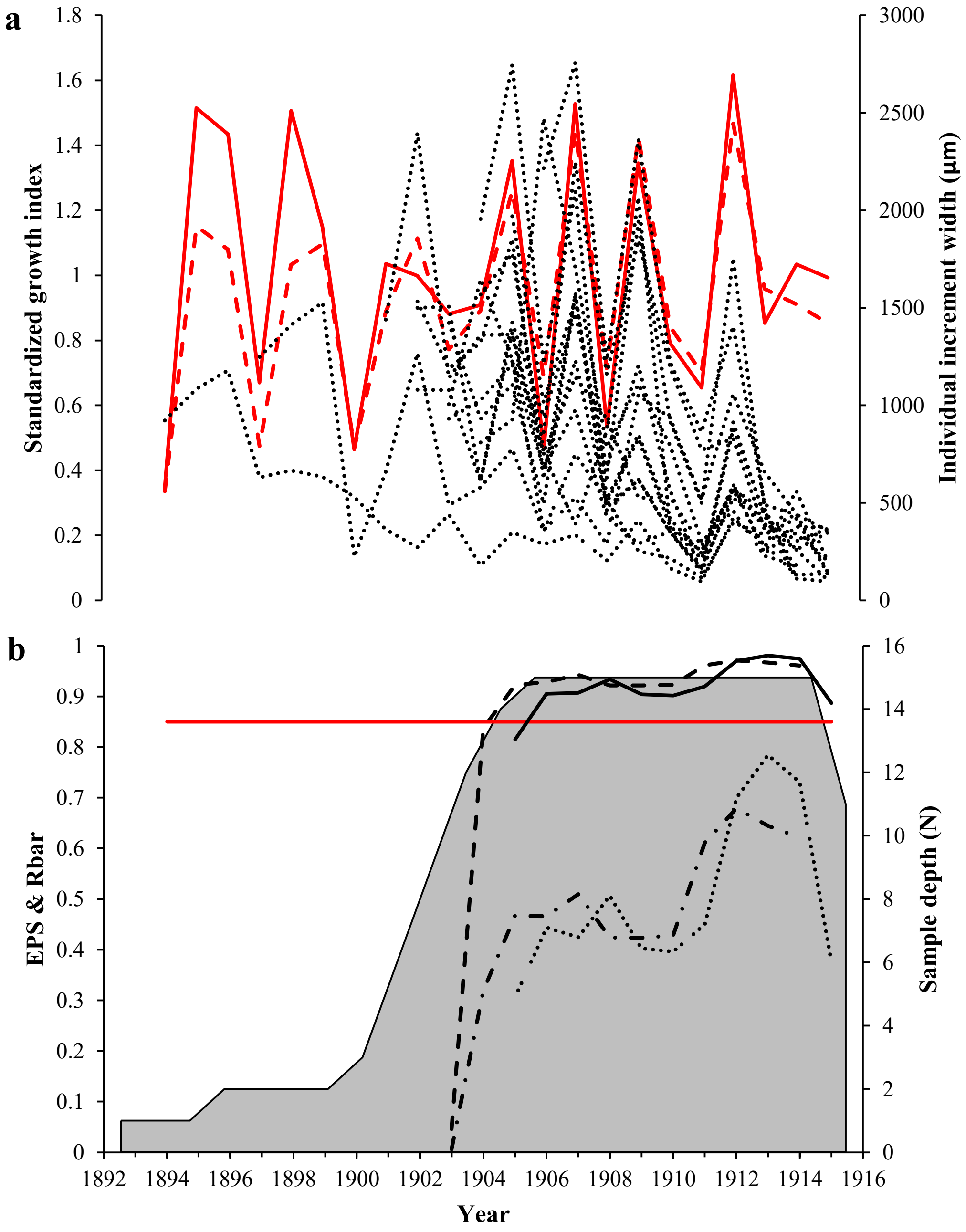

Fig. 6.18 a) AB1915 NE-chronology (solid red line, primary Y-axis) and RCS-chronology (dashed red line, primary Y-axis) and individual undetrended growth histories are also shown (black dotted lines, secondary Y-axis) **b)** EPS from the NE-chronology (solid black line), EPS

from the RCS-chronology (dashed black line), Rbar of the NE chronology (dotted black line) and of the RCS-chronology (dashed-dotted black line) and sample depth (N) as a grey shaded area, the EPS = 0.85 threshold suggested by (Wigley et al., 1984) is represented with a solid red line.

6.2.2 1927 Discovery investigations

The small quantity of specimens available from the 1927 *Discovery* investigations, prevented the construction of a chronology. The lifespan of specimen 192702001 was between 14 and 19 years (**Fig 6.19**). Since the work on 1927 *Discovery* samples is preliminary it was not possible to develop any chronology; the deep-collected dry-preserved specimen (192702003) was not processed and was left for future research. As this shell presented little erosion at the umbo it was possible to measure almost the entire length along its maximum growth axis; however, no ontogenetic trend can be observed in the growth increment width series suggesting either that some disturbance marks have been measured as annually formed increments or that there is a significant part of the early growth that was not measured (**Fig. 6.19**). It is, however, not possible to identify the position of any missing increments due to lack of additional specimens to carry out crossdating and due to the fact that this specimen presented a faint pattern at the hinge plate (in order to carry out a margin *vs.* hinge plate calibration). The growth history of specimen 192702001 showed little variation apart from an alternating period of reduced/rapid/reduced growth between 1925 and 1927 (**Fig. 6.19**).

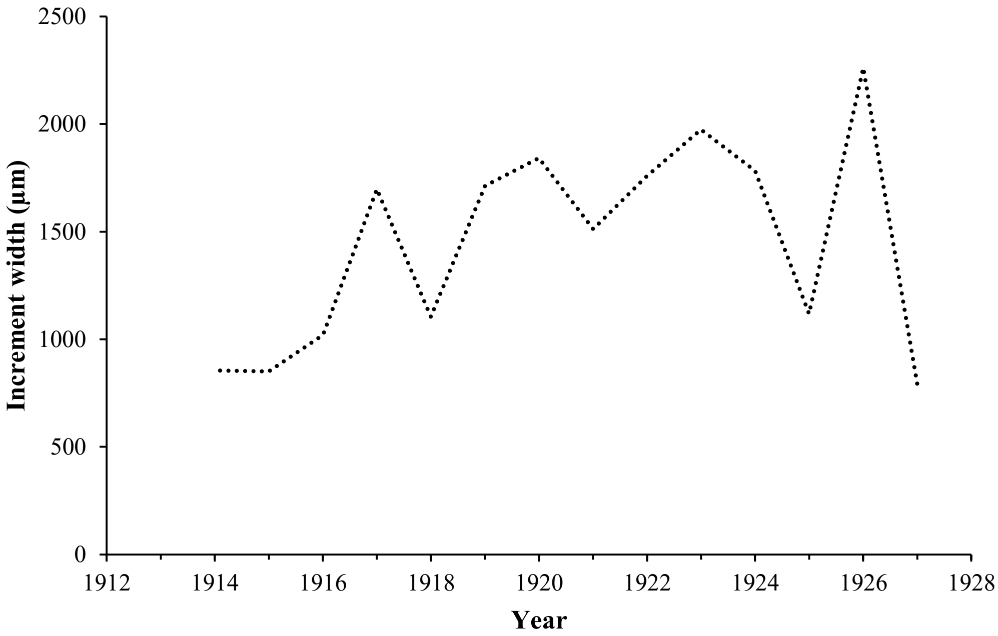

Fig. 6.19 Undetrended growth history from specimen 192702001 from the 1927 *Discovery* investigations collection measured on the margin.

6.2.3 1988 British Antarctic Survey collection

The chronologies (NE, and RCS) presented here constitute a development of the previously published NE-chronology by Roman-Gonzalez (2011), which was developed from 12 *A. eightsii* specimens. These data and the comparison with the environmental data available have been published by Roman-Gonzalez et al. (2016). The chronologies presented here were constructed by successfully crossdating eight additional specimens into the earlier chronology ($n = 20$; **Fig. 6.20**). The average lifespan of all the specimens incorporated into the chronologies was 30 years and the longest-lived specimen was 41 years. The comparison between both chronologies demonstrates, that they are very similar ($r = 0.92$, $R^2 = 0.85$, $n = 40$, $p \leq 0.01$; **Fig. 6.20**).

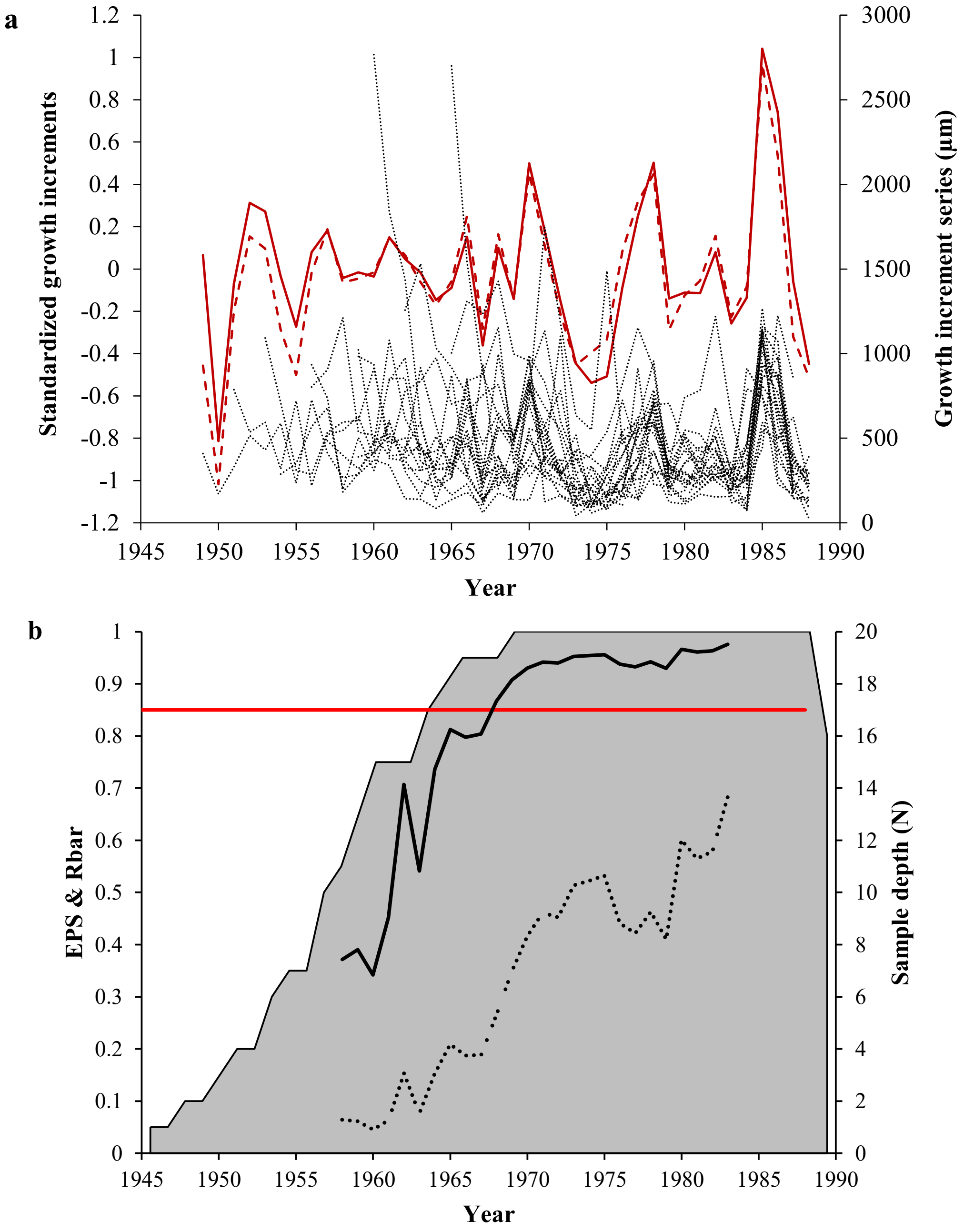

Fig. 6.20 a) Factory Cove NE-chronology (solid red line, primary Y-axis) and RCS-chronology (dashed red line, primary Y-axis) with individual undetrended growth histories (black dotted lines, secondary Y-axis) **b)** EPS (solid black line) and Rbar of the NE-chronology (black dotted line)

from the Factory Cove master chronology. The EPS = 0.85 threshold suggested by (Wigley et al., 1984) is also shown (solid red line) and sample depth (N) is shown as a grey shaded area.

6.2.4 Comparison with instrumental records

Correlation coefficients between the RCS-chronology and the monthly HadISST1 dataset showed stronger positive correlations with the months April-November (with the exception of September; significant for June, July, October and November) and weaker correlations for the December-March, even negative in the case of December (**Table 6.5**).

Table 6.5 Pearson's product-moment correlation (r) of the RCS-chronology from Factory Cove, Signy Island, and the monthly averaged seawater temperature record from the from the HadISST1 dataset. * significant correlations $p < 0.05$ and ** significant correlations $p < 0.01$.

Location / Month	**Jan**	**Feb**	**Mar**	**Apr**	**May**	**Jun**	**Jul**	**Aug**	**Sep**	**Oct**	**Nov**	**Dec**
Factory Cove	0.15	0.19	0.10	0.30	0.39	0.50*	0.53**	0.34	0.22	0.54**	0.44*	-0.04

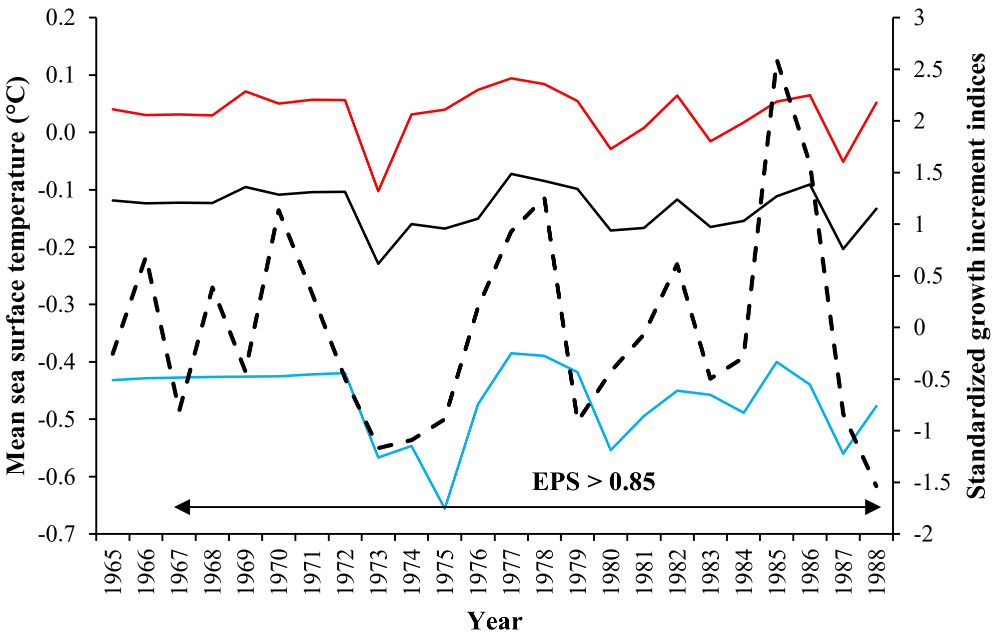

Fig. 6.21 RCS-chronology (dashed black line) mean annual (August-July, solid black line) SST record, summer (November-March) record (red line) and mean winter (April-October, blue line) record from the HadISST1 record. The robust part of the chronology (EPS > 0.85) is also indicated with a double arrow.

A significant positive correlation between the Factory Cove RCS-chronology and the mean winter (July-October) sea surface temperature (SST) record was found ($r = 0.57$, $n = 24$, $p \leq 0.01$) for the period (1965/88 when the EPS > 0.85, **Fig. 6.21**); a weaker positive correlation, although still significant, with the mean summer (November-June) SST record ($r = 0.46$, $n = 24$, $p \leq 0.05$, **Fig. 6.21**) for the same period was also present and with the mean annual (August-July) SST record ($r = 0.48$, $n = 24$, $p \leq 0.05$; **Fig. 6.21**). Additionally a significant negative correlation was found between the Factory Cove RCS-chronology and the fast-ice duration record ($r = -0.41$, $n = 24$, $p \leq 0.05$; **Fig. 6.22**). The combination of both mean winter SST and fast-ice duration into a multiple regression significantly predicted the Factory Cove RCS-chronology $F_{2,23} = 6.361$, $p \leq 0.01$, $R^2 = 0.38$.

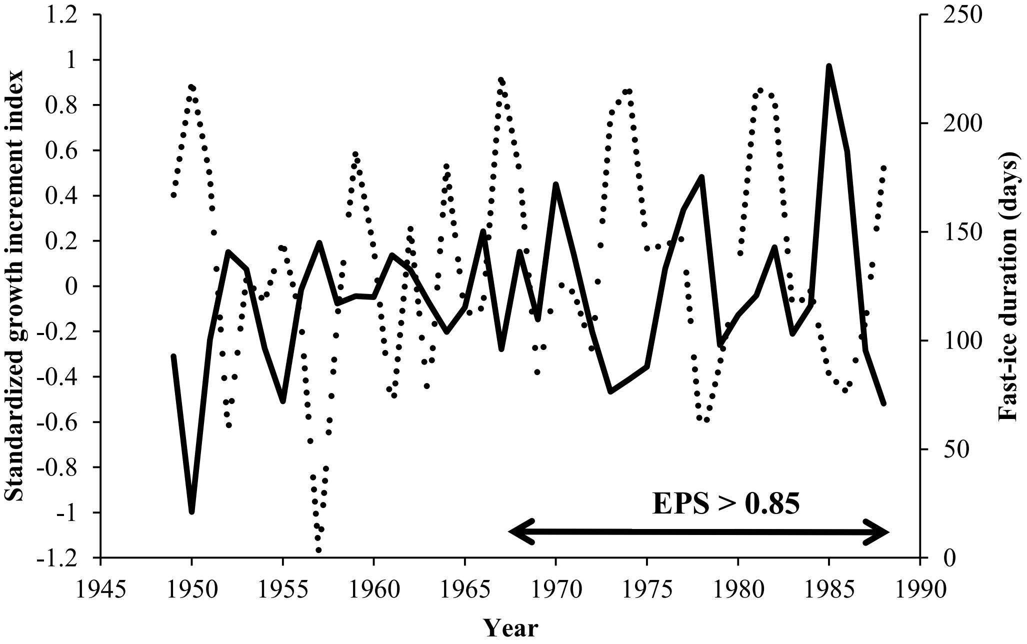

Fig. 6.22 RCS-chronology (solid line) and the fast-ice duration record from Signy Station (dotted line) between 1949 and 1988. The robust part of the chronology (EPS > 0.85) is also indicated with a double arrow (Roman-Gonzalez et al., 2016).

Running correlations based on a 15-year window between the Factory Cove RCS-chronology and environmental parameters are presented in **Fig. 6.23**. Correlations between the RCS-chronology and the fast-ice duration record for the South Orkney Islands shows a negative correlations for the period 1963/88 (**Fig. 6.23**); on the contrary, a clear shift in the running correlations between the RCS-chronology and SST records (mean annual, summer and winter) can be observed in 1972 (**Fig. 6.23**), from no correlation to positive correlations (on average $r = 0.04 \pm 0.08$ SD for the period 1963/72 and $r = 0.58 \pm 0.07$ SD for the period 1973/88).

A comparison between the Factory Cove RCS-chronology and the bimonthly MEI and monthly SAM values shows no significant correlation for either the full length of the overlap between the chronology and the climatic indices (1950/88 for MEI and 1957/88 for SAM) or for the period when the chronology is robust (1965/88; **Table 6.6**).

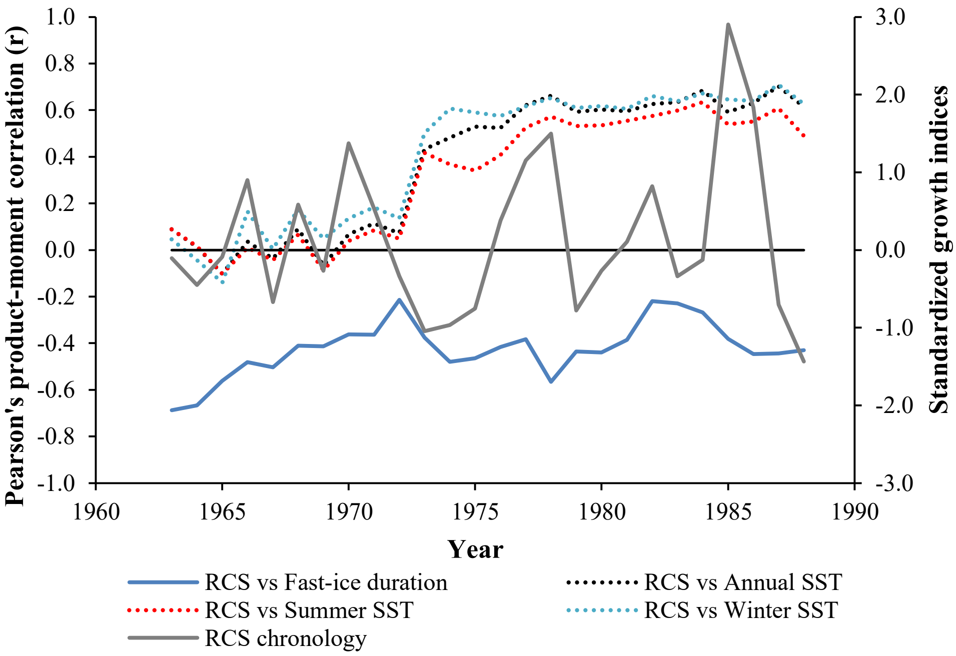

Fig. 6.23 Running correlations in a 15 year window between the RCS-chronology (solid grey line) from Factory Cove, South Orkney Islands and different environmental parameters: fast-ice duration (solid blue), summer (November-June) sea surface temperatures (SST, dotted red line), annual (August-July) SST (dotted black line) and winter (July-October) SST (dotted light blue line, (Roman-Gonzalez et al., 2016). SST data were extracted from the HadISST1 dataset (Rayner et al., 2003).

Table 6.6 Pearson's product-moment correlation (r) between the Factory Cove RCS-chronology and the bimonthly MEI values and the monthly SAM values. The period 1965/88 corresponds with the overlapping period between the series where the RCS-chronology is robust whereas the 1950/88 period in the MEI comparison and the 1957/88 period in the SAM comparison correspond with the maximum overlapping periods of the datasets with the RCS-chronology.

MEI	**DJ**	**JF**	**FM**	**MA**	**AM**	**MJ**	**JJ**	**JA**	**AS**	**SO**	**ON**	**ND**
1950/88	-0.19	-0.14	-0.18	-0.14	-0.14	-0.12	-0.06	-0.02	0.07	0.05	0.03	0.03
1965/88	-0.07	0.00	-0.05	-0.07	0.03	0.12	0.11	0.16	0.20	0.20	0.24	0.24
SAM	**Jan**	**Feb**	**Mar**	**Apr**	**May**	**Jun**	**Jul**	**Aug**	**Sep**	**Oct**	**Nov**	**Dec**
1957/88	-0.08	0.23	-0.06	0.18	0.10	0.09	-0.16	-0.24	-0.30	0.09	0.02	-0.28

1965/88	0.06	-0.25	0.04	-0.16	-0.04	-0.13	0.20	0.31	0.29	-0.07	-0.04	0.31

6.3 Discussion

6.3.1 West Antarctic Peninsula

The mixed results regarding the construction of the chronologies at Rothera demonstrate challenges associated with chronology development and the environmental interpretations. Whereas specimens collected at Hangar Cove show a consistent population growth pattern over a period of ten years (**Fig. 6.2b**), the South Cove chronology shows a drop in the EPS centred around 2001 (**Fig. 6.1b**), the Back Bay chronology shows a lack of correlation between the specimens in the most modern period of the chronology (from 2009 to 2014; **Fig. 6.3b**) and no chronology could be developed from Trolval (**Fig. 6.6**). The drop in correlation of the South Cove chronology is probably due to the reduced sample depth (i.e. number of contemporary specimens at any time in the chronology; 11 specimens compared to the 16 specimens from the Hangar Cove chronology). However, the lack of agreement in the shell growth records of specimens from Back Bay (partially) and from Trolval appears to be more significant than with the specimens from South Cove. Nonetheless the lack of agreement between the shell growth records from both locations could be an indication of the local environmental conditions that prevent the expression of a common population shell growth pattern. Ice-scour has significantly increased in Lagoon Island (the main island where Back Bay is located) since 2006 which has resulted in assemblage level changes in local benthic ecosystem (Barnes et al., 2014). This period overlaps with the Back Bay chronology (**Fig. 6.3**), which presents a lack in common growth pattern since 2009. Ice-scour peaked at Lagoon Island in 2008 (Barnes et al., 2014), intense physical disturbance caused by ice-scour, which has a stochastic nature, and assemblage level changes could be possible reasons for the lack of a common growth pattern in *A. eightsii* at Back Bay. On the other hand, a comparison study indicates that benthos mortality, reduced biodiversity and reduced average lifespan of long-lived benthic species are some of the predicted outcomes linked to current trends of increasing iceberg scouring caused by rising global temperatures (Smale et al., 2008; Smale and Barnes, 2008; Barnes and Souster, 2011).

The comparison between the chronologies (i.e. South Cove, Back Bay and Hangar Cove) and the environmental records collected at the RaTS site allow a spatial interpretation of the results presented here. Chronologies developed from nearby locations can show different growth patterns depending the environmental drivers acting upon shell growth (Reynolds et al., 2017). Inner Ryder Bay locations (i.e. South Cove and Back Bay) show a higher agreement between them than any of the chronologies with the Hangar Cove chronology (**Fig. 6.7**); this indicates that the conditions driving shell growth in shallow coastal waters may be substantially different between inner Ryder Bay and at Hangar Cove. The only period where all studied locations showed a common growth pattern is between 2006 and 2008, when the chronologies indicate a shift from rapid to low to rapid shell growth conditions; this may indicate the presence of a wider strong environmental forcing which was able to overprint the effect of local environmental drivers of shell growth. Ryder Bay experienced a change of state in its oceanography conditions in 2007/08 from shallow mixing, high chlorophyll concentration, long fast-ice duration to deep mixing, low chlorophyll concentration, short fast-ice duration (see Chapter IV section 4.4). The low shell growth in all studied locations during 2007 suggest that the environmental conditions that caused the change in Ryder Bay oceanographic state, and ultimately the climatic driver controlling this change (c.f. section 4.4), had a detrimental impact on *A. eightsii* growth. The chronologies presented in this study add to other Antarctic chronologies based on marine mollusc bivalves (Brey et al., 2011; Ivany et al., 2011); once new chronologies are developed and replication over time becomes increasingly available it will be possible to carry out more complex regional climate reconstructions (Briffa, 1999), such as the *A. islandica* chronology network developed from coastal waters around the British Isles (c.f. Reynolds et al., 2017).

One unexpected outcome of the Ryder Bay specimens is the lack of success in developing a chronology from Trolval Island (**Fig. 6.6**). The shallow coastal areas surrounding Troval Island were considered ideal for developing sclerochronological records since they present low disturbance levels caused by iceberg scouring (Dunlop et al., 2014); therefore, other factor may be contributing to the lack of a population common growth pattern or the inability to distinguish one from the specimens collected. Based on the current information from the shell growth record and the limited environmental data available from Trolval Island, it is not possible to determine the cause of the lack of a common growth pattern in the local *A. eightsii* population. The disturbance lines present in the shell growth record from the Trolval Island *A. eightsii* specimens may not be related to iceberg scouring and may be caused by other biological or physical process such as predatory attacks or extreme local events affecting seawater salinity or temperature (Richardson, 2001). Harper et al. (2012) analysed the effects of iceberg scouring in the *Laternula elliptica* population at Ryder Bay and found that specimens from Hangar Cove presented a high frequency of shell repair followed by South Cove and Back Bay (**Fig. 2.1b**). This is confirmed by the study of underwater concrete markers, which highlights the difference between either sides of Rothera Point, with higher iceberg disturbance in the outer Ryder Bay side (Brown et al., 2004). Hangar Cove specimens showed the most consistent population common growth pattern compared to South Cove or Back Bay, which shows that current frequencies of iceberg scouring have little or no effect in the development of a population common growth pattern in Hangar Cove and another driver of shell must the origin of the lack of correlation between specimens from South Cove and Back Bay.

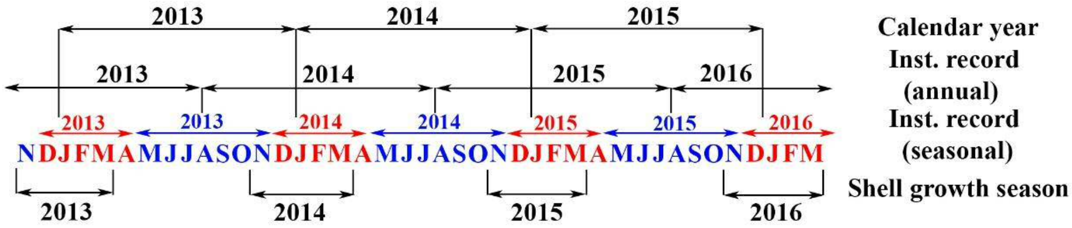

Fig. 6.24 Diagram showing an example of the differences between the calendar year, the calendar used to calculated annual averages in the instrumental record (inst. record annual) and the seasonal instrumental records (winter in blue and summer in red) and the shell growth season (chronologies). Capital letters represent calendar months by their initial letter.

Shell growth can be controlled by a combination of several complex and sometimes interrelated environmental and biological parameters such as temperature, availability of food sources and disturbance levels (e.g. Pannella and MacClintock, 1968; Wilbur, 1972; Clark, 1974; Rhoads and Lutz, 1980; Bayne and Newell, 1983; Witbaard, 1996; Ramsay et al., 2000; Richardson, 2001). The comparison between the South Cove NE-chronology and the upper 15 m temperature records from RaTS indicates positive correlations between shell growth and mean annual (August-July; $r = 0.48$, $p = 0.09$, $n = 13$) and mean summer (December-April; $r = 0.61$, $p = 0.03$, $n = 13$) seawater temperatures at plus one-year lag (**Fig. 6.10a** and **Fig. 6.10b**); in addition, lagged correlations show a negative correlation with the winter (May-November; $r = -0.32$, $p = 0.26$, $n = 14$) seawater temperature records at minus one-year lag (**Fig. 6.10c**). **Fig. 6.24** helps to illustrate the differences between calendar years, the instrumental records calendar and the shell growth calendar. The positive correlations with the mean annual and mean summer temperature records at plus one-year lag has *a priori* no meaning since it would imply that shell growth in the South Cove *A. eightsii* population is significantly affected by seawater temperatures occurring during the previous austral summer. Alternatively, the South Cove chronology might present the plus one year offset if the first increment of the time series has been misidentified, which then would result in the temporal alignment between the seawater temperature record and the increment width record. A misidentification of the first increment can happen if this is particularly small and/or a high number of disturbance increments are present. The specimens used to construct the South Cove chronology were collected at the beginning of February 2015 and in theory these specimens could have had two extra months of growth. If shell growth conditions were not optimum during the 2015 growing season, this could have resulted in a very small increment at the tip of the margin. The minus one-year lag in the correlation between the South Cove chronology and the winter seawater temperature record is most likely an statistical artefact since it would imply that shell growth is negatively affected by the winter temperatures of three winter seasons in advance. Consequently, the seasonal analysis indicates positive correlations with summer seawater temperatures if a one year lag is introduced in the South Cove chronology. It has been suggested that growth in *A. eightsii* does not stop during winter, although the majority of the growth occurs within the summer season (Nolan and Clarke, 1993; Peck et al., 2000); therefore is expected that if seawater temperature has an effect on shell growth, this would be primarily during the austral summer, when food supplies are available and higher temperatures promote high metabolic rates which translate into fast growth and the accumulation of energetic reserves (Peck et al., 2000, 2006).

Conversely to the South Cove chronology, the Hangar Cove NE-chronology does not show any significant correlation with the upper 25 m seawater temperature records (**Fig. 6.9b**) and does not present any significant lagged correlation (**Fig. 6.11**). This suggests that the local conditions affecting shell growth in *A. eightsii* population at Hangar Cove are different from those from the inner Ryder Bay.

No clear relationship was apparent between the chronologies and the chlorophyll concentration records measured at the RaTS sampling site (upper 15 m and upper 25 m of the water column; **Fig. 6.12**). This suggests that neither of the *A. eightsii* populations are food limited even during years of low chlorophyll concentration such as 2008/09 (**Fig. 6.12**). The relationship between growth in Antarctic marine ectotherms, including *A. eightsii*, and primary production has already been discussed (e.g. Brey and Clarke, 1993; Nolan and Clarke, 1993; Peck et al., 2000), suggesting that growth at low temperatures is controlled both thermodynamically and by the food supply. The lagged correlations between the chronologies and the chlorophyll concentration records (**Fig. 6.13**) showed a negative relationship at minus one-year lag, in the case of South Cove (r = -0.46, p = 0.07, n = 16 for the period 1999/2014) and no apparent lagged correlations in the case of the Hangar Cove. This correlation may be spurious since it would imply that shell growth is negatively affected by high chlorophyll concentrations whereas low chlorophyll concentrations are beneficial. This relationship will be especially considered if a one-year offset is introduced in the South Cove chronology, as mentioned above when discussing the relationship between the chronology and the temperature records. High concentrations of suspended matter can have detrimental effects in the growth of bivalve molluscs since it can collapse the gills and the animal is forced to produce pseudofaeces in order to avoid gill damage. However, it was not expected to find a negative relationship between shell growth and chlorophyll concentrations (if the one year offset is introduced in the South Cove chronology).

Sea ice is a critical component of the Southern Ocean ecosystems (Massom and Stammerjohn, 2010b). The comparison of the chronologies with the fast-ice duration record showed positive correlations, only significant in the case of South Cove (**Fig. 6.14**). The reason why the Hangar Cove NE-chronology presented no significant correlation with the fast-ice duration record is apparent when the running correlations between the records are analysed (**Fig. 6.13b**); at zero-year lag, correlation coefficients show weaker correlation after 2005. In addition, strong autocorrelation with a period of three years can be observed between the records (**Fig. 6.13b**); this can be seen in the SHELLCORR plot as an alternation between positive (red colour) and negative (blue colour) lagged correlations with a defined period. Lagged correlations between the South Cove NE-chronology and the fast-ice duration record also showed positive correlations at minus one-year lag centred around 2005/06 (**Fig. 6.13a**); however, this correlation is spurious since it would imply that shell growth is affected negatively by the sea-ice duration during the next austral winter season. If the one-year offset is introduced in the South Cove chronology as previously discussed, then the relationship between shell growth and fast-ice duration becomes negative although not significant ($r = -0.37$, $p = 0.13$, $n = 18$ for the period 1997-2014; lag plus one year in **Fig. 6.13**). Peck and Bullough (1993) have already highlighted the close relationship between sea ice and *A. eightsii* population structure at Factory Cove. The authors suggested that iceberg scour poses a limiting factor in the longevity of *A. eightsii* population at this site; calculating that all areas within Factory Cove would experience iceberg scour every 50 to 75 years. The positive correlation between fast-ice duration and shell growth in the present study seems at first sight contradictory, since longer fast-ice duration would imply shorter duration for the phytoplankton bloom via reduced irradiance. However, it has been pointed out the importance of sea ice in the stability of the water column and how a reduced water column stability leads to reduced phytoplankton bloom due to dispersion of the phytoplankton out of their optimal depth (Mitchell and Holm-Hansen, 1991; Dierssen et al., 2002; Meredith et al., 2010). In addition, longer fast-ice duration can exert a buttressing effect against iceberg scouring, protecting the soft bottom benthic environments (Gutt and Starmans, 2002; Massom and Stammerjohn, 2010b; Barnes and Souster, 2011; Barnes et al., 2014). However, there are contradictory relationships with fast-ice duration at Factory Cove (South Orkney Islands), which present a negative relationship, and at the Western Antarctic Peninsula (WAP) sites (**Fig. 6.22**), which present a positive relationship (**Fig. 6.14**) with shell growth. This contradiction may be caused by the particular effects of reduced/increased fast-ice duration upon the environment at Factory Cove and at the WAP sites. Negative relationships between sea-ice duration and formation of carbonate structures by marine organisms have also been reported for Antarctic bryozoans (Barnes, 2015), which is important in terms of carbon fixation at high latitudinal seas. Sea-ice duration and extent is being currently affected by rising global temperatures (e.g. Vaughan et al., 2003; Stammerjohn et al., 2008; Cook et al., 2016), this is likely to affect benthic ecosystems around Antarctica via e.g. increased iceberg scouring, increased mixed layer depth, ecosystems shifts (Smale et al., 2007; Clarke et al., 2008). Longer and more intense phytoplankton blooms are some of the environmental responses to shorter sea-ice duration at high latitude seas (e.g. Arrigo et al., 2008; Peck et al., 2010; Constable et al., 2014; Gutt et al., 2015). It can be argued that whereas increased melting at the WAP sites have deleterious effects in benthic communities via increased iceberg scouring and increased turbidity, the Factory Cove specimens do not experience these effects as no major local glaciers and less frequent drifting icebergs are present in the region. Conversely, Factory Cove *A. eightsii* population will be affected by enhanced (longer and more intense) phytoplankton blooms, which can have positive effects on growth. In addition, reduced iceberg scouring will also have an impact in the maximum lifespan attained by *A. eightsii* (i.e. extended in the case of the South Orkney Island specimens).

All the comparisons with the instrumental records suggest that the South Cove chronology represents better the environmental conditions measured at the RaTS sampling site than the Hangar Cove chronology, even though the two sites are located close to one another, on either side of Rothera Point (**Fig. 2.1b**). As South Cove is located closer to the RaTS sampling site, in the inner bay side of Rothera Point, and due to the shallow nature of the sampling sites, the very local environmental conditions of each site are expected to exert a great influence upon growth of the local *A. eightsii* population. Regarding the lagged correlations found between the South Cove chronology and the instrumental records, an alternative explanation could be that shell growth during 2015 was so minimal that the annually formed increment in all specimens could not be read or was misidentified as a disturbance growth check. If this is the case then correlations between the chronology and the instrumental record would not present any lag. However, based on the observation of the sectioned valves this explanation is highly unlikely.

It could be perhaps be expected that the oceanographic conditions operating in Ryder Bay in 2007/08 would have affected aversively the local *A. eightsii* populations, especially since the phytoplankton bloom yield was significantly diminished. However, in spite of observing a substantial reduction in shell growth in all three sites (Back Bay, Hangar Cove and South Cove; **Fig. 6.7**), the mean population shell growth for the period prior to and the period following 2007, do not differ (**Table A6.2**). The South Cove chronology showed reduced shell growth for 2007 and 2008 whereas the Back Bay and Hangar Cove chronologies showed rapid growth in 2008 (**Fig. 6.7**), which may be an indication of the very local conditions. Subsequently in 2009/10 the phytoplankton bloom yield recovered to around half of the usual yield prior to 2007 (**Fig. 4.12**). Currently nothing is known about the energetic budget of *A. eightsii*, therefore it is possible that even at this reduced ambient chlorophyll levels, the *A. eightsii* populations have still enough food resources to grow normally and as a result there is no difference between the shell growth indices prior to and following 2007 (**Table A6.2**). Peck et al. (2000) indicated that *A. eightsii* could still grow under reduced winter food availability, utilising local benthic microalgae whose bloom is partly controlled by sea-ice cover (Gilbert, 1991). Antarctic benthic bryozoans were found to be able to maintain feeding (i.e. filter-feeding) during winter at a very low level of suspended cell concentration (Barnes and Clarke, 1994). Microphytobenthic communities were found to be able to survive during winter at the South Orkney Islands and accounted for most of the sediment chlorophyll concentration (Gilbert, 1991), which can be a significant food source for benthic deposit feeders, such as *A. eightsii*, for periods with poor phytoplankton bloom yields. Extended availability of food independent from the phytoplankton bloom can be an explanation for the lack of correlation between the shell growth indices and the RaTS chlorophyll record.

To date there is a gap in the literature comparing high-resolution (i.e. annually or sub-annually) stable isotope records ($\delta^{18}O_{shell}$ and $\delta^{13}C_{shell}$) directly with the shell growth record (i.e. chronologies) from specimens collected from the same location, as presented in **Fig. 6.16** and **Fig. 6.17**. Traditionally the shell growth record has been used to clearly identify the increment growth pattern in the shell, to reduce possible errors due to the misidentification of growth checks during drilling and to validate the calendar record of the growth increment series, if a known date is available, prior to developing isotope records that can be compared to environmental parameters (Jones et al., 1983; Lorrain et al., 2004; Gillikin et al., 2006; Goman et al., 2008; Brey et al., 2011; Schöne et al., 2011; Freitas et al., 2012; Scourse et al., 2012; Wanamaker et al., 2012; Royer et al., 2013; Mette et al., 2016; Reynolds et al., 2016). This gap in the literature may be due to lack of correlation with the shell growth record (publication bias) as reported for *A. eightsii* (**Fig. 6.16** and **Fig. 6.17**), the main aim of most of the studies in the literature has been to compare the geochemical records against environmental parameters, climatic modes or ontogenetic growth trends. However, the comparison of the shell growth records and the geochemical records could offer some insights into the relationship between isotope incorporation into the shell matrix and shell growth rates (e.g. McConnaughey, 1989; McConnaughey et al., 1997; Goodwin et al., 2003; Wanamaker et al., 2006; Owen et al., 2008; Butler et al., 2011; Trevisiol et al., 2013).

The comparison between the Hangar Cove and South Cove chronologies and the MEI and SAM climatic indices showed contrasting results between both locations (**Table 6.3 and Table 6.4**). Due to the shortness of the records, especial caution must be exercised in interpreting the results; especially so when only the robust periods of the chronologies are considered. Whereas, the South Cove chronology shows moderate correlations, although not significant, with the MEI at around six-months lag (**Table 6.4**), the Hangar Cove chronology does not show any apparent correlation with the MEI and neither of the chronologies showed any apparent correlation with the SAM. As explained in more detail in the introduction (c.f. Chapter I subsection 1.1.5), the MEI consists of sliding bimonthly (e.g. Jan-Feb, Feb-Mar, Mar-Apr) data on sea surface temperature, surface air temperature, total cloudiness fraction and sea-level pressure, which results in positive (negative) values for El Niño (La Niña) conditions (Wolter and Timlin, 1993, 1998). ENSO and SAM have been found to have significant expression on the Antarctic Peninsula (Li, 2000; Kwok and Comiso, 2002; Liu et al., 2002; Meredith et al., 2004; Turner, 2004; Yuan, 2004; Holland et al., 2005; Clarke et al., 2008; Stammerjohn et al., 2008a and 2008b; Meredith et al., 2010). SAM is the dominant mode of atmospheric variability in the Southern Hemisphere and it represents the change in westerlies wind belt between 40^{o}-70^{o}S (Thompson and Wallace, 2000; Yuan, 2004; Marshall, 2007; Stammerjohn et al., 2008b). During La Niña and positive SAM, increased northerly warm and wet winds affect the WAP mediated by negative atmospheric pressure anomalies in the southeast Pacific Ocean and vice versa for El Niño and negative SAM (Yuan, 2004; Marshall, 2007; Stammerjohn et al., 2008b; Meredith et al., 2017). The combination in the climatic variability of the different phases of these two climatic modes can enhance or damp climatic anomalies at the WAP (Stammerjohn et al., 2008b). The sea surface temperature (SST) anomalies in the South Pacific are advected towards higher latitudes via atmospheric teleconnections (Li, 2000; Yuan and Martinson, 2001; Yuan, 2004; Stammerjohn et al., 2008a) which can lag from over two to three years (Trathan and Murphy, 2002; Turner, 2004) to just a few months (Meredith et al., 2005, 2008b). Locally at the WAP, El Niño conditions were found to be associated with intense sea-ice formation, an enhanced winter mixed layer, reduced stratification of the water column and ice-edge retreat (Kwok and Comiso, 2002; Meredith et al., 2004), which in turn have cascading effects on the local ecosystems (Clarke et al., 2008). The exact cause of the positive relationship between El Niño and *A. eightsii* growth is still obscure, although the connection must be related to sea-ice dynamics, winter mixed layer depth and phytoplankton activity (Clarke et al., 2008; Massom and Stammerjohn, 2010; Barnes and Souster, 2011; Barnes et al., 2014). No clear relationship has been found between ENSO activity and seawater temperature at King George Island, South Shetland Islands, South Georgia and Anvers Island, WAP (Barnes et al., 2006), which shows the complex interactions and/or that seawater temperature may not be the main ENSO vector along the WAP. The lack of correlation between the South Cove chronology and SAM index (**Table 6.3**) is also surprising since it should present a similar inverse correlation to that between the South Cove chronology and the MEI.

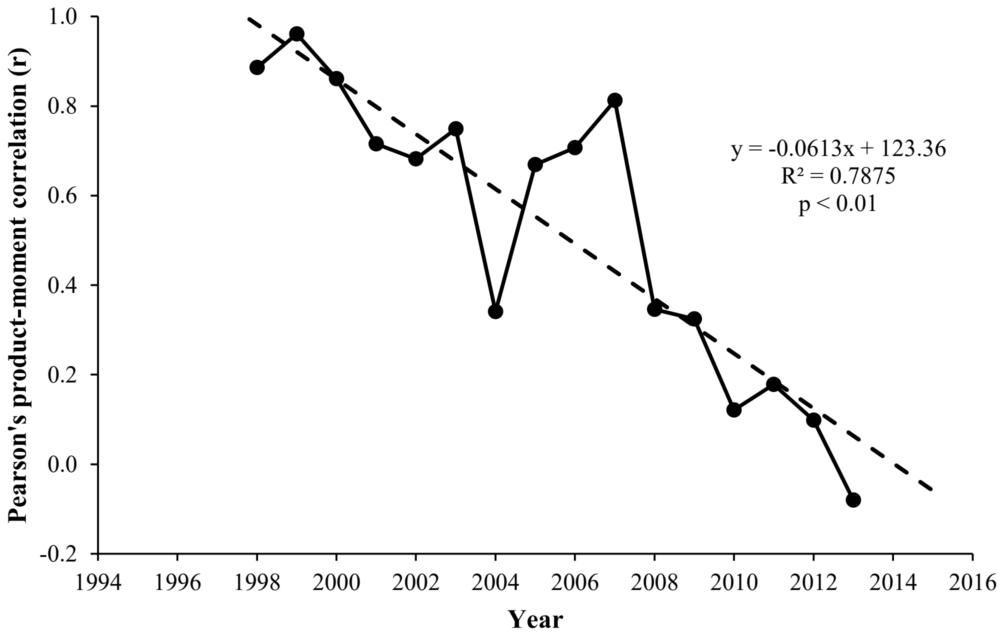

Fig. 6.25 Running correlations based on a five year window between the South Cove chronology and the averaged MEI for the period between June and September. A linear regression was applied to the data (dashed line) and the regression equation and the R^2 are provided.

In addition the declining relationship between the lagged MEI and shell growth (**Fig. 6.25**) may indicate either a decoupling in the ecosystem response in the WAP to ENSO activity or the presence of a longer-term cycle between ENSO activity and ecosystem response. The period covered by the running correlation is contemporary to major climatic changes occurring across the South Pacific and the Southern Ocean. During 1999/2014 the Southern Ocean along the WAP experienced a cooling trend which was caused by enhanced cool east and south-easterly atmospheric circulation mediated by increased cyclonic conditions, associated with mid-latitude jet blocking, in the Drake Passage and north-western Weddell Sea (Turner et al., 2016b). In addition, La Niña-like conditions became more dominant over the same period, which would have resulted in rising temperatures at the WAP if not for the enhanced east and south-easterly atmospheric circulation (Turner et al., 2016). Similarly, Ivany et al. (2011)

found that the fossilised shell growth record of *Cucullaea raea* shells that grew in shallow marine environments during the early Eocene at Seymour Island, Weddell Sea, presented a quasi-periodic variability associated with ENSO despite climatic differences (global average temperature was 10 °C warmer compared to the current value) and geomorphological (the Drake Passage was not yet open) in comparison with present conditions. The study of *C. raea* shows the potential of sclerochronological records to provide insights into climatological conditions far removed from the beginning of the instrumental record; however, the assumptions considered in their analysis add a significant amount of uncertainty to the comparison between the early Eocene and modern times.

6.3.2 South Orkney Islands

The historical specimens from the 1915 A. Bennett collection located at the Natural History Museum, London, proved to have a strong population growth pattern (**Fig. 6.18**). The AB1915 chronology constitutes the first floating chronology from *A. eightsii* as it is separated from the Factory Cove chronology by 34 years (from 1915/49). Based on the current information about historical *A. eightsii* specimens and the availability of dead-collected material present in the wild it is not likely that this gap will be bridged, unless dead-collected material in a good state of preservation (c.f. Chapter II subsection 2.3.1) can be found in the soft sediments from around the South Orkney Islands. In addition, based on the lifespan of the specimens available from this region, it is likely that two to three *A. eightsii* cohorts (e.g. early 1930s, mid-1950s and late 1960s, suggested dates represent the end of their lifespan) would be necessary to cover the gap between the chronologies.

The comparison of the growth histories between the deep-collected specimen from the 1927 *Discovery* investigations (**Fig. 6.19**) and the shallow-collected specimens from the 1915 A. Bennett collection (**Fig. 6.18**) showed, as expected, that the deep specimen presents a low inter-annual variability when compared to the shallow specimens. This result, in addition to the results presented on the shell geochemistry (c.f. Chapter V section 5.1), points to a much more stable (seasonally and inter-annually) environment at depth than in shallower coastal waters, which was also expected. The analysis of the specimen from the 1927 *Discovery* investigations showed that this individual was not particularly long-lived (14-19 years of age, **Fig. 6.19**). Peck and Bullough (1993) hypothesised, based on the study of smaller shallow-collected *A. eightsii* specimens, that the large specimens from the 1927 *Discovery* investigations could reach 150 years of age. Conversely, the specimen analysed here suggests rapid growth so that the large shell (40.34 mm in shell length) is not due to an extended lifespan. The study of other deep-sea mollusc bivalves such as *Megayoldia thraciaeformis* and *Nuculana pernula* collected from between 895 and 1490 m water depth from the North West Atlantic Ocean showed also very fragile and thin shells (1-2 mm for *M. thraciaeformis* and 0.5 mm for *N. pernula*) and very narrow (80 to 100 μm for *M. thraciaeformis* and approximately 13 μm for *N. pernula*) bands that were assumed to be annual (Gilkinson et al., 1986). Although shell size was not reported for *M. thraciaeformis* and *N. pernula* nor the difference in water depth of the collection site, the deep-collected *A. eightsii* specimen here analysed is characterised by significantly wider increments (on average 1448 μm).

Regarding the Factory Cove (South Orkney Islands) chronology (**Fig. 6.20**), its most prominent features are increases in growth in 1970, 1977 and 1985, and a noticeable period of weak growth between 1973 and 1976 (**Fig. 6.20a**). Between 1973 and 1976 a phenomenon known as the Weddell Polynya (WP) influenced the region, characterised by convective water circulation formed by surface salinity changes in the Weddell Sea (Gordon, 1982). Holland (2001) identified deep upwelling processes surrounding the Maud Rise seamount (66°0′S, 3°0′E) as playing a major role in the development of the

WP. Since the physical processes driving the formation of the WP altered the whole water column stratification, the decrease in mean annual SST observed at Signy Island was likely related to the same processes that formed the WP. Gordon (1982) reported the existence of a subsurface 'cold spot', which migrated westwards (i.e. towards Signy Island) at an annual average drift rate of 1.3 cm sec^{-1}. This suggests that waters surrounding Signy Island could have been affected by this cold regime. The satellite SST data indicate a pronounce decrease in mean summer SST (1973) and mean winter SST (1973/75; **Fig. 6.21**). The RCS-chronology indices show a sharp decline in shell growth between 1970 and 1973 that subsequently remained low for the period 1973/76 (**Fig. 6.21**). Additionally the RCS-chronology indices show a period of fast growth between 1975 and 1977, which coincides with an increase in the mean annual SST due mainly to relatively warm temperatures during winter (**Fig. 6.21**). Subsequently there is sharp decline in growth (1978/79) that coincides with a decrease in mean annual SST that lasted until 1980. It is difficult to determine whether the *A. eightsii* population at Signy Island responded to the effects of the cold conditions that originated in the WP before even the full development of the WP, as indicated by the sharp decline in growth between 1970 and 1973. The lack of quality winter SST data prior to 1973 (note the lack of variability in the mean winter SST values prior to 1973; **Fig. 6.22**), prevents the determination of the onset of this cold regime. This indicates some degree of sensitivity of *A. eightsii* to changes in SST, especially during the winter season. *Aequiyoldia eightsii* sensitivity to winter SST can be also detected in the monthly-calculated correlation coefficients with stronger positive correlations between April and November (except September) and weaker correlations during the summer (December-March). This suggests that another environmental parameter is controlling shell growth during the summer months. It is very likely that deposited organic matter availability due to the phytoplankton bloom is the main environmental driver during the summer and as winter progresses and food availability becomes scarce, SST starts to play a more important role in regulating shell growth.

The SST data need to be viewed with caution as the mean SST values are based on oceanic SST values calculated from satellite measurements and the sparse instrumental data available (**Fig. 6.21**; Rayner et al., 2003). The variability in the data prior to 1973 is likely a result of differences in the methodology used to produce the SST records between the two periods (Rayner et al., 2003). Local instrumental SST data between 1988 and 1994 showed stable winter temperatures around -1.8 °C, although the winter duration seems to differ greatly from year to year. Assuming similar conditions between 1949 and 1988 (i.e. the period covered by the RCS-chronology) and considering the positive correlation between the chronology and mean winter SST and the negative correlation with core winter duration, the correlation with the mean winter SSTs could be interpreted as a relationship between shell growth and winter length. Changes in the length of the winter season will likely have a significant impact on the growth of *A. eightsii* by affecting its food availability. The WP, in combination with the potentially unreliable SST data up to 1973, when monthly satellite data records start (Rayner et al., 2003), could explain the lack of any clear correlation between the growth index and the SST record between 1949 and 1973. Due to the lack of instrumental data for the region such as salinity, *in situ* temperature measurement or reliable SST satellite measurements (prior to 1973), this remains speculative. The correlation of environmental parameters shows conflicting results in the relationships between SST, core winter duration and fast-ice duration. Whilst negative correlation between core winter duration and SST and fast-ice duration and SST are expected, a positive correlation between core winter duration and fast-ice duration was also expected although not present. This may be a reflection of other parameters affecting the formation and stability of fast-ice such as arrival of pack-ice and wind patterns. The marked shift in the running correlations between the RCS-chronology and the SST measurements (**Fig. 6.23**) also coincides with the start of monthly satellite measurements (i.e. 1973) and this is probably a reflection of this improvement in the quality of the environmental data. HasISST1 *in situ* SST observations prior to 1973 are very limited and sea-ice data were derived from two unconnected climatological records; the gaps between the sea-ice records and 1973 were interpolated (Rayner et al., 2003). This, alongside the greater ice extent values prior to 1973 in HadISST1 may explain the closer resemblance of annual SST values to winter SST values (**Fig. 6.22**). Instrumental data collected by Clarke et al. (1988) from Factory Cove between 1972 and 1981 reveal similarities between the HadISST1 winter and annual SST values and the instrumental data. On the contrary, summer SST values seem to be contradictory between the two records. Unfortunately a more robust analysis between the two records and the chronology was not possible due to the brevity and gaps in the instrumental series.

The comparison between the Factory Cove RCS-chronology and the bimonthly MEI values and the monthly SAM values does not show any significant correlation nor any pattern in sign of the correlation coefficients over a period of almost 40 years (**Table 6.6**). This contrasts with the case of the WAP chronologies, which showed some sub-annual pattern in the sign of the correlation coefficients (**Table 6.3**) for over a period 20 years. Considering the relative shortness of the overlap between the records, caution must be exercised when interpreting these results. Similar results to those considering the WAP chronologies were expected in the case of Factory Cove chronology since ENSO has also been reported to have an effect in the oceanographic conditions around the South Orkney Islands lagging around three to six months (Meredith et al., 2005, 2008). Any explanation for the difference in the relationship between the climatic indices and the Factory Cove and WAP chronologies remains speculative.

6.4 Appendix – Tables and figures

Table A6.1 List of *A. eightsii* specimens used to construct the different chronologies. HCd: Hangar Cove deep, HCs: Hangar Cove shallow, SC: South Cove, BL: Back Lagoon, FC: Factory Cove.

Specimen ID	Sampling location	Collection date	Age (yr)	Shell length (mm)	Shell height (mm)	Water depth (m)
8803002	FC, Signy Island	Mar-88	41	30.27	18.45	< 8
8803006	FC, Signy Island	Mar-88	37	30.66	19.14	< 8
8803010	FC, Signy Island	Mar-88	29	28.42	18.25	< 8
8804007	FC, Signy Island	Apr-88	28	28.45	17.55	< 8
8804041	FC, Signy Island	Apr-88	22	28.15	17.52	< 8
8804054	FC, Signy Island	Apr-88	28	29.49	18.49	< 8
8804058	FC, Signy Island	Apr-88	25	28.53	17.1	< 8
8804076	FC, Signy Island	Apr-88	31	29.47	18.41	< 8
8804083	FC, Signy Island	Apr-88	25	30.62	18.37	< 8
8804102	FC, Signy Island	Apr-88	34	29.38	17.53	< 8
8804110	FC, Signy Island	Apr-88	19	28.62	17.98	< 8
8804111	FC, Signy Island	Apr-88	36	30.62	18.42	< 8
8808002	FC, Signy Island	Aug-88	24	31.00	19.13	< 8
8808003	FC, Signy Island	Aug-88	29	30.74	19.21	< 8
8808005	FC, Signy Island	Aug-88	31	30.7	18.93	< 8
8808006	FC, Signy Island	Aug-88	37	29.53	18.47	< 8
8808008	FC, Signy Island	Aug-88	28	32.97	20.45	< 8
8811007	FC, Signy Island	Nov-88	31	31.24	19.65	< 8

8811028	FC, Signy Island	Nov-88	34	30.55	18.88	< 8
8811029	FC, Signy Island	Nov-88	33	30.22	19.64	< 8
20102005	HCd, Rothera	31-Jan-14	16	24.5	7.9	25-30
21402007	HCd, Rothera	31-Jan-14	11	22.4	7.1	25-30
21402010	HCd, Rothera	31-Jan-14	14	24.3	7.8	25-30
21402013	HCd, Rothera	31-Jan-14	13	23.2	7.4	25-30
21402016	HCd, Rothera	31-Jan-14	13	22.7	7.7	25-30
21402042	HCd, Rothera	31-Jan-14	20	24.8	8.6	25-30
21402049	HCd, Rothera	31-Jan-14	11	23.2	7.2	25-30
21402053	HCd, Rothera	31-Jan-14	17	22.5	7.4	25-30
21402059	HCd, Rothera	31-Jan-14	15	22.0	6.7	25-30
21403001	HCs, Rothera	03-Feb-14	18	22.4	6.7	~ 15
21403002	HCs, Rothera	03-Feb-14	11	22.5	7.0	~ 15
21403010	HCs, Rothera	03-Feb-14	13	22.2	8.0	~ 15
21403025	HCs, Rothera	03-Feb-14	12	25.2	8.3	~ 15
21403027	HCs, Rothera	03-Feb-14	15	22.6	8.0	~ 15
21403045	HCs, Rothera	03-Feb-14	17	22.0	7.5	~ 15
21403049	HCs, Rothera	03-Feb-14	13	22.4	7.1	~ 15
21504003	SC, Rothera	10-Feb-15	21	26.0	8.7	~ 15
21504010	SC, Rothera	10-Feb-15	9	23.4	7.9	~ 15
21504012	SC, Rothera	10-Feb-15	15	27.6	10.7	~ 15
21504031	SC, Rothera	10-Feb-15	17	28.6	9.5	~ 15
21504034	SC, Rothera	10-Feb-15	15	26.3	8.4	~ 15

21504035	SC, Rothera	10-Feb-15	20	26.9	8.5	~ 15
21504044	SC, Rothera	10-Feb-15	19	26.3	8.4	~ 15
21504046	SC, Rothera	10-Feb-15	15	27.5	8.8	~ 15
21504047	SC, Rothera	10-Feb-15	19	25.9	8.2	~ 15
21504050	SC, Rothera	10-Feb-15	17	25.4	9.3	~ 15
21504054	SC, Rothera	10-Feb-15	15	26.2	8.5	~ 15
21505003	BL, Rothera	13-Feb-15	19	23.54	7.81	~ 11
21505004	BL, Rothera	13-Feb-15	15	23.81	7.14	~ 11
21505008	BL, Rothera	13-Feb-15	14	23.5	7.15	~ 11
21505011	BL, Rothera	13-Feb-15	15	24.13	7.52	~ 11
21505012	BL, Rothera	13-Feb-15	16	23.24	8	~ 11
21505019	BL, Rothera	13-Feb-15	13	24.89	8.86	~ 11
21505028	BL, Rothera	13-Feb-15	17	23.97	7.16	~ 11
21505029	BL, Rothera	13-Feb-15	13	24.32	7.27	~ 11
21505034	BL, Rothera	13-Feb-15	20	24.25	7.8	~ 11
21505038	BL, Rothera	13-Feb-15	20	24.40	7.99	~ 11
21505002	BL, Rothera	13-Feb-15	16	23.98	7.82	~ 11
191501003	Signy Island	1915	11	25.32	6.6	~ 11
191501004	Signy Island	1915	22	25.42	7.54	~ 11
191501013	Signy Island	1915	13	25.92	7.34	~ 11
191501015	Signy Island	1915	9	25.32	6.9	~ 11
191501017	Signy Island	1915	13	25.82	7.58	~ 11
191501021	Signy Island	1915	13	24.78	6.51	~ 11

191501024	Signy Island	1915	14	25.4	6.98	~ 11
191501026	Signy Island	1915	10	25.67	7.14	~ 11
191501027	Signy Island	1915	14	25.16	6.87	~ 11
191501029	Signy Island	1915	19	25.08	6.92	~ 11
191501030	Signy Island	1915	14	26.14	6.98	~ 11
191501031	Signy Island	1915	11	25.21	7.02	~ 11
191501032	Signy Island	1915	14	25.88	7.48	~ 11
191501036	Signy Island	1915	12	25.71	7.04	~ 11
191501038	Signy Island	1915	12	24.88	6.99	~ 11

Table A6.2 One-way ANOVA test results comparing the standardized shell growth indices for the periods prior and after 2007.

Location	F	df	p-value
Back Bay	0.298	18	0.592
Hangar Cove	0.069	18	0.769
South Cove	0.085	19	0.774

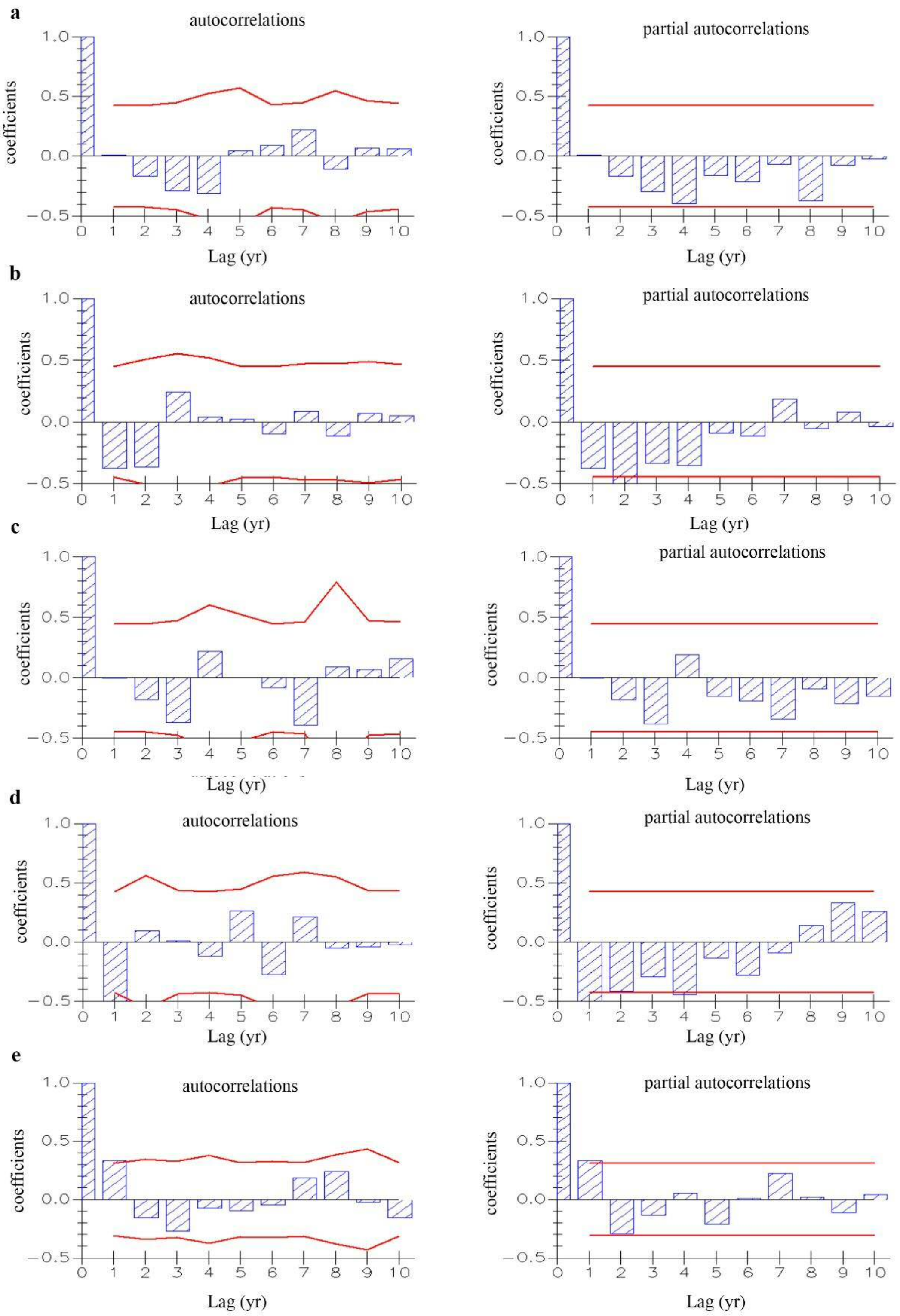
a
autocorrelations
partial autocorrelations
b
autocorrelations
partial autocorrelations
c
partial autocorrelations
d
autocorrelations
partial autocorrelations
e
autocorrelations
partial autocorrelations
coefficients
1.0
0.5
0.0
−0.5
0 1 2 3 4 5 6 7 8 9 10
Lag (yr)

Fig. A6.1 Pooled autocorrelation results (autocorrelations and partial autocorrelation indices) from ARSTAN for the negative exponential chronologies from **a)** South Cove, **b)** Hangar Cove, **c)** Back Bay, **d)** 1915 A. Bennett collection and **e)** Factory Cove.

Chapter VII: Conclusions and final remarks

This chapter contains the conclusion and final remarks regarding each area of study presented in the thesis. In addition, recommendations are given for improving in the future the techniques and analysis used in the thesis. Some of the relationships between the Factory Cove chronology and the instrumental record are not included in this chapter since they were already published in a previous pilot study and the results presented in Chapter VI are a refinement of that previous pilot study, although a significant amount of work was carried out during the PhD program. During the PhD program: i) six additional specimens were crossdated to the existing 1988 South Orkney Islands (SOI) chronology, ii) the RCS 1988 SOI chronology was created, iii) comparisons between the chronologies and the geochemical records were carried out and iv) the relationships between shell growth and the environmental parameters was reassessed.

7.1 Conclusions

The research carried out for this thesis allowed the analysis and comparison of historically-collected specimens (1915 A. Bennett and 1927 *Discovery* collections at the Natural History Museum, London) with more modern-collected specimens. The analysis of the biometrics and the increment growth history of the 1927 *Discovery* investigations *A. eightsii* specimens showed a clear difference between them and all other *A. eightsii* specimens collected (recently-collected or historical specimens; c.f. Chapter III section 3.1). The reason for this difference remains equivocal, but is likely to be related either to habitat adaptation or that the 1927 *Discovery* investigations specimens belong to a different or undescribed *Aequiyoldia* species. Surprisingly, the large 1927 *Discovery* specimen did not have an extended lifespan, as other authors

(Peck and Bullough, 1993) had previously suggested based on shell size, but a modest lifespan of approximately 14 to 19 years.

In addition, the study of growth increment series of *A. eightsii* proved useful as it helped to identify a secondary ontogenetic growth rhythm (c.f. Chapter III section 3.2), which may be related to the reproductive cycle of *A. eightsii*. To date there is no other example of such secondary ontogenetic growth rhythm in Antarctic bivalve molluscs. Identifying pure biological trends in the shell growth records is key in order to develop sclerochronological proxies in the marine realm for the modern calibration period and for periods prior to the instrumental record. Therefore the work presented in this thesis establishes a methodological background for constructing chronologies using *A. eightsii*.

During the analysis of the specimens, number of rounded orange-coloured markings were found in the carbonate part of the shell underneath the periostracum (c.f. Chapter III section 3.1). These marking were associated with shell damage and possibly remineralization and shell dissolution.

Aequiyoldia eightsii has the potential to provide annually-resolved shallow-marine proxy records for the Antarctic continent spanning several decades, if enough fossil or sub-fossil material is available. In this thesis, the first *A. eightsii* chronologies for the West Antarctic Peninsula (WAP) are presented (c.f. Chapter VI section 6.1) and an additional chronology from the South Orkney Islands is constructed (c.f. Chapter VI section 6.2). In addition, a previously established chronology from the South Orkney Islands (SOIs) is strengthened by crossdating additional specimens (c.f. Chapter VI section 6.2). Significant differences between the WAP chronologies are most likely due to the shallow nature of the sampling sites and the local variability in the environmental parameters driving shell growth (c.f. Chapter VI section 6.3). Hangar Cove and South

Cove *A. eightsii* specimens provided the most robust chronologies, whereas Back Bay specimens provided mixed results and it was not possible to develop a chronology from Trolval. South Cove was identified as the most favourable location to develop an *A. eightsii* proxy for WAP coastal waters since the local population shows a synchronous growth pattern and since there is a stronger relationship between the shell growth record and the long-term instrumental record from the RaTS program. Contrary to what was previously found (from a population in the SOIs), *A. eightsii* at South Cove (WAP) showed a significant positive correlation with fast-ice duration (c.f. Chapter VI subsection 6.1.6); this difference may relate to the role of fast-ice and iceberg and sea-ice disturbance in both regions (c.f. Chapter VI section 6.3). South Cove chronology also showed a positive relationship with climate variability in the South Pacific Ocean (represented in the MEI index) lagged by approximately six months (shell growth leading; c.f. Chapter VI subsection 6.1.6); however, this relationship is becoming less strong with time.

The current investigation shows the presence of subannual cycles in *A. eightsii* $\delta^{18}O_{shell}$ and $\delta^{13}C_{shell}$ records, which are the first sub-annual and annual stable isotope records developed from *A. eightsii* (c.f. Chapter V). The comparison between the high and low-resolution stable isotope records showed agreement between the two sampling methodologies, especially in the case of $\delta^{13}C_{shell}$ (c.f. Chapter V **Fig. 5.12** and **Fig. 5.23**), which will facilitate the development of *A. eightsii* stable isotope records in future investigations. The comparison between the instrumental $\delta^{18}O_{shell}$ records with the instrumental $\delta^{18}O_{water}$, collected in the RaTS program, showed an offset in the average values of approximately 0.5 ‰ (water higher; c.f. Chapter V subsection 5.2.3); this is most probably due to differences in the local conditions between the RaTS sampling site and the shell sampling sites (c.f. Chapter V subsection 5.4.2). It was also established that the annually-formed increment line coincided with heavy $\delta^{18}O_{shell}$ values, within the subannual cycle. The $\delta^{18}O_{shell}$ records developed from contemporary specimens collected in the WAP showed similar interannual variability which indicates a common environmental driver (c.f. Chapter V **Fig. 5.17a** and **Fig. 5.17b**). In addition, all specimens showed a trend towards lower isotopic values with time in $\delta^{18}O_{shell}$ which indicates that the waters in which the specimens lived have been becoming either fresher, warmer or a combination of both (c.f. Chapter V section 5.4, **Fig. 5.8** and **Fig. 5.17a**).

The presence of ontogenetic trends in the *A. eightsii* $\delta^{13}C_{shell}$ record remains inconclusive, although it is expected to be present based on analyses of other bivalve mollusc species. The *A. eightsii* $\delta^{13}C_{shell}$ record seems to reflect partly primary production activity during the calibration periods, although further work is required to assess the importance of benthic algae blooms in *A. eightsii* $\delta^{13}C_{shell}$. The $\delta^{13}C_{shell}$ records from the *A. eightsii* specimens collected in the WAP seem to have recorded a major change of state in Ryder Bay, which occurred in 2007, from a high chlorophyll concentration state to a lower chlorophyll concentration state (c.f. Chapter IV subsection 4.1.3 and Chapter V subsection 5.2.3).

Lateral fractionation of stable isotopes in shell material has surprisingly received little attention in comparison with the development of long-term isotopic records. The preliminary study on stable isotope lateral fractionation in *A. eightsii* shell material presented here (c.f. Chapter V section 5.3) provides some indications of its importance. Some of the analysed specimens showed intra-increment differences in $\delta^{18}O_{shell}$ and $\delta^{13}C_{shell}$ depending on the anatomical position of the sample in the shell (i.e. anterior, ventral, posterior; c.f. Chapter V section 5.3), which could be related to either isotope fractionation depending on shell growth or to differences in the shell structure between anatomical regions (c.f. Chapter V subsection 5.4.3).

7.2 Limitations of the study

7.2.1 Specimen collection

It was shown that hand picking and suction pump sampling by the British Antarctic Survey (BAS) scuba divers were successful techniques for collecting live medium-sized specimens in shallow Antarctic coastal waters down to approximately 30 m water depth. BAS scuba divers indicated that the difficulty in finding dead shell specimen was not, in principle, due to the sampling techniques used but due to their real absence in the studied locations. In addition, they suggested that the cause of the lack of fossil shell material was most likely due to the intense physical reworking that the soft sediment is subjected to by frequent iceberg and sea-ice scouring.

Time, monetary and diving-depth limitations are some of the restrictions identified for sample collection during the present research. A remotely video-controlled Van-Veen grab deployed from a rib boat and the use of an underwater ROV were discussed during the course of the current investigation as an alternative method for collection of *A. eightsii* specimens, although the idea was discarded due to time and logistical constraints of the current project. Incorporating new effective sampling techniques in Antarctic shallow coastal waters can be challenging, although it could be a solution to some of the limitations identified here.

The present study is the first attempt to develop a species-specific network of chronologies in the Southern Ocean. Since the present study is framed within a doctoral training programme, funds available for sampling and fieldwork are more limited than in standard research programmes. This limitation and logistical impediments, especially for working at Signy Research Station prevented the collection of modern samples from the South Orkney Islands. A more recent chronology could likely have been developed for Factory Cove if samples had been available, which potentially could have overlapped with the existing Factory Cove chronology; this would have enabled further calibration with modern instrumental data. In addition, this chronology would also have provided a comparative temporal frame with the chronologies developed from the WAP.

7.2.2 Study locations

The coastal environments close to the Rothera and Signy Research Stations proved excellent sites of study since they are both located in regions of scientific interest for studying Antarctic climate variability and processes. Signy Research Station has been for a long time the focus of many environmental and climatological studies, which provide, even if for short periods, a background information on local and regional variability. Rothera Research Station is especially ideal due to the availability of the modern long-term environmental time series from the RaTS program (c.f. Chapter IV section 4.1), which allowed direct comparison and calibration between the shell growth records and the environmental conditions present during shell deposition. In contrast, Signy Research Station presents some limitations since no modern long-term year-round instrumental record program, such as RaTS, is available; however, given that only historical samples from Signy Research Station were available this was not problematic within the context of the current investigation.

There are several other locations of scientific interest around Antarctica suitable for the use of *A. eightsii* as a sclerochronological archive; however, the inclusion of more sampling locations would have proved not only logistically and economically difficult but also out of the scope of the aim of this research project.

7.2.3 Laboratory procedures

Laboratory work with the thin and fragile *A. eightsii* shells proved challenging and extremely laborious, especially when compared with other established bivalve molluscs used in chronology. More care has to be taken than when working with other species with larger and more robust shells. Some methodological examples include: i) the removal of the periostracum from the shell by inserting a razor blade between the carbonate part and the periostracum, ii) hydrochloric acid (HCl) etching of the shell for the acetate peel replica preparation, iii) imaging of shell sections and drilling of shells in order to obtain samples for geochemical analysis.

Identification of the growth increments in the shell sections was extremely challenging and impossible in some cases during the first year of the PhD program due to the old imaging system available at that time at Bangor University. This was only solved after the acquisition of new high-resolution cameras (c.f. Chapter II subsection 2.3.4). The cross-calibration between shell section images, acetate peel replica images and the composite photographs of the external surface of the shell was crucial in the development of the records presented in this doctoral thesis; however, it has to be acknowledged that this task is very time consuming.

Hydrochloric acid etching of *A. eightsii* shells required substantial experimentation in the laboratory. The use of a weak HCl solution (i.e. 0.01 M) was found to give more control during the etching process, although there were considerable inter-specimen differences in the required etching degree. However, a standardized methodology for etching *A. eightsii* shells was refined during the course of the current investigation (Chapter II subsection 2.3.3), which provides quality acetate peel replicas for the majority of *A. eightsii* specimens. In addition the observation of polished section of *A. eightsii* shells provided images of high quality to the same standard as the acetate peel replica technique. To date, the most commonly used technique in chronology has been the acetate peel replica; directly observing the polished sections provides a workable alternative to the above mentioned technique. In addition, the use of the polished section alone has further advantages as no chemicals are required, less time is required in sample processing and there is no chemical alteration of the processed specimens (e.g. carbonate dissolution).

The collection of shell powder samples for geochemical analysis proved to be the most challenging task of all laboratory techniques carried out (c.f. Chapter II section 2.8). A new protocol for drilling on the outer surface of the thin and fragile *A. eightsii* shell was developed using a computerised micromill. However, this technique has the potential to be refined further for achieving more precise samples (c.f. Chapter V section 5.4).

7.2.4 Aequiyoldia eightsii chronologies

During the course of the present investigation it was found that the average lifespan of the specimens from the WAP was shorter than initially expected (c.f. Chapter VI), based on prior investigations of historical specimens. This fact and the apparent lack of fossil material may pose a limitation in the use of *A. eightsii* in certain regions of the shallow Antarctic coastal waters.

Unfortunately, it is very likely that it will prove impossible to cover the gap between the most recent (i.e. 1988) Factory Cove chronology and the 1915 chronology due to the intense reworking of the soft sediments by iceberg activity unless a sheltered site can be located and *A. eightsii* dead specimens are found. At present no knowledge of such a site exists; however, if discovered, it could (with the addition of modern specimens from the same site) provide a continuous century-long chronology for the South Orkney Islands, which would allow the investigation of a longer temporal shift in environmental parameters.

New *A. eightsii* specimens, from the already curated WAP *A. eightsii* collection, will be added in the near future to these chronologies; this will strengthen the signal of the population common growth pattern and will allow a more robust comparison with environmental records. This is especially relevant for the Back Bay chronology which shows a high inter-specimen variability in the most modern part of the shell (c.f. Chapter VI subsection 6.1.3).

7.3 Scope for future research

Exploration of the origin and formation processes of the orange marks (c.f. Chapter III from **Fig. 3.4** to **Fig. 3.10**) found in the outer shell layer beneath the periostracum has the potential to offer further insights into how Antarctic lightly calcifying marine organisms are being affected by ocean acidification.

The use of *A. eightsii* as a sclerochronological proxy for Antarctic coastal waters has considerable potential for development. In terms of the development of new records, the construction of a more recent chronology from Factory Cove would not only extend the shell growth record to the present day, but it would also aid in the calibration with modern, more precise instrumental record. This will also allow direct comparison with the contemporary *A. eightsii* sclerochronological records developed from Rothera Research Station. There is also an opportunity to develop new sclerochronological records from specimens collected at greater depths, these records will allow a comparison between shallow coastal marine environments and deeper marine habitats and the environmental drivers in each habitat. At present, there is a lack of such comparisons in the chronology literature. A comparison between shallow and deep collected *A. eightsii* specimens could also offer some insight into significant oceanographic processes such as incursions of upper Circumpolar Deep Water onto the WAP oceanic shelf, which is believed to play a major role in regional deglaciation. In addition new sclerochronological proxies can be developed from unexplored locations and provide information of the local environment where instrumental records are sparse or absent.

When enough chronologies are available, there will be the possibility to construct a network of chronologies to address spatial variability in the climate and environmental drivers over large areas (e.g. Weddell Sea, whole WAP).

Future work with the current collection of *A. eightsii* specimens from Rothera should be aimed at developing a fully robust chronology from Back Bay and South Cove by adding new specimens to the chronologies (c.f. Chapter VI section 6.1). Once this is done, further investigations can be undertaken in order to investigate further the differences between sites from within and from outside Ryder Bay. If sufficient specimens are added to the existing chronologies, the RCS detrending method could be used instead of NE detrending, this should provide shell growth records more representative of the environmental parameters driving shell growth (c.f. Chapter III section 3.2). Further investigation of the lack of an *A. eightsii* common growth pattern at Trolval, or if there is a masked underlying growth pattern, could offer an insight into the environmental conditions present at this site (c.f. Chapter VI section 6.3).

Collection of dead specimens has the potential to extend the existing chronologies back in time. However, the collection of dead specimens has been found to be difficult; this may be related to the intense reworking of the soft bottoms in Antarctic shallow marine coastal environments and the chemical dissolution of the thin carbonate shells. A few dead-collected specimens are already available for analysis, which will be analysed in the near future, although more specimens will be needed in order to robustly extend the chronologies over significant periods of time.

The addition of dead-collected specimens to modern collected specimens has the potential to extend the *A. eightsii* increment width series and stable isotope records over a few decades. Environmental information prior to the instrumental record is particularly valuable especially in the Southern Ocean where environmental information is sparse. Some potential examples of the use of annually-resolved multicentennial *A. eightsii* records are: i) the establishment of the onset of the intense warming trend that the WAP has experienced during the 20th century, ii) effects of deglaciation on Antarctic shallow coastal benthic ecosystems, iii) leading driver (ocean *vs*. atmosphere) of WAP regional warming trends, iv) long-term trends in primary production associated with warming trend, deglaciation and modification of the mixed depth layer.

Understanding the energetic budget and reproductive cycle of *A. eightsii* could offer some insight into the ontogenetic growth rhythms presented in this study (c.f. Chapter III section 3.2). This investigation has the potential to offer some clues about adaptations of bivalve molluscs to the Antarctic marine environment.

As indicated earlier, there is still potential for improving the micromilling technique used for sampling *A. eightsii* shells, or any other bivalve shell for that matter. Understanding the external and internal structure of the specimens is a critical factor that has to be studied in parallel with the refinement of the sampling technique, as it potentially has significant effects on the samples produced.

Possible ontogenetic patterns in the stable isotope geochemistry, especially in the $\delta^{13}C_{shell}$, of *A. eightsii* can be addressed by selecting specimens with a wide age range and then developing high-resolution stable isotope series that can be combined together into a single ontogenetic geochemical record. This species-specific ontogenetic geochemical record could be used for generating a detrending curve for all individual geochemical records, which should provide a more clear relationship between the isotope fractionation between *A. eightsii* shell and the environment.

Further work should be directed to understanding the lateral variation in thickness of the different shell layers from the posterior part to the anterior part of the shell.

Understanding of the internal structure of the shell will help to confirm whether the preliminary results presented here on lateral fractionation (c.f. Chapter V section 5.3) are due to true fractionation or due to biases in the sampling methodology used.

At present, there is no study available investigating trace element distribution and incorporation in *A. eightsii* shell. Consequently, pioneering work can still be carried out in this field, which could potentially increase our understanding of processes such as ocean acidification, deglaciation and ecology dynamics.

Reference List

Abele, D., Philipp, E., 2013. Environmental Control and Control of the Environment: The Basis of Longevity in Bivalves. Gerontology 59, 261–266. doi:10.1159/000345331

Abele, D., Tesch, C., Wencke, P., Pörtner, H.-O., 2001. How does oxidative stress relate to thermal tolerance in the Antarctic bivalve *Yoldia eightsi*? Antarct. Sci. 13 111–118.

Allison, N., Finch, A.A., EIMF, 2010. The potential origins and palaeoenvironmental implications of high temporal resolution δ18O heterogeneity in coral skeletons. Geochim. Cosmochim. Acta 74, 5537–5548. doi:10.1016/j.gca.2010.06.032

Antarctic Treaty, 1959. Washington D.C. October 15th, 1959. Accessed: http://www.ats.aq/documents/ats/treaty_original.pdf

Annett, A.L., Skiba, M., Henley, S.F., Venables, H.J., Meredith, M.P., Statham, P.J., Ganeshram, R.S., 2015. Comparative roles of upwelling and glacial iron sources in Ryder Bay, coastal western Antarctic Peninsula. Mar. Chem. 176, 21–33. doi:10.1016/j.marchem.2015.06.017

Arrigo, K.R., van Dijken, G.L., Bushinsky, S., 2008. Primary production in the Southern Ocean, 1997-2006. J. Geophys. Res. 113. doi:10.1029/2007JC004551

Barnes, D.K., Brockington, S., 2003. Zoobenthic biodiversity, biomass and abundance at Adelaide Island, Antarctica. Mar. Ecol. Prog. Ser. 249, 145–155.

Barnes, D.K., Clarke, A., 1994. Seasonal variation in the feeding activity of four species of Antarctic bryozoan in relation to environmental factors. J. Exp. Mar. Biol. Ecol. 181, 117–133.

Barnes, D.K.A., 2015. Antarctic sea ice losses drive gains in benthic carbon drawdown. Curr. Biol. 25, R789–R790.

Barnes, D.K.A., Fenton, M., Cordingley, A., 2014. Climate-linked iceberg activity massively reduces spatial competition in Antarctic shallow waters. Curr. Biol. 24, R553–R554. doi:10.1016/j.cub.2014.04.040

Barnes, D.K.A., Fuentes, V., Clarke, A., Schloss, I.R., Wallace, M.I., 2006. Spatial and temporal variation in shallow seawater temperatures around Antarctica. Deep Sea Res. Part II Top. Stud. Oceanogr. 53, 853–865. doi:10.1016/j.dsr2.2006.03.008

Barnes, D., Peck, L., 2008. Vulnerability of Antarctic shelf biodiversity to predicted regional warming. Clim. Res. 37, 149–163. doi:10.3354/cr00760

Barnes, D.K.A., Souster, T., 2011. Reduced survival of Antarctic benthos linked to climate-induced iceberg scouring. Nat. Clim. Change 1, 365–368. doi:10.1038/nclimate1232

Barrera, E., Tevesz, M.J.S., Carter, J.G., 1990. Variations in oxygen and carbon isotopic compositions and microstructure of the shell of *Adamussium colbecki* (Bivalvia). PALAIOS 5, 149. doi:10.2307/3514811

Barrera, E., Tevesz, M.J.S., Carter, J.G., McCall, P.L., 1994. Oxygen and carbon isotopic composition and shell microstructure of the bivalve *Laternula elliptica* from Antarctica. PALAIOS 9, 275. doi:10.2307/3515202

Bayne, B.L., Newell, R.C., 1983. Physiological energetics of marine molluscs, in: The Molluca, volume IV: Physiology. Academic Press, New York and London, pp. 407–515.

Brand, W.A., 2004. Mass spectrometer hardware for analyzing stable isotope ratios. Handb. Stable Isot. Anal. Tech. 1, 835–856.

Brey, T., Clarke, A., 1993. Population dynamics of marine benthic invertebrates in Antarctic and subantarctic environments: are there unique adaptations? Antarct. Sci. 5. doi:10.1017/S0954102093000343

Brey, T., Dahm, C., Gorny, M., Klages, M., Stiller, M., Arntz, W.E., 1996. Do Antarctic benthic invertebrates show an extended level of eurybathy? Antarct. Sci. 8. doi:10.1017/S0954102096000028

Brey, T., Mackensen, A., 1997. Stable isotopes prove shell growth bands in the Antarctic bivalve *Laternula elliptica* to be formed annually. Polar Biol. 17, 465–468.

Brey, T., Voigt, M., Jenkins, K., Ahn, I.-Y., 2011. The bivalve Laternula elliptica at King George Island — A biological recorder of climate forcing in the West Antarctic Peninsula region. J. Mar. Syst. 88, 542–552. doi:10.1016/j.jmarsys.2011.07.004

Briffa, K.R., 1995. Interpreting high-resolution proxy climate data — The example of dendroclimatology, in: Analysis of climate variability. Springer Berlin Heidelberg, pp. 77–94.

Briffa, K.R., 1999. Interpreting high-resolution proxy climate data - The example of dendroclimatology, in: Analysis of climate variability - Applications of statistical techniques. Springer, Berlin, New York, pp. 77–94.

Briffa, K.R., Jones, P.D., 1990. Basic chronology statistics and assessment, in: Methods of dendrochronology. Kluwer Academic Publishers, Dordrecht, pp. 137–152.

Briffa, K.R., Jones, P.D., Bartholin, T.S., Eckstein, D., Schweingruber, F.H., Karlen, W., Zetterberg, P., Eronen, M., 1992. Fennoscandian summers from AD 500: temperature changes on short and long timescales. Clim. Dyn. 7, 111–119.

Briffa, K.R., Jones, P.D., Schweingruber, F.H., Karlen, W., Shiyatov, S.G., 1996. Tree-ring variables as proxy-indicators: problems with low-frequency signals, in: Climatic variations and forcing mechanisms of the last 2000 years. Springer, Berlin, Germany, pp. 9–41.

Brocas, W.M., Reynolds, D.J., Butler, P.G., Richardson, C.A., Scourse, J.D., Ridgway, I.D., Ramsay, K., 2013. The dog cockle, *Glycymeris glycymeris* (L.), a new annually-resolved sclerochronological archive for the Irish Sea. Palaeogeogr. Palaeoclimatol. Palaeoecol. 373, 133–140. doi:10.1016/j.palaeo.2012.03.030

Brown, K.M., Fraser, K.P.P., Barnes, D.K.A., Peck, L.S., 2004. Links between the structure of an Antarctic shallow-water community and ice-scour frequency. Oecologia 141, 121–129. doi:10.1007/s00442-004-1648-6

Bušelić, I., Peharda, M., Reynolds, D.J., Butler, P.G., González, A.R., Ezgeta-Balić, D., Vilibić, I., Grbec, B., Hollyman, P., Richardson, C.A., 2015. *Glycymeris bimaculata* (Poli, 1795) — A new sclerochronological archive for the Mediterranean? J. Sea Res. 95, 139–148. doi:10.1016/j.seares.2014.07.011

Butler, P.G., Richardson, C.A., Scourse, J.D., Wanamaker, A.D., Shammon, T.M., Bennell, J.D., 2010. Marine climate in the Irish Sea: analysis of a 489-year marine master chronology derived from growth increments in the shell of the clam *Arctica islandica*. Quat. Sci. Rev. 29, 1614–1632. doi:10.1016/j.quascirev.2009.07.010

Butler, P.G., Richardson, C.A., Scourse, J.D., Witbaard, R., Schöne, B.R., Fraser, N.M., Wanamaker, A.D., Bryant, C.L., Harris, I., Robertson, I., 2009. Accurate increment identification and the spatial extent of the common signal in five *Arctica islandica* chronologies from the Fladen Ground, northern North Sea. Paleoceanography 24, n/a-n/a. doi:10.1029/2008PA001715

Butler, P.G., Wanamaker, A.D., Scourse, J.D., Richardson, C.A., Reynolds, D.J., 2011. Long-term stability of δ13C with respect to biological age in the aragonite shell of mature specimens of the bivalve mollusk *Arctica islandica*. Palaeogeogr. Palaeoclimatol. Palaeoecol. 302, 21–30. doi:10.1016/j.palaeo.2010.03.038

Cerrano, C., Bavestrello, G., Calcinai, B., Cattaneo-Vietti, R., Chiantore, M., Guidetti, M., Sarà, A., 2001. Bioerosive processes in Antarctic seas. Polar Biol. 24, 790–792. doi:10.1007/s003000100294

Clark, G.R., 1968. Mollusk shell: daily growth lines. Science 161, 800–802.

Clark, G.R., 1974. Growth lines in invertebrate skeletons. Annu. Rev. Earth Planet. Sci. 2, 77.

Clarke, A., 1988. Seasonality in the Antarctic marine environment. Comp. Biochem. Physiol. B Biochem. Mol. Biol. 90B, 461–473.

Clarke, A., Holmes, L.J., White, M.G., 1988. The annual cycle of temperature, chlorophyll and major nutrients at Signy Island, South Orkney Islands, 1969-82. Br. Antarct. Surv. Bull. 80, 65–86.

Clarke, A., Leakey, R.J.G., 1996. The seasonal cycle of phytoplankton, macronutrients, and the microbial community in a nearshore Antarctic marine ecosystem. Limnol. Oceanogr. 1281–1294.

Clarke, A., Meredith, M.P., Wallace, M.I., Brandon, M.A., Thomas, D.N., 2008. Seasonal and interannual variability in temperature, chlorophyll and macronutrients in northern Marguerite Bay, Antarctica. Deep Sea Res. Part II Top. Stud. Oceanogr. 55, 1988–2006. doi:10.1016/j.dsr2.2008.04.035

Clarke, A., Murphy, E.J., Meredith, M.P., King, J.C., Peck, L.S., Barnes, D.K.., Smith, R.C., 2007. Climate change and the marine ecosystem of the western Antarctic Peninsula. Philos. Trans. R. Soc. B Biol. Sci. 362, 149–166. doi:10.1098/rstb.2006.1958

Clarke, A., Peck, L.S., 1991. The physiology of polar marine zooplankton. Polar Res. 10, 355–370. doi:10.1111/j.1751-8369.1991.tb00659.x

Comiso, J.C., 2012. Large Decadal Decline of the Arctic Multiyear Ice Cover. J. Clim. 25, 1176–1193. doi:10.1175/JCLI-D-11-00113.1

Connolley, W.M., 2002. Long-term variation of the Antarctic Circumpolar Wave. J. Geophys. Res. 108. doi:10.1029/2000JC000380

Constable, A.J., Melbourne-Thomas, J., Corney, S.P., Arrigo, K.R., Barbraud, C., Barnes, D.K.A., Bindoff, N.L., Boyd, P.W., Brandt, A., Costa, D.P., Davidson, A.T., Ducklow, H.W., Emmerson, L., Fukuchi, M., Gutt, J., Hindell, M.A., Hofmann, E.E., Hosie, G.W., Iida, T., Jacob, S., Johnston, N.M., Kawaguchi, S., Kokubun, N., Koubbi, P., Lea, M.-A., Makhado, A., Massom, R.A., Meiners, K., Meredith, M.P., Murphy, E.J., Nicol, S., Reid, K., Richerson, K., Riddle, M.J., Rintoul, S.R., Smith, W.O., Southwell, C., Stark, J.S., Sumner, M., Swadling, K.M., Takahashi, K.T., Trathan, P.N., Welsford, D.C., Weimerskirch, H., Westwood, K.J., Wienecke, B.C., Wolf-Gladrow, D., Wright, S.W., Xavier, J.C., Ziegler, P., 2014. Climate change and Southern Ocean ecosystems I: how changes in physical habitats directly affect marine biota. Glob. Change Biol. 20, 3004–3025. doi:10.1111/gcb.12623

Convey, P., Chown, S.L., Clarke, A., Barnes, D.K., Bokhorst, S., Cummings, V., Ducklow, H.W., Frati, F., Green, T.G., Gordon, S., others, 2014. The spatial structure of Antarctic biodiversity. Ecol. Monogr. 84, 203–244.

Cook, A.J., Holland, P.R., Meredith, M.P., Murray, T., Luckman, A., Vaughan, D.G., 2016. Ocean forcing of glacier retreat in the western Antarctic Peninsula. Science 353, 283–286. doi:10.1126/science.aae0017

Cook, E.R., 1985. A time series analysis approach to tree ring standardization. University of Arizona, School of Renewable Natural Resources, Arizona, USA.

Cook, E.R., Briffa, K., Shiyatov, S., Mazepa, V., Jones, P.D., 1980. Data analysis, in: Methods in Dendrochronology, Applications in the Environmental Sciences. Springer Netherlands, pp. 97–162.

Cook, E.R., Briffa, K., Meko, D., Graybill, D., Funkhouser, G., 1995. The "segment length curse" in long tree-ring chronology development for palaeoclimatic studies. The Holocene 5, 229–237. doi:10.1177/095968369500500211

Cook, E.R., Briffa, K., Shivatoc, S., Mazepa, V., 1990. Tree-ring standardization and growth-trend estimation, in: Methods in dendrochronology: application in the environmental sciences. Kluwer Academic Publishers, Dordrecht, Netherlands, pp. 104–123.

Cook, E.R., Krusic, P.J., 2007. Program ARSTAN - A tree-ring standardization program based on detrending and autoregressive time series modelling, with interactive graphics.

Cook, E.R., Peters, K., 1997. Calculating unbiased tree-ring indices for the study of climatic and environmental change. The Holocene 7, 361–370. doi:10.1177/095968369700700314

Cook, E.R., Peters, K., 1981. The smoothing spline: A new approach to standardizing forest interior tree-ring width series for dendroclimatic studies. Tree-Ring Bull. 41, 45–53.

Cunningham, S.A., 2005. Southern ocean circulation. Arch. Nat. Hist. 32, 265–280.

Datos climatologicos y geomagneticos Islas Orcadas del Sur. Periodo 1903 - 1950 (No. 11), 1951. , B. Direccion general del servicio meteorologico nacional, Argentina.

Davenport, J., 1988. The feeding mechanism of *Yoldia* (= *Aequiyoldia*) *eightsi* (Courthouy). Proc. R. Soc. Lond. B Biol. Sci. 232, 431–442.

Davenport, J., 1989. Feeding, oxygen uptake, ventilation rate and shell growth in the Antarctic protobranch bivalve mollusc *Yoldia eightsi* (Courthouy). Proc. Br. Antarct. Surv. Spec. Top. Award Scheme Symp. 57–63.

Dell, R.K., 1990. Antarctic Mollusca. R. Soc. N. Z. Bull. 27, 1–311.

DeLong, K.L., Quinn, T.M., Taylor, F.W., Shen, C.-C., Lin, K., 2013. Improving coral-base paleoclimate reconstructions by replicating 350years of coral Sr/Ca variations. Palaeogeogr. Palaeoclimatol. Palaeoecol. 373, 6–24. doi:10.1016/j.palaeo.2012.08.019

Dettman, D.L., Reische, A.K., Lohmann, K.C., 1999. Controls on the stable isotope composition of seasonal growth bands in aragonitic fresh-water bivalves (unionidae). Geochim. Cosmochim. Acta 63, 1049–1057. doi:10.1016/S0016-7037(99)00020-4

Dierssen, H.M., Smith, R.C., Vernet, M., 2002. Glacial meltwater dynamics in coastal waters west of the Antarctic peninsula. Proc. Natl. Acad. Sci. 99, 1790–1795.

Dunlop, K.M., Barnes, D.K.A., Bailey, D.M., 2014. Variation of scavenger richness and abundance between sites of high and low iceberg scour frequency in Ryder Bay, west Antarctic Peninsula. Polar Biol. 37, 1741–1754. doi:10.1007/s00300-014-1558-y

Elliot, M., deMenocal, P.B., Linsley, B.K., Howe, S.S., 2003. Environmental controls on the stable isotopic composition of *Mercenaria mercenaria* : Potential application to paleoenvironmental studies: isotopic composition of *M. mercenaria*. Geochem. Geophys. Geosystems 4. doi:10.1029/2002GC000425

Esper, J., Cook, E.R., Krusic, P.J., Kenneth, P., 2003. Tests of the RCS method for preserving low-frequency varibility in long tree-ring chronologies. Tree-Ring Res. 59, 81–98.

Esper, J., Frank, D., Büntgen, U., Kirdyanov, A., 2009. Influence of pith offset on tree-ring chronology trend. Trace 7, 205–210.

Fahrbach, E., Hoppema, M., Rohardt, G., Schroeder, M., Wisotzki, A., 2004. Decadal-scale variations of water mass properties in the deep Weddell Sea. Ocean Dyn. 54, 77–91. doi:10.1007/s10236-003-0082-3

Foster, T.D., Carmack, E.C., 1976. Frontal zone mixing and Antarctic Bottom water formation in the southern Weddell Sea. Deep Sea Res. Oceanogr. Abstr. 23, 301–317. doi:10.1016/0011-7471(76)90872-X

Freitas, P.S., Clarke, L.J., Kennedy, H., Richardson, C.A., 2012. The potential of combined Mg/Ca and δ18O measurements within the shell of the bivalve *Pecten maximus* to estimate seawater δ18O composition. Chem. Geol. 291, 286–293. doi:10.1016/j.chemgeo.2011.10.023

Gazeau F., Parker, L.M., Comeau, S., Gattuso, J-P., O'Connor, W.A., Martin, S., Pörtner H-O., Ross, P.M., 2013. Impacts of ocean acidification on marine shelled molluscs. Mar. Biol. 160: 2207-2245. Doi: 10.1007/s00227-013-2219-3

Gardner, A.S., Moholdt, G., Cogley, J.G., Wouters, B., Arendt, A.A., Wahr, J., Berthier, E., Hock, R., Pfeffer, W.T., Kaser, G., Ligtenberg, S.R.M., Bolch, T., Sharp, M.J., Hagen, J.O., van den

Broeke, M.R., Paul, F., 2013. A reconciled estimate of glacier contributions to sea level rise: 2003 to 2009. Science 340, 852–857. doi:10.1126/science.1234532

Ghil, M., Allen, M.R., Dettinger, M.D., Ide, K., Kondrashov, D., Mann, M.E., Robertson, A.W., Saunders, A., Tian, Y., Varadi, F., others, 2002. Advanced spectral methods for climatic time series. Rev. Geophys. 40.

Gilbert, N.S., 1991. Microphytobenthic seasonality in near-shore marine sediments at Signy Island, South Orkney Islands, Antarctica. Estuar. Coast. Shelf Sci. 33, 89–104.

Gilkinson, K.D., Hutchings, J.A., Oshel, P.E., Haedrich, R.L., 1986. Shell microstructure and observations on internal banding patterns in the bivalves *Yoldia thraciaeformis* Storer, 1838, and Nuculana pernula Muller, 1779 (Nuculanidae), from a deep-sea environment. The Veliger 29, 70–77.

Gillett, N.P., Stone, D.A., Stott, P.A., Nozawa, T., Karpechko, A.Y., Hegerl, G.C., Wehner, M.F., Jones, P.D., 2008. Attribution of polar warming to human influence. Nat. Geosci. 1, 750–754. doi:10.1038/ngeo338

Gillett, N.P., Thompson, D.W., 2003. Simulation of recent Southern Hemisphere climate change. Science 302, 273–275.

Gillikin, D.P., De Ridder, F., Ulens, H., Elskens, M., Keppens, E., Baeyens, W., Dehairs, F., 2005. Assessing the reproducibility and reliability of estuarine bivalve shells (*Saxidomus giganteus*) for sea surface temperature reconstruction: Implications for paleoclimate studies. Palaeogeogr. Palaeoclimatol. Palaeoecol. 228, 70–85. doi:10.1016/j.palaeo.2005.03.047

Gillikin, D.P., Lorrain, A., Bouillon, S., Willenz, P., Dehairs, F., 2006. Stable carbon isotopic composition of *Mytilus edulis* shells: relation to metabolism, salinity, δ13CDIC and phytoplankton. Org. Geochem. 37, 1371–1382. doi:10.1016/j.orggeochem.2006.03.008

Gillikin, D.P., Lorrain, A., Meng, L., Dehairs, F., 2007. A large metabolic carbon contribution to the δ13C record in marine aragonitic bivalve shells. Geochim. Cosmochim. Acta 71, 2936–2946. doi:10.1016/j.gca.2007.04.003

Goman, M., Ingram, B.L., Strom, A., 2008. Composition of stable isotopes in geoduck (*Panopea abrupta*) shells: a preliminary assessment of annual and seasonal paleoceanographic changes in the northeast Pacific. Quat. Int. 188, 117–125.

Goodwin, D.H., Schöne, B.R., Dettman, D.L., 2003. Resolution and fidelity of oxygen isotopes as paleotemperature proxies in bivalve mollusk shells: models and observations. Palaios 18, 110–125.

Gordon, A.L., 1982. Weddell Deep Water variability. J. Mar. Res. 40, 199–217.

Gordon, A.L., Visbeck, M., Comiso, J.C., 2007. A Possible Link between the Weddell Polynya and the Southern Annular Mode*. J. Clim. 20, 2558–2571. doi:10.1175/JCLI4046.1

Gordon, L., Codispoti, L., Jennings, J., Millero, F., Morrison, J., Sweeney, C., 2000. Seasonal evolution of hydrographic properties in the Ross Sea, Antarctica, 1996–1997. Deep Sea Res. Part II Top. Stud. Oceanogr. 47, 3095–3117. doi:10.1016/S0967-0645(00)00060-6

Grossman, E.L., Ku, T.-L., 1986. Oxygen and carbon isotope fractionation in biogenic aragonite: Temperature effects. Chem. Geol. Isot. Geosci. Sect. 59, 59–74. doi:10.1016/0168-9622(86)90057-6

Gutt, J., Barratt, I., Domack, E., d'Acoz, C. d'Udekem, Dimmler, W., Grémare, A., Heilmayer, O., Isla, E., Janussen, D., Jorgensen, E., others, 2011. Biodiversity change after climate-induced ice-shelf collapse in the Antarctic. Deep Sea Res. Part II Top. Stud. Oceanogr. 58, 74–83.

Gutt, J., Bertler, N., Bracegirdle, T.J., Buschmann, A., Comiso, J., Hosie, G., Isla, E., Schloss, I.R., Smith, C.R., Tournadre, J., Xavier, J.C., 2015. The Southern Ocean ecosystem under multiple climate change stresses - an integrated circumpolar assessment. Glob. Change Biol. 21, 1434–1453. doi:10.1111/gcb.12794

Gutt, J., Cape, M., Dimmler, W., Fillinger, L., Isla, E., Lieb, V., Lund?lv, T., Pulcher, C., 2013. Shifts in Antarctic megabenthic structure after ice-shelf disintegration in the Larsen area east of the Antarctic Peninsula. Polar Biol. 36, 895–906. doi:10.1007/s00300-013-1315-7

Gutt, J., Starmans, A., 2002. Quantification of iceberg impact and benthic recolonisation patterns in the Weddell Sea (Antarctica), in: Arntz, W.E., Clarke, A. (Eds.), Ecological Studies in the Antarctic Sea Ice Zone. Springer Berlin Heidelberg, Berlin, Heidelberg, pp. 210–214. doi:10.1007/978-3-642-59419-9_27

Halfar, J., Hetzinger, S., Adey, W., Zack, T., Gamboa, G., Kunz, B., Williams, B., Jacob, D.E., 2011. Coralline algal growth-increment widths archive North Atlantic climate variability. Palaeogeogr. Palaeoclimatol. Palaeoecol. 302, 71–80. doi:10.1016/j.palaeo.2010.04.009

Harangozo, S.A., 2000. A search for ENSO teleconnections in the west Antarctic Peninsula climate in austral winter. Int. J. Climatol. 20, 663–679. doi:10.1002/(SICI)1097-0088(200005)20:6<663::AID-JOC493>3.0.CO;2-I

Harper, E.M., Clark, M.S., Hoffman, J.I., Philipp, E.E.R., Peck, L.S., Morley, S.A., 2012. Iceberg scour and shell damage in the Antarctic bivalve *Laternula elliptica*. PLoS ONE 7, e46341. doi:10.1371/journal.pone.0046341

Harper, E.M., Peck, L., 2003. Predatory behaviour and metabolic costs in the Antarctic muricid gastropod *Trophon longstaffi*. Polar Biol. 26, 208–217.

Held, C., Waegele, J.W., 2005. Cryptic speciation in the giant Antarctic isopod *Glyptonotus antarcticus* (Isopoda: Valvifera: Chaetiliidae)*. Sci. Mar. 69, 175–181.

Hendy, E.J., Gagan, M.K., Lough, J.M., 2003. Chronological control of coral records using luminescent lines and evidence for non-stationary ENSO teleconnections in northeast Australia. The Holocene 13, 187–199. doi:10.1191/0959683603hl606rp

Henley, S.F., Annett, A.L., Ganeshram, R.S., Carson, D.S., Weston, K., Crosta, X., Tait, A., Dougans, J., Fallick, A.E., Clarke, A., 2012. Factors influencing the stable carbon isotopic composition of suspended and sinking organic matter in the coastal Antarctic sea ice environment. Biogeosciences 9, 1137–1157. doi:10.5194/bg-9-1137-2012

Hofmann, E.E., Klinck, J.M., 1998. Thermohaline variability of the waters overlying the west Antarctic Peninsula continental shelf. Antarct. Res. Ser. 75, 67–81.

Holland, D.M., 2001. Explaining the Weddell Polynya--a Large Ocean Eddy Shed at Maud Rise. Science 292, 1697–1700. doi:10.1126/science.1059322

Holland, M.M., Bitz, C.M., Hunke, E.C., 2005. Mechanims forcing an Antarctic dipole in simulated sea ice and surface ocean conditions. J. Clim. 18, 2052–2066. doi:10.1175/JCLI3396.1

Hollyman, P., Chenery, S.R., Righton, D., Richardson, C.A., 2014. Timing of growth line formation in accreted structures of the whelk *Buccinum undatum*. doi:10.13140/2.1.4356.5446

Holmes, R.L., Adams, R.K., Fritts, H.C., 1986. Tree-ring chronologies of western north America: California, Eastern Oregon and Northern Great Basin with procedures used in the chronology development work including users manuals for computer programs COFECHA and ARSTAN. Laboratory of Tree-Ring Research, University of Arizona (Tucson, AZ), Arizona, USA.

Ivany, L.C., Brey, T., Huber, M., Buick, D.P., Schöne, B.R., 2011. El Niño in the Eocene greenhouse recorded by fossil bivalves and wood from Antarctica: EOCENE EL NIÑO. Geophys. Res. Lett. 38, n/a-n/a. doi:10.1029/2011GL048635

Jacobs, S., 2006. Observations of change in the Southern Ocean. Philos. Trans. R. Soc. Math. Phys. Eng. Sci. 364, 1657–1681. doi:10.1098/rsta.2006.1794

Jacobs, S.S., Giulivi, C.F., Mele, P.A., 2002. Freshening of the Ross Sea during the late 20th century. Science 297, 386–389.

Jones, D.S., 1983. Sclerochronology: reading the record of the molluscan shell: annual growth increments in the shells of bivalve molluscs record marine climatic changes and reveal surprising longevity. Am. Sci. 71, 384–391.

Jones, D.S., Williams, D.F., Arthur, M.A., 1983. Growth history and ecology of the Atlantic surf clam, *Spisula solidissima* (Dillwyn), as revealed by stable isotopes and annual shell increments. J. Exp. Mar. Biol. Ecol. 73, 225–242.

Jones, M.E., Fenton, M., Meredith, M.P., Clargo, N.M., Ossebaar, S., Ducklow, H.W., Venables, H.J., de Baar, H.J.W., 2017. Ocean acidification and calcium carbonate saturation states in the coastal zone of the West Antarctic Peninsula. Deep-Sea Res. II 139, 181-194. doi: 10.1016/j.dsr2.2017.01.007

Keith, M.L., Anderson, G.M., Eichler, R., 1964. Carbon and oxygen isotopic composition of mollusk shells from marine and fresh-water environments. Geochim. Cosmochim. Acta 28, 1757–1786.

Klinck, J.M., Hofmann, E.E., Beardsley, R.C., Salihoglu, B., Howard, S., 2004. Water-mass properties and circulation on the west Antarctic Peninsula Continental Shelf in Austral Fall and Winter 2001. Deep Sea Res. Part II Top. Stud. Oceanogr. 51, 1925–1946. doi:10.1016/j.dsr2.2004.08.001

Korb, R.E., Whitehouse, M.J., Thorpe, S.E., Gordon, M., 2005. Primary production across the Scotia Sea in relation to the physico-chemical environment. J. Mar. Syst. 57, 231–249. doi:10.1016/j.jmarsys.2005.04.009

Korb, R.E., Whitehouse, M.J., Ward, P., 2004. SeaWiFS in the southern ocean: spatial and temporal variability in phytoplankton biomass around South Georgia. Deep Sea Res. Part II Top. Stud. Oceanogr. 51, 99–116. doi:10.1016/j.dsr2.2003.04.002

Krantz, D.E., Williams, D.F., Jones, D.S., 1987. Ecological and paleoenvironmental information using stable isotope profiles from living and fossil molluscs. Palaeogeogr. Palaeoclimatol. Palaeoecol. 58, 249–266.

Kukal, O., Heinrich, B., Duman, J.G., 1988. Behavioural thermoregulation in the freeze-tolerant Arctic caterpillar, Gynaephora groenlandica. J. Exp. Biol. 138, 181–193.

Kwok, R., Comiso, J.C., 2002. Southern Ocean climate and sea ice anomalies associated with the Southern Oscillation. J. Clim. 15, 487–501.

Lartaud, F., Chauvaud, L., Richard, J., Toulot, A., Bollinger, C., Testut, L., Paulet, Y-M., 2010. Experimental growth pattern calibration of Antarctic scallop shells (*Adamussium colbecki*, Smith 1902) to provide a biogenic archive of high-resolution records of environmental and climatic changes. J. Exp. Mar. Bio. Ecol. 393: 158-167. doi: 10.1016/j.jembe.2010.07.016

Li, Z.X., 2000. Influence of tropical Pacific El Niño on the SST of the Southern Ocean Through Atmospheric Bridge. Geophys. Res. Lett. 27, 3505–3508. doi:10.1029/1999GL011182

Liu, J., Yuan, X., Rind, D., Martinson, D.G., 2002. Mechanism study of the ENSO and southern high latitude climatic teleconnections. Geophys. Res. Lett. 29, 1679. doi:10.1029/2002GL015143

Lorrain, A., Paulet, Y.-M., Chauvaud, L., Dunbar, R., Mucciarone, D., Fontugne, M., 2004. δ13C variation in scallop shells: Increasing metabolic carbon contribution with body size? Geochim. Cosmochim. Acta 68, 3509–3519. doi:10.1016/j.gca.2004.01.025

Mäkinen, H., Vanninen, P., 1999. Effect of sample selection on the environmental signal derived from tree-ring series. For. Ecol. Manag. 113, 83–89. doi:10.1016/S0378-1127(98)00416-2

Mann, M.E., Lees, J.M., 1996. Robust estimation of background noise and signal detection in climatic time series. Clim. Change 33, 409–445.

Marshall, G.J., 2003. Trends in the Southern Annular Mode from observations and reanalyses. J. Clim. 16, 4134–4143. doi:http://dx.doi.org/10.1175/1520-0442(2003)016<4134:TITSAM>2.0.CO;2

Marshall, G.J., 2007. Half-century seasonal relationships between the Southern Annular mode and Antarctic temperatures. Int. J. Climatol. 27, 373–383. doi:10.1002/joc.1407

Marshall, G.J., Connolley, W.M., 2006. Effect of changing Southern Hemisphere winter sea surface temperatures on Southern Annular Mode strength. Geophys. Res. Lett. 33. doi:10.1029/2006GL026627

Martinson, D.G., Iannuzzi, R.A., 2003. Spatial/temporal patterns in Weddell gyre characteristics and their relationship to global climate. J. Geophys. Res. 108. doi:10.1029/2000JC000538

Martinson, D.G., McKee, D.C., 2012. Transport of warm Upper Circumpolar Deep Water onto the western Antarctic Peninsula continental shelf. Ocean Sci. 8, 433–442. doi:10.5194/os-8-433-2012

Martinson, D.G., Stammerjohn, S.E., Iannuzzi, R.A., Smith, R.C., Vernet, M., 2008. Western Antarctic Peninsula physical oceanography and spatio–temporal variability. Deep Sea Res. Part II Top. Stud. Oceanogr. 55, 1964–1987. doi:10.1016/j.dsr2.2008.04.038

Massom, R.A., Stammerjohn, S.E., 2010. Antarctic sea ice change and variability – Physical and ecological implications. Polar Sci. 4, 149–186. doi:10.1016/j.polar.2010.05.001

McClintock, J.B., Angus, R.A., McDonald, M.R., Amsler, C.D., Catledge, S.A., Vohra, Y.K., 2009. Rapid dissolution of shells of weakly calcified Antarctic benthic macroorganisms indicates high vulnerability to ocean acidification. Antarct. Sci. 21(5), 449-456. Doi:10.1017/S0954102009990198

McConnaughey, T., 1989. 13C and 18O isotopic disequilibrium in biological carbonates: I. Patterns. Geochim. Cosmochim. Acta 53, 151–162. doi:10.1016/0016-7037(89)90282-2

McConnaughey, T.A., Burdett, J., Whelan, J.F., Paull, C.K., 1997. Carbon isotopes in biological carbonates: Respiration and photosynthesis. Geochim. Cosmochim. Acta 61, 611–622. doi:10.1016/S0016-7037(96)00361-4

McConnaughey, T.A., Gillikin, D.P., 2008. Carbon isotopes in mollusk shell carbonates. Geo-Mar. Lett. 28, 287–299. doi:10.1007/s00367-008-0116-4

McKenzie, J.A., 1985. Carbon isotopes and productivity in the lacustrine and marine environment, in: Chemical Processes in Lakes. Wiley-Interscience, New York, pp. 99–118.

McNeil, B.I., Matear, R.J., 2008. Southern Ocean acidification: A tipping point at 450-ppm atmospheric CO_2. Proc. Natl. Acad. Sci. USA 105(48): 18860-18864. doi: 10.1073/pnas.0806318105

Meehl, G.A., Arblaster, J.M., Bitz, C.M., Chung, C.T.Y., Teng, H., 2016. Antarctic sea-ice expansion between 2000 and 2014 driven by tropical Pacific decadal climate variability. Nat. Geosci. 9, 590–595. doi:10.1038/ngeo2751

Meredith, M.P., Brandon, M.A., Murphy, E.J., Trathan, P.N., Thorpe, S.E., Bone, D.G., Chernyshkov, P.P., Sushin, V.A., 2005. Variability in hydrographic conditions to the east and northwest of South Georgia, 1996?2001. J. Mar. Syst. 53, 143–167. doi:10.1016/j.jmarsys.2004.05.005

Meredith, M.P., Brandon, M.A., Wallace, M.I., Clarke, A., Leng, M.J., Renfrew, I.A., van Lipzig, N.P.M., King, J.C., 2008a. Variability in the freshwater balance of northern Marguerite Bay, Antarctic Peninsula: Results from δ18O. Deep Sea Res. Part II Top. Stud. Oceanogr. 55, 309–322. doi:10.1016/j.dsr2.2007.11.005

Meredith, M.P., King, J.C., 2005. Rapid climate change in the ocean west of the Antarctic Peninsula during the second half of the 20th century. Geophys. Res. Lett. 32, L19604. doi:10.1029/2005GL024042

Meredith, M.P., Murphy, E.J., Hawker, E.J., King, J.C., Wallace, M.I., 2008b. On the interannual variability of ocean temperatures around South Georgia, Southern Ocean: Forcing by El Niño/Southern Oscillation and the Southern Annular Mode. Deep Sea Res. Part II Top. Stud. Oceanogr. 55, 2007–2022. doi:10.1016/j.dsr2.2008.05.020

Meredith, M.P., Nicholls, K.W., Renfrew, I.A., Boehme, L., Biuw, M., Fedak, M., 2011. Seasonal evolution of the upper-ocean adjacent to the South Orkney Islands, Southern Ocean: Results from a "lazy biological mooring." Deep Sea Res. Part II Top. Stud. Oceanogr. 58, 1569–1579. doi:10.1016/j.dsr2.2009.07.008

Meredith, M.P., Renfrew, I.A., Clarke, A., King, J.C., Brandon, M.A., 2004. Impact of the 1997/98 ENSO on upper ocean characteristics in Marguerite Bay, western Antarctic Peninsula. J. Geophys. Res. 109. doi:10.1029/2003JC001784

Meredith, M.P., Stammerjohn, S.E., Venables, H.J., Ducklow, H.W., Martinson, D.G., Iannuzzi, R.A., Leng, M.J., van Wessem, J.M., Reijmer, C.H., Barrand, N.E., 2017. Changing distributions of sea ice melt and meteoric water west of the Antarctic Peninsula. Deep Sea Res. Part II Top. Stud. Oceanogr. 139, 40–57. doi:10.1016/j.dsr2.2016.04.019

Meredith, M.P., Wallace, M.I., Stammerjohn, S.E., Renfrew, I.A., Clarke, A., Venables, H.J., Shoosmith, D.R., Souster, T., Leng, M.J., 2010. Changes in the freshwater composition of the upper ocean west of the Antarctic Peninsula during the first decade of the 21st century. Prog. Oceanogr. 87, 127–143. doi:10.1016/j.pocean.2010.09.019

Mette, M.J., Wanamaker, A.D., Carroll, M.L., Ambrose, W.G., Retelle, M.J., 2016. Linking large-scale climate variability with *Arctica islandica* shell growth and geochemistry in northern Norway: Linking climate and shell records in Norway. Limnol. Oceanogr. 61, 748–764. doi:10.1002/lno.10252

Milano, S., Schöne, B.R., Witbaard, R., 2017. Changes of shell microstructural characteristics of *Cerastoderma edule* (Bivalvia) — A novel proxy for water temperature. Palaeogeogr. Palaeoclimatol. Palaeoecol. 465, 395–406. doi:10.1016/j.palaeo.2015.09.051

Mitchell, V.L., 1967. An investigation of certain aspects of tree growth rates in relation to climate in the central Canadian boreal forest, University of Winsonsin, Dept. Meteorology. ed, Technical report. Madison, USA.

Mitchell, B.G., Holm-Hansen, O., 1991. Observations and modeling of the Antarctic phytoplankton crop in relation to mixing depth. Deep Sea Res. 34, 981–1007.

Moffat, C., Beardsley, R.C., Owens, B., van Lipzig, N., 2008. A first description of the Antarctic Peninsula Coastal Current. Deep Sea Res. Part II Top. Stud. Oceanogr. 55, 277–293. doi:10.1016/j.dsr2.2007.10.003

Moffat, C., Owens, B., Beardsley, R.C., 2009. On the characteristics of Circumpolar Deep Water intrusions to the west Antarctic Peninsula Continental Shelf. J. Geophys. Res. 114. doi:10.1029/2008JC004955

Montes-Hugo, M., Doney, S.C., Ducklow, H.W., Fraser, W., Martinson, D., Stammerjohn, S.E., Schofield, O., 2009. Recent Changes in Phytoplankton Communities Associated with Rapid Regional Climate Change Along the Western Antarctic Peninsula. Science 323, 1470–1473. doi:10.1126/science.1164533

Moore, G.W.K., Alverson, K., Renfrew, I.A., 2002. A reconstruction of the air-sea interaction associated with the Weddell Polynya. J. Phys. Oceanogr. 32, 1685–1698.

Morewood, W.D., Ring, R.A., 1998. Revision of the life history of the High Arctic moth *Gynaephora groenlandica* (Wocke) (Lepidoptera: Lymantriidae). Can. J. Zool. 76, 1371–1381.

Motoi, T., Ono, N.B., Wakatsuchi, M., 1987. A Mechanism for the Formation of the Weddell Polynya in 1974. J. Phys. Oceanogr. 17, 2241–2247. doi:10.1175/1520-0485(1987)017<2241:AMFTFO>2.0.CO;2

Murphy, E.J., Clarke, A., Abram, N.J., Turner, J., 2014. Variability of sea-ice in the northern Weddell Sea during the 20th century. J. Geophys. Res. Oceans 119, 4549–4572. doi:10.1002/2013JC009511

Murphy, E.J., Clarke, A., Symon, C., Priddle, J., 1995. Temporal variation in Antarctic sea-ice: analysis of a long term fast-ice record from the South Orkney Islands. Deep Sea Res. Part Oceanogr. Res. Pap. 42, 1045–1062.

Murphy, E.J., Hofmann, E.E., Watkins, J.L., Johnston, N.M., Piñones, A., Ballerini, T., Hill, S.L., Trathan, P.N., Tarling, G.A., Cavanagh, R.A., Young, E.F., Thorpe, S.E., Fretwell, P., 2013. Comparison of the structure and function of Southern Ocean regional ecosystems: The Antarctic Peninsula and South Georgia. J. Mar. Syst. 109–110, 22–42. doi:10.1016/j.jmarsys.2012.03.011

Murphy, E.J., Trathan, P.N., Watkins, J.L., Reid, K., Meredith, M.P., Forcada, J., Thorpe, S.E., Johnston, N.M., Rothery, P., 2007. Climatically driven fluctuations in Southern Ocean ecosystems. Proc. R. Soc. B Biol. Sci. 274, 3057–3067. doi:10.1098/rspb.2007.1180

Nolan, C.P., Clarke, A., 1993. Growth in the bivalve *Yoldia eightsi* at Signy Island, Antarctica, determined from internal shell increments and calcium-45 incorporation. Mar. Biol. 117, 243–250.

Orsi, A.H., Johnson, G.C., Bullister, J.L., 1999. Circulation, mixing, and production of Antarctic Bottom Water. Prog. Oceanogr. 43, 55–109.

Orsi, A.H., Nowlin, W.D., Whitworth, T., 1993. On the circulation and stratification of the Weddell Gyre. Deep Sea Res. Part Oceanogr. Res. Pap. 40, 169–203. doi:10.1016/0967-0637(93)90060-G

Orsi, A.H., Smethie, W.M.J., Bullister, J.L., 2002. On the total input of Antarctic waters to the deep ocean: A preliminary estimate from chlorofluorocarbon measurements. J. Geophys. Res. 107. doi:10.1029/2001JC000976

Orsi, A.H., Whitworth, T., Nowlin, W.D., 1995. On the meridional extent and fronts of the Antarctic Circumpolar Current. Deep Sea Res. Part Oceanogr. Res. Pap. 42, 641–673. doi:10.1016/0967-0637(95)00021-W

Owen, E.F., Wanamaker, A.D., Feindel, S.C., Schöne, B.R., Rawson, P.D., 2008. Stable carbon and oxygen isotope fractionation in bivalve (*Placopecten magellanicus*) larval aragonite. Geochim. Cosmochim. Acta 72, 4687–4698. doi:10.1016/j.gca.2008.06.029

Pannella, G., MacClintock, C., 1968. Biological and environmental rhythms reflected in molluscan shell growth. Mem. Paleontol. Soc. 64–80.

Peck, L.S., 2005. Prospects for surviving climate change in Antarctic aquatic species. Front. Zool. 2, 9.

Peck, L.S., Ansell, A.D., Webb, K.E., Hepburn, L., Burrows, M., 2004. Movements and burrowing activity in the Antarctic bivalve molluscs *Laternula elliptica* and *Yoldia eightsi*. Polar Biol. 27, 357–367. doi:10.1007/s00300-003-0588-7

Peck, L.S., Barnes, D.K.A., Cook, A.J., Fleming, A.H., Clarke, A., 2010. Negative feedback in the cold: ice retreat produces new carbon sinks in Antarctica: negative climate feedbacks in Antarctica. Glob. Change Biol. 16, 2614–2623. doi:10.1111/j.1365-2486.2009.02071.x

Peck, L.S., Brockington, S., Vanhove, S., Beghyn, M., 1999. Community recovery following catastrophic iceberg impact in a soft-sediment shallow-water site at Signy Island, Antarctica. Mar. Ecol. Prog. Ser. 186, 1–8.

Peck, L.S., Brockington, S., Brey, T., 1997. Growth and metabolism in the Antarctic brachiopod *Liothyrella uva*. Philos. Trans. R. Soc. B Biol. Sci. 352, 851–858. doi:10.1098/rstb.1997.0065

Peck, L.S., Bullough, L.W., 1993. Growth and population structure in the infaunal bivalve *Yoldia eightsi* in relation to iceberg activity at Signy Island, Antarctica. Mar. Biol. 117, 235–241.

Peck, L.S., Colman, J.G., Murray, A.W.A., 2000. Growth and tissue mass cycles in the infaunal bivalve *Yoldia eightsi* at Signy Island, Antarctica. Polar Biol. 23, 420–428.

Peck, L.S., Convey, P., Barnes, D.K.A., 2006. Environmental constraints on life histories in Antarctic ecosystems: tempos, timings and predictability. Biol. Rev. 81, 75–109. doi:10.1017/S1464793105006871

Peharda, M., Black, B.A., Purroy, A., Mihanović, H., 2016. The bivalve *Glycymeris pilosa* as a multidecadal environmental archive for the Adriatic and Mediterranean Seas. Mar. Environ. Res. 119, 79–87. doi:10.1016/j.marenvres.2016.05.022

Potter, J.R., Paren, J.G., 1985. Interaction Between Ice Shelf and Ocean in George VI Sound, Antarctica.

Prézelin, B.B., Hofmann, E.E., Moline, M., Klinck, J.M., 2004. Physical forcing of phytoplankton community structure and primary production in continental shelf waters of the Western Antarctic Peninsula. J. Mar. Res. 62, 419–460.

Rabarts, L.W., 1970. Physiological aspects of the ecology of some Antarctic lamellibranchs. British Antarctic Survey Base Report N9b/1970/H. British Antarctic Survey, Cambridge, England.

Ramsay, K., Kaiser, M.J., Richardson, C.A., Veale, L.O., Brand, A.R., 2000. Can shell scars on dog cockles (*Glycymeris glycymeris*, L.) be used as an indicator of fishing disturbance? J. Sea Res. 43, 167–176.

Rayner, N.A., Parker, D.E., Horton, E.B., Folland, C.K., Alexander, L.V., Rowell, D.P., Kent, E.C., Kaplan, A., 2003. Global analyses of sea surface temperature, sea ice, and night marine air temperature since the late nineteenth century. J. Geophys. Res. 108. doi:10.1029/2002JD002670

Reynolds, D.J., Butler, P.G., Williams, S.M., Scourse, J.D., Richardson, C.A., Wanamaker, A.D., Austin, W.E.N., Cage, A.G., Sayer, M.D.J., 2013. A multiproxy reconstruction of Hebridean (NW Scotland) spring sea surface temperatures between AD 1805 and 2010. Palaeogeogr. Palaeoclimatol. Palaeoecol. 386, 275–285. doi:10.1016/j.palaeo.2013.05.029

Reynolds, D.J., Richardson, C.A., Scourse, J.D., Butler, P.G., Hollyman, P., Román-González, A., Hall, I.R., 2017. Reconstructing North Atlantic marine climate variability using an absolutely-dated sclerochronological network. Palaeogeogr. Palaeoclimatol. Palaeoecol. 465, 333–346. doi:10.1016/j.palaeo.2016.08.006

Reynolds, D.J., Scourse, J.D., Halloran, P.R., Nederbragt, A.J., Wanamaker, A.D., Butler, P.G., Richardson, C.A., Heinemeier, J., Eiríksson, J., Knudsen, K.L., Hall, I.R., 2016. Annually resolved North Atlantic marine climate over the last millennium. Nat. Commun. 7, 13502. doi:10.1038/ncomms13502

Rhoads, D.C., Lutz, R.A. (Eds.), 1980. Skeletal growth of aquatic organisms: biological records of environmental change, Topics in geobiology. Plenum Pr, New York.

Richardson, C.A., 1988. Exogenous and endogenous rhythms of band formation in the shell of the clam *Tapes philippinarum* (Adams et Reeve, 1850). J. Exp. Mar. Biol. Ecol. 122, 105–126.

Richardson, C.A., 2001. Molluscs as archives of environmental change. Oceanogr. Mar. Biol. Annu. Rev. 39, 103–164.

Richardson, C.A., Crisp, D.J., Runham, N.W., 1980. An endogenous rhythm in shell deposition in *Cerastoderma edule*. J. Mar. Biol. Assoc. U. K. 60, 991–1004.

Ridgway, I.D., Richardson, C.A., 2010. *Arctica islandica*: the longest lived non colonial animal known to science. Rev. Fish Biol. Fish. 21, 297–310. doi:10.1007/s11160-010-9171-9

Rintoul, S.R., 2007. Rapid freshening of Antarctic Bottom Water formed in the Indian and Pacific oceans. Geophys. Res. Lett. 34. doi:10.1029/2006GL028550

Rintoul, S.R., Hughes, C., Olbers, D., 2001. The Antarctic Circumpolar Current System. Academic Press, San Diego, CA, pp. 271–302.

Robertson, R., Visbeck, M., Gordon, A.L., Fahrbach, E., 2002. Long-term temperature trends in the deep waters of the Weddell Sea. Deep Sea Res. Part II Top. Stud. Oceanogr. 49, 4791–4806.

Roman-Gonzalez, A., 2011. Climate change in the Antarctic: The search for sclerochronological proxies (MSc. dissertation). Bangor University, School of Ocean Sciences, Bangor (Gwynedd), Wales, United Kingdom.

Román-González, A., Scourse, J.D., Butler, P.G., Reynolds, D.J., Richardson, C.A., Peck, L.S., Brey, T., Hall, I.R., 2017. Analysis of ontogenetic growth trends in two marine Antarctic bivalves *Yoldia eightsi* and *Laternula elliptica*: Implications for sclerochronology. Palaeogeogr. Palaeoclimatol. Palaeoecol. 465, 300–306. doi:10.1016/j.palaeo.2016.05.004

Román-González, A., Scourse, J.D., Richardson, C.A., Peck, L.S., Bentley, M.J., Butler, P.G., 2016. A sclerochronological archive for Antarctic coastal waters based on the marine bivalve *Yoldia eightsi* (Jay, 1839) from the South Orkney Islands. The Holocene 27(2): 271-281. doi:10.1177/0959683616658525

Royer, C., Thébault, J., Chauvaud, L., Olivier, F., 2013. Structural analysis and paleoenvironmental potential of dog cockle shells (*Glycymeris glycymeris*) in Brittany, northwest France. Palaeogeogr. Palaeoclimatol. Palaeoecol. 373, 123–132. doi:10.1016/j.palaeo.2012.01.033

Sahade, R., Lagger, C., Torre, L., Momo, F., Monien, P., Schloss, I., Barnes, D.K.A., Servetto, N., Tarantelli, S., Tatian, M., Zamboni, N., Abele, D., 2015. Climate change and glacier retreat drive shifts in an Antarctic benthic ecosystem. Sci. Adv. 1, e1500050–e1500050. doi:10.1126/sciadv.1500050

Schöne, B.R., 2013. *Arctica islandica* (Bivalvia): A unique paleoenvironmental archive of the northern North Atlantic Ocean. Glob. Planet. Change 111, 199–225. doi:10.1016/j.gloplacha.2013.09.013

Schöne, B.R., Fiebig, J., Pfeiffer, M., Gleβ, R., Hickson, J., Johnson, A.L.A., Dreyer, W., Oschmann, W., 2005. Climate records from a bivalved Methuselah (*Arctica islandica*, Mollusca; Iceland). Palaeogeogr. Palaeoclimatol. Palaeoecol. 228, 130–148. doi:10.1016/j.palaeo.2005.03.049

Schöne, B.R., Gillikin, D.P., 2013. Unraveling environmental histories from skeletal diaries — Advances in sclerochronology. Palaeogeogr. Palaeoclimatol. Palaeoecol. 373, 1–5. doi:10.1016/j.palaeo.2012.11.026

Schöne, B.R., Wanamaker, A.D., Fiebig, J., Thébault, J., Kreutz, K., 2011. Annually resolved δ13Cshell chronologies of long-lived bivalve mollusks (*Arctica islandica*) reveal oceanic carbon dynamics in the temperate North Atlantic during recent centuries. Palaeogeogr. Palaeoclimatol. Palaeoecol. 302, 31–42. doi:10.1016/j.palaeo.2010.02.002

Shumway, S.E., Parsons, G.J., 2006. Scallops biology, ecology, and aquaculture. Elsevier, Amsterdam; Boston.

Scourse, J., Richardson, C., Forsythe, G., Harris, I., Heinemeier, J., Fraser, N., Briffa, K., Jones, P., 2006. First cross-matched floating chronology from the marine fossil record: data from growth lines of the long-lived bivalve mollusc *Arctica islandica*. The Holocene 16, 967–974. doi:10.1177/0959683606hl987rp

Scourse, J.D., Wanamaker, A.D., Weidman, C., Heinemeier, J., Reimer, P.J., Butler, P.G., Witbaard, R., Richardson, C.A., 2012. The marine radiocarbon bomb pulse across the temperate north Atlantic: a compilation of Δ14C time histories from *Arctica Islandica* growth increments. Radiocarbon 54, 165–186.

Seed, R., 1980. Shell growth and form in the bivalvia, in: Skeletal Growth of Aquatic Organisms. Plenum press, New York and London, pp. 23–68.

Serebrennikova, Y.M., Fanning, K.A., 2004. Nutrients in the Southern Ocean GLOBEC region: variations, water circulation, and cycling. Deep Sea Res. Part II Top. Stud. Oceanogr. 51, 1981–2002. doi:10.1016/j.dsr2.2004.07.023

Shackleton, N.J., 1974. Attainment of isotopic equilibrium between ocean water and the benthonic foraminifera genus Uvigerina: isotopic changes in the ocean during the last glacial.

Smale, D.A., Barnes, D.K., 2008. Likely responses of the Antarctic benthos to climate-related changes in physical disturbance during the 21st century, based primarily on evidence from the West Antarctic Peninsula region. Ecography 31, 289–305.

Smale, D.A., Barnes, D.K.A., Fraser, K.P.P., 2007. The influence of ice scour on benthic communities at three contrasting sites at Adelaide Island, Antarctica. Austral Ecol. 32, 878–888. doi:10.1111/j.1442-9993.2007.01776.x

Smale, D.A., Brown, K.M., Barnes, D.K.A., Fraser, K.P.P., Clarke, A., 2008. Ice Scour Disturbance in Antarctic Waters. Science 321, 371–371. doi:10.1126/science.1158647

Speer, K., Rintoul, S.R., Sloyan, B., 2000. The diabatic Deacon cell. J. Phys. Oceanogr. 30, 3212–3222.

Stammerjohn, S., Massom, R., Rind, D., Martinson, D., 2012. Regions of rapid sea ice change: An inter-hemispheric seasonal comparison: regions of rapid sea ice change. Geophys. Res. Lett. 39, n/a-n/a. doi:10.1029/2012GL050874

Stammerjohn, S.E., Martinson, D.G., Smith, R.C., Iannuzzi, R.A., 2008a. Sea ice in the western Antarctic Peninsula region: Spatio-temporal variability from ecological and climate change perspectives. Deep Sea Res. Part II Top. Stud. Oceanogr. 55, 2041–2058. doi:10.1016/j.dsr2.2008.04.026

Stammerjohn, S.E., Martinson, D.G., Smith, R.C., Yuan, X., Rind, D., 2008b. Trends in Antarctic annual sea ice retreat and advance and their relation to El Niño–Southern Oscillation and Southern Annular Mode variability. J. Geophys. Res. 113. doi:10.1029/2007JC004269

Sturrock, A.M., Hunter, E., Milton, J.A., EIMF, Johnson, R.C., Waring, C.P., Trueman, C.N., 2015. Quantifying physiological influences on otolith microchemistry. Methods Ecol. Evol. 6, 806–816. doi:10.1111/2041-210X.12381

Talley, L.D., 1999. Some aspects of ocean heat transport by the shallow, intermediate and deep overturning circulations, in: Clark, U., Webb, S., Keigwin, D. (Eds.), Geophysical Monograph Series. American Geophysical Union, Washington, D. C., pp. 1–22. doi:10.1029/GM112p0001

Talley, L.D., Pickard, G.L., Emery, W.J., Swift, J.H. (Eds.), 2011. Descriptive physical oceanography: an introduction, 6. ed. ed. Elsevier, Amsterdam.

Thompson, D.W., Wallace, J.M., 2000. Annular modes in the extratropical circulation. Part I: month-to-month variability*. J. Clim. 13, 1000–1016.

Thompson, D.W., Wallace, J.M., Hegerl, G.C., 2000. Annular modes in the extratropical circulation. Part II: Trends. J. Clim. 13, 1018–1036.

Thompson, D.W.J., Solomon, S., 2002. Interpretation of Recent Southern Hemisphere Climate Change. Science 296, 895–899. doi:10.1126/science.1069270

Thompson, I., Jones, D.S., 1977. The ocean quahog, *Arctica islandica*, “tree” of the North Atlantic shelf. Abstract. Annu. Meet. Geol. Soc. Am. Programs 9, 1199.

Trathan, P.N., Murphy, E.J., 2002. Sea surface temperature anomalies near South Georgia: Relationships with the Pacific El Niño regions. J. Geophys. Res. 108. doi:10.1029/2000JC000299

Trenberth, K.E., 2015. Has there been a hiatus? Science 349, 691–692. doi:10.1126/science.aac9225

Trenberth, K.E., Large, W.G., Olson, J., 1990. The Mean Annual Cycle in Global Ocean Wind Stress. J. Phys. Oceanogr. 20, 1742–1760.

Trevisiol, A., Bergamasco, A., Montagna, P., Sprovieri, M., Taviani, M., 2013. Antarctic seawater temperature evaluation based on stable isotope measurements on *Adamussium colbecki* shells: kinetic effects vs. isotopic equilibrium. J. Mar. Sys. 126, 43-55. doi: 10.1016/j.jmarsys.2012.10.012

Tunnicliffe, V., Davies, K.T.A., Butterfield, D.A., Embley, R.W., Rose, J.M., Chadwick Jr, W.W., 2009. Survival of mussels in extremely acidic waters on a submarine volcano. Nat. Geosci. 2, 344-348. doi: 10.1038/ngeo500

Turner, J., 2004. The El Niño–southern oscillation and Antarctica. Int. J. Climatol. 24, 1–31. doi:10.1002/joc.965

Turner, J., Lu, H., White, I., King, J.C., Phillips, T., Hosking, J.S., Bracegirdle, T.J., Marshall, G.J., Mulvaney, R., Deb, P., 2016. Absence of 21st century warming on Antarctic Peninsula consistent with natural variability. Nature 535, 411–415. doi:10.1038/nature18645

Turner, J., Marshall, G.J., 2011. Climate change in the polar regions. Cambridge Univ. Press, Cambridge.

Urrutia, M.B., Ibarrola, I., Iglesias, J.I.P., Navarro, E., 1999. Energetics of growth and reproduction in a high-tidal population of the clam *Ruditapes decussatus* from Urdaibai Estuary (Basque Country, N. Spain). J. Sea Res. 42, 35–48.

Vaughan, D.G., Comiso, J.C., Allison, I., Carrasco, J., Kaser, G., Kwok, R., Mote, P., Murray, T., Paul, F., Ren, J., others, 2013. Observations: cryosphere. Clim. Change 317–382.

Vaughan, D.G., Marshall, G.J., Connolley, W.M., Parkinson, C., Mulvaney, R., Hodgson, D.A., King, J.C., Pudsey, C.J., Turner, J., 2003. Recent rapid regional climate warming on the Antarctic Peninsula. Clim. Change 60, 243–274.

Venables, H.J., Clarke, A., Meredith, M.P., 2013. Wintertime controls on summer stratification and productivity at the western Antarctic Peninsula. Limnol. Oceanogr. 58, 1035–1047. doi:10.4319/lo.2013.58.3.1035

Venables, H.J., Meredith, M.P., 2014. Feedbacks between ice cover, ocean stratification, and heat content in Ryder Bay, western Antarctic Peninsula. J. Geophys. Res. Oceans 119, 5323–5336. doi:10.1002/2013JC009669

Wallace, M.I., 2008. Ocean circulation, properties and variability in Marguerite Bay, West Antarctic Peninsula. Open University.

Wanamaker, A.D., Butler, P.G., Scourse, J.D., Heinemeier, J., Eiríksson, J., Knudsen, K.L., Richardson, C.A., 2012. Surface changes in the North Atlantic meridional overturning circulation during the last millennium. Nat. Commun. 3, 899. doi:10.1038/ncomms1901

Wanamaker, A.D., Kreutz, K.J., Borns, H.W., Introne, D.S., Feindel, S., Barber, B.J., 2006. An aquaculture-based method for calibrated bivalve isotope paleothermometry: bivalve isotope paleothermometry. Geochem. Geophys. Geosystems 7, n/a-n/a. doi:10.1029/2005GC001189

Weidman, C.R., Kyger, G.A.J., 1994. The long-lived mollusc *Arctica islandica*: A new paleoceanographic tool for the reconstruction of bottom temperatures for the continental shelves of the northern North Atlantic Ocean. J. Geophys. Res. 99, 18305. doi:10.1029/94JC01882

White, M.G., 1977. Ecological adaptations by antarctic poikilotherms to the polar marine environment, in: Adaptations within Antarctic Ecosytems. The Smithsonian Institution, Washington D.C., pp. 197–208.

White, W.B., Peterson, R.G., 1996. An Antarctic circumpolar wave in surface pressure, wind, temperature and sea-ice extent. Nature 380, 699–702. doi:10.1038/380699a0

Wigley, T.M.L., Briffa, K.R., Jones, P.D., 1984. On the average value of correlated time series, with application in dendroclimatology and hydrometeorology. J. Clim. Appl. Meteorol. 23, 201–213.

Wilbur, K.M., 1972. Shell Formation in Mollusks, in: Chemical Zoology Volume VII Mollusca. Academic Press, New York and London, pp. 103–145.

Witbaard, R., 1996. Growth variations in *Arctica islandica* L.(Mollusca): a reflection of hydrography-related food supply. ICES J. Mar. Sci. J. Cons. 53, 981–987.

Witbaard, R., Jenness, M.I., Van Der Borg, K., Ganssen, G., 1994. Verification of annual growth increments in *Arctica islandica* L. from the North Sea by means of oxygen and carbon isotopes. Neth. J. Sea Res. 33, 91–101.

Wolter, K., Timlin, M., 1993. Monitoring ENSO in COADS with a seasonally adjusted principal component index. Presented at the 17th Climate Diagnostics Workshop, NOAA/NMC/CAC, NSSL, Oklahoma Clim. Survey, CIMMS and the School of Meteor., Univ. of Oklahoma, Norman, OK, pp. 52–57.

Wolter, K., Timlin, M.S., 1998. Measuring the strength of ENSO events: How does 1997/98 rank? Weather 53, 315–324. doi:10.1002/j.1477-8696.1998.tb06408.x

Young, D.A., Wright, A.P., Roberts, J.L., Warner, R.C., Young, N.W., Greenbaum, J.S., Schroeder, D.M., Holt, J.W., Sugden, D.E., Blankenship, D.D., van Ommen, T.D., Siegert, M.J., 2011. A dynamic early East Antarctic Ice Sheet suggested by ice-covered fjord landscapes. Nature 474, 72–75. doi:10.1038/nature10114

Yuan, X., 2004. ENSO-related impacts on Antarctic sea ice: a synthesis of phenomenon and mechanisms. Antarct. Sci. 16, 415–425. doi:10.1017/S0954102004002238

Yuan, X., Martinson, D.G., 2001. The Antarctic dipole and its predictability. Geophys. Res. Lett. 28, 3609–3612.

Zachos, J., 2001. Trends, rhythms, and aberrations in global climate 65 Ma to present. Science 292, 686–693. doi:10.1126/science.1059412

Zazulie, N., Rusticucci, M., Solomon, S., 2010. Changes in Climate at High Southern Latitudes: A Unique Daily Record at Orcadas Spanning 1903–2008. J. Clim. 23, 189–196. doi:10.1175/2009JCLI3074.1

Zenk, W., Morozov, E., 2007. Decadal warming of the coldest Antarctic Bottom Water flow through the Vema Channel. Geophys. Res. Lett. 34. doi:10.1029/2007GL030340

Zitto, M.E., Barrucand, M.G., Piotrkowski, R., Canziani, P.O., 2015. 110 years of temperature observations at Orcadas Antarctic Station: multidecadal variability. Int. J. Climatol. n/a. doi:10.1002/joc.4384